UNIVERSITY OF SOUTHAMPTON

THE X-RAY CRYSTAL STRUCTURES OF CYTOCHROME C_L AND METHANOL DEHYDROGENASE FROM *METHYLOBACTERIUM EXTORQUENS*

By

PAUL ANTONY WILLIAMS

A thesis submitted for the degree of DOCTOR OF PHILOSOPHY

Department of Biochemistry

June 2003

UNIVERSITY OF SOUTHAMPTON

ABSTRACT

DIVISION OF BIOCHEMISTRY AND MOLECULAR BIOLOGY
SCHOOL OF BIOLOGICAL SCIENCES
Doctor of Philosophy

THE X-RAY CRYSTAL STRUCTURES OF CYTOCHROME c_L AND METHANOL DEHYDROGENASE FROM *METHYLOBACTERIUM EXTORQUENS*

by Paul Antony Williams

The soluble proteins involved in the oxidation of methanol in the methylotrophic bacteria *Methylobacterium extorquens* provide an ideal system in which to study electron transfer. Methanol is oxidized to formaldehyde by methanol dehydrogenase (MDH), reducing the pyrroloquinoline quinone (PQQ) prosthetic group to quinol. Electrons are then passed, one at a time, to the *c*-type cytochrome, cytochrome c_L, creating the semiquinone PQQ free radical after the first transfer. Cytochrome c_L is reoxidised by the typical class I *c*-type cytochrome, cytochrome c_H, which in turn passes electrons to the terminal electron acceptor, the membrane bound cytochrome oxidase, cytochrome aa_3.

The crystal structures of MDH and cytochrome c_H have been solved prior to this project. The principal aim of this thesis was to grow crystals and solve the structure of the hitherto uncrystallized cytochrome c_L. The 1.6 Å X-ray crystal structure of cytochrome c_L reported in this thesis was solved by molecular replacement; the search model was cytochrome c_{551i}. As expected, the haem was covalently bonded to the protein through thioether bonds to Cys65 and Cys68 and the fifth ligand to the haem iron was provided by His69. Somewhat unexpectedly, the sixth ligand to the haem iron was provided by His112, and not Met109, which is homologous to Met101, the sixth ligand to the haem in cytochrome c_{551i}. The absence of the N-terminal region of the protein in the electron density maps strongly suggested the protein has been truncated during crystallization, leading to an increase in the flexibility and solvent exposure of the loop region which contains Met109. This, along with the labile nature of the Met-Fe bond in cytochrome c_L is the most-likely explanation for the bis-histidine haem iron coordination. The crystal structure also revealed that a calcium ion was bound close to the inner haem propionate; this region is most commonly occupied by an arginine or a histidine side chain in eukaryotic cytochromes *c* and bacterial cytochromes c_2. The calcium ion interacts with the inner haem propionate through a conserved water molecule, suggesting that it may affect the redox potential.

MDH was analysed from methanol oxidation mutants, where mutations have been introduced into the *mxaC* and *mxaD* genes. The *mxaC* gene was shown to code for a protein involved in calcium insertion into MDH, and the *mxaD* gene product was thought to modify MDH to improve the electron transfer to cytochrome c_L. Although no gross structural changes were observed in the MDH structures from both methanol oxidation mutants, the calcium occupancy in *mxaC31*-MDH was only 60%, consistent with the proposed role of the *mxaC31* gene product in calcium insertion. The structural similarity of *mxaD11*-MDH to wild type-MDH does not account for its lower rate of methanol oxidation in whole cells, and suggests that the *mxaD* gene product does not alter the structure of MDH in order to improve electron transfer to cytochrome c_L, as was previously postulated.

Contents

List of Figures

Chapter 2

Chapter 3

Chapter 4

Chapter 6

Chapter 7

List of Tables

Chapter 5

Chapter 6

Chapter 7

I would like to thank Professor Chris Anthony for giving me the opportunity to study for a PhD at Southampton, and for his patience and advice concerning work matters.

I owe a large debt of gratitude to Professor Steve Wood and Dr Jon Cooper for giving me the opportunity to learn X-ray crystallography, especially to Jon for managing to find extra funding during the latter stages of my project, and also providing moments of comic genius. Thanks a lot!

Thanks to the postgrads and postdocs, past and present, for saying hello in the corridor and sharing a drink with me from time to time; these include, Jed, Rob, Donald, Katie, Graham, Darren, Raj, Gordon, Nick, Dave, Steve, Terry, Michelle, Peter and Sanjay. Cheers to Leighton and Fiyaz for guiding me through all things crystallographic (and for being top lads), and Monty, for being an absolute ripper.

Special thanks to my friends outside of work. Cheers Pete for being a great friend; things would have been tough if we didn't have our daily discussions on anything and everything, hope everything works out for you and Sarah in the future. My big buddy Claire, for being sheer quality. Gaz, Big G and the Coventry, soon to be Bolton posse, Kev, Karen and Harrison.

Finally, I would like to thank my brother and Mum. Rob for his encouragement, the odd £50, free meals and holidays to Australia, and Ma for supporting me and always looking out for me.

Abbreviations

α	Alpha
Å	Angstrom
ADH	Alcohol dehydrogenase
ATP	Adenosine-5'-triphosphate
$Å^2$	Angstrom squared
β	Beta
Ba^{2+}	Barium ion
BCA	Bicinchoninic acid assay
Ca^{2+}	Calcium ion
CTQ	Cysteine tryptophylquinone
CO	Carbon monoxide
Cu^{2+}	Copper ions
CCD	Charged-coupled device
C	C-centered lattice
CCP4	Collaborative computational project number 4
CNS	Crystallography and NMR system
cyt c_2	Cytochrome c_2
cyt c_L	Cytochrome c_L
cyt c_{551i}	Cytochrome c_{551i}
cyt c_M	Mitochondrial cytochrome *c*
DCPIP	2, 6-dichlorophenolindophenol
DEAE	Diethylaminoethyl
d_{hkl}	Interplanar distance
DTT	Dithiothreitol
EDTA	Ethylenediamine-N,N,N',N'-tetraacetic acid
ELISA	Enzyme-linked immunosorbent assay
ESRF	European synchrotron radiation facility
F_{hkl}	Structure factor $_{hkl}$
F	Face-centered lattice
FT	Fourier transform
F*o*	Observed structure factors
F*c*	Calculated structure factors
GDH	Glucose dehydrogenase
GeV	Bilion (in US counting) electron volts
HP7	Outer haem propionate
HP6	Inner haem propioante
IMS	Inter-membrane space
IM	Inner membrane
I	Internal lattice / body-centered lattice
I_{hkl}	Intensity $_{hkl}$
kDa	Kilodalton
KCN	Potassium cyanide
LINAC	Linear accelerator
MDH	Methanol dehydrogenase

MMO	Methane monooxygenase
mGDH	Membrane glucose dehydrogenase
Mg^{2+}	Magnesium ion
M	Membrane
m.c.d	Magnetic circular dichroism
MSE	Mounted ultrasonic disintegrator
MES	3-(N-morpholino) ethane sulphonic acid
MOPS	3-[N-morpholino] propane sulphonic acid
ORF	Open reading frame
OM	Outer membrane
PQQ	Pyrroloquinoline quinone
PMF	Proton motive force
PES	Phenazine ethosulphate
PEG	Polyethylene glycol
$\rho(xyz)$	Electron density (xyz)
P	Primitive
QH-ADH	Quinohaemoprotein alcohol dehydrogenase
sGDH	Soluble glucose dehydrogenase
Sr^{2+}	Strontium ion
SDS-PAGE	Sodium dodecyl sulfate polyacrylamide gel electrophoresis
TTQ	Tryptophan tryptophylquinone
Tris	Tris (hydroxymethyl) aminomethane

Chapter 1

Introduction

1.1 Introduction

Methanol dehydrogenase (MDH) and cytochrome c_L are soluble proteins from the periplasm of methylotrophic Gram negative bacteria, such as *Methylobacterium extorquens*. MDH has a pyrroloquinoline quinone (PQQ) prosthetic group and catalyses the conversion of methanol to formaldehyde (Anthony, 1986), reducing the prosthetic group quinone to quinol. The reaction mechanism for the oxidation of methanol relies on the quinone portion of PQQ being polarized by a tightly bound calcium ion. Cytochrome c_L is an unusual *c*-type cytochrome and is the physiological electron acceptor from MDH (Anthony, 1992). MDH donates electrons in two single steps to cytochrome c_L; a semi-quinone PQQ is formed after the first electron is transferred (Dijkstra *et al.*, 1989). The aims of this project were to characterize MDH from the calcium insertion mutant *mxaC*31 and to solve the structures of cytochrome c_L and the reduced form of cytochrome c_H using X-ray crystallography.

1.2 Methylotrophs

Methylotrophic bacteria are microorganisms able to grow on reduced carbon compounds with one or more carbon atoms but no carbon-carbon bonds (Colby & Zatman, 1972). There are two types of methylotrophic bacteria; those that absolutely require such compounds for growth, termed obligate methylotrophs, or those that can also use organic multicarbon compounds, termed facultative methylotrophs (Anthony, 1982).

Methylobacterium extorquens (formerly *Pseudomonas* AM1), the bacterium used in this study, is a pink facultative methylotroph capable of using methanol and methylamine as a C_1 source, but unable to use methane. It can also utilize multicarbon compounds, such as pyruvate and succinate.

1.3 The electron transport chain

Methanol is oxidized by MDH to formaldehyde. Methanol can be synthesised from methane in some methylotrophs; methane monooxygenase (MMO) catalyses this reaction,

although this enzyme is not present in *M. extorquens*. Figure 1.1 shows the short electron transport chain for methanol oxidation; MDH transfers electrons to cytochrome c_L, which is oxidized by cytochrome c_H, a typical class I *c*-type cytochrome, which is in turn oxidised by the membrane-bound terminal oxidase, cytochrome aa_3 (Anthony, 1992). The pathway of electrons from methanol to O_2 produces a proton motive force (PMF) sufficient to produce about 1 molecule of ATP (Anthony, 1988; O'Keeffe & Anthony, 1978), although this is dependent on the relative concentrations of ADP and ATP.

1.4 **Pyrroloquinoline quinone (PQQ)**

PQQ (Figure1.2) is a non-covalently bound prosthetic group found in many periplasmic dehydrogenases of Gram negative bacteria. Enzymes containing PQQ are now classed as quinoproteins (Goodwin & Anthony, 1998). PQQ is formed from the fusion of glutamate and tyrosine and is synthesized independently of the apoenzyme dehydrogenase and transported into the periplasm, where it is incorporated into the enzyme. PQQ was first isolated from glucose dehydrogenase and methanol dehydrogenase (Hauge, 1964; Anthony & Zatman, 1967). The compound is easily released from the enzyme by denaturation and once characterized it was shown to be a red, highly polar, acidic compound with a characteristic green fluorescence. Its structure was subsequently solved by X-ray crystallography (Salisbury *et al.*, 1979) and its chemistry was fully described by Frank and Duine (Duine *et al.*, 1987; Duine, 1991). The key feature of PQQ is the *ortho*-quinone at the C-4 and C-5 positions of the quinone ring, which becomes reduced to a quinol during catalysis. The C-5 is readily attacked by nucleophiles such as ammonia, cyclopropanol and methanol amongst others. These reactions form adducts at the C-5 position (Frank *et al.*, 1989), an important feature when considering the enzyme mechanism. Another important feature of PQQ is the ability to coordinate divalent cations in solution; this was first shown by Mutzel and Gorisch (1991) and further developed by Itoh (1997). Ca^{2+} is tightly coordinated to the PQQ in the active site by way of the C7-carboxylate group, the N-6 in the ring and the C-5 carbonyl oxygen; all quinoproteins whose structures have been determined contain calcium bound in this way. Active site residues also coordinate to the Ca^{2+} (Figure 1.3).

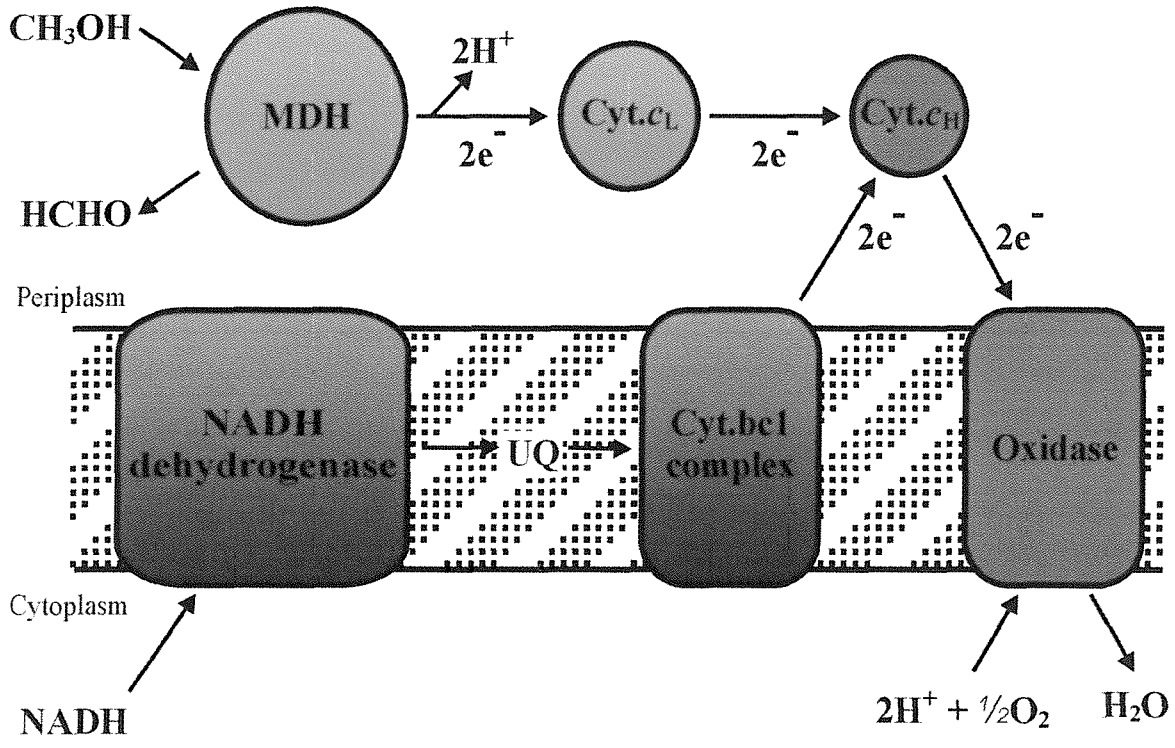

Figure 1.1 The electron transport chain for methanol oxidation

All the proteins involved in the transfer of electrons from methanol to O_2 are periplasmic, except for the oxidase. Once formed, formaldehyde is used for assimilation in the cell or is further oxidized to carbon dioxide.

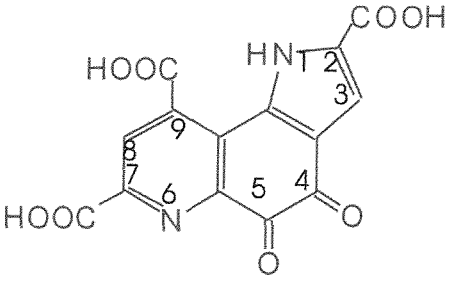

PQQ

(Quinone)

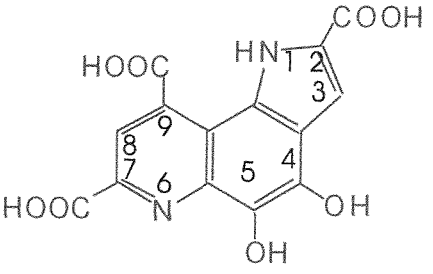

$PQQH_2$

(Quinol)

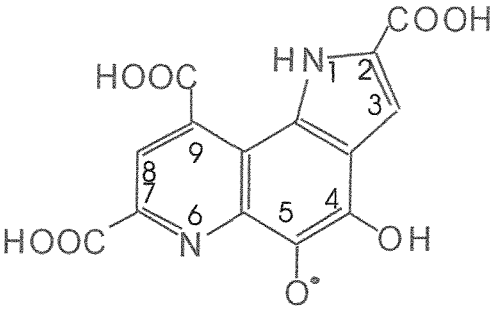

$PQQH^{\bullet}$

(Semiquinone)

Figure 1.2 The structures of the various forms of pyrroloquinoline quinone (PQQ)

The quinone is reduced by substrate in the enzymes active site, producing quinol which is re-oxidized (by way of the semi-quinone) in two single electron transfer steps back to the quinone.

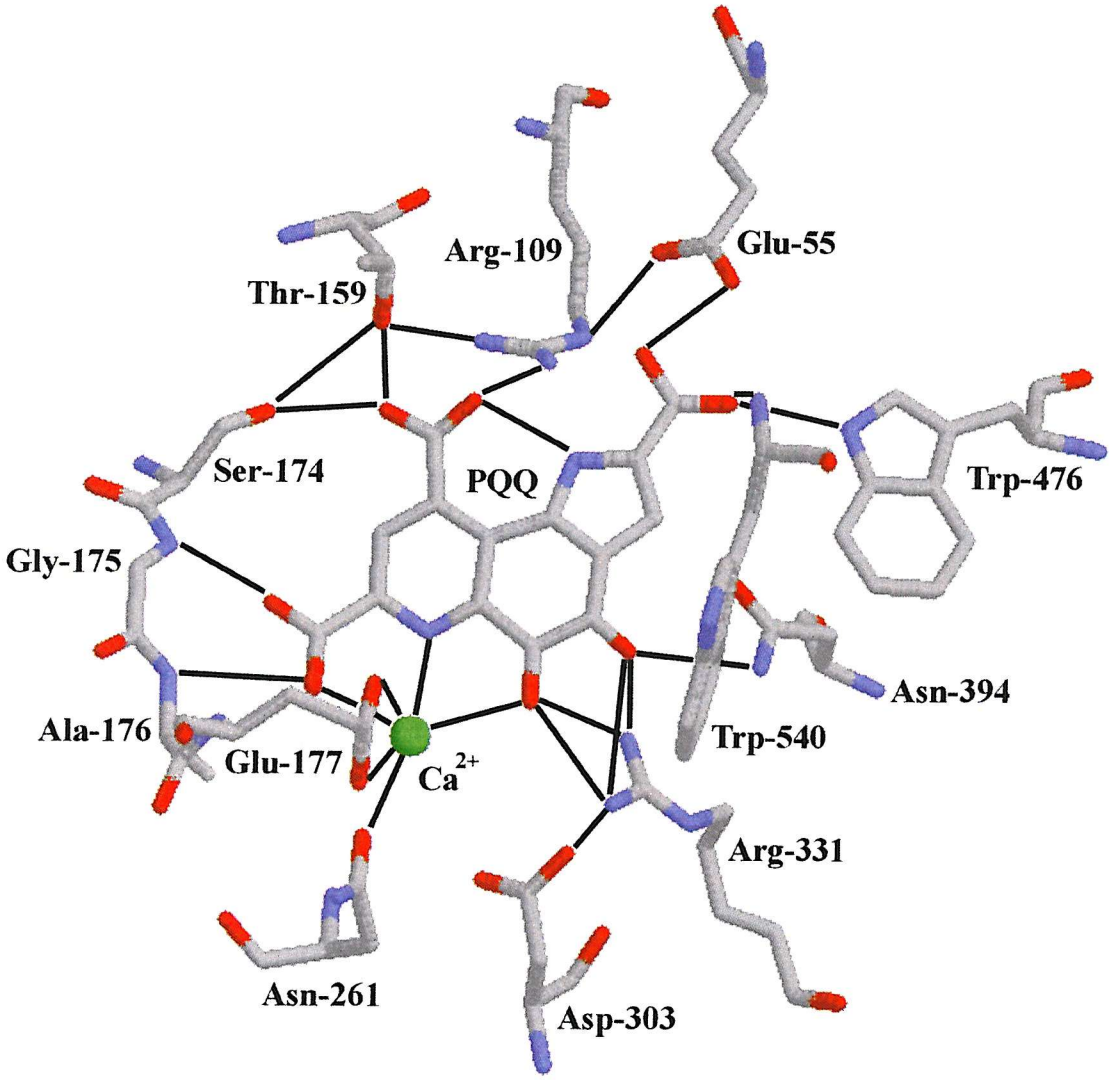

Figure 1.3 The many interactions of PQQ and calcium in the active site of MDH

These interactions were calculated from the X-ray structure of MDH from *M. extorquens* (Ghosh *et al.*, 1995).

1.5 **The main types of quinoproteins**

Quinoproteins include all enzymes whose catalytic mechanisms involve quinone-containing prosthetic groups in their active sites (Anthony, 1996). Quinoprotein dehydrogenases which oxidize alcohols and aldoses contain PQQ as their prosthetic group, whereas amine dehydrogenases contain prosthetic groups derived from modified tryptophan residues: TTQ (tryptophan tryptophylquinone) (Davidson, 1993a, 2000) or CTQ (cysteine tryptophylquinone) (Satoh *et al.*, 2002). By contrast with TTQ and CTQ, which are derived from the amino acid chain of the proteins, PQQ is synthesized separately and bound non-covalently into the active site of the protein. The reactions are catalysed in the periplasm, either by membrane-bound enzymes which pass electrons to ubiquinone, or by soluble dehydrogenases which react with *c*-type cytochromes or blue copper proteins.

There are three classes of PQQ-containing alcohol dehydrogenases. Type I enzymes are soluble and contain a single PQQ molecule; MDH is a member of this class and is further discussed below. Type II alcohol dehydrogenases are soluble quinohaemoproteins, which have a C-terminal extension containing a haem *c* domain (Section 1.11). Type III enzymes are similar to type II but they have two additional subunits (including a multi-haem cytochrome *c*) and are bound to the periplasmic membrane. There two types of glucose dehydrogenase; an atypical soluble quinoprotein (sGDH) whose function is not understood, and a more widely-distributed glucose dehydrogenase which is bound to the membrane by transmembrane helices at the N-terminus (mGDH).

1.6 **The structure of MDH**

Several structures of MDH from methylotrophic bacteria have been solved (See Table 1.1 for a complete list of references). The highest resolution structure for MDH from *M. extorquens* was 1.94 Å (Ghosh *et al.*, 1995), and it is the structure that will be referred to. When relating structure to function the results from the active site D303E mutant of MDH (Afolabi *et al.*, 2001) will be considered.

MDH is a tetrameric protein with an $\alpha_2\beta_2$ structure which consists of two almost spherical $\alpha\beta$ units (Figure 1.4). Figure 1.5 shows a single $\alpha\beta$ subunit from MDH. The α-subunit is 66 kDa and is the catalytic subunit of the enzyme as it contains the Ca^{2+} ion, the PQQ and the catalytic amino acid Asp303. The β-subunit is a small 8.5 kDa subunit which is thought to have

Table 1.1 A list of references to all the MDH structures solved

Organism	Reference:
Methylobacterium extorquens	Ghosh *et al.*, 1995
Methylobacterium extorquens	Anthony, Ghosh & Blake, 1994
Methylobacterium extorquens	Afolabi *et al.*, 2001
Methylobacterium extorquens	Anthony & Ghosh, 1998
Methylophilus W3A1	Zheng *et al.*, 2001
Methylophilus W3A1	Xia *et al.*, 1996
Parracoccus denitrificans	Xia *et al.*, 1999
Methylophilus W3A1	Xia *et al.*, 1992
Methylophilus methylotrophus	Xia *et al.*, 1992
Methylophilus W3A1	White *et al.*, 1993

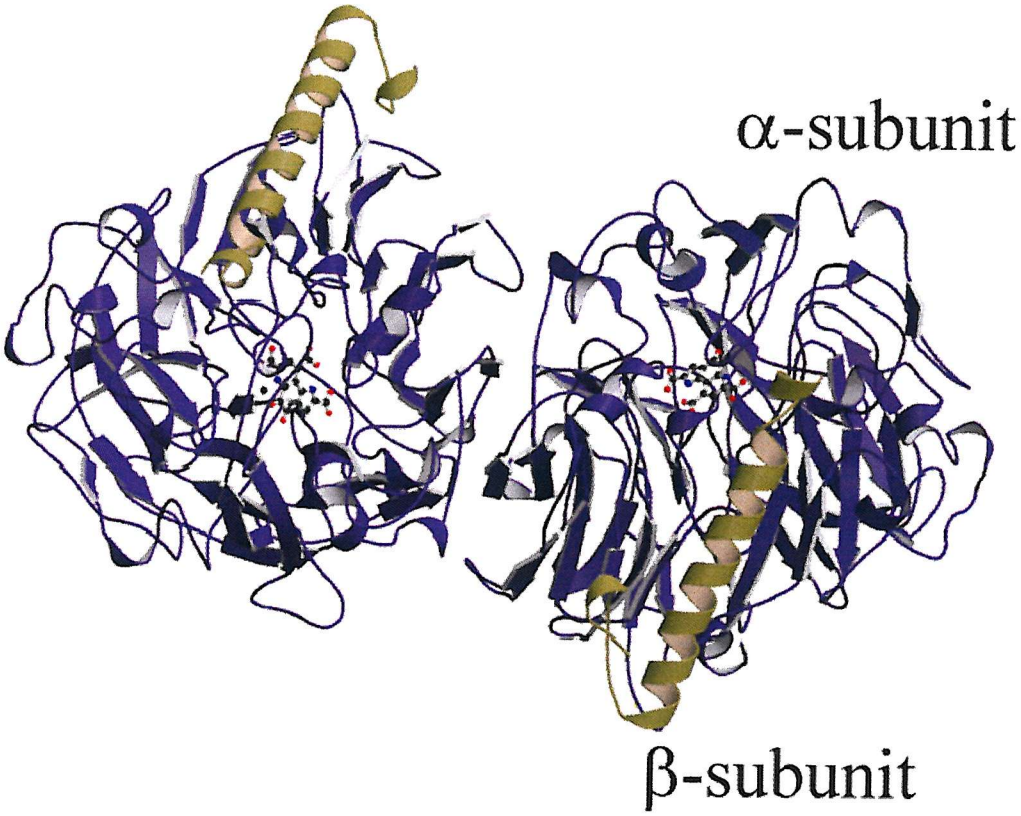

Figure 1.4 The $\alpha_2\beta_2$ tetrameric structure of MDH

The protein is comprised of 2 roughly spherical αβ units. The α-subunit is shown in blue and the β-subunit in gold (Ghosh *et al.*, 1995).

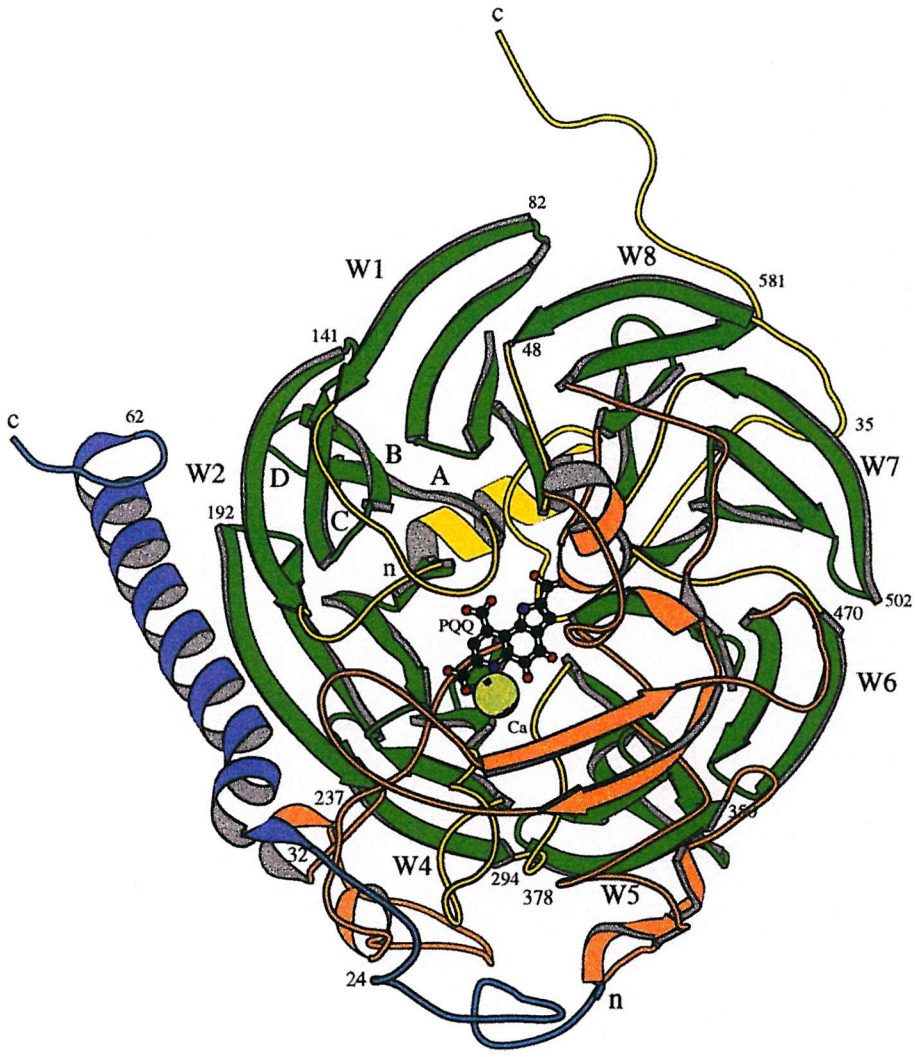

Figure 1.5 The αβ subunit of MDH

This view looks down the pseudo 8-fold axis and is simplified to show only the 'W' motifs of the α-chain (shown in green) and the long α-helix of the β-chain (shown in blue), but excludes other β-structures and short α-helices. The PQQ is in skeletal form and the calcium ion shown as a small sphere. The Figure is based on the structure from Ghosh *et al.* (1995).

no catalytic function. A mutation in the gene which codes for the β-subunit produces bacteria incapable of producing MDH (Nunn *et al.*, 1989). MDH is the only PQQ-containing enzyme with a β-subunit, which suggests that it may have a unique role in MDH

1.6.1 **The α-subunit of MDH**

The X-ray crystal structure of MDH shows the α-subunit is a superbarrel structure made up of eight twisted antiparallel β-sheets (W-shaped) stacked radially around a pseudo eight-fold symmetry axis running through the centre of the subunit. The structure has been referred to as a propeller fold, each W motif representing a propeller blade. The fold is held together by tryptophans which link together the eight β-sheets, these residues constitute the 'tryptophan docking motif'. The tryptophan docking motifs make planar, stabilizing girdles around the periphery of the α-subunit (Figure 1.6). The interaction occurs by way of an eleven-residue consensus sequence in the region of the C and D β-strands all 'W' motifs, except number eight. The relevant characteristics of the tryptophan residues are their planar conjugated rings and their ability to act as a hydrogen bond donor through the indole ring NH group. Figure 1.7 shows how the tryptophan at position eleven in the consensus sequence is stacked between the alanine at position one of the same motif (W_n) and the peptide bond which exists between residue six and the invariant glycine at position seven of the next motif (W_{n+1}). The same tryptophan is also hydrogen bonded between its indole NH and the main-chain carbonyl of residue four in the next motif (W_{n+1}). The third type of interaction involving the conserved tryptophan is a β-strand hydrogen bond between its carbonyl oxygen and the backbone nitrogen of position one (usually an alanine) of the same motif. Examples of proteins which have a propeller fold with four, six, seven or eight propeller blades have been previously described. Haemopexin (Faber *et al.*, 1995) and synovial collagenase (Li *et al.*, 1995) have four blades; viral neuraminidase (Varghese *et al.*, 1983) and bacterial sialidase (Crennell *et al.*, 1993) have six blades; the β-subunit of the G-protein transducin (Sondek *et al.*, 1996; Lambright *et al.*, 1996) and the heavy chain of methylamine dehydrogenase have seven, while MDH and nitrite reductase (Fulop *et al.*, 1995) have eight. Each α-subunit of MDH has a single PQQ molecule which is coordinated to a Ca^{2+} ion and is highly hydrogen bonded to the protein (Figure 1.3).

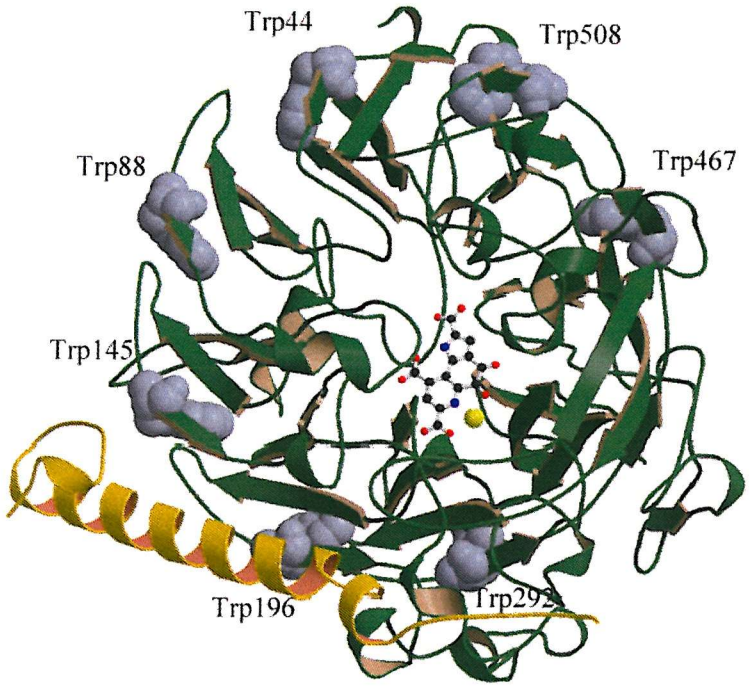

Figure 1.6 The girdle of tryptophan residues, which are involved in docking the β sheets together

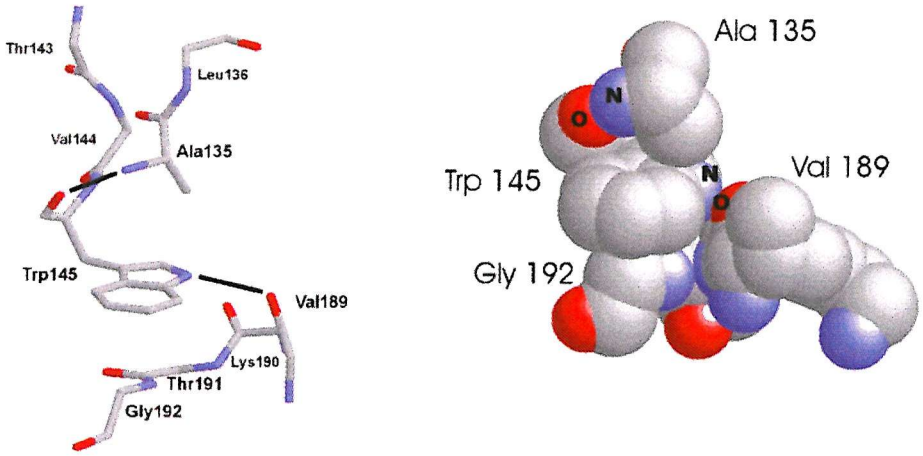

Figure 1.7 A typical example of a tryptophan docking motif, as seen in MDH

The Figure is taken from Anthony & Goodwin (1998).

1.6.2 **The β-subunit of MDH**

Each 8.5 kD 74 residue β-subunit forms a 'J' shaped structure around one side of the α-subunit. Figure 1.5 shows that the subunit consists of a long straight α-helix as its stem. It hooks around the α-subunit and forms mainly ionic interactions with the larger subunit, although there are several hydrophobic interactions. The β-subunit makes contact with the edges of the W1-W4 of the α-subunit with ion pair interactions involving Glu148, Glu193, Arg197, Lys236, Glu267 and Glu301 on the α-chain, with Lys16, Glu48, Arg50, Arg54 and Lys59 of the β-chain. In the absence of any other known function for the subunit, it is possible that it acts to stabilize the folded form of the α-chain. It was previously thought that the high number of lysine residues in the β-subunit (15 out of the 74 residues) indicated a role in docking with cytochrome c_L (Nunn *et al.*, 1989) but this was later shown not to be the case (Section 1.19).

1.6.3 **The active site of MDH**

The active site of MDH is located in an internal chamber within each α-subunit, which is located approximately at the centre of the pseudo eight-fold symmetry axis. The active site contains the catalytic amino acid Asp303, the Ca^{2+} ion, a PQQ molecule and an unusual eight-membered disulphide ring structure which is formed from adjacent Cys103 and Cys104 residues joined by an atypical non-planar peptide bond; the disulphide forms the ceiling of a chamber enclosing the PQQ and the base of the chamber is formed from the indole ring of Trp243 (Figure 1.8). Recent research on quinohaemoproteins has postulated that conserved water molecules in the active site are important in the transfer of electrons from PQQ to a C-terminal *c*-type cytochrome *c* domain (Chen *et al.*, 2002; Oubrie *et al.*, 2002) (Section 1.13). This electron transfer could be conserved in the MDH/cytochrome c_L system as MDH has these water molecules in the active site. The disulphide bridge between Cys103 and Cys104 is not present in the membrane bound glucose dehydrogenase but it is present in other quinoprotein alcohol dehydrogenases. The transfer of electrons from membrane bound glucose dehydrogenase to ubiquinone probably does not involve the formation of a semi-quinone prosthetic group as happens in MDH; this disulphide ring structure has therefore been postulated to stabilize the semi-quinone free radical formed in soluble alcohol dehydrogenases (Avezoux *et al.*, 1995).

The X-ray structure of MDH showed that the calcium ion in the active site is coordinated

a)

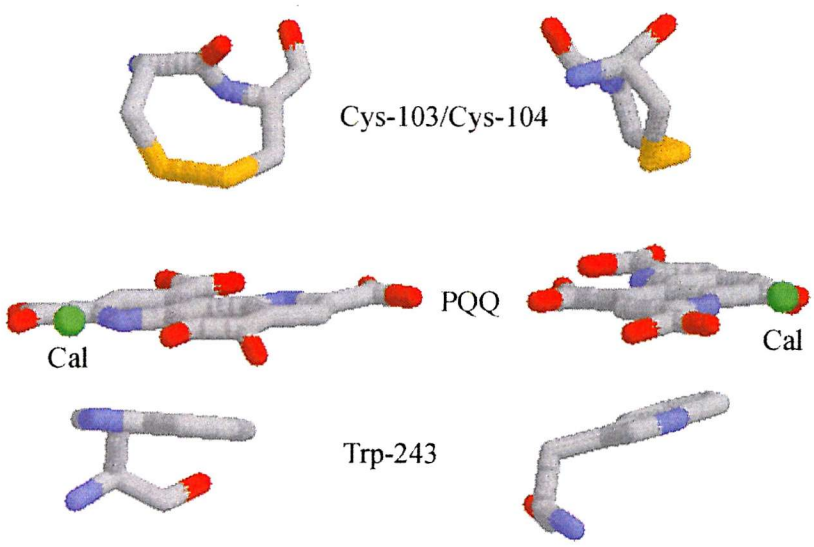

b)

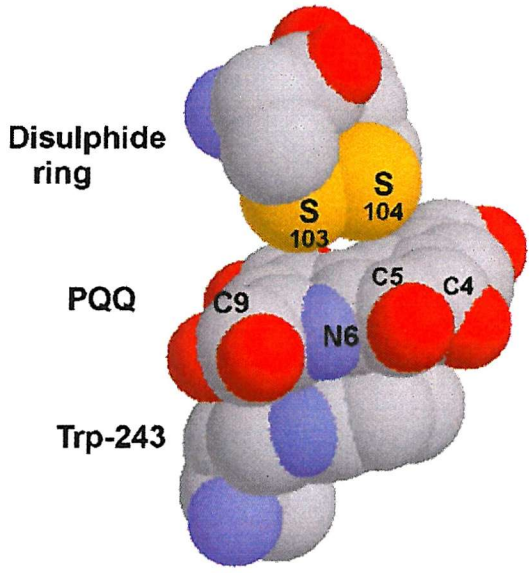

Figures 1.8 The stacking of PQQ between the indole ring of Trp243 and the disulphide ring formed from Cys103 and Cys104 in MDH

Figure 1.8a shows the two orientations of the stacking interaction between PQQ and the eight membered ring formed between adjacent cysteines 103 and 104 and Trp243. These Figures are taken from Anthony and Goodwin (1998).

by six ligands; three atoms from amino acid side-chains (both carboxylate oxygens of Glu177 and the amide of Asn261) and three PQQ atoms (the C-5 quinone oxygen, one oxygen of the C-7 carboxylate group and the N-6 ring atom) (Ghosh *et al.*, 1995); this arrangement is shown in Figure 1.3. The calcium ion is proposed to perform two roles in the enzyme. It keeps the PQQ in the correct conformation for electron transfer and secondly it acts as a Lewis acid in the reaction mechanism; the definition of a Lewis acid is 'a substance that can accept a lone pair of electrons'. This second function of the calcium ion is to facilitate the attack by the hydride or the oxyanion on the C-5 of PQQ in the reaction mechanism by polarising the C-5 carbonyl group (see Section 1.7). Calcium-free MDH from *M. extorquens* mutants (Section 1.17) was inactive and had an abnormal absorption spectrum (Richardson & Anthony, 1992; Goodwin *et al.*, 1996; Goodwin & Anthony, 1996). The absorption spectrum was different from wild type MDH in the region of 345 and 400 nm; it is in this region that PQQ produces a characteristic peak and shoulder respectively. The recovery of enzyme activity and wild type absorption spectrum could be achieved by reconstituting MDH at high pH with high concentrations of not only calcium but also barium or strontium ions (Goodwin & Anthony, 1996); this produced the only example of a characterised enzyme with barium in the active site.

1.7 **The reaction mechanism for MDH.**

The C-5 carbonyl in oxidized PQQ is very reactive towards nucleophiles, such as alcohols, ammonia, amines, cyanide and amino acids. This led to the proposal of a substrate-PQQ covalent complex (a hemiketal) forming in the reaction mechanism (Frank *et al.*, 1988; Frank *et al* 1989; Anthony, 1996). Support for the hemiketal-intermediate mechanism has come from the reaction of MDH with cyclopropanol (a suicide inhibitor) which gives a C-5 propanol adduct (Frank *et al.*, 1989). Therefore it was suggested that a similar mechanism occurs during methanol oxidation. The proposed mechanism begins with an initial proton extraction from the substrate by Asp303 which allows the resulting oxyanion to attack the C-5 of the PQQ, and form a hemiketal intermediate, as shown in Figure 1.9a. The subsequent reduction of the PQQ with release of aldehyde is facilitated by prior ionisation of the hemiketal complex, which involves the pyrrole nitrogen atom. The calcium ion coordinated to the PQQ O-5 facilitates this reaction by acting as a Lewis acid, making the C-5 more reactive and susceptible to attack by the oxyanion.

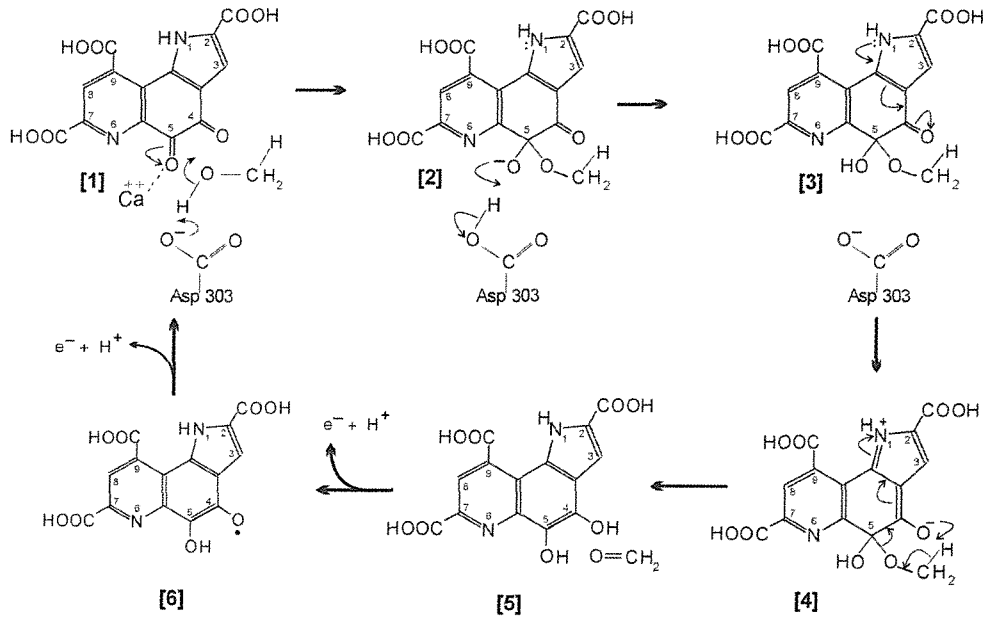

Figure 1.9a) The hemiketal intermediate reaction mechanism for the oxidation of methanol to formaldehyde

The Figure is taken from Anthony (2001).

An alternative mechanism is an acid/base-catalysed hydride transfer mechanism (Figure 1.9b) (Anthony, 1996). This mechanism now seems the more likely reaction mechanism. The Asp303 again initiates the reaction by a proton abstraction from methanol, the reaction continues with a direct hydride transfer from the methanol to the C-5 of the PQQ which produces the first intermediate, a tetrahedral C-5 reduced intermediate. The rate-limiting step of the reaction is the breaking of the C-H bond and the hydride transfer to the C-5 atom of the PQQ, this step is greatly facilitated by the Ca^{2+}, which polarises the C-5 carbonyl bond. What follows is a tautomerisation of the PQQ, presumably facilitated by the catalytic base Asp303, resulting in $PQQH_2$. Both mechanisms have been considered for sGDH where the evidence strongly supports the hydride transfer mechanism. A high resolution structure (1.9 Å) of sGDH was solved where glucose was bound in the active site. Figure 1.10 is created using the pdb file from the X-ray structure of sGDH; the structure showed how glucose interacts with the PQQ. The orientation of the glucose in the active site is ideal for direct hydride transfer from the glucose C-1 atom to the PQQ C-5 atom; the distance between the two atoms is only 3.2 Å in the sGDH-glucose complex. Since the C-1 hydrogen atom is expected to point down towards the PQQ C-5 atom a hydride ion thus has to be transferred over a distance of only 1.2 Å for covalent addition to the C-5 atom. A similar proximity (3.2 to 3.5 Å) and geometry of substrate and cofactor reactive groups has been observed in several nicotinamide and flavin-dependent oxido-reductases (Karplus & Schulz, 1989; Mattevi *et al.*, 1996, 1997), which also make use of a hydride transfer mechanism. Further inspection of the active site shows that His144 is the only base close to the glucose O-1 atom; this suggests that in the case of sGDH, His144 acts as the general base that abstracts a proton from the glucose O-1 atom. There is also substantial evidence for the hydride transfer mechanism in MDH. A 1.90 Å structure of MDH from *Methylophilus methylotrophus* showed PQQ in a reduced sate, with the C-5 carrying a hydroxyl, this is not an intermediate in the hemiketal mechanism; this would suggest a hydride transfer mechanism (Zheng *et al.*, 2001). There was also a failure to observe a spectroscopic intermediate during the course of the reaction and along with the observation from the D303E MDH mutant from *Methylobacterium extorquens* that Glu303 is able to make a hydrogen bond with the O-5 oxygen of PQQ, which would only be possible if there was a hydroxyl in this position.

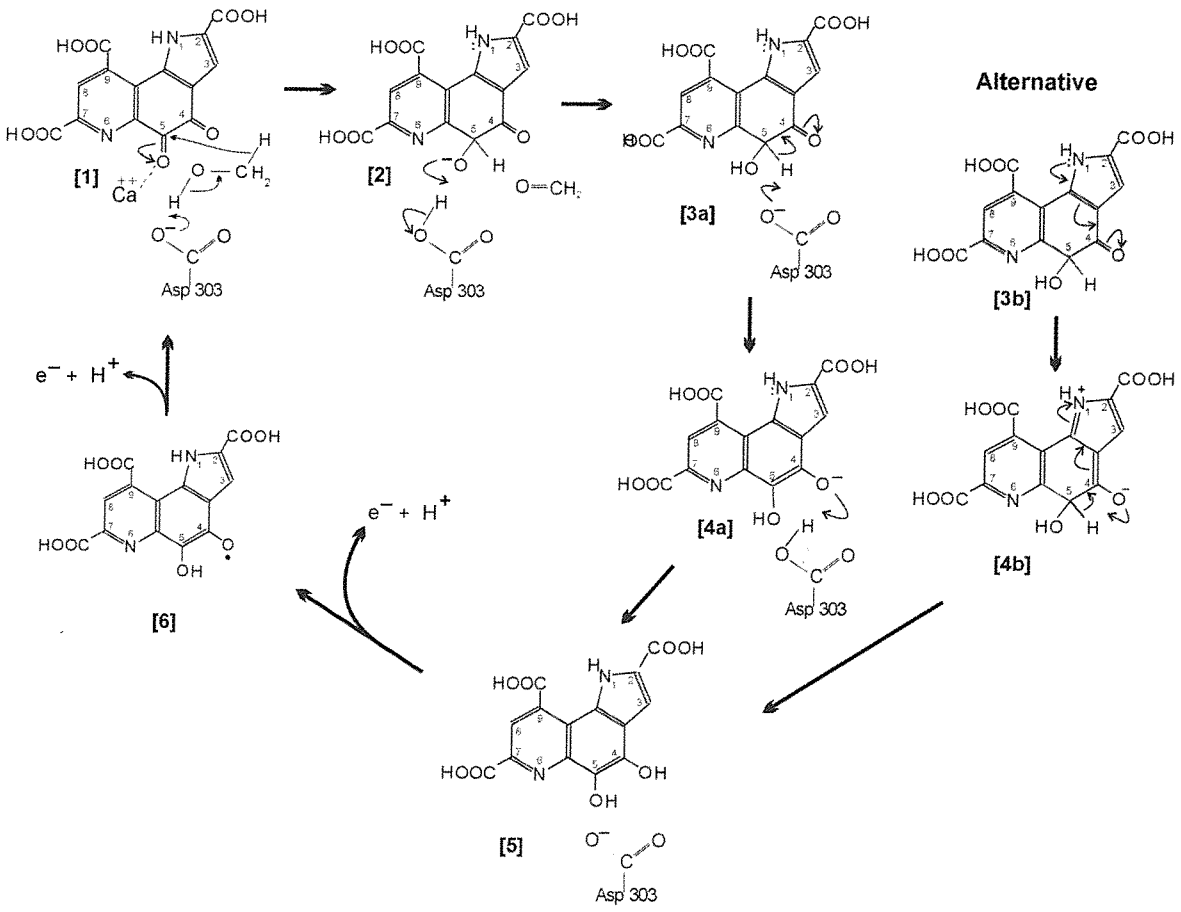

Figure 1.9b) The acid/base-catalysed hydride transfer mechanism for the oxidation of methanol to formaldehyde

The Figure is taken from Anthony & Williams (2002).

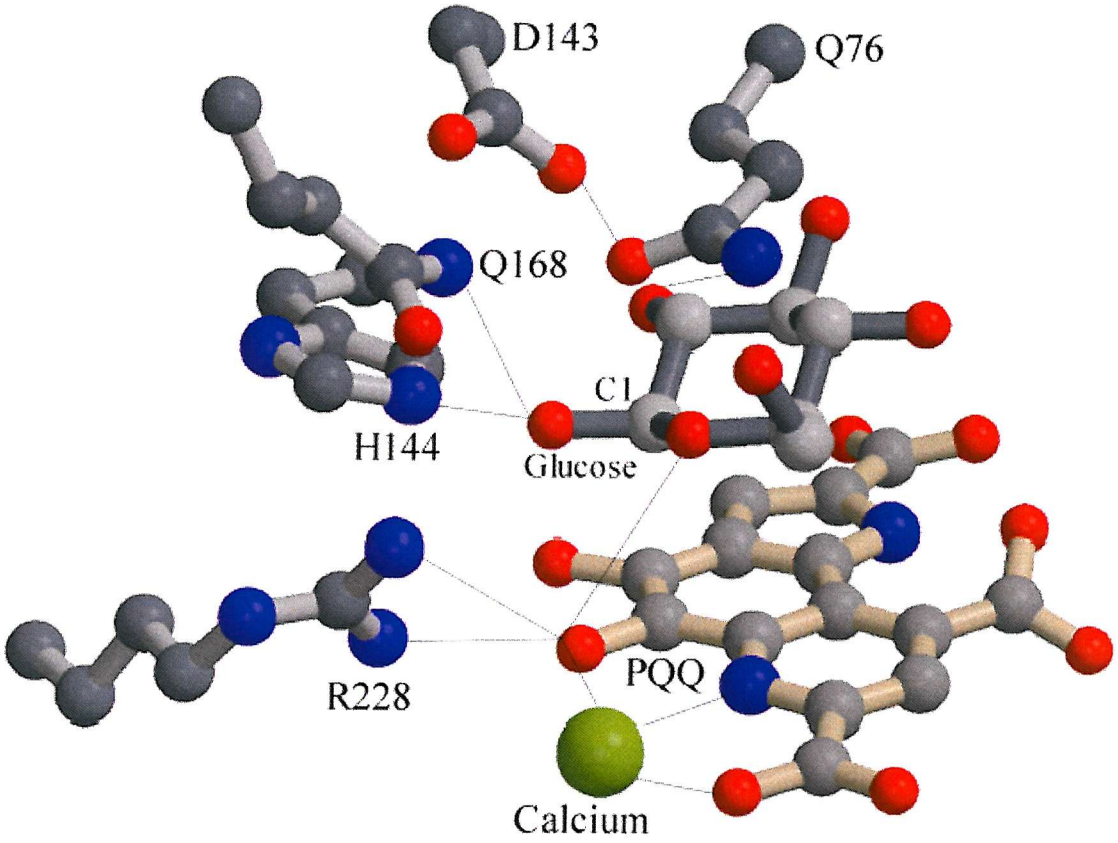

Figure 1.10 The active site of sGDH

The Figure is constructed using the deposited pdb coordinates from Oubrie *et al* (1999).

1.8 **Quinohaemoproteins**

Quinohaemoproteins are ideal proteins to study the electron transfer between PQQ and the haem of cytochrome *c* as each of the redox centres are present in separate domains within the same protein; this allows potential routes for electrons to travel between the redox centres to be postulated. Recently high resolution X-ray structures of type II alcohol dehydrogenases have been solved, from *Comamonas testosteroni* (Oubrie *et al.*, 2002) and *Pseudomonas putida* (Chen *et al.*, 2002). The overall tertiary structure of the 1.44 Å resolution structure of alcohol dehydrogenase from *Comamonas testosteroni* is shown in Figure 1.11. As the Figure shows, the protein has two easily identifiable domains which are joined by a linker region which extends from Pro590 and Gly566, (the linker is a flexible region and is not shown in Figure 1.11 as the deposited pdb file does not contain this segment of the structure). The larger domain (the 566 amino acid N-terminal domain) contains one molecule of PQQ and a calcium ion, which is coordinated to the PQQ and amino acid side chains. Also present in the active site was a region of ring-shaped electron density; this density was interpreted as being tetrahydrofuran-2-carboxylic acid in the proposed substrate binding cleft, which is a hydrophobic cavity located near the PQQ. Tetrahydrofuran-2-carboxylic acid is an oxidation product of tetrahydrofurfuryl alcohol; this oxidation reaction takes place in the highly related alcohol dehydrogenase quinohaemoprotein from *Ralstonia eutropha* (Zarnt *et al.*, 2001; Zarnt *et al.*, 1997). Also tetrahydrofuran-2-carboxylic acid is similar to the oxidation products of the bulky primary alcohols which the *Comamonas* enzyme is capable of oxidizing. The PQQ domain has a β-propeller fold similar to that seen in MDH and in other PQQ-containing enzymes. As with MDH the propeller fold is formed by eight four stranded β-sheets arranged in a radial manner creating a pseudo eight-fold symmetry with PQQ at the centre. Six of the eight β-sheets contain the tryptophan-docking motif to stabilize the β-propeller fold. The smaller C-terminal domain is an α-helical type I cytochrome *c* (amino acids 591-677) and is composed of five α-helical segments that enclose the covalently bound haem *c* which is covalently attached to the protein via thioether linkages to Cys604 and Cys607. The haem iron is coordinated to the protein via His608 and Met647 and is in a low-spin hexa-coordinated state. The residues around the methionine coordinated to the haem iron are atypical when compared to mitochondrial cytochrome *c* and many bacterial cytochrome c_2 proteins. The conserved tyrosine residue which is adjacent to the methionine ligated to the haem iron and is thought to stabilize the redox related conformational

Figure 1.11 The tertiary structure of the quinohaemoprotein alcohol dehydrogenase from *Comamonas testosteroni*

The Figure is taken from the 1.44 Å X-ray crystal structure (Oubrie *et al.*, 2002).

changes is absent and is replaced by a phenylalanine residue; apart from several water molecules in the cleft surrounding the Met647, the area is mainly hydrophobic. Also no water molecule is close enough to interact with Met647 and regulate redox related conformational changes as is postulated in mitochondrial cytochrome *c* (Berguist & Brayer, 1992). His608, on the opposite side of the haem, forms a conserved hydrogen bond via the ND1 atom to the carbonyl group of a proline amino acid (Pro620), as is seen with all known cytochrome *c* structures, and it is also surrounded by hydrophobic residues.

Pseudomonas putida HK5 produces two type II alcohol dehydrogenases, ADH IIB and ADH IIG (Toyama *et al.*, 1995), the former is produced when the bacteria are grown on butanol and the latter when grown on glycerol or 1,2 propanediol. ADH IIB exhibits high activity against long-chain primary and secondary alcohols, while ADH IIG has higher activity with diols but not with primary and secondary alcohols. The structure of ADH IIB is described below. The X-ray crystal structure was solved to a resolution of 1.90 Å and is, as expected, very similar to the quinohaemoprotein from the *Comamonas* enzyme (discussed above). The large N-terminal domain (~60 kDa) contains the PQQ moiety and the C-terminal domain (~10 kDa) constitutes the cytochrome *c* domain. The overall rms deviation between the quinohaemoproteins from *Pseudomonas putida* and *Comamonas testosteroni* for 576 equivalent Cα atoms is 1.08 Å. For the separately aligned domains, the rms deviations are 0.85 Å for 516 equivalent quinoprotein Cα atoms and 1.28 Å for 76 equivalent cytochrome Cα atoms. The sequence identities for equivalent residues in the two types of domain are 56.8 % and 31.6 % respectively. Although there is a higher rms deviation between the two cytochrome domains the folding pattern is almost identical when comparing the two domains. The only other major difference between the two alcohol dehydrogenases is that the *Comomonas* protein has the reaction product tetrahydrofuran-2-carboxylic acid in the active site whereas the *Pseudomonas* enzyme has a molecule of bound acetone.

1.8.1 **Reaction mechanism in type II ADHs**

The reaction mechanism for alcohol oxidation has been extensively studied for MDH and sGDH (see Sections 1.10). The widely accepted theory is that the reaction is initiated by a proton abstraction from the substrate in concert with a direct hydride transfer from the substrate to the C-5 atom of PQQ and subsequent tautomerization of the PQQ intermediate to $PQQH_2$. The

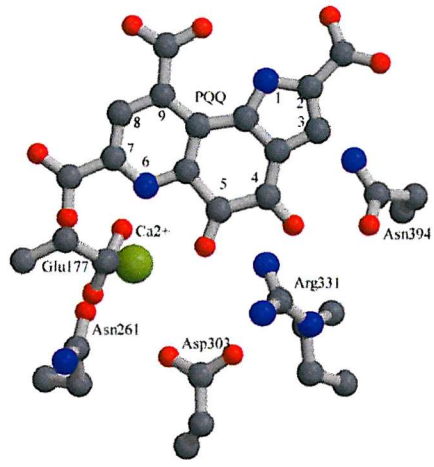

Active site of MDH (above)

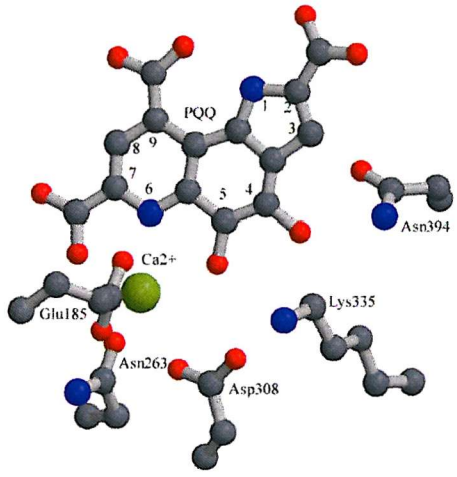

Active site of the quinohaemoprotein

Figure 1.12 The active site of MDH (top diagram) and the type II alcohol dehydrogenase from *Comamonas testeroni* (Oubrie *et al.*, 2002)

The Figure shows that the residues in the active site of both proteins are very similar. Molecular modelling predicts that the active site of mGDH retains the active site lysine (Lys335), aspartate (Asp466) and the two asparagines (Asn607 and Asn355); the metal ion is also predicted to have an extra ligand to the active site metal ion, Thr424 (Cozier & Anthony, 1995).

amino acid residues surrounding the PQQ are essentially the same in type II alcohol dehydrogenases as they are in MDH (Figure 1.12) and so the mechanisms of oxidation are most likely to be identical for both types of enzyme. The *Comamonas* enzyme has tetrahydrofuran-2-carboxylic acid in the active site, hydrogen bonded to oxygen atoms from both Asp308 and Glu185; either amino acid might therefore be the catalytic base, which initiates the reaction. The Asp308 is thought to act as the catalytic base as it is in a similar position relative to the PQQ as His144 in sGDH (Oubrie *et al.*, 1999), which is the catalytic amino acid in the sGDH. Also in MDH the aspartate is hydrogen bonded to the only active site water molecule (Ghosh *et al*, 1995), which has been displaced by tetrahydrofuran-2-carboxylic acid in the quinohaemoprotein from *Comamonas testeroni*; it seems clear therefore that the aspartate rather than the glutamate is the most likely catalytic amino acid.

1.8.2 **Electron transfer from $PQQH_2$ to haem *c* in quinohaemoproteins**

Because haem *c* is a single electron acceptor, the two electrons from $PQQH_2$ must be transferred in two single steps; after the first electron is transferred a semi-quinone PQQ is formed. The shortest distance between the PQQ and haem *c* redox centres is 12.9 Å in the quinohaemoprotein from the *Comamonas* organism. The conserved disulphide bridge formed from adjacent cysteine residues 116 and 117 is positioned directly between the PQQ and haem *c*. Asp118 and Arg67 are also located between the cofactors; Asp118 is conserved in all alcohol dehydrogenases and Arg67 is present in all ADHs with the exception of MDH (Oubrie *et al.*, 2002). There are other non-conserved residues located between the two sites along with several water molecules. Electron transfer rates between redox centres in biological systems are strongly related to edge-to-edge distance (Moser *et al.*, 1992); the maximum distance electrons can travel between two redox centres without additional redox centres is 14 Å (Page *et al.*, 1999) thus 12.9 Å is a considerable distance for electrons to travel. When using this distance and a calculated value for the atomic density of 0.63 between the co-factors, a maximum electron transfer rate of 1.0×10^5 s^{-1} can be calculated, which is a much higher rate than is calculated for substrate oxidation (k_{cat} = 17 s^{-1}), suggesting that the intraprotein electron transfer has little influence on the kinetic mechanism of QH-ADH.

In principle the disulphide bridge could act as a secondary redox centre, the two cysteines residues acting as such, by accepting two electrons and two protons; a disulphide bond which is

involved in redox reactions is indeed located close to an iron-sulphur cofactor in the ferredoxin: thioredoxin reductase system (Dai *et al.*, 2000). Biochemical evidence, however, suggests that the disulphide bond of the related quinoprotein MDH is not reduced during the redox cycle (Avezoux *et al.*, 1995). The disulphide bridge may also act to confer rigidity on the loop between the PQQ and the haem *c* (Page *et al.*, 1999).

The protein medium may also be directly involved in the conduction of electrons from $PQQH_2$ to haem *c*; the electrons could be transferred through specific pathways which may or may not be dynamically controlled (Balabin & Onuchic, 2000). Two suggested pathways for electrons to travel to haem *c* were calculated using the computer program Harlem (Kurnikov, 2000) (Figure 1.13). These pathways, in conclusion, predict that the disulphide bond between Cys116 and Cys117 and possibly the side chains of Asp118 and Arg67 are essential for electron transfer from $PQQH_2$ to haem *c* (Oubrie *et al.*, 2002).

The *Pseudomonas* QH-ADH is slightly different from the *Comamonas* enzyme. The PQQ C-5 and the haem *c* iron are separated by 20.6 Å but the planes of the two rings are tilted to each other by 70 °, making the distance between the two redox centres about 15 Å (Chen *et al.*, 2002). The authors have postulated four potential pathways by which the electrons could travel to the haem *c* from $PQQH_2$; all four pathways include either or both cysteines from the disulphide bridge, but only the fourth involves the actual sulphur atoms in the disulphide bridge (Chen *et al.*, 2002).

During oxidation of reduced PQQ, protons are released into the periplasm. Proton pathways in proteins usually consist of hydrogen-bonded networks of proton donor and acceptor groups, which are either water molecules or amino acid side-chains (Iwata *et al.*, 1995: Stowell *et al.*, 1997). Such a network extends from the hydroxyl groups of $PQQH_2$ to the solvent in QH-ADH from *Comamonas testeroni*. This network involves Lys335, Asp308, Glu185 and Arg67; a water-filled chamber also exists between the two domains and Arg67 (Figure 1.14). A network was proposed by the authors for the release of protons into the periplasm involving the above residues and water molecules. These residues and water molecules except Arg67, which is replaced by an asparagine, are conserved in MDH and it is therefore likely that the proposed proton translocation pathway is conserved in MDH. This pathway allows the release of protons into the periplasm to create a proton motive force sufficient to drive ATP synthesis.

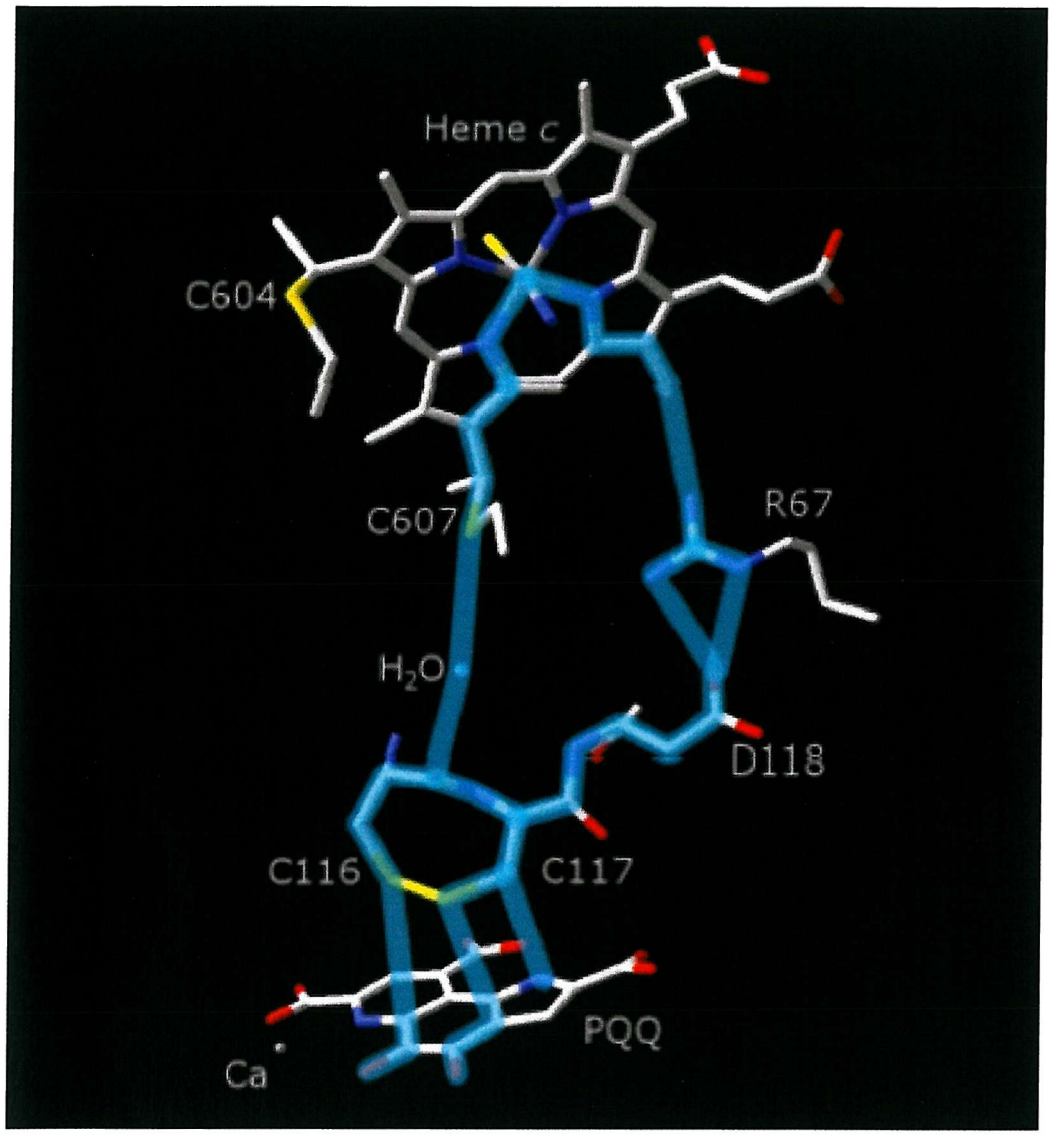

Figure 1.13 Two proposed routes for electron transfer from $PQQH_2$ to the haem *c* in the type II alcohol dehydrogenase from *Comamonas testeroni*

The Figure is taken from Oubrie *et al* (2002).

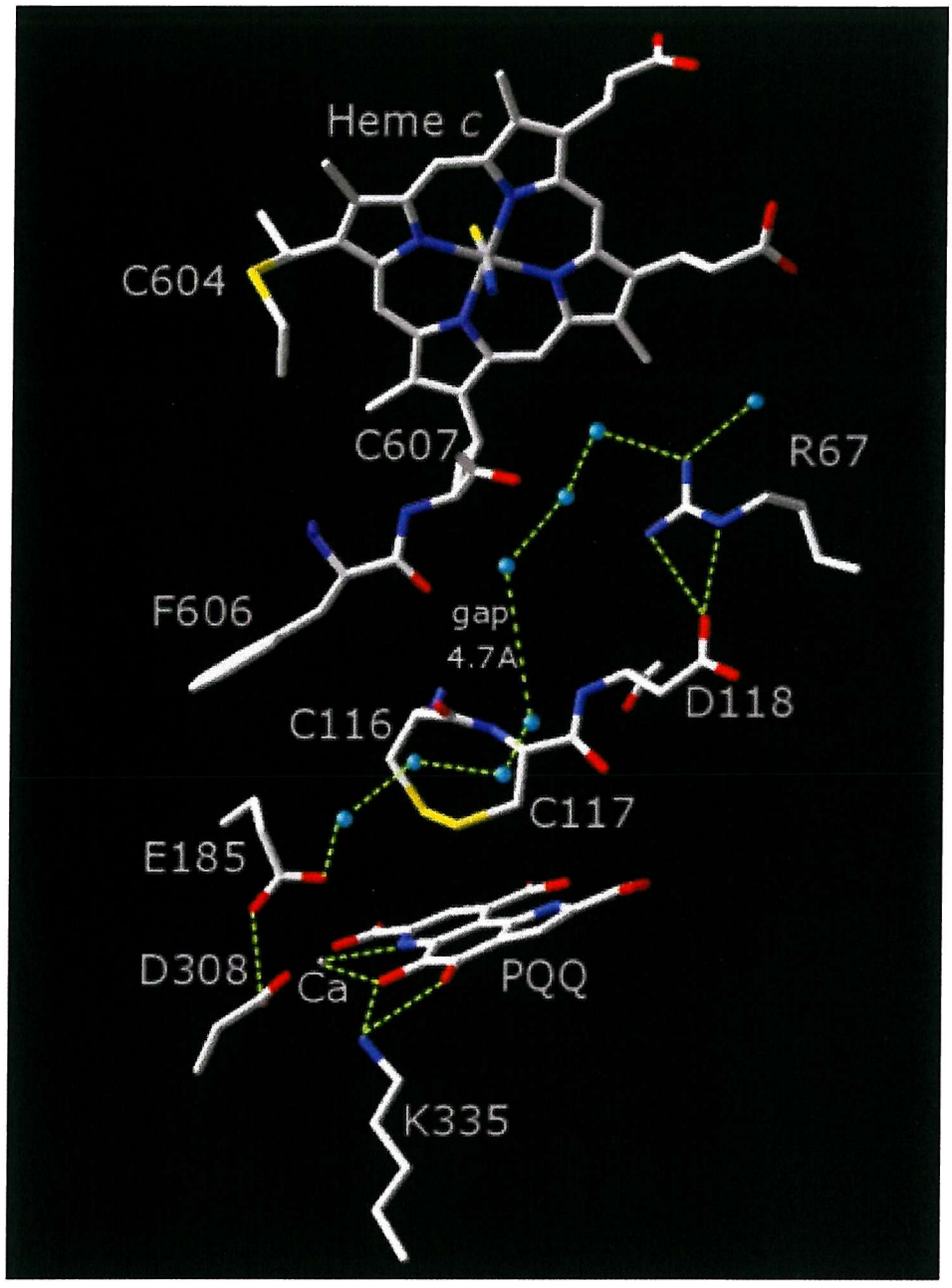

Figure 1.14 The proposed pathway for proton transfer from $PQQH_2$ to the periplasm in the QH-ADH from *Comamonas testeroni*

The blue spheres are water molecules. The protons enter the periplasm after Arg67. The Figure is taken from Oubrie *et al* (2002).

1.9 **Glucose dehydrogenase**

There are two types of glucose dehydrogenase found in bacteria, a soluble periplasmic protein (sGDH) and a membrane bound protein (mGDH). There is little sequence similarity between the two proteins and they differ slightly in some properties such as stability and substrate specificity; both enzymes can oxidize a wide range of monosaccharides although mGDH is unable to oxidize disaccharides.

1.9.1 **Membrane bound glucose dehydrogenase**

The mGDH is an 87 kDa monomer and contains one PQQ molecule. The enzyme catalyses the oxidation of D-glucose to D-gluconate in the periplasm, whilst the electrons are transferred to cytochrome oxidase via ubiquinone. GDH is expressed as an apo-enzyme in *Escherichia coli* because this enzyme is unable to synthesis PQQ; the active holo-enzyme is readily reconstituted with PQQ and Mg^{2+} ions (but not Ca^{2+} ions). The N-terminal domain (154 amino acids) anchors the protein to the membrane (Yamada *et al.*, 1993) and the remaining amino acids (155-796) form a periplasmic superbarrel domain. The periplasmic domain has 26 % sequence identity to the α-subunit of MDH; this sequence similarity has allowed the molecular modelling of the periplasmic domain of mGDH structure from the pdb coordinates of MDH (Cozier & Anthony, 1995; Cozier *et al.*, 1999).

In the model structure of mGDH the PQQ molecule is in the periplasmic domain and it has fewer equatorial interactions with amino acids in the active site than it does in MDH; this explains why it is possible to effect the reversible dissociation of PQQ from mGDH but not from MDH. A major difference between MDH and mGDH is that there is more space in the active site of mGDH, perhaps to accommodate a larger substrate. A second difference is that Arg331 in MDH which may play a catalytic role is replaced by Lys493 in mGDH. Finally, the novel disulphide bridge in MDH is replaced by a histidine in mGDH

The ligation of the divalent ion (Ca^{2+} or Mg^{2+}) to PQQ is similar, suggesting that they play a similar role in both enzymes; that of a Lewis acid through coordination to the C-5 carbonyl oxygen, thus stabilising the electrophilic C-5 of PQQ. By analogy with the MDH structure, Asp466 is likely to be involved in the abstraction of a proton from the substrate (Cozier & Anthony, 1995), followed by an attack from a hydride ion from the glucose oxyanion, leading directly to the formation of the lactone and the quinol form of PQQ. In all PQQ-

containing proteins whose structure has been determined the PQQ is coordinated to a calcium ion, suggesting that this is a common feature of the dehydrogenases, but mGDH appears to be different. It is usually isolated as an apoenzyme and requires PQQ plus a divalent ion for reconstitution. For this process Mg^{2+} or other divalent metal ions can be used instead of Ca^{2+} (Matsushita *et al.*, 1995). If the function of Mg^{2+} during reconstitution is to provide a metal ion in the active site as Ca^{2+} does for other quinoproteins then this will have implications for the understanding of the mechanism of mGDH, as it is unlikely that Mg^{2+} could replace Ca^{2+} for some functions (James & Anthony, 2003). The modelling studies on mGDH have suggested that some of the residues important in coordinating the calcium at the active site are different in glucose dehydrogenase (Cozier & Anthony, 1995), when compared to MDH. After site-directed mutagenesis of these active site residues, the most remarkable observation was that reconstitution of apoenzyme with PQQ of the mutant enzymes was not supported by Mg^{2+} ions as in wild-type GDH, but could be supported by Ca^{2+}, Sr^{2+} or Ba^{2+} ions. This was competitively inhibited by Mg^{2+}. This result along with other kinetic data have led to the conclusion that although a Ca^{2+} ion is able to form part of the active site in genetically-modified GDH, as in other quinoproteins, a Mg^{2+} ion surprisingly replaces Ca^{2+} in the active site of wild-type GDH (James & Anthony, 2003).

1.9.2 **Soluble glucose dehydrogenase**

Although the amino acid sequence of soluble GDH has little similarity to other PQQ enzymes the structures have some remarkably similarities. The X-ray crystal structure of the enzyme shows the protein is a dimer of identical subunits of approximately 50 kDa (Oubrie *et al.*, 1999). Each monomer contains one molecule of PQQ which is coordinated to one calcium ion, in the same manner as in MDH. Soluble GDH also has calcium binding sites at the dimer interface, where four Ca^{2+} ions stabilize the structure. Each monomer exhibits the characteristic β-propeller superbarrel structure, although in the case of sGDH there are only 6 four-stranded anti-parallel β-sheets as opposed to the eight seen in MDH. The PQQ is coordinated in a similar fashion to that seen in MDH which suggests a common reaction mechanism; the X-ray structure of the active site (Figure 1.10) greatly supports the hydride transfer mechanism (Section 1.10)

1.10 **The genes involved in methanol oxidation**

Over thirty genes have been shown to be involved in the oxidation of methanol. Many of these genes were identified from different organisms, so some genes that encoded proteins carrying out different functions were given the same names, while genes with the same names were later found to encode different protein. Some of these genes were found to be involved in PQQ synthesis, which is not specific to methanol oxidation and are therefore now termed pqq genes (Lidstrom *et al.*, 1994). Due to this confusion the previous *mox* system was replaced by a linkage system in which the genes were named according to chromosome linkage. The genes that encode the α and β-subunits of MDH (*mxaF* and *mxaI*) and cytochrome c_L (*mxaG*) are situated in an operon together with *mxaJ* (Anderson & Lidstom, 1988; Anderson *et al.*, 1990; van Spanning *et al.*, 1991). The protein encoded for by *mxaJ* is 30 kDa. A mutation in this gene has no effect on the transcription and translation of cytochrome c_L although neither subunit of MDH is produced suggesting a role for the 30 kDa protein in processing MDH (Amaratunga *et al.*, 1997). The genes *mxaFJGI* are transcribed from a promoter upstream of *mxaF*. Figure 1.15 shows the *mxa* gene cluster. There are two putative reading frames between the *mxaFJGI* and the *mxaACKLD* genes in *Methylobacterium extorquens*. The predicted amino acid sequence of the first open reading frame (ORF) has 60 % identity with the *mxaR* protein found in *P. denitrificans*; there is no obvious signal peptide or hydrophobic membrane-spanning regions and the sequence indicates that MxaR (38.6 kDa) is a typical cytoplasmic protein. Its sequence suggests that there are two motifs relevant to MgATP binding. It can therefore be reasonably concluded that the MxaR protein has a function involved in binding ATP. Also sequencing of the cluster suggests that there is a single ORF after *mxaR*, which could code for a 22.3 kDa protein. The C-terminal part of the predicted protein shows 37 % identity with the putative MxaS of *P. denitrificans*. This gene sequence should be interpreted with caution and *mxaS* is depicted in parenthesis as the predicted amino acid sequence is highly dubious as it containing a high proportion of proline and arginine amino acids but no glutamates and only a few lysines. And there is no initiation codon (ATG or GAG) in the sequence which corresponds to the start of *mxaS* in *P. dentrificans*.

About 2 kb downstream from *mxaI* in the gene cluster there is the group of genes *mxaACKLD*. This group of genes has not been described in *P. denitrificans*. Predicted amino acid sequences suggest that the five proteins reside in different compartments of the cell; MxaD

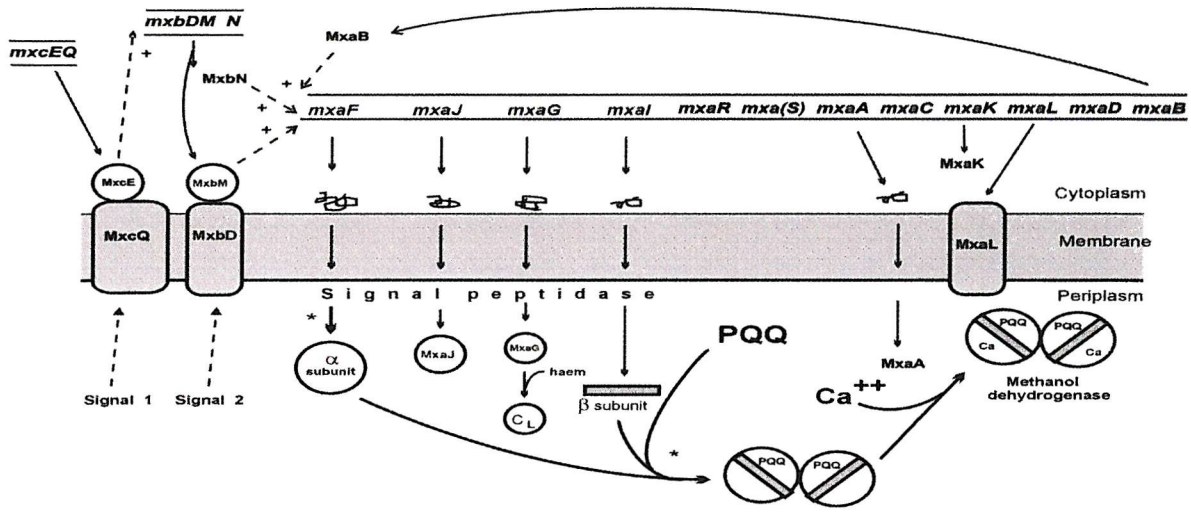

Mdperi.cdr

mdperi97.cdr

Figure 1.15 A model for the expression of MDH in *Methylobacterium extorquens*

The *mxaFJGI* preproteins are transported into the periplasm where they are assembled into the proteins that are specifically involved in methanol oxidation. The * indicates two possible stages where PQQ may possibly be inserted. At least 3 proteins (MxaA, MxaK, MxaL) are involved in the incorporation of Ca^{2+} into MDH and MxaC and MxaD may also be involved in this. The Figure is taken from Goodwin and Anthony (1998).

and MxaA are periplasmic, MxaL and MxaC are bound to the periplasmic membrane and MxaK is cytoplasmic. Mutations in any of *mxaA, K* and *L* genes has led to the production of a calcium free MDH, leading to the obvious conclusion that the proteins transcribed from these three genes are important in calcium insertion into the active site of MDH. The reconstitution of calcium-free MDH with high levels of calcium, strontium or barium ions (>5 mM), leads to a return of an active enzyme, and a characteristic absorption spectrum (Richardson & Anthony, 1992). This reconstitution process is also pH-dependent; the reconstitution is optimal at about pH 9.5 (Goodwin *et al*, 1996). When MDH is reconstituted with barium to give (Ba^{2+}-MDH) the modified enzyme has a relatively low affinity for methanol (K_m, 3.4 mM instead of 10 μM) and also a lower K_m for the activator, ammonia, but its activation energy is less than half (and its V_{max} twice) that of the normal Ca^{2+} enzyme (Goodwin & Anthony, 1996). This is probably due to a change in conformation at the active site caused by the large ionic radius of barium relative to calcium; this change in conformation leads to a decrease in free energy of binding and hence a decrease in activation energy (Goodwin & Anthony, 1996). The Ba^{2+}-MDH was subsequently used to prepare fully oxidised MDH (Ca^{2+}-MDH is isolated in the semi-quinone or fully reduced forms) for spectroscopy; these studies were aimed at trying to identify a spectroscopically identifiable covalent-adduct intermediate in the reaction mechanism, but no intermediate could be identified.

1.11 **The reaction of MDH with cytochrome c_L**

The redox mechanism proposed for the oxidation of MDH is shown in Figure 1.16. Initially, methanol-dependent reduction of cytochrome c_L was difficult to prove due to an endogenous substrate present with each MDH preparation; there are thought to be about 90 molecules of unidentified reductant associated with each preparation (Anthony, 1986: Ghosh & Quayle, 1981), which cannot be removed by dialysis. A dye-linked assay using DCPIP as the terminal electron acceptor has since been developed for cytochrome c_L activity (Cox *et al.*, 1992; Chan & Anthony, 1991). As Figure 1.16, shows the reaction requires ammonia as an activator for the oxidation of the substrate. Step one shows the semi-quinone form of the prosthetic group (which is the form in which it is normally present in isolated MDH) reducing cytochrome c_L; substrate binds to the oxidized MDH at step two; step three shows the release of product. The rate limiting step in the dye linked assay is the breaking of the methyl C-H bond in the substrate

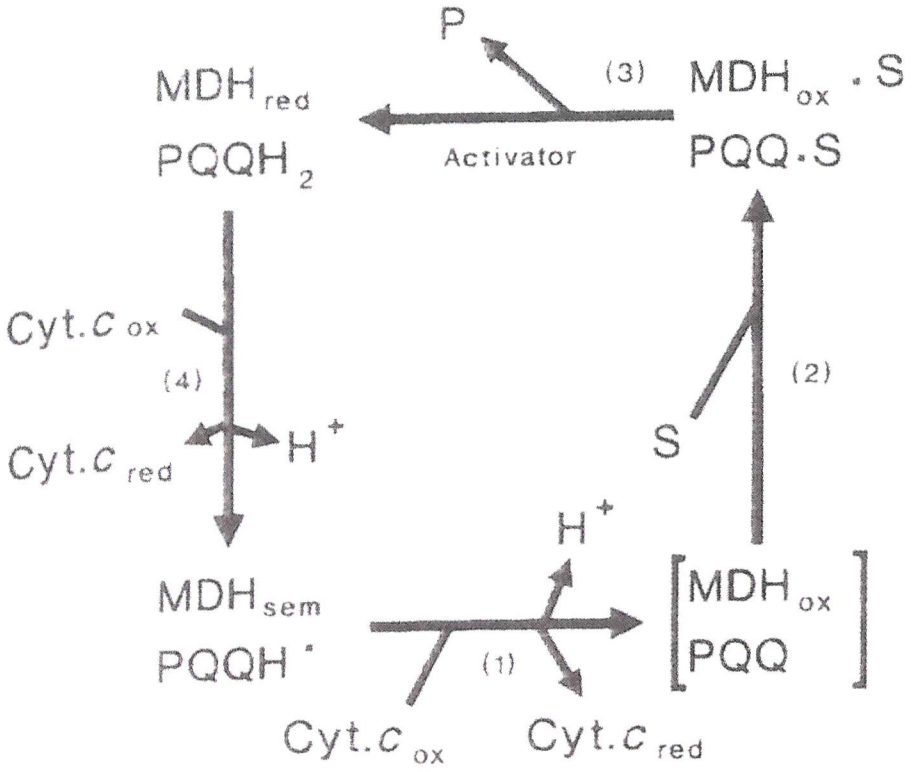

Figure 1.16 The reaction cycle of MDH

This reaction cycle is based on the work of Dijkstra , Frank and Duine (Dijkstra *et al.*, 1989). The electron acceptor is either a dye, such as phenazine ethosulphate, or cytochrome c_L. The starting point for the cycle is the semi-quinone form of the enzyme MDH_{semi}

(Frank *et al.*, 1988; Goodwin & Anthony, 1996; Afolabi *et al.*, 2001); this is the step which is affected by the activator ammonia although the mechanism of this activation is not understood. The final step is the release of one electron to cytochrome c_L, creating the semi-quinone PQQ.

1.11.1 The interaction of cytochrome c_L with MDH

The interaction between cytochrome c_L and MDH occurs in the periplasm of the bacterium where both are present in high concentrations (~0.05 mM) (Anthony, 1986). Once reduced, cytochrome c_L is oxidized by cytochrome c_H. Suggestions that electrostatic "docking" interactions of MDH with cytochrome c_L, involving ionic interactions between the lysine or arginine residues on MDH and carboxyl residues on cytochrome c_L, were put forward (Nunn *et al.*, 1989) following the observation that a very high number of lysine residues (15 out of 74) are present on the β-subunit and that these lysines formed a well defined positively charged region on one side of an amphipathic helix. However, studies have shown that these residues are not involved in this interaction. Firstly, the comparison of the amino acid sequence of the β-subunit from other methylotrophs showed that the proposed lysine residues are not conserved (Chan & Anthony, 1991). Secondly, studies using *M. extorquens* and *Methylophilus methylotrophus* (Cox *et al.*, 1992) and *Acetobacter methanolicus* (Chan & Anthony, 1991) have subsequently confirmed that ionic interactions are between the α-subunit and cytochrome c_L, and not the β-subunit. The interaction is inhibited by low concentrations of salts; the degree of inhibition was proportional to the square root of the ionic strength of the medium, as expected if the interaction is ionic in nature. Changing the charge on lysine residues of MDH by chemical modifications led to an inactive enzyme, whereas modification with retention of charge had little effect. The modified MDH always retained activity in the dye-linked assay system, demonstrating that the active site for the reaction with substrate had been maintained. In similar experiments, chemical modification of the lysine residues of cytochrome c_L yielded an active protein, but modification of the carboxyl groups on the cytochrome led to loss of activity. After chemical modification with trinitrobenzene sulphonate (TNBS) of the minimum number of lysine residues on MDH to lead to loss of activity (average of nine per $\alpha_2\beta_2$ tetramer), and separation of the subunits of MDH it was shown that TNBS was incorporated into the α-subunit and not the β-subunit (Cox *et al.*, 1992). Further evidence that the lysines involved in the docking are from the α-subunit came from cross-linking studies. Using zero-length cross-linking methods (Grabarek & Gerely, 1990)

it was possible to demonstrate that carboxyl groups on cytochrome c_L cross-linked with lysine residues on the α-subunit of MDH (Chan & Anthony, 1991; Cox *et al.*, 1992).

To distinguish whether the three periplasmic proteins involved in electron transfer (MDH, cytochrome c_L and cytochrome c_H) form a stable three-way complex in a "wire" type system or form a bimolecular complex for electron transfer, cross-linking studies were used. In the case of a "wire" system, electrons would flow from MDH through cytochrome c_L to cytochrome c_H, suggesting a different point of entry and exit on the cytochrome c_L for the electrons to pass. In the case of a bimolecular interaction, the cytochrome c_L must separate from MDH before associating with cytochrome c_H, therefore requiring a single site for electron transfer. Attempts to cross-link the three proteins failed (Cox *et al.*, 1992), with the MDH and cytochrome c_H competing for the same site on cytochrome c_L. In these competition experiments tuna cytochrome *c* was used as a model for the typical class I cytochrome (cytochrome c_H). When cytochrome c_L was reacted separately with equimolar amounts of either MDH or tuna cytochrome *c*, cross-linked products with the tuna cytochrome *c* and the α-subunit of MDH were formed. When cytochrome c_L was modified and reacted with equimolar amounts of both tuna cytochrome *c* and the α-subunit of MDH at the same time cross-linked products with the tuna cytochrome *c* and the α-subunit of MDH were formed, but not with both together, indicating that there is a single site on cytochrome c_L that reacts with both proteins. Further evidence for this is that when the concentration of MDH was increased 3-fold, more cross-linking occurred with MDH (α-subunit), and less occurred with tuna cytochrome *c*. Similarly, when the tuna cytochrome was in excess it formed more cross-linked product and MDH cross-linking was diminished.

EDTA is a known inhibitor of methanol oxidation although it has no effect on the dye-linked activity of the enzyme. It was suggested that EDTA inhibits electron transfer from MDH to cytochrome c_L, by reacting with lysyl residues on MDH, thus preventing the docking process (Chan & Anthony, 1992); however the observation that EDTA has no effect on the docking was shown by using fluorescence spectroscopy (Dales & Anthony, 1995). On binding of MDH and cytochrome c_L the fluorescence of tryptophans from MDH was quenched by the haem present on cytochrome c_L; the K_m for the initial interaction between the lysines (MDH) and carboxylates (cytochrome c_L) was insensitive to EDTA. Therefore EDTA inhibition of methanol oxidation has been postulated to act by binding to lysine residues on the α-subunit of MDH which are close to

those which interact with cytochrome c_L and stop the complex, once formed, from moving into the conformation optimal for electron transfer (Dales & Anthony, 1995).

1.12 **Cytochrome *c***

Cytochromes are electron transfer proteins which have one or several haem groups and are classified according to their haem iron coordination, by haem type and further by their amino acid sequence. Cytochrome *c* can be defined as an electron transfer protein having one or more haem *c* groups bound to the protein by one (or more commonly) two thioether bonds, involving sulphydryl groups of cysteines residues. The fifth haem iron ligand is always provided by a histidine residue, which is always adjacent to one of these cysteines.

There are four classes of cytochrome *c*, I, II, III, IV. Both of the soluble cytochromes in *M. extorquens* are class I *c*-type cytochromes. Class I cytochromes *c* have a low spin iron in the single haem group, which is attached towards the N-terminus of the protein (within the first 20 residues), and the 6^{th} ligand to the haem iron is provided by a methionine, a further 40 residues towards the C-terminus (Moore & Pettigrew, 1987; Moore & Pettigrew, 1990). The haem prosthetic group is enveloped by three conserved α-helices, forming a basket around the haem group which leaves only one haem edge exposed to solvent (Moore & Pettigrew, 1990). Cytochrome c_H exhibits all of the above class I characteristics (Read *et al.*, 1999). Apart from the haem binding motif the amino acid sequence of cytochrome c_L does not fit into an established sequence class; it is possible that cytochrome c_L has a long terminal extension to the class I domain (Moore & Pettigrew, 1990) (Section 1.15).

1.12.1 **Mitochondrial cytochrome *c***

The main function of mitochondrial cytochrome *c* is to transport electrons in the inner mitochondrial space between the cytochrome bc_1 complex and the terminal oxidase, cytochrome aa_3 (Wilkstrom *et al.*, 1981). Mitochondrial cytochrome *c* also interacts with other intermembrane redox partners; these include cytochrome b_5, cytochrome *c* peroxidase, cytochrome b_2 and sulfite oxidase (Figure 1.17).

The structure of eukaryotic cytochrome *c* has been solved from tuna (Takano and Dickerson, 1981a, b), rice (Ochi *et al.*, 1983), horse (Bushnell *et al.*, 1990) and from yeast (Louie & Brayer, 1990). Of these structures yeast iso-1-cytochrome *c* has been solved to the highest

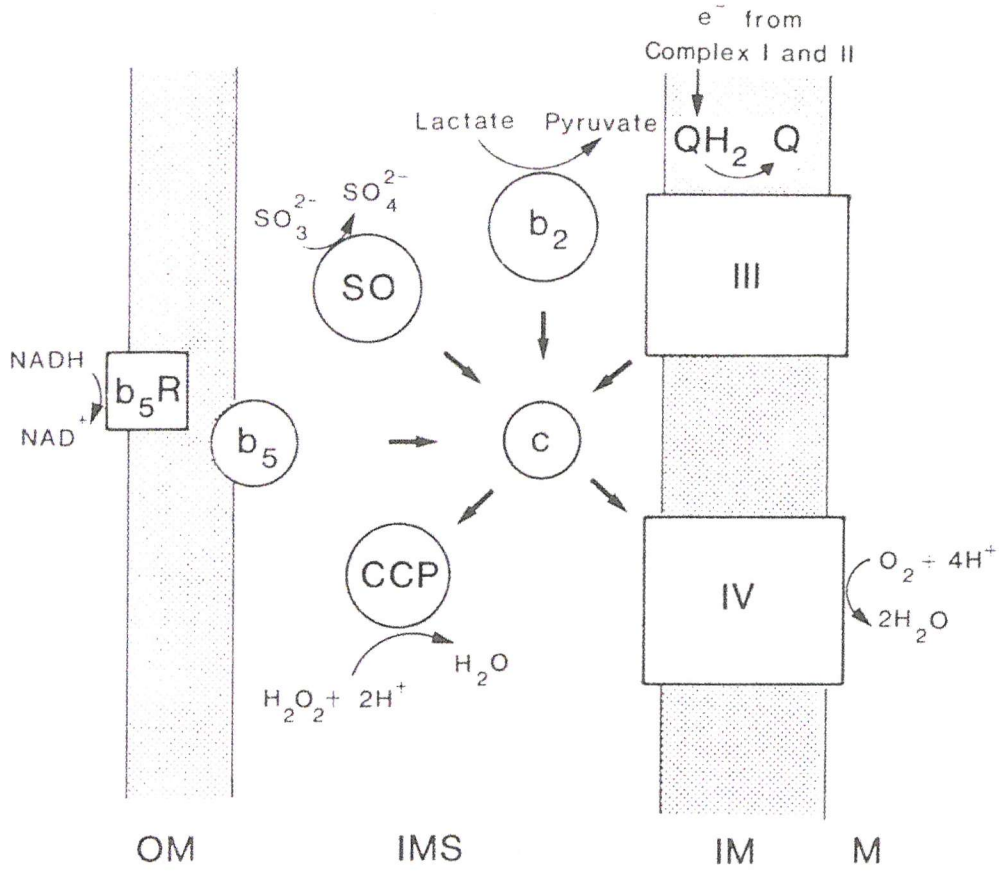

Figure 1.17 The role of cytochrome *c* in mitochondrial electron transport

Cytochrome *c* acts as a shuttle between membrane proteins and also interacts with soluble redox partners. The Figure is taken from Moore and Pettigrew (1987).

OM = Outer membrane
IMS = Inter membrane space
IM = Inner mitochondrial membrane
M = Matrix
III = Complex III
IV = Complex IV

SO = Sulfite oxidase
CCP = Cytochrome *c* peroxidase
b_2 = Cytochrome b_2
b_5 = Cytochrome b_5
b_5R = Cytochrome b_5 (reduced)

resolution, 1.23 Å (Louie & Brayer, 1990).Yeast iso-1-cytochrome *c* is the more abundant of two iso-enzymes. It is a 108 amino acid protein which has a single haem group; it is easy to obtain commercially and can be mutated, which allows residues of interest that are involved in structure and function to be studied. The eukaryotic cytochromes *c* all have similar structures and therefore the yeast cytochrome *c* is used as the general model for eukaryotic cytochrome *c*. Extensive work by Brayer and his co-workers using site-directed mutagenesis has helped formulate a theory on the structural changes that occur on changing redox state (Berghuis & Brayer, 1992). Several conserved residues and internal solvent molecules have been highlighted by these studies to be apparently crucial in redox state conformational change. These slight structural alterations help stabilize the two oxidation states (Section 1.13.1).

1.12.2 **Bacterial cytochrome c_2**

Cytochromes c_2 are biological electron shuttles involved in cyclic redox processes. They are structurally and evolutionarily closely related to mitochondrial cytochrome *c*. They can be separated into two groups by size; large (13-14 kDa) and small (~12 kDa). The % sequence identity of the 'small' cytochromes c_2 group with mitochondrial cytochromes *c* fall within the range of 41-56 %. The midpoint redox potential for eukaryotic cytochrome *c* is about +260 mV, whereas it can vary from +260 mV to +450 mV for cytochromes c_2. Cytochromes c_2 are class-I *c*-type cytochromes involved in the electron transport chains of photosynthesis and respiration in most photosynthetic non-sulfur bacteria. In non-photosynthetic bacteria it is only involved in respiration. In the photosynthetic process, it functions as a water-soluble electron carrier which shuttles between two membrane proteins: the photosynthetic reaction center and the cytochrome bc_1 complex (Pettigrew, G. W. & Moore, G. R, 1987)). In the respiration process cytochromes c_2 functions as a soluble protein which donates electrons to membrane bound terminal oxidases. Listed in Table 1.2 are the protein structures of cytochromes c_2. These are proteins whose molecular mass range from 12 kDa ("small type") to 13-14 kDa ("large type"). Regarding the amino acid sequence, they form a fairly homogeneous group of proteins with 30-40 % homology (Ambler *et al.*, 1979; Moore & Pettigrew, 1990). The X-ray structures solved so far confirm that the cytochromes c_2 share with mitochondrial cytochrome *c* the highly conserved folding motif of five or six helices arranged around the haem; also the haem in cytochrome c_2 has a characteristically low-spin iron with a histidine and a methionine as the extra planar iron ligands;

Table 1.2 A table of references for previously solved structures of cytochromes c_2

Organism	Reference
Rhodospirillum rubrum	Salemme *et al.*, 1973
Rhodobacter capsulatus	Benning *et al.*, 1991
Paracoccus denitrificans	Benning *et al.*, 1994
Rhodobacter sphaeroides	Axelrod *et al.*, 1994
Rhodopseudomonas viridis	Sogabe & Miki, 1995
Methylobacterium extorquens	Read *et al.*, 1999
Rhodopseudomonas palustris	Geramia *et al.*, 2002
Paracoccus denitrificans	Harrenga *et al.*, 2000

the haem is attached covalently to the protein by thioether linkages with cysteines positioned near the N-terminus, as is also seen in mitochondrial cytochrome *c*.

1.13 **Structure of the mitochondrial cytochrome c**

Mitochondrial cytochrome *c* contains a single polypeptide chain to which a protoporphyrin IX haem prosthetic group is covalently attached through two thioether linkages with the side chains from Cys14 and Cys17. The overall structural fold of yeast iso-1-cytochrome *c* shows the typical 'cytochrome *c* fold' (Figure 1.18). The thioether linkages that connect the haem to the polypeptide chain are formed. The haem iron ligands are provided by the side chain of His18 on the right hand side of the haem and Met80 on the left hand side of the haem (Figure 1.19). It is the amino acids and buried water molecules in and around that haem binding pocket that are of interest; these undergo conformational changes during a change in redox state of mitochondrial cytochrome *c*.

1.13.1 **Oxidation state-dependent conformation changes in yeast cytochrome *c***

High resolution crystal structures of the reduced and oxidized cytochrome *c* show subtle conformational differences. These include adjustments to the haem structure, movement of internally-bound water molecules and disruption of a hydrogen bond network on the left hand side of the haem (Figure 1.19) (Berghuis & Brayer, 1991). The hydrogen bond network around the Met80 changes between redox states; the conserved water molecule 166 (Wat166) moves 1.7 Å towards the positively charged haem Fe^{3+} on oxidation and this appears crucial in stabilizing the oxidized haem. Movement of Wat166 breaks the established hydrogen bond between Ty67 and Met80 that exists in the reduced state and stabilizes the positively charged iron by decreasing the electron-withdrawing potential of the Met80 ligand. Tyr67 maintains a hydrogen bond with the repositioned Wat166 (Figure 1.19). Therefore the role of Wat166 is to modify the hydrogen bond network, which involves several residues near Met80, in an oxidation state-dependent manner. This alteration in the electro-negativity of Met80 is said to be crucial to the controlling of the redox potential of cytochrome *c*. Also Wat166 mediates a change in mobility of three segments of the polypeptide chain; there is an increase in mobility when the protein is oxidized. Mutations which lead to the removal of Wat166 remove the change in polypeptide chain mobility that occurs when the protein is oxidized.

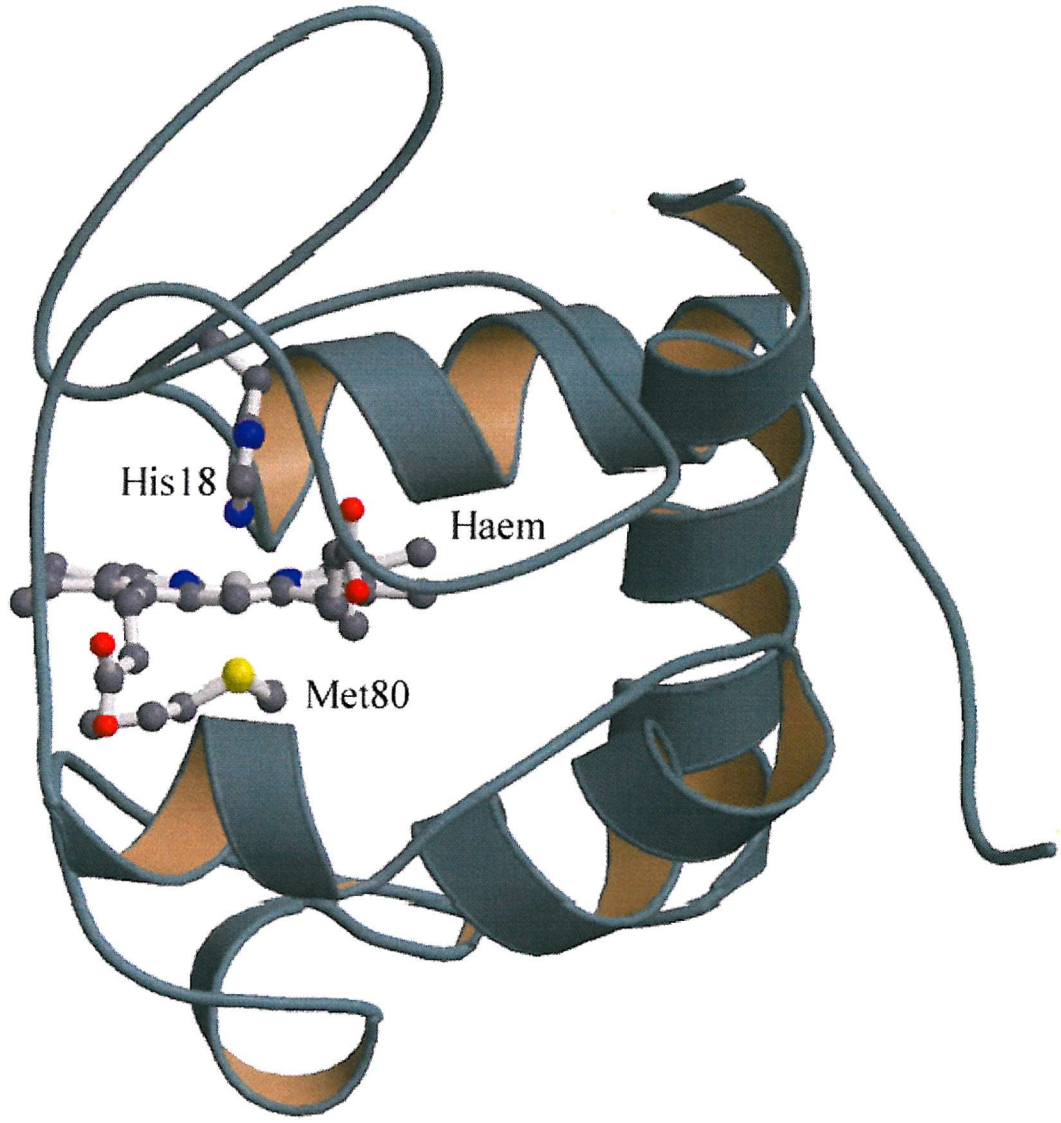

Figure 1.18 The tertiary structure of mitochondrial cytochrome *c* from yeast

The cytochrome exhibits the typical cytochrome *c* fold which wraps the three central α-helices around the haem *c* prosthetic group. The Figure is from the pdb file coordinates from Berghuis & Brayer (1991).

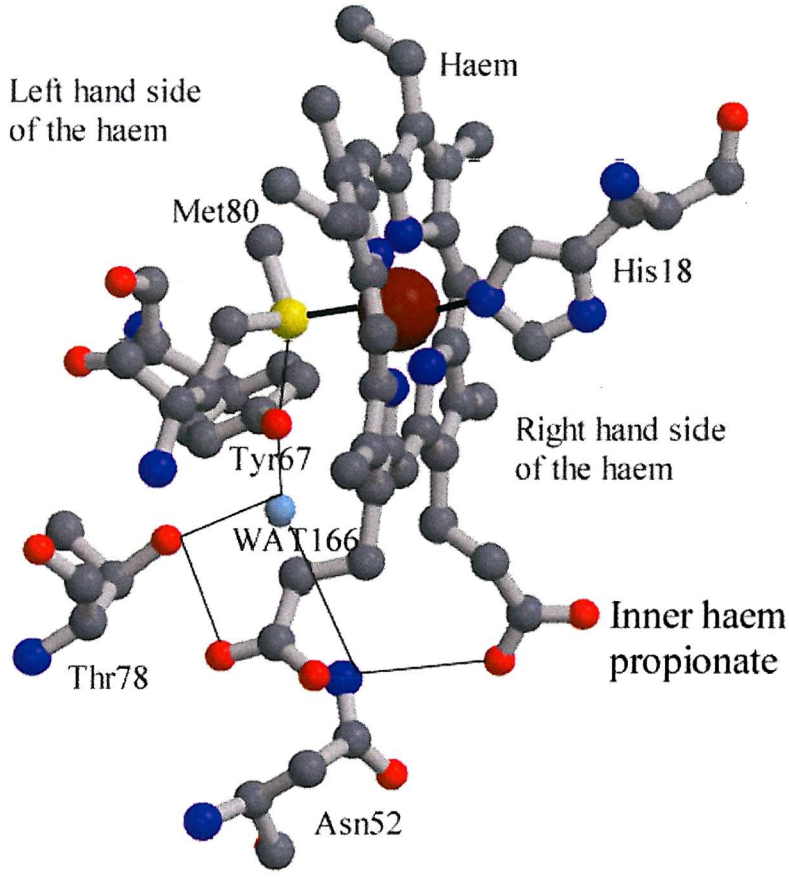

Figure 1.19 The residues and water molecules in and around the left hand side of the haem cleft of the reduced mitochondrial cytochrome *c*

The lines indicate hydrogen bonds. When the protein becomes oxidized Wat166 moves 1.7 Å towards the Fe^{3+}. The conformational change removes the hydrogen bonds between Asn52 and Wat166 and between Asn52 and inner haem propionate. Tyr67 maintains a hydrogen bond to the newly position water but is no longer hydrogen bonded to Met80. Thr78 maintains a hydrogen bond to the haem propionate and Wat166.

1.13.2 **Site directed mutagenesis studies on yeast iso-1-cytochrome c.**

The importance of Tyr67 in the cytochrome *c* mechanism was illustrated by mutating this residue to a phenylalanine (Berghuis *et al.*, 1994). By removing the tyrosine's hydroxyl group this mutation was expected to increase the hydrophobic nature of the region around haem, and thus to increase the redox potential. The internal water molecule (Wat166) was expected to be absent in the mutant as it would be energetically unfavorable to be in the haem pocket because it could not form the required number of hydrogen bonds. However, the mutation caused an increase in the size of the internal cavity where the Wat166 is present in wild type; this cavity not only retained the conserved Wat166 molecule but it acquired a second water molecule (Wat300), in roughly the same position as the hydroxyl group from Tyr67 in the reduced wild type protein (Figure 1.20). Therefore the hydrophobicity of the region in the mutant was actually decreased due to the extra water molecule. The Y67F cytochrome maintains the Asn52 hydrogen bond to the inner haem propionate (HP7) side chain; which stabilizes the oxidized Y67F protein relative to oxidized wild type. In wild type protein the Asn52 hydrogen bond to the propionate is lost on oxidation, which increases the flexibility of the polypeptide chain. The electrochemical properties of the Y67F cytochrome *c* are altered having a redox potential of 234 mV at pH 6.0, which is 56 mV lower than wild-type protein (290 mV). This same mutation showed a similar lowering of redox potential in both horse and rat cytochrome *c* (Luntz *et al.*, 1989; Frauenhoff & Scott, 1992). Brayer and co-workers postulated that the redox potential is modulated by the Tyr67 and Met80 hydrogen bond (Berghuis *et al.*, 1994).

The mutation of Asn52 to an isoleucine, and X-ray structure determination of the protein in both redox states was also studied (Berguis *et al.*, 1994). Asn52 participates in the redox related conformation changes (this Section). Mutating of Asn52 to isoleucine caused the loss of the conserved Wat166, which led to a decrease of the midpoint potential by 56 mV (as observed in the Y67F yeast cytochrome *c* mutant). As with Y67F, N52I loses the hydrogen bond between Tyr67 and Met80. Also the loss of Wat166 eliminates the change in mobility of the polypeptide on oxidation, which the internal water mediates in the wild-type protein. Therefore Asn52 is essential in mediating the Wat166 interaction with Tyr67, which in turn is essential in setting the redox potential of cytochrome *c* and increasing the flexibility of the oxidized protein. Arg38 and Trp59 are also highly conserved in cytochrome *c* structures; they are located internally and interact with the buried inner haem propionate (Figure 1.20) and they undergo only a slight

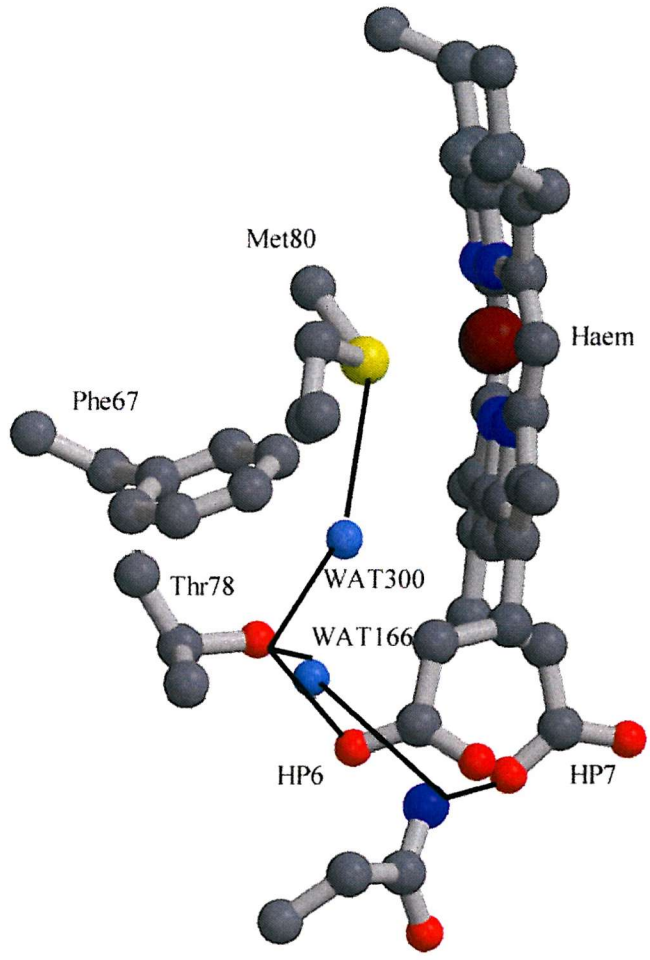

Figure 1.20 The active site of the Y67F mutant

The mutation leads to an extra water molecule (Wat300) being introduced into the cleft on the left hand side of the haem (Berguist *et al.*, 1991); the wild-type protein is shown in Figure 1.19. The lines indicate hydrogen bonds.

conformational change on change of redox state. The hydrogen bond between the haem and the tryptophan is absolutely conserved throughout the class I *c*-type cytochromes, which does suggest a vital function. The arginine appears essential in protecting the haem propionate from the bulk solvent. The interaction of Arg38 with the propionate is mediated through water molecules Wat121 and Wat168 (Figure 1.21). Chemical modifications of the side chains of either Arg38 or Trp59, which prevented the interaction with the inner haem propionate, caused the dissociation of the methionine ligand to the iron (Wallace & Rose, 1983). The length of the hydrogen bond between Trp59 and the haem propionate increases slightly on oxidation and leads to small shift in the main chain atoms of this amino acid. No other redox-related conformation change occurs.

1.14 **The structure of oxidized cytochrome c_H**

Cytochrome c_H is a typical class I *c*-type cytochrome and is the physiological electron acceptor from cytochrome c_L in *M. extorquens* and also from the cytochrome bc_1 complex. It donates these electrons is to the terminal oxidase cytochrome aa_3 (Figure 1.1). Cytochromes c_L and c_H are named to distinguish between them; cytochrome c_L has a low isoelectric point (3.5-4.0) and cytochrome c_H a high isoelectric point (9.0) (O'Keeffe & Anthony, 1980a; Anthony, 1992). It is 11 kDa and has a haem attachment site towards the N-terminus and the sixth ligand to the iron is provided by a methionine ligand sixty residues further on towards the C-terminus. This provides a histidinyl-methionyl-Fe coordination which leads to the characteristic 695 nm absorbance in the ferric state (Moore & Pettigrew, 1990).

The X-ray crystal structure of oxidized cytochrome c_H has been solved to 2.0 Å, and has several interesting features not seen in other class I *c*-type cytochromes (Read *et al.*, 1999). The tertiary structure of cytochrome c_H is typical of class I *c*-type cytochromes, the central three α-helices forming the 'cytochrome *c* fold' enveloping the haem group in a hydrophobic environment. Figure 1.22 shows that it bears a closer resemblance to mitochondrial cytochrome *c* than to other cytochrome c_2 proteins. The two cysteines that form thioether linkages with the haem vinyl groups are Cys14 and Cys17; the 5th ligand to the haem is a histidine at position 18 and the 6th ligand is a methionine at position 78. The structure differs from conventional *c*-type cytochromes only in the region surrounding this 6th ligand to the haem. In all other known eukaryotic and prokaryotic class I *c*-type cytochromes a conserved tyrosine (Tyr67 from yeast

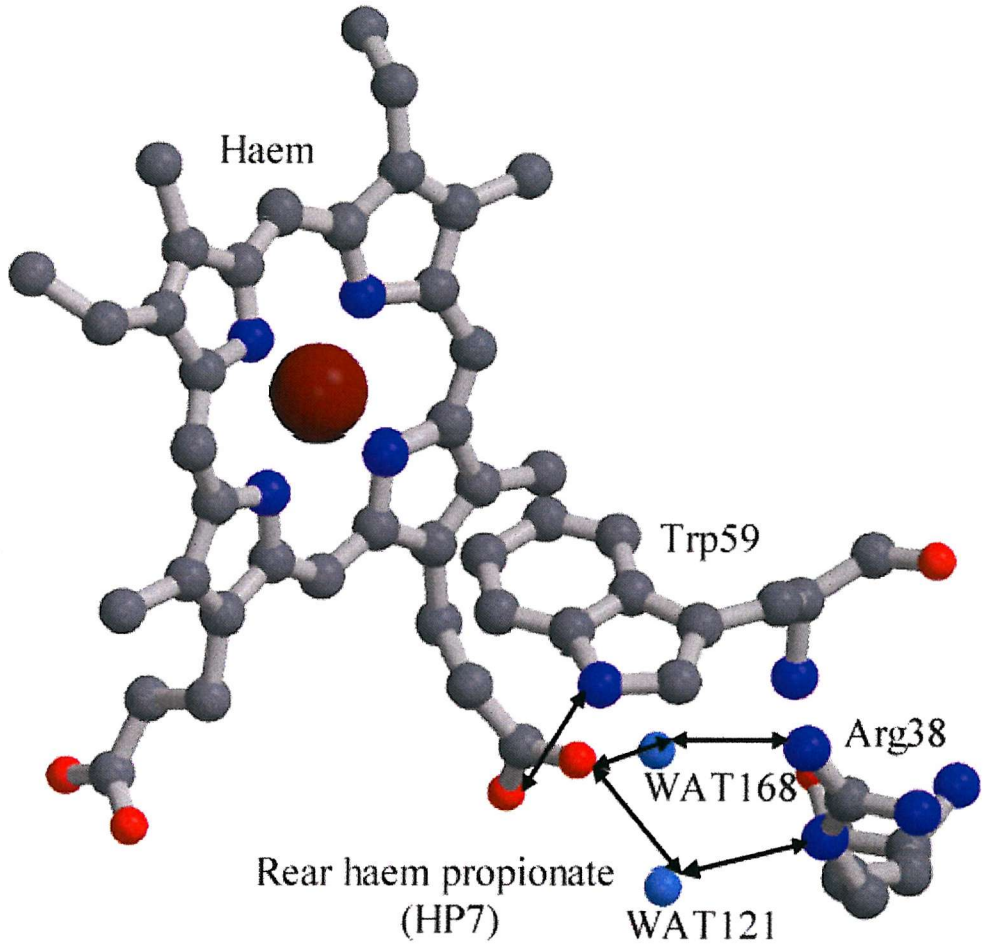

Figure 1.21 The interactions between the haem, Arg38 and Trp59 in yeast cytochrome *c* (arrows indicate hydrogen bonds)

Arg38 interacts with the haem propionate through two conserved water molecule (Wat121 & 168); Trp59 forms a hydrogen bond to the same propionate The Figure is from the pdb file coordinates from Berghuis & Brayer (1991).

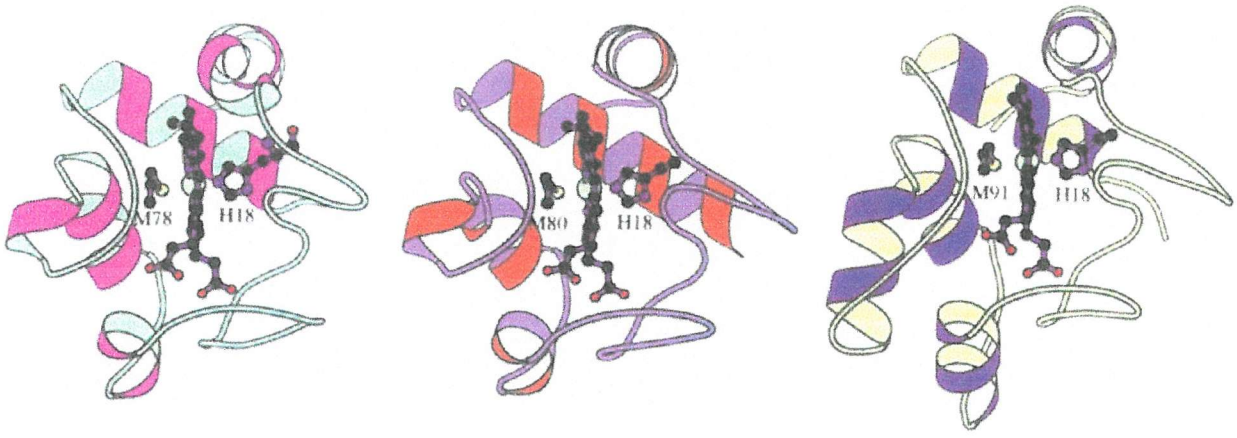

Figure 1.22 The overall X-ray structure of cytochrome c_H, and a comparison with cytochrome c_2 from *Rsp. rubrum* and tuna cytochrome *c*

The Figure shows the 5th and 6thligands to the haem iron and the common cytochrome *c* fold. It also shows how cytochrome c_H bears a closer gross resemblance to mitochondrial cytochrome *c* than to the typical bacterial cytochrome c_2. The Figure is taken from Read *et al.*, 1999.

cytochrome *c*), hydrogen bonds to the 6th ligand to the haem (Met78) when the protein is reduced; however this tyrosine is replaced by a tryptophan in cytochrome c_H. The tyrosine to methionine hydrogen bond is believed to be essential in mitochondrial cytochrome *c* for the structural changes that occur on a change in redox state (Section 1.13.1). This substitution suggests that other mechanisms are required to stabilize the oxidized iron in cytochrome c_H. It was proposed that the Trp65 which replaces the conserved tyrosine could form a potential hydrogen bond with the ring A haem π cloud if the tryptophan indole ring is slightly rotated; this would bring the NE1 atom closer to the haem plane to form a hydrogen bond (Figure 1.23) (Read *et al.*, 1999). This conformational change could happen in the protein when it becomes reduced. Trp65 is also within van der Waals contact with the conserved Trp57 (Figure 1.23) which in turn hydrogen bonds to the inner haem propionate (HP7).

Cytochrome c_H has other features which are rare in class I cytochromes *c*. For example the conserved Arg38 in mitochondrial cytochrome *c* is replaced by an alanine. Arg38 in mitochondrial cytochromes *c* and cytcochromes c_2 is thought to protect the haem from solvent and this substitution increases the solvent exposure of the inner haem propionate. It is possible therefore that dissociation of the exceptionally exposed inner haem propionate contributes to the unusual pH dependence of redox potential as previously proposed for this cytochrome (O'Keeffe & Anthony, 1980a).

Cytochrome c_H also lacks a conserved water molecule which is seen in mitochondrial cytochrome *c* (Wat166). This water molecule modulates the hydrogen bond network which involves Tyr67, Asn52, and Met80 in an oxidation state-dependent manner (Section 1.24). Also absent from cytochrome c_H is Asn52, which is replaced by the non polar residue, leucine. This substitution contributes to the surprisingly hydrophobic conditions in the region around the 6th haem ligand. This contributes to the large positive redox potential of cytochrome c_H (254 mV at pH 7.0). The features seen in cytochrome c_H suggest that the triggers behind the redox-related conformational shifts which occur in class I cytochromes *c* are not universal and that members of the class I cytochrome *c* family protect the oxidized haem iron via alternative methods.

1.15 **Cytochrome c_L**

Cytochrome c_L is the physiological single electron acceptor from MDH (Anthony, 1992: Dales & Anthony, 1995). Once reduced, cytochrome c_L is oxidized by the smaller, typical class I

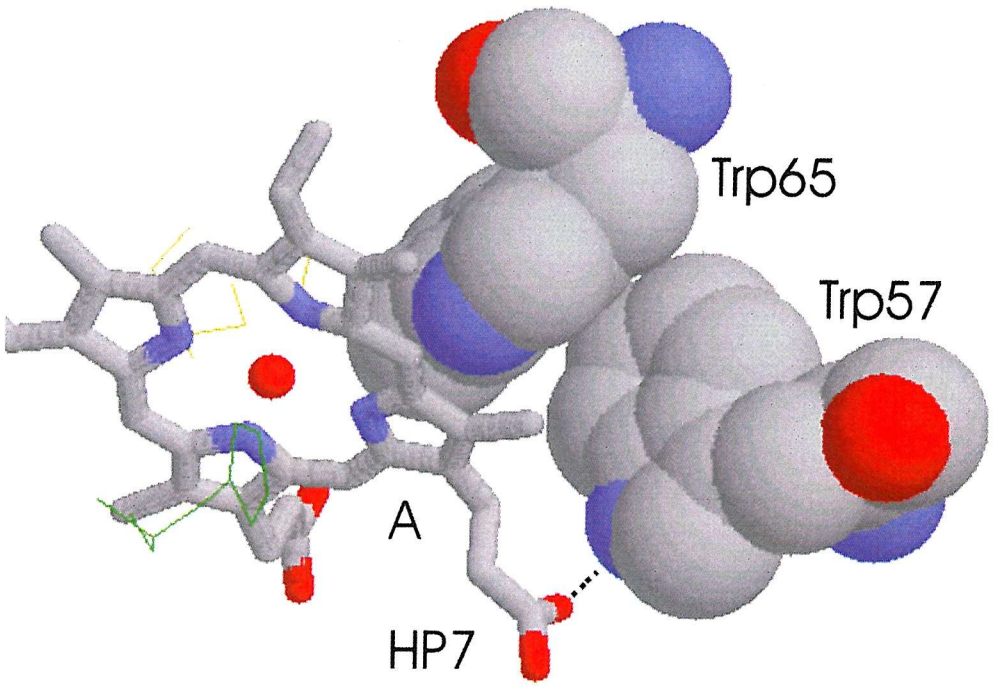

Figure 1.23 The interaction between the haem and the two tryptophans, Trp65 and Trp57

The Figure is taken from Read *et al.*, (1999).

c-type cytochrome, cytochrome c_H (Read *et al.*, 1999). Cytochrome c_L is a large, soluble, high potential cytochrome which has a single haem prosthetic group with a low spin iron. The haem is ligated to the protein by two thioether linkages involving cysteine residues. Previous work indicated that histidine is the 5th ligand to the haem and a methionine is the 6th ligand, as in typical class I *c*-type cytochromes (Beardmore-Gray *et al.*, 1982; Anthony, 1992; Afolabi *et al.*, 2001). However cytochrome c_L has many properties which are different from those of typical class I *c*-type cytochromes. It is uncharacteristically large (18,750 Da), (class I *c*-type cytochromes are usually no larger that 14 kDa); secondly, except for the haem binding motif (Cys65, Ser66, Gly67, Cys68, His69), cytochrome c_L shows no sequence homology with other *c*-type cytochromes; and thirdly the haem binding motif is 57 residues from the N terminus, (in typical class I *c*-type cytochromes the haem binding site is within the first 20 residues of the N-terminus). The 6th ligand to the haem (a methionine) is usually over 60 residues towards the C-terminus from the haem binding motif, whereas in cytochrome c_L all methionines are within 50 residues of the haem binding site (Anthony, 1992). As a result of these features it has been proposed that cytochrome c_L is the sole member of a sub-class of class I cytochrome *c* which has an N-terminal extension (Moore & Pettigrew, 1990).

1.15.1 **Autoreduction of cytochrome c_L and cytochrome c_H**

In the absence of reducing agent, it has been observed that the haem of both cytochrome c_L and cytochrome c_H can undergo rapid autoreduction when the pH is raised; this has been observed in a cytochromes from a number of methylotrophic bacteria, namely *Methylobacterium extorquens* (O'keeffe & Anthony, 1980b), *Methylophilus methylotrophus* (Beardmore-Gray *et al.*, 1982), *Hyphomicrobium X* (Dijkstra *et al.*, 1988) and *Acetobacter methanolicus* (Elliot & Anthony, 1988). The proposed mechanism involves the dissociation of a weakly acidic group on the cytochrome which, following a pH increase, dissociates to give a negatively charged species. This is then able to donate an electron to the haem and the free radical produced can then be stabilized by sharing an electron with the haem iron. This process, a first order intra-molecular reaction is reversible and can be repeated (Elliot & Anthony, 1982). The ferricytochrome of both cytochrome c_L and cytochrome c_H has a well-defined absorbtion band at 695 nm which disappears on reduction with dithionite at pH 7.0, and was restored with subsequent oxidation with ferricyanide. When the pH was raised to 10 (leading to autoreduction), the 695 nm band

immediately disappeared as the methionine was presumably replaced by an alternative strong field ligand; it could not be restored by oxidation with ferricyanide, although lowering the pH to 7.0 led to its reappearance. By contrast no displacement of the methionine ligand occurs on reduction of cytochrome c_L by MDH at pH 7.0. (Beardmore-Gray *et al.*, 1982)

1.15.2 **The haem environment of cytochrome c_L, and its interaction with CO**

Cytochrome c_L is able to bind with CO; this can only happen if the iron-methionine bond is broken. Such a reaction has previously been used to indicate an oxidase function, but there is no evidence to suggest that cytochrome c_L functions as an oxidase (Anthony, 1986; Anthony, 1992). The slow incomplete reaction with CO probably reflects the structure around the haem pocket that allows a more readily dissassociable iron-methionine bond (O'Keeffe & Anthony, 1980b). That the haem environment is slightly unusual is also indicated by the response of the midpoint redox potential to the changing pH values; there are two ionizing groups affecting redox potentials, the pK values being 3.5 and 5.5 in the oxidized form and 4.5 and 6.5 in the reduced form (O'Keeffe & Anthony, 1980). If these dissociations arise from the haem, the higher of the pK values is likely to be due to the inner haem propionate in the hydrophobic environment of the haem cleft, and the lower pK values due to the outer propionate in its more hydrophilic environment. The suggestion that the haem environment may be unusual is supported by the demonstration that the axial methionine ligand has a novel configuration as directly observed in NMR studies (Santos & Turner., 1988). Although the authors were not specific, the resonances of the axial ligands of diamagnetic haems are shifted to low frequency in NMR spectra because of the haem-ring current. The range observed for the methyl group of the methionine chemical shift is 2.7-3.7 ppm, reflecting the different types of side chain in the immediate environment of the methionine and the variations in the stereochemistry.

1.15.3 **The reduction of cytochrome c_L by MDH**

The reduction of cytochrome c_L by MDH occurs when the two proteins are mixed at pH 7.0, and does not require added substrate (Anthony, 1992); therefore proof of methanol-dependent reduction of cytochrome c_L was difficult to demonstrate. Two possible explanations for MDH-dependant reduction have been proposed. One suggests that it is due to an endogenous reductant, each molecule of MDH having about 90 molecules of this unidentified reductant

which cannot be removed by extensive dialysis (Ghosh & Quayle, 1981). A second proposal suggests that autoreduction of cytochrome c_L is stimulated by MDH to occur at a lower pH value than usual by changing the pK of an acidic group on the cytochrome which is involved in the autoreduction. Because the second proposal would not involve electron transport, a substrate would not be necessary and the kinetics should be first order with respect to the oxidized cytochrome c_L (O'Keeffe & Anthony, 1980b). Indeed, this was shown to be the case for *Methylobacterium extorquens* (O'Keeffe & Anthony, 1980b) and for *Acetobacter methanolicus* (Elliot & Anthony, 1988). However arguments against the participation of autoreduction in the reaction mechanism have also been put forward. Most importantly is that the observed rate of MDH-stimulated reduction of cytochrome c_L was much faster than the rate of autoreduction of the cytochrome c_L in MDH from *Hyphomicrobium X* (Dijkstra *et al.*, 1988). In addition, cyclopropanol-inactivated MDH from *Hyphomicrobium X* could not reduce ferricytochrome c_L in the absence of methanol, suggesting the need for electron transfer. From these experiments it is more probable that MDH-dependent cytochrome reduction in the absence of substrate is due to the endogenous substrate.

Methanol-dependent reduction of cytochromes *c* by MDH was eventually demonstrated using a linked system (Anthony, 1982). When MDH and a 50-fold excess of mammalian cytochrome *c* were mixed, the cytochrome remained oxidized. Addition of a small amount of cytochrome c_L led to the reduction of the mammalian cytochrome *c*, presumably due to the oxidation of endogenous reductant on MDH. Added mammalian cytochrome oxidase then rapidly oxidized all of the reduced cytochrome *c*, after which KCN was added to inhibit the oxidase. Addition of methanol then led to the complete reduction of all the cytochrome *c* present; the final rate being proportional to the concentration of MDH, but independent of mammalian cytochrome *c*.

1.15.4 **The absorption spectrum of cytochrome c_L**

Cytochromes c_L and c_H differ by no more than 1.5nm in their absorbance maxima. In the reduced cytochromes there are three major peaks (Figure 1.24). The highest peak is the γ peak at 416 nm (Soret band) which is due to a π to π^* electronic transition in the iron of the haem. On oxidation, this peak is slightly decreased and 'blue shifted' (to about 410 nm). The other two

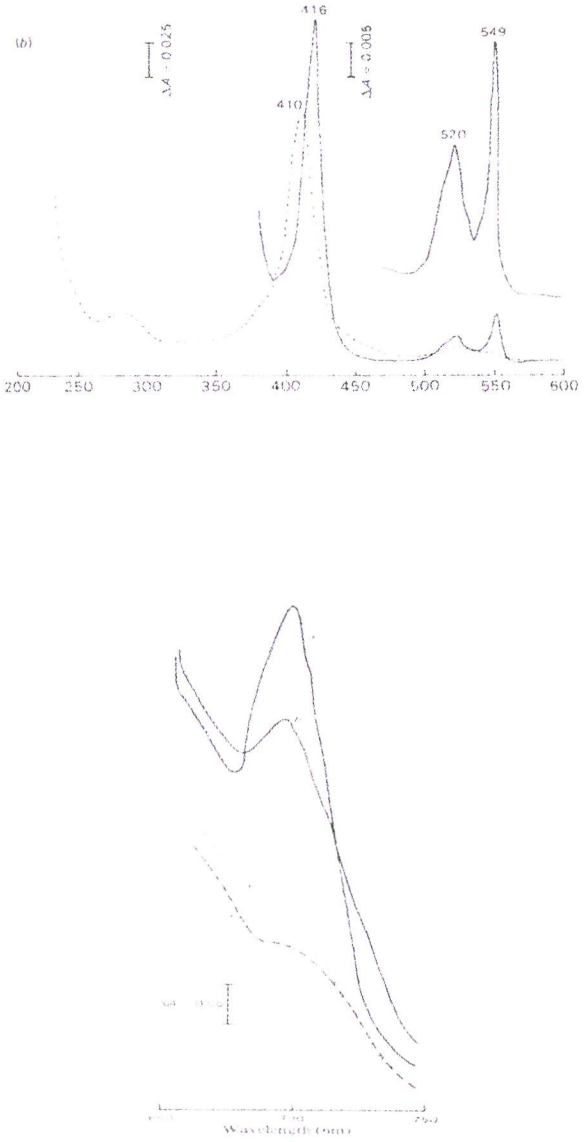

Figure 1.24 The oxidized and the reduced absorbance spectrum of cytochrome c_L

The oxidized spectrum is shown with a dashed line and the reduced with a solid line (O'Keeffe & Anthony, 1980a). The Figure at the top of the page shows the region from 200-600nm, and the Figure beneath shows the 695nm absorbance band, which indicates a methionine is the sixth ligand to the haem

peaks in the reduced cytochrome are the α and β-peaks (about 550 nm and 520 nm); on oxidation these peaks are lost. Of special interest is a peak at 695 nm (only in the oxidized cytochrome) produced by the methionine-iron ligation in class I *c* type cytochromes (Senn *et al.*, 1980; Senn & Wuthrich, 1985). This peak has been reported in both cytochrome c_L and c_H (Beardmore-Gray *et al.*, 1982). When the protein becomes autoreduced (this occurs at high pH >8.5), the methionine is replaced by an alternative strong-field ligand; this is shown by the loss of the 695 nm peak. This displacement does not occur on reduction of cytochrome c_L by MDH (Beardmore-Gray *et al.*, 1982).

1.15.5 **The structure of cytochrome c_{551i}**

Cytochrome c_{551i} is the physiological electron acceptor for MDH in *P. denitrificans* (Ferguson, 1991), as in *M. extorquens* and could reasonably be called cytochrome c_L (Anthony, 1992). Cytochrome c_{551i} is a large 17.5 kDa *c*-type cytochrome. It has 155 amino acids, of which 52 % are identical to those in cytochrome c_L, making this a good model for molecular replacement should X-ray diffraction data for cytochrome c_L be obtained. The X-ray crystal structure of cytochrome c_{551i} has been solved in a three-component protein complex with methylamine dehydrogenase and its electron acceptor, the blue copper protein amicyanin (Chen *et al.*, 1994). Cytochrome c_{551i} shows some typical bacterial *c*-type cytochrome structural properties; the one haem group is enveloped in the characteristic cytochrome *c* fold by the three central α-helices of the five found in the protein (helices II, III and IV) (Figure 1.25). This structure shows that it is similar to other cytochromes, but with a sizeable peptide extensions at both the N and C-termini (Figure 1.25). This cytochrome, like cytochrome c_L is highly acidic and the charged groups are mainly at the back and the sides of the molecules, away from the haem. In contrast, the front of the cytochrome, where the haem group is partially exposed, is almost totally hydrophobic, with the exception of two conserved tyrosines (Tyr78 and Tyr80) and Thr79. Tyrosine 78 is conserved within class I cytochromes *c* and forms a hydrogen bond with the outer haem propionate (HP6). Cytochrome c_{551i} and cytochrome c_L both have properties atypical of class I *c*-type cytochromes. For both cytochromes the haem binding motif is over 20 residues from the C-terminus (in cytochrome c_{551i} it is 59 residues away, and in cytochrome c_L it is 65 residues); secondly, the 6th ligand to the haem iron (Met101) is only 45 residues away from the haem binding motif. The haem binding motif is usually more than 60 residues away from the

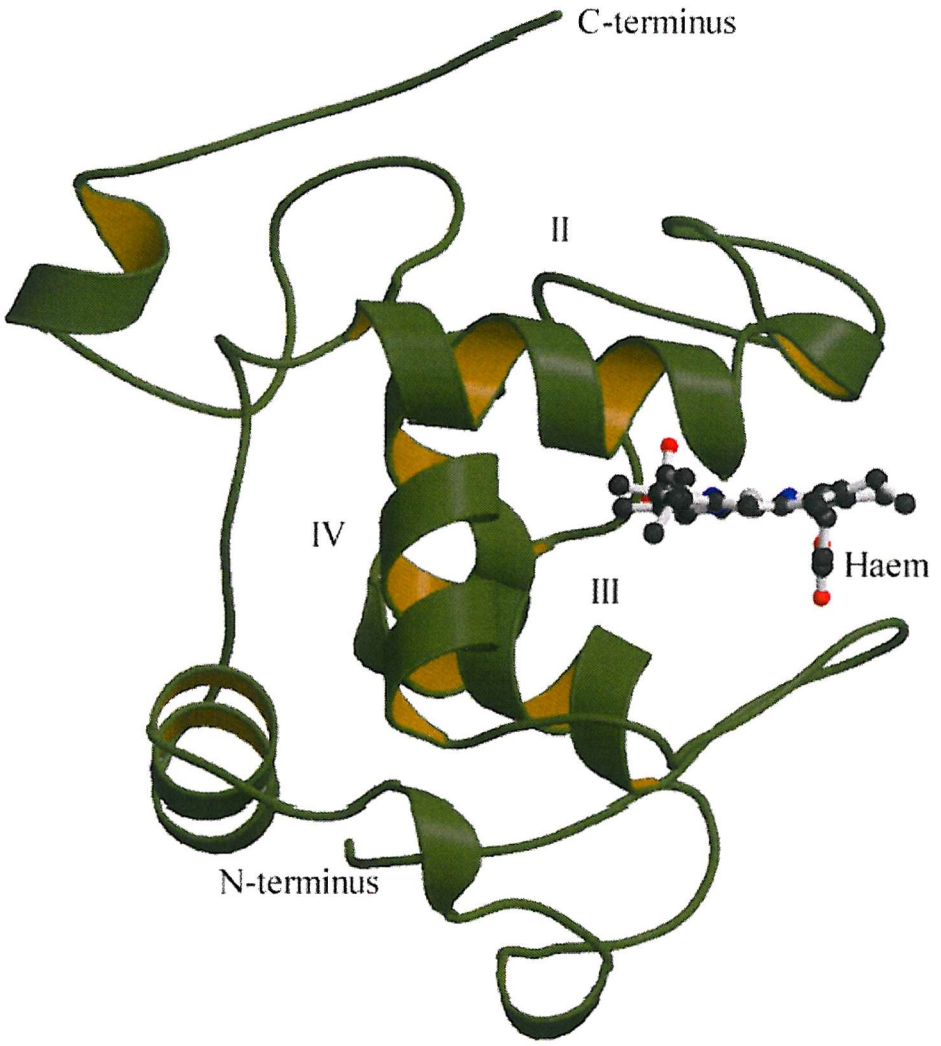

Figure 1.25 The tertiary structure of cytochrome c_{551i} from *P. denitrificans*

The symbols II, III and IV refer to the three α-helices which enclose the haem group and constitute the cytochrome *c* fold.

methionine ligand in typical *c*-type cytochromes

To determine if methionine is the ligand to the haem iron in cytochrome c_L mutants were made of the two methionine residues which are conserved between cytochrome c_L and cytochrome c_{551i}; these are Met109 and Met121 (cytochrome c_L numbering). In both mutants the methionine was replaced with an alanine. The presence of the 695 nm absorbance band which is present in cytochrome c_L and signifies a Met-Fe bond was used to determine which of the two methionines was coordinated to the iron. It was the M109A mutant which lost the characteristic 695 nm absorbance band, whereas the M121A mutant retained the wild type absorption spectrum. Also the M109A protein was inactive when it was assayed with MDH and DCPIP. These experiments demonstrated that Met109 was the methionine that is coordinated to the iron in the haem (Afolabi *et al.*, 2001).

1.16 **Spin state of the iron in cytochrome *c***

The spin state of the iron in cytochrome *c* can be in either a high-spin state or a low-spin state corresponding to different arrangements of electrons in the 3d orbitals. A high-spin arrangement is when the five electrons in the 3d orbitals are unpaired. When the electrons pair up in the three lower energy 3d orbitals, the t_{2g} orbitals, leaving the higher energy 3d orbitals, (the e_g orbitals) empty, this constitutes the low-spin state (Moore & Pettigrew, 1990). The alternative electron arrangements stem from the fact that the five 3d orbitals are not spatially equivalent and are differentially affected by ligands to the haem. The two e_g orbitals lie along the Cartesian axes whereas the three t_{2g} orbitals lie between the axes. Whether electrons stay unpaired is dependent on whether the pairing energy requires less energy to pair electrons in the t_{2g} orbitals than it does to keep them unpaired in the e_g orbitals, which are at a higher energy level due to being destabilized by incoming ligands. Both cytochrome c_H and cytochrome c_L have a low-spin configuration this was previously shown by an m.c.d (magnetic circular dichroism) spectrum (Beardmore-Gray & Anthony, 1980a).

1.17 **Aims of the work described in this thesis**

The work in this thesis describes studies conducted on methanol dehydrogenase and cytochrome c_L. Chapter four describes the X-ray crystal structure of cytochrome c_L from *Methylobacterium extorquens*. The goal was to produce a detailed three-dimensional structure of

this unusual cytochrome *c* and to compare the structure to other cytochrome structures. In addition, it was hoped that the structure would held to explain the physical and chemical properties of cytochrome c_L which have been mentioned in Sections 1.15-1.15.3. Chapters five and six describe work performed on MDH from the methanol oxidation mutants, *mxaC31* and *mxaD11*. Again X-ray crystallography was used to try and determine a structural basis for the properties exhibited by MDH from these mutants.

Chapter 2

Materials and Methods

2.1 Media and growth conditions for *M. extorquens*

Wild type *M. extorquens* and the *M. extorquens* mutants *mxaC31* and *mxaD11* (Toyama *et al.*, 1998) were the bacteria used in this study. The minimal medium was made up as described by Day and Anthony (1990a), by mixing 100 ml stock 1, 0.5 ml of stock 3 and autoclavable carbon sources (methylamine hydrochloride) at pH 7.0, for every litre of culture medium required. The volume was made up to 1 litre with deionised water and autoclaved at 121°C for 20 minutes. Once cooled to below 45 °C, 2 ml of stock 2 (autoclaved separately), and any other carbon sources and antibiotics were added just before use. Both mutant and wild type bacteria were grown on minimal agar with one or more carbon source/s; the growth medium which was used for *mxaC31* and *mxaD11* was supplemented with the antibiotic kanamycin (300 μg/ml). All agar plates and liquid cultures were incubated at 30 °C; agar plates for 5-12 days; liquid cultures were incubated without shaking for 24 hours, followed by 3-5 days with vigorous shaking.

Table 2.1 The three stock solutions which were used to grow *M. extorquens*.

	Component	grams/litre
Stock 1	$(NH_4)_2SO_4$	30.0
	$NaH_2PO_4.2H_2O$	5.7
	K_2HPO_4	15.3
Stock 2	$MgSO_4.7H_2O$	100.0
Stock 3	$CaCl_2.2H_2O$	5.3
	$FeSO_4.7H_2O$	2.0
	$MnSO_4.4H_2O$	0.2
	$ZnSO_4.7H_2O$	0.2
	$CuSO_4.5H_2O$	0.04
	$CoCl_2.6H_2O$	0.04
	Na_2MoO_4	0.04

H_3BO_3	0.03
1M HCL	10 ml

2.1.1 **Harvesting and preparation of cell free extract**

Cells were harvested by centrifugation for 8 minutes at 8,000 rpm (Beckman J2-21) and washed in 20 mM Tris buffer pH 8.0 three times. The cell pellet was resuspended in 20 mM Tris buffer to a ratio of 1.5 g of cells per ml of added buffer in preparation for sonication. The cells were broken by sonicating for 20 cycles (30 seconds on/30 seconds off), using a MSE 150 ultrasonic disintegrator. Throughout the sonication the cells were kept cool in an ice water bath.

The sonicated material was centrifuged at 10,000 rpm (Beckman L-7 ultracentrifuge) at 4 °C for 15 minutes to remove the cell debris. The supernatant was removed and centrifuged at 40,000 rpm for 1 hour at 4 °C to remove the cell membranes. MDH, cytochrome c_L and cytochrome c_H were separated and purified from the resulting supernatant (the crude extract).

2.2 **Purification of MDH**

The purification was based on the method described by Day and Anthony (1990a), with a slight alteration to the protocol. The pH of the crude extract was lowered to pH 4.0 with 1 M acetic acid. This formed a thick precipitate, which was removed by centrifuging for 15 minutes at 10,000 rpm, 4 °C. The pellet was discarded and the pH of the soluble fraction was increased back to 8.0 using 1 M NaOH. The material was then added to an ion exchange DEAE-sepharose fast flow column (Pharmacia, 16 mm x 30 cm), which had been previously equilibrated in 20 mM Tris-HCl buffer, pH 8.0. MDH and cytochrome c_H do not bind to the column whereas cytochrome c_L does bind. The fractions containing MDH and cytochrome c_H were identified using SDS-PAGE, pooled together and concentrated using a 3 kDa cut off YM3 Amicon membrane in a concentrating cell under N_2 pressure to approximately 5 % of its initial volume (5 mls). The sample was then applied in 1 ml runs to a high load superdex 200 gel-filtration column (Pharmacia, 16 mm x 60 cm) which had been previously equilibrated in 20 mM Tris-HCl buffer pH 8.0 containing 200 mM NaCl. Fractions containing MDH were identified using the microtiter dye-linked assay (Section 2.7), pooled and concentrated to 20 % of the volume (5 mls) and dialysed against 25 mM MES buffer, pH 5.5. The final step in the purification was to apply a 1 ml sample to an ion exchange Mono S column, which had been previously equilibrated in 25

mM MES buffer, pH 5.5. MDH binds to the column and is eluted using a 0-1 M salt gradient; the MDH eluted at 125 mM NaCl. Pure MDH was finally dialysed against 20 mM Tris-HCl buffer pH 8.0 and stored in 1 ml vials at -20 °C.

2.3 **Purification of cytochrome c_H**

The material which did not bind to the DEAE-sepharose column contained both cytochrome c_H and MDH; these were separated on the high load superdex 200 gel filtration column (as described above). The fractions which contained cytochrome c_H were identified using SDS page, and concentrated to approximately 20 % of the volume (5 mls) and dialysed against 25 mM MES buffer, pH 5.5. The final step in the purification was to apply a 1 ml sample to an ion exchange Mono S column which had been previously equilibrated in the same buffer. Cytochrome c_H binds to the column and is eluted using a 0-1 M salt gradient. Pure protein is passed through a buffer exchange PD10 column, which had been previously equilibrated in 20 mM MOPS, pH 7.0 and stored at 20 °C.

2.4 **Purification of cytochrome c_L**

Cytochrome c_L remained bound to the DEAE-sepharose fast column and was eluted using a salt gradient of 0-250 mM NaCl over a total volume of 500 ml; it eluted at approximately 100 mM NaCl. Fractions containing cytochrome c_L were identified using SDS-PAGE and pooled together. A slight alteration to the Day and Anthony (1990b) purification procedure was carried out at this stage. Ammonium sulphate was added to the sample to give a concentration of 2 M. The material was centrifuged at 10,000 rpm for 15 minutes, 4 °C to remove a pale precipitate; the cytochrome at this stage remained in solution. The pellet was discarded and ammonium sulphate was added (final concentration 3 M) to precipitate the cytochrome c_L, which was collected by centrifuging at 10,000 rpm for 15 minutes, 4 °C. The pellet was resuspended in 5 ml of 20 mM Tris buffer, pH 8.0 and passed down a buffer exchange PD10 column to remove the ammonium sulphate and NaCl. A 1 ml sample was then applied to a high load S-75 superdex gel-filtration column (Pharmacia, 16 mm x 60 cm) which had been previously equilibrated in a 20 mM Tris-HCl buffer, pH 8.0 containing 200 mM NaCl; the fractions containing cytochrome c_L were pooled and concentrated to approximately 20 % of the volume (5 mls). The final step in the purification was to add a 1 ml sample to a Mono Q anion-exchange column equilibrated in 20

mM Tris-HCl buffer, pH 8.0. Oxidized cytochrome c_L was eluted using a 0-1 M NaCl salt gradient at approximately 100 mM NaCl. The pure protein was pooled and dialysed against 20 mM Tris buffer pH 8.0 and stored in 1 ml vials at –20 °C.

2.5 **Methanol dehydrogenase assay systems**

Measurements of MDH activity using the dye-linked assay system were done at room temperature using a Hitachi U-2000 spectrophotometer as described by Day and Anthony (1990a). The activity was measured at pH 9.0 in 100 mM Tris-HCl buffer containing 5 mM methanol as substrate, 87 µM 2, 6-dichlorophenolindophenol (DCPIP), 15 mM ammonium chloride as an activator and enzyme in a 1 ml total volume; the reaction was initiated by the addition of 1.0 mM phenazine ethosulphate (PES), which acts as the primary electron acceptor and is coupled to the terminal electron acceptor, the dye DCPIP. The reaction was monitored by the decrease in absorbance of the DCPIP measured at 600 nm.

2.5.1 **Methanol dehydrogenase detection: the microtiter assay**

This assay is a modification of the MDH dye-linked assay outlined above and is used to detect MDH in collected fractions. A working mixture is made up of all the reagents used in the dye-linked system; 10 µl of sample is placed in the well of the microtiter plate and the reaction is initiated by adding 200 µl of the working mixture. The presence of active enzyme is indicated by a colour change from blue-green to yellow/olive.

2.6 **Protein detection and measurement**

a) SDS-polyacrylamide gel electrophoresis (SDS-PAGE)

The mini apparatus Bio-rad Protean II system and the discontinuous Tris-HCl/glycine system of Laemmli (1970) were employed throughout the study. Loading buffer, with or without β-mercaptoethanol was used when appropriate. A 12 % (MDH samples) or 15 % (cytochrome samples) running gel and a 4.5 % stacking gel were used, and the gel run at 20 mA. Detection of the proteins was by staining with Coomassie brilliant blue R250 as described by Weber and Osborn (1975). The positions of the protein band/s were compared to a set of molecular weight markers (SDS-PAGE, low range markers, Bio-Rad).

b) Bicinchoninic acid (BCA) assay

Protein concentrations were determined using the bicinchoninic acid assay (BCA assay) as described by Smith *et al.* (1985) and adapted for microtiter plates by Redinbaugh and Turley (1986). The reading of the microtiter plates was done on a Dynatech MR5000 micro-ELISA auto reader. In this assay the protein reacts with alkaline Cu^{2+} to produce cuprous ions which react with BCA to yield a purple colour with absorbance at 562 nm. The standard assay procedure involves the addition of 20 times the volume of working reagent (200 µl 4 % $CuSO_4.H_2O$ made up to 10 ml in BCA reagent, Sigma) to one volume of the sample. Bovine serum albumin fraction V (Sigma), in the range 0-1.0 mg/ml was used as the standard.

2.7 **Crystallization of cytochrome c_L**

Cytochrome c_L crystals were grown over one month at room temperature in the dark, using the hanging drop-vapour diffusion method (Figure 2.1). The protein samples for the crystallisation were 20-25 mg/ml. Initial crystal hits were obtained using the Molecular Dimensions crystal screen, containing 100 different solutions which have previously been used to produce protein crystals. The hanging drop method involves mixing a 2-4 µl protein sample with the same volume of the precipitant (termed the mother liquor) on a siliconised glass cover slip (siliconising stops the solution spreading over the cover slip). The cover slip is then placed over a well containing approximately 1 ml of mother liquor solution. A seal is formed between the well and the cover slip using vacuum grease which had previously been added around the circumference of the well. The hanging drop is then left in its enclosed environment over a period of time, during which time a state of equilibrium is set up within the well, where water diffuses between the protein-mother liquor mix in the drop and the more concentrated stock mother solution in the well. It is during this process of equilibration that the crystals form, as the concentration of the precipitant increases in the hanging drop. From the Molecular Dimensions crystal screen, three solutions produced crystal hits; the best of these hits was with a solution composed of 0.2 M calcium acetate (pH 6.5) together with 0.1 M sodium cacodylate and 18 % PEG 8,000. Optimisation by varying pH and concentrations of sodium cacodylate and PEG produced better crystals. The final optimised crystal growth condition was 0.2 M calcium acetate, pH 6.5 with 24 % PEG 8,000 and 0.25 M sodium cacodylate.

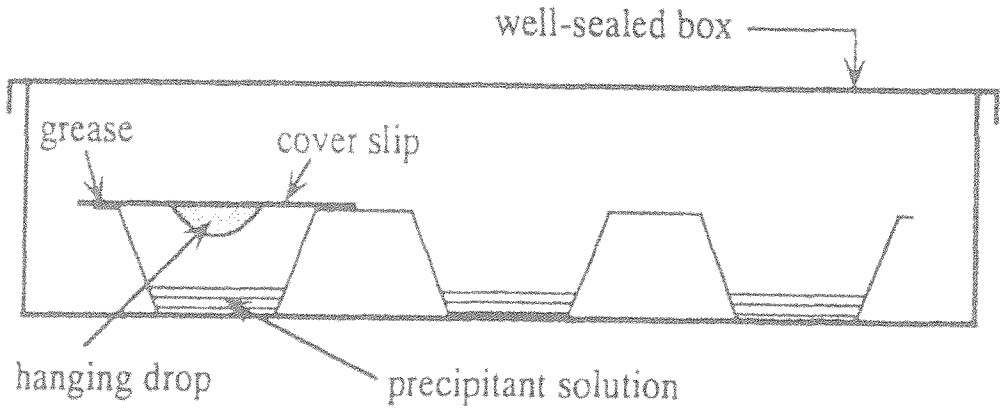

Figure 2.1 The experimental arrangement for the hanging-drop vapour diffusion method of protein crystallisation

The Figure is taken from Drenth (1994).

2.8 **Crystal freezing**

The crystal was flash frozen in an Oxford Cryosystems liquid nitrogen cryostream. To protect the crystal from the effects of freezing it was placed in a drop of mother solution and several drops of glycerol.

2.9 **Crystallization of MDH**

The conditions required for the crystallisation of MDH were duplicated from Afolabi *et al.* (2001). The protein concentration used for crystallisation was 16-20 mg/ml; the mother solution was 100 mM Tris buffer (pH 9.0) which contained 15.5 % PEG 6,000. Crystals were formed using the hanging-drop method as described above and appeared over one month, at room temperature in the dark.

2.9.1 **Crystal soaking and co-crystallization of MDH with cinnamyl alcohol**

Wild type MDH crystals were soaked in 1 mM cinnamyl alcohol for 4 hrs to soak the substrate into the active site of the enzyme. After soaking, the crystals were removed from the drop and flash frozen exactly as described for the cytochrome c_L. Co-crystallisation of MDH with cinnamyl alcohol was attempted by adding 1-20 mM cinnamyl alcohol to the mother solution (as described above), and using this as the crystallisation solution. Crystals appeared after 2 months. The crystals were removed from the drops and flash frozen as described for cytochrome c_L.

2.10 **Crystal micro-spectrophotometry**

This method was used to confirm the oxidation state of the cytochrome c_L crystal used for data collection by taking an absorption spectrum of the crystal in the 500-600 nm range. Also the technique was used to measure between 300-360 nm, which measures the characteristic PQQ absorbance spectrum for the *mxaC31*-MDH crystal used for data collection.

2.11 **Mass spectrometry analysis**

Samples were first desalted, using R2 and R3 reverse phase resin. 2 µl of R2/R3 resin was applied to a micro bore needle. The resin was subsequently washed with 2 x 4 µl dH_2O. A 4 µl sample was applied to the resin and washed with 3 x dH_2O. The sample was eluted of the

resin and into an electro-spray coated needle with 45 % acetonitrile: 5 % formic acid: 55 % dH_2O. Between each desalting phase the sample was spun down using a bench top centrifuge. Samples were then applied to the Time-of Flight Electrospray Mass spectrometer.

Chapter 3

X-ray crystallography, data collection and processing

3.1 X-ray sources for protein crystallography

X-rays are waves of electromagnetic radiation, defined as having wavelengths in the range of 0.1-100 Å (Rhodes, 1993). X-rays can physically interact with the electron clouds of atoms which are of similar dimensions to the wavelength. From this interaction structural information can be obtained about the three-dimensional positions of electrons and hence atoms, in space. X-rays in the useful range for crystallography can be produced by bombarding a metal target (most commonly copper or molybdenum) with electrons which are produced by a heated filament and accelerated by an electric field. A high energy electron collides with a metal atom and an electron from an inner electron orbital can be driven out, away from the nucleus. This allows an electron from a higher energy shell to drop down to the lower level. The excess energy is emitted in the form of an X-ray photon (Rhodes, 1993).

There are three common X-ray sources: *X-ray tubes*, *rotating anode tubes* and *particle accelerators*. The latter produce synchrotron radiation in the X-ray region. In the X-ray tube, electrons from a hot filament are accelerated by electrically charged plates and collide with a water cooled anode made of the target metal; X-rays emerge from the tube through windows of beryllium. Output from X-ray tubes is limited by the amount of heat that can be dissipated from the anode by circulating water. A higher X-ray output can be obtained from rotating anode tubes, in which the target is a rapidly rotating metal disk. This method improves heat dissipation by spreading the electron bombardment over a much larger area of metal. Particle accelerators are the most powerful X-ray sources and are utilized at synchrotron facilities. The X-rays are generated when electrons, which are traveling at, or close to the speed of light and in a circular motion are forced into a curved motion. A charged body like an electron emits energy (synchrotron radiation) when forced into a curved motion, and this energy is emitted as an X-ray. Additional devices called "wigglers" cause further bending of the beam and thus increase the intensity of the radiation.

3.2 **The Synchrotron**

Because the X-rays produced by the synchrotron are more concentrated together and produce a higher beam intensity (Drenth, 1994), it allows rapid data collection; typically data can be collected over a few hours as opposed to several days from a conventional X-ray source, such as a rotating anode device. Decreasing data collection time is not only convenient but it also limits the amount of radiation damage caused to the crystal (Drenth, 1994). Data collected from a synchrotron also has the advantage that the high intensity X-ray beam produces stronger X-ray diffraction by the crystal and usually to a higher resolution. Protein molecules in the unit cell (the unit cell is a single repeating block in the three-dimensional crystal lattice) can be large and consequently have few diffracting particles. Since the strength of diffraction is proportional to the number of diffracting particles in the crystal, crystals of large proteins produce diffraction which is generally weak. A more intense X-ray source can provide stronger diffraction per unit time.

The basic apparatus of a typical synchrotron radiation source is shown in Figure 3.1. The initial stage is the generation and acceleration of the electrons up to velocities approaching the speed of light. Electrons are generated using a linear accelerator (or LINAC) and accelerated by electric fields. The final energies of the particles should be in the region of 1-8 GeV (Mitchell, 1999). At these energies the electrons emit electromagnetic radiation in the X-ray range when exposed to an accelerating force (Drenth, 1994). After this stage the particles enter the storage ring; this allows the X-rays to be released for experimentation. The ring has bending magnets to guide the electron beam around the central cavity, and linear sections which contain insertion devices (Mitchell, 1999). At certain positions around the storage ring, beam lines branch off at tangents to the ring, and around each of these beam lines, these are work stations where experimental data from crystals or other samples can be collected. X-rays emerge from the storage ring when the electrons experience acceleration; this occurs when charged particles are forced to deviate from their circular path by magnets. After the release of X-rays, the accelerated particles return to their original path (Mitchell, 1999; Drenth, 1994). To compensate for the loss of energy by the electrons energy boosters are present in the synchrotron ring; this arrangement is shown in Figure 3.1

Once X-rays are generated they need to be monochromatised, passed through a focusing mirror and finally a collimator. Monochromators for a synchrotron are normally crystals of

germanium or silicon since these select out a very narrow X-ray wavelength from the incident beam (Mitchell, 1999). A single wavelength source of X-rays is desirable because a source producing two distinct wavelengths of radiation would produce two interspersed sets of reflections, which would make indexing of the reflections very difficult due to overlapping reflections. Mirrors are used to further reduce the diameter of the beam and focus the X-rays onto the crystal and are usually made from rhodium-coated silicon or glass (Mitchell, 1999). Collimation at a synchrotron is achieved using slits to eliminate unwanted scattered radiation, the collimator is a narrow metal tube which selects, and reflects the X-rays into parallel paths, producing a narrow beam.

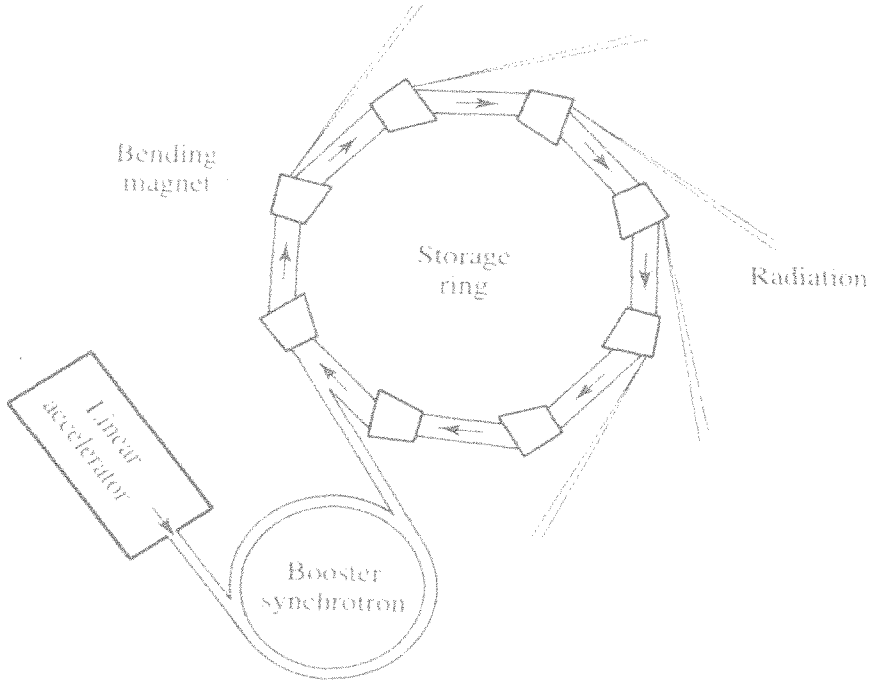

Figure 3.1 The typical storage ring of a synchrotron facility

The number of bending magnets is usually 16 or more and the diameter of the ring is of the order of 30 metres as is the case at the synchrotron installation at Daresbury laboratory, UK (Figure taken from Woolfson, 1997).

3.3 **Detectors for X-ray protein crystallography**

When an X-ray beam hits a target it becomes diffracted into many X-ray beams which emerge from the crystal. Each diffracted X-ray beam contains structural information derived from all the electrons within the crystal, and as such it is advantageous to collect as many of these diffracted X-ray beams as possible and measure their relative intensities within the shortest possible time. Detectors used to collect these X-rays need to fulfill certain criteria; these include the ability to collect the intensity of waves over a large intensity range (dynamic range); this allows both strong and weak diffracted beams to be recorded on a single diffraction image. Sensitivity is another factor; that is the ability to detect individual X-ray photons. Accuracy of the detector response to X-rays is another important aspect, i.e. to ensure that a uniform signal is registered and is output by the detector in response to the number of X-rays that strike it. Speed is another consideration; the quicker the detector can transfer a collected image into stored computer data, the more data can be collected and this is especially important on synchrotron trips. The resolution of the detector is also vital so that each spot produced has every chance of being identified as a separate entity. In this work only the CCD detector was used.

3.3.1 **The charged coupled device (CCD) detector**

The charge coupled device (CCD) detector is one of the most advanced detector types used in X-ray crystallography today. There are two basic designs for these devices. Firstly there is an arrangement where X-rays strike the CCD directly; this device encounters certain problems as the detector is susceptible to radiation damage; signal saturation can also occur due to each X-ray photon transferring energy directly to the plate (Westbrook & Naday, 1997). Because of these problems this design is rarely seen.

The second design incorporates an X-ray-sensitive phosphor surface at the front end of the CCD to shield it from the radiation, and to convert the X-ray signal to visible light immediately after radiation exposure. This immediate conversion of X-ray photons to visible light minimizes radiation damage and the overall signal detection process is rapid. The CCD functions by converting the visible light from the phosphor into a digital signal.

3.4 X-ray diffraction data processing: theory and programs

Once diffraction data has been collected the role of the crystallographer is to interpret the images correctly to determine the three-dimensional picture of the electron density and thus the atoms in the crystal. The processing of the diffraction data can be broken down into three stages:

1) Determination of the structure factor amplitudes of all the diffracted X-ray beams which give rise to the dark spots seen on X-ray diffraction patterns. The structure factor amplitudes are represented by $|F_{hkl}|$
2) Determination of the phase of each of the diffracted X-ray beams; this means elucidation of how the wave oscillates relative to the others.
3) Production of an electron density map and refining the structure obtained from the electron density map are the final stages in determining the three-dimensional structure of the molecule/s in the crystal.

Equation 1 below is the electron density equation; this summarizes the task of the X-ray crystallographer.

Equation 1: $$\rho(xyz) = \frac{1}{V}\sum_{h}\sum_{k}\sum_{l} F_{hkl}\, e^{-2\pi i(hx+ky+lz)}$$

In equation 1 ρ (xyz) represents the electron density at any particular point (*xyz*) in the unit cell; V is the unit cell volume; F_{hkl} are the structure factor terms for the reflection (*hkl*).

From the diffraction data, the structure factor amplitude can be obtained directly as it is directly proportional to the square root of the intensity of the diffraction spot (I_{hkl}). The phase information of the X-ray wave cannot be obtained directly from the diffraction pattern. To obtain phase information, molecular replacement is commonly used, where the phase information from a homologous protein whose three-dimensional structure has been previously determined is used as a phasing model for the unknown structure. The phasing model can be superimposed in three-dimensional space onto the unknown structure, where phase information is in effect applied to the unknown structure. Other methods used to obtain phase information are reliant on heavy atom binding to the protein molecules present in the crystal. There are two methods which utilize heavy atoms.

The first method is isomorphous replacement. Each atom in the unit cell contributes to every reflection in the diffraction pattern; if an atom which diffracts X-rays strongly, for example a heavy atom, could be incorporated into identical sites in all unit cells in the crystal you would expect to see changes in the diffraction pattern, caused by the additional contribution of the heavy atom. This slight perturbation in the diffraction pattern caused by the additional atoms can be used to obtain initial estimates of the phases. Thus the crystallographer must obtain a native data set (no heavy atom incorporation) and a data set with heavy atoms incorporated into identical sites in each unit cell. For the method to be successful the heavy atom incorporation must not significantly disturb the crystal packing or the protein conformation in the crystal; this means the native and derivative crystal must have the same unit cell dimensions and symmetry, in other words they must be *isomorphic*. The isomorphous replacement method depends on the assumption that the scattering by the derivative crystal, PH, which contains the heavy atom, is the sum of the scattering by the native crystal, P, and the scattering by the heavy ions, H.

A second means of obtaining phases from heavy-atom derivatives takes advantage of the heavy atoms capacity to absorb X-rays of a specified wavelength. As a result of this absorption, Friedels law, which states that reflection *hkl* and *-h-k-l* have the same intensity but phase of opposite sign does not hold. Atoms are able to absorb X-rays as well as emit them; absorption falls dramatically at wavelengths just below their characteristic emission wavelengths, this change in absorption as a function of wavelength being called an absorption edge. An element exhibits *anomalous scattering* when the X-ray wavelength used to collect diffraction data is near the atoms absorption edge. Under these conditions a fraction of the radiation is absorbed by the heavy atom and re-emitted with altered phase, this is termed anomalous scattering. In anomalous scattering, the members of a Friedel pair can be used to establish the phase of a reflection in the heavy atom data set, thus establishing the phase of the corresponding reflection in the native data.

Both of these methods determine the phase angle component of F_{hkl} by representing waves as complex numbers. Briefly, a complex number is composed of two parts, a real part and an imagionary part; this can be imagined as horizontal and vertical coordinates which represent a complex number (z) on a two-dimensional sheet of graph paper. Further, the complex can be thought of as a vector from the origin to this point (z). A type of diagram which is used to

represent a complex number is an Argand diagram, in which F_{hkl} is the point on the two-dimensional graph. The length of the vector is proportional to the amplitude of the reflection, whereas the angle between the real axis and F_{hkl} is the phase contribution to the reflection.

3.5 **Space groups**

The contents of the unit cell are symmetric and therefore certain sets of reflections are equivalent. In theory only one set of equivalent reflections need be measured, so awareness of unit cell symmetry eliminates recording the same reflection more than once and therefore reduces the data collection time substantially. The symmetry of the unit cell is described by its space group which is represented with a capital letter followed by numbers, for example $P2_12_12_1$. The capital letter designates the lattice type (Figure 3.2) and the numbers represent symmetry operations that can be carried out in the unit cell without changing its appearance.

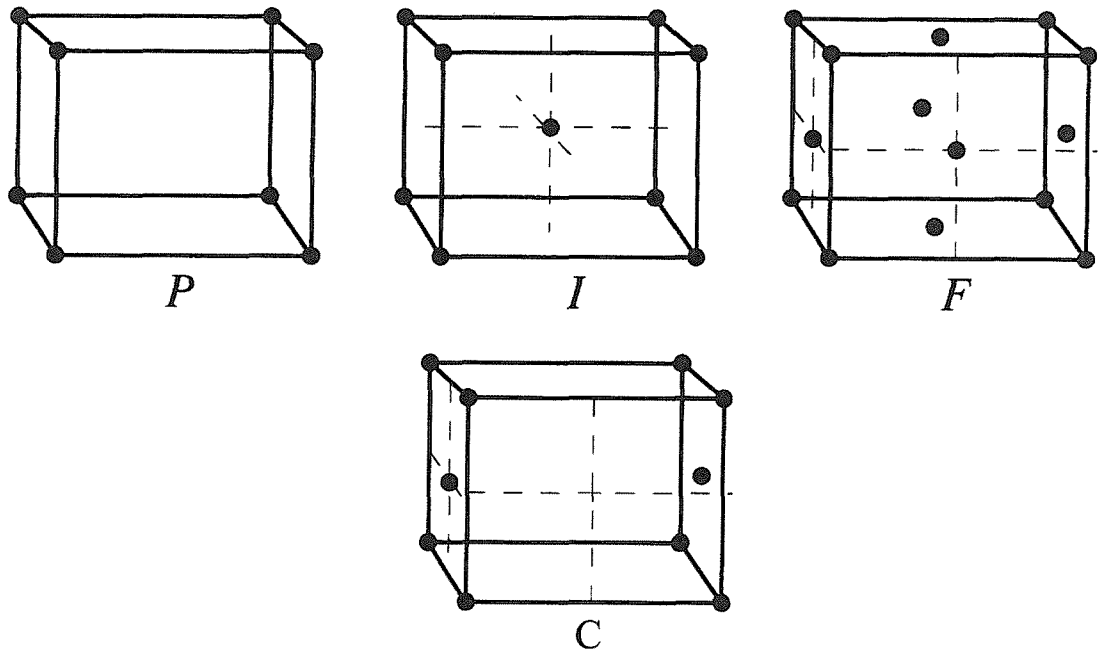

Figure 3.2 The lattice types *P, I, F* and *C*

Figure 3.2 shows a few lattice types. Lattice type *P* describes a primitive lattice type. A primitive lattice contains one lattice point at each corner of the unit cell. Each lattice point is

shared among eight neighboring unit cells and therefore a primitive lattice contains eight times one eighth of a lattice point or one lattice point in a unit cell. Symbol *I* represents a body-centred lattice, with a lattice point at the centre of each unit cell and one eighth at each corner therefore each unit cell contains two lattice points. Symbol *F* describes a face-centred lattice which has lattice points on the centre of each face.

The unit cell contains a large asymmetrical molecule (the protein) which contains no symmetry elements but which can be juxtaposed onto other identical entities by symmetry operations; this symmetry describes the contents of the unit cell. The symmetry elements that can be imposed on protein crystals are translation, rotation and screw axis (translation and rotation elements combined).

Translation simply means to move the molecule a specified distance along x, y or z. When the distance is equal to the length of that axis, superimposing the atoms of one unit cell onto those adjacent to it; this translation by one axial length is called *unit translation*. Unit cells often exhibit symmetry that entails translation by a fraction of axial length e.g. *a*/4. If the contents of the unit cell exhibits, for example, a 4 fold rotational symmetry, it means that it has the same appearance after each 90 ° rotation. This rotational symmetry is in general denoted by a number following the lattice type in the space group symbol; a four-fold rotational axis gives a P4 space group.

A screw axis results from a combination of translation and rotation. Figure 3.3 shows a $P2_1$ unit cell where successive molecules are rotated 180 ° (two-fold rotational symmetry) and translated one half of the axis length; for a two-fold screw rotational symmetry there is only one possible translation.

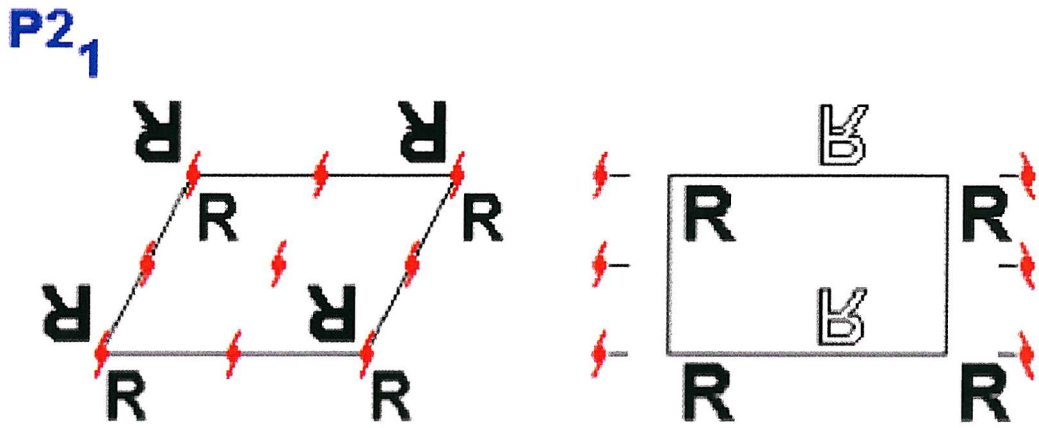

Figure 3.3 An illustration of a $P2_1$ space group

A $P2_12_12_1$ unit cell possesses three perpendicular twofold screw axes parallel to x, y and z. For $P4$ symmetry there are four possible space groups: $P4$ and three possible screw axis $P4_1$, $P4_2$ and $P4_3$, that is three possible translations.

3.6 **Data processing**

The first task for the crystallographer is to index all the spots from the diffraction images collected. This process involves assigning each spot a three-digit number comprising the integers h, k, and l. These are known as Miller integers and they represent coordinates which describe the position of each reflection in a three-dimensional reciprocal-space lattice. It is termed a three-dimensional reciprocal lattice as there is an inverse relationship between the lattice spacing in the crystalline lattice (real unit-cell) and the spacing of reflections in the lattice on the film. The method used to index all spots is **autoindexing**. Figure 3.4 shows that only part of the three-dimensional diffraction can be recorded at once and in order to measure the directions and intensities of all additional spots the crystallographer must rotate the crystal and record the diffraction pattern from all unique orientations of the crystal relative to the X-ray beam.

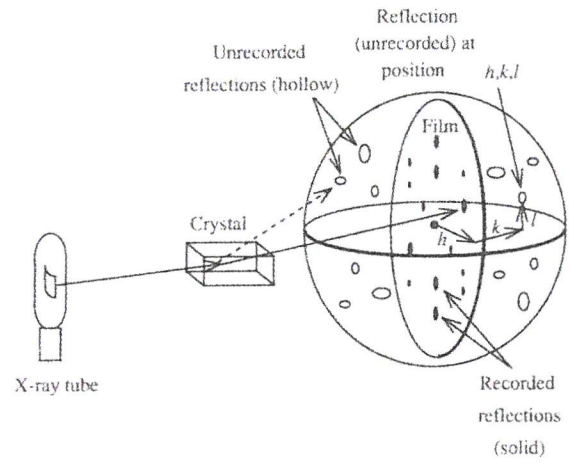

Figure 3.4 Crystallographic data collection

Reflections measured at one particular crystal orientation (solid, on film) and those that could be measured at other orientations (hollow, within the sphere but not on the film) (Rhodes, 1993).

For autoindexing to work best, it is preferable to have prior information about the space group of the crystal, and unit cell dimensions, although this is not essential. Autoindexing gives us predicted positions for all spots in the reciprocal-space lattice (*hkl*) and also the intensity of the reflection is recorded (I_{hkl}). The indices *hkl* refer to the atoms on a particular set of parallel planes in the crystal (real-lattice).

Each reflection that arrives at the detector can be seen as a complex wave. The wave can be described by a Fourier series composed of Fourier terms, where each term is a simple sine or cosine function whose wavelength is an integral fraction of the wavelength. The Fourier series that describes a diffracted X-ray can be described by a *structure factor equation* and the computed sum of the series for reflection *hkl* is called the *structure factor amplitude* (F_{hkl}). A useful way to visualize F_{hkl} is as a Fourier series where each Fourier term describes diffraction by one atom in the unit cell and thus the series contains the same number of terms as there are number of atoms in the unit cell. Therefore the structure factor amplitude is a wave created by the superposition of many individual waves. This can be mathematically expressed as below in equation 2:

Equation 2

$$F_{hkl} = \sum_{j=1}^{n} f_j e^{2\pi i(hxj+kyj+lzj)}$$

Equation 2 means the structure factor that describes reflection *hkl* is a Fourier series in which each term is the contribution of one atom, treated as a simple sphere of density. So the contribution of each atom *j* to F_{hkl} depends on (1) what the element is, which determines the f_j, the amplitude of the contribution, and (2) its position in the unit cell (x_j, y_j, z_j), which establishes the phase of its contribution.

3.6.1 **Data processing: methods and programs**

In my study the X-ray data were processed using **MOSFLM** (Leslie, 1994). Once the reflections have been autoindexed, the predicted positions in the three-dimensional lattice need to be refined so they accurately predict all the reflections in the reciprocal lattice. To do this MOSFLM refines certain experimental parameters such as the beam centre, crystal orientation, unit cell lengths and angles, crystal to detector distance and beam divergence. This allows a closer match of the reflection predictions with the reflections on the image. Once the prediction–spot match is optimised for several images, integration of the reflection intensity information from the full data set can proceed. Intensities are corrected by subtracting the background and the application of Lorentz-polarization corrections. All reflections are now sorted; this combines data sets from a high-resolution pass and a low-resolution pass and sorts the reflections on the basis of *h*, *k* and *l*.

The next task is to scale all the images together and combine symmetry-related reflections (known as multiplicity in the data) and thence to determine $\mathbf{R_{merge}}$ values for these symmetry-related reflections. The R_{merge} values represent a measure of the accuracy of the integration and scaling steps, as well as the strength of the diffraction signal and the correctness of the space group. For high resolution data the R_{merge} limits are from 3-10 %. Scaling is crucial to the process as it smoothes out fluctuations from one image to the next which can be brought about by crystal damage, crystal slippage, absorption or beam fluctuations. The way scaling works is to compare symmetry-related reflections from different images which should in theory have the same intensity, and to determine a scale factor to apply to the images to make their intensity values uniform. The B-factor for each of the images can also be estimated at this stage. This is a numerical value associated with the flexibility of the position of atoms within the crystal. The final stage in scaling is to merge the data together and calculation of the R_{merge}.

Finally, after scaling the data, a program is used to convert each reflection intensity into the all important structure factor amplitude, this program (truncate) produces the reflection file which can be used for molecular replacement. The programs used to sort, scale and truncate the reflections are all from the programs from the CCP4 suite (CCP4, 1994).

3.6.2 **Systematic absences**

Unique reflections often come from multiple observations of the same symmetry-related reflections, which are merged and averaged into one unique intensity value. Extra symmetry in the diffraction pattern arises from space group elements. For example a two-fold symmetry along the z axis will give rise to four reflections: (*h, k, l*) (*-h, -k, l*) (*h, k, -l*) and *–h, -k, -l*) all with equal intensity Although the screw character of a two-fold screw axis is not detected in the symmetry of the diffraction pattern it has an effect on along the corresponding axis in the diffraction pattern. All operations involving translations such as screw axes yield extinctions in the diffraction pattern (systematically absent reflections). The systematically absent reflections reveal symmetry elements in the unit cell. Using $P2_1$ as an example, the two-fold screw axis along the b axis, causes reflections on the 0*k*0 (*hkl*) axis to be systematically absent every other reflection. These systematic absences can be used to confirm the space group of the crystal.

3.7 **From diffraction to electron density**

The result of X-ray data collection is a list of reflection intensities. Each is assigned an index *hkl* which corresponds to its position in the reciprocal lattice. The intensity of the reflection is a measure of the strength of the reflection from the set of lattice planes which have an index *hkl* (bear in mind it is the complete set of parallel planes which contribute to the reflection as opposed to a single plane). The reflections close to the centre of the diffraction pattern have low indices and those with high indices lie further away. It is the reflections close to the centre of the pattern which come from sets of planes with a large interplanar distance (d_{hkl}); these reflections carry information about gross features of the contents of the unit cell; reflections further from the centre are from sets of planes with high indices and thus from a set of planes with a small d_{hkl} and these reflections carry information about the finer details of the contents of the unit cell. It is these outermost reflections which contain the high frequency terms in the Fourier series, which enable the three-dimensional electron density map to be more accurate.

To determine the electron density for the unit cell $\rho(xyz)$ from the structure factor amplitudes another mathematical term has to be introduced; this is the *Fourier Transform*. Fourier demonstrated that for any function $f(x)$ there exists another function $F(h)$, where $F(h)$ is the *Fourier Transform* (FT) of $f(x)$, and the units of the variable h are reciprocals of x; for example if x is a function of time then h is reciprocal time or frequency measured in reciprocal seconds (s^{-1}). How to compute the $F(h)$ of $f(x)$ is shown below in equation 3.

Equation 3: $$F(h) = \int_{-\infty}^{+\infty} f(x) e^{2\pi i(hx)} dx$$

Computation of the Fourier transform involves the multiplying of the function $f(x)$ by $e^{2\pi i(hx)}$ and integration of the combined functions with respect to x; the result is the new function $F(h)$ which is the Fourier transform of $f(x)$. The Fourier transform is reversible; therefore the same mathematical operation can be carried out in the opposite direction to give $f(x)$ from $F(h)$. The Fourier transform also applies to periodic functions in any number of dimensions; therefore to express $F(hkl)$ in terms of a three-dimensional function $f(xyz)$, equation 4 shows the Fourier transform of $f(x,y,z)$.

Equation 4: $$F(hkl) = \int_x \int_y \int_z f(x, y, z) e^{2\pi i(hx+ky+zl)} dxdydz$$

As before, the $F(h,k,l)$ is the Fourier transform of $f(x,y,z)$, and in turn, $f(x,y,z)$ is the Fourier transform of $F(h,k,l)$. Thus, we can use the Fourier transform to obtain information about the contents of the unit-cell $f(x,y,z)$ obtained from the diffraction pattern, $F(h,k,l)$.

The structure factor amplitude (F_{hkl}) can be written as the sum of contributions from each volume element of electron density in the unit cell. We can make our volume elements infinitesimally small so that the average value of $\rho(xyz)$ is precisely equal to the actual values at every point and integrating these volume elements. The resulting integral can be seen as the sum of the contributions of an infinite number of small volume elements. This is shown in equation 5.

Equation 5: $$F_{hkl} = \int_x \int_y \int_z \rho(x, y, z) e^{2\pi i(hx+ky+lz)} dxdydz$$

This equation can be represented as in equation 6:

Equation 6: $$F_{hkl} = \int_V \rho(x, y, z) e^{2\pi i(hx+ky+lz)} dV$$

The equation describes the integral over V, the unit-cell volume (equal to the integral over all values of *x, y,* and *z* in the unit cell). Each electron density volume element contributes to the F_{hkl} with a phase determined by its coordinates *(x,y,z)*. In addition, since the transform is reversible, the electron density, $\rho(x,y,z)$ is in turn the transform of the structure factors as shown in the equation 7.

Equation 7: $$\rho(x, y, z) = \frac{1}{V} \sum_h \sum_k \sum_l F_{hkl} e^{-2\pi i(hx+ky+lz)}$$

This equation explains how we can obtain the electron density in the unit-cell by constructing a Fourier series from all the structure factors. The structure factor describes a diffracted X-ray and like all descriptions of a periodic function it must include two parameters, namely, amplitude and phase. The amplitude can be obtained directly from the diffraction pattern, but the phase of the diffracted beam is not recorded on the diffraction pattern. In my study molecular replacement was used to obtain initial phase estimates.

3.8 **Molecular replacement**

The protein structures solved in this study were done using molecular replacement. After processing the data, the crystallographer has directional and intensity data on each reflection (the structure factor amplitude) but has no information about the phase of the wave that leads to the reflection spots. To obtain the phase information, the phases from structure factors of a known crystal structure are used as initial estimates of the phases for the unknown structure. Molecular

replacement allows the crystallographer to determine the structure of a protein by using just one native data set and does not require multiple data sets to be collected, as is required when using heavy atom methods to solve the phases of the reflections. When using molecular replacement, the known protein model is referred to as the *phasing model* and the unknown structure as the *target structure*. The principle behind molecular replacement depends on superimposing the search model on the target structure in its unit cell. This allows the phases from the correctly orientated and positioned model to be calculated and used as initial estimates for the target protein. The method involves determining the orientation and the position of the phasing model in the unit cell, relative to the target protein.

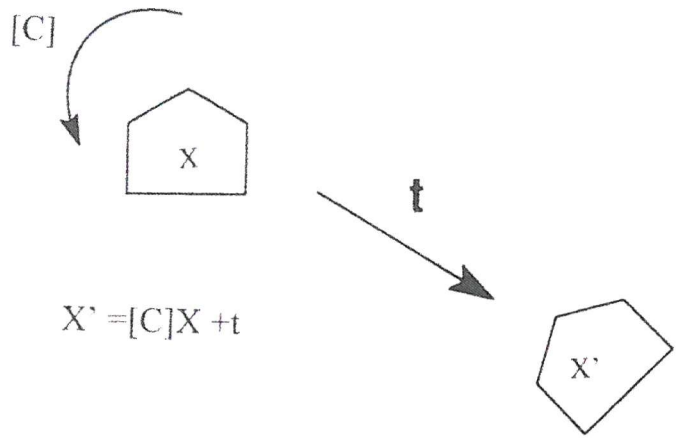

Figure 3.5 The aim of molecular replacement

If X is the matrix of the position vectors of the search model and X' the matrix of position vectors of the target model, the transformation between them can be described as in equation 8.

Equation 8: $$X' = [C]X + t$$

In equation 8, C is the matrix that rotates co-ordinates X into the new orientation and $\underline{t}$ is the vector defining the translation. The rotation matrix consists of 3 parameters usually defined as the Eulerian angles α, β and γ; the translational vector ($\underline{t}$) is also defined by 3 translation parameters (t_x, t_y and t_z). This leaves 6 parameters to search for; this would require a large

amount of computing time and therefore an alternative solution was devised by Rossman and Blow (1962). They demonstrated that the search for the orientation of similar proteins in the crystal cell could be achieved by using the Patterson function (see Section 3.11); this allows the search to be split into 2 parts, a search for rotation solution and a search for a translation solution.

3.8.1 **The Patterson function**

The Patterson function is the Fourier transform of the experimental intensities and therefore requires no phase information. The Patterson map consists of peaks corresponding to all inter-atomic vectors. Each pair of atoms in the unit cell gives rise to two peaks in the Patterson cell; for N atoms in the unit cell (where N = number of atoms) there would be N^2 peaks in the Patterson cell. The Patterson cell also contains an origin peak which consists of vectors of zero length, corresponding to vectors between each atom and itself. Therefore, the Patterson unit cell consists of N^2-N non-origin peaks. By increasing the number of atoms in the unit cell, the corresponding Patterson cell becomes more densely packed and hence more difficult to interpret.

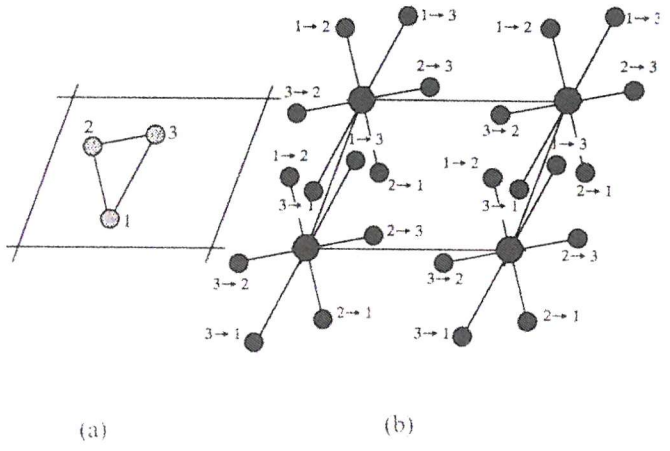

Figure 3.6 An illustration of the Patterson function

The 2-dimensional real-cell containing 3 atoms (a) and its corresponding Patterson cell (b) is shown. The Patterson cell consists of peaks corresponding to all inter-atomic vectors.

In a Patterson map from a known structure the intramolecular vectors are independent of the position of the structure in the unit cell as long as the molecule is not rotated. Whereas by rotating the structure in the unit cell the Patterson map rotates around the origin, altering the arrangement of the vectors in a single Patterson unit cell. This is how the Patterson map is used to determine the orientation of a molecule in the unit cell. If the phasing protein and the target proteins are indeed similar and orientated the same way in the unit cell they should give very similar Patterson maps. This allows a series of trials in which the Patterson map is rotated and compared to the Patterson map of the target protein. This finds the best orientation of the model (rotation function), which is then used to determine the best position of the molecule (the translation function). The translation function relies on the cross-vectors in the Patterson function, i.e. the search molecule is moved around in the cell and the calculated cross-vectors are compared with the native Patterson map, which can be calculated from the diffraction data.

3.9 **Refinement and model building**

Refinement is the process for improving the agreement between the calculated and the observed structure factor amplitudes. This method is often referred to as reciprocal space refinement and involves adjusting atomic positions (x, y, and z) to values that best fit the observed structure factor amplitudes. With least squares refinement, atom positions are selected that minimize the squares of the difference between corresponding calculated and observed structure factor amplitudes. This can be expressed by equation 9.

Equation 9:
$$\phi = \sum W_{hkl} \left(|F_o| - |F_c| \right)^2_{hkl}$$

Where ϕ =the sum of squared differences between the observed (Fo) and the calculated (Fc) structure factor amplitudes

W_{hkl}= weighting of the difference depending on the reliability of the measured intensity.

The parameters to be refined include atomic positions, temperature factors (B-factors) and occupancy. A major problem with refining protein molecules is the large number of atoms in

the structure, which results in a poor observations-to-parameters ratio. Therefore, constraints or restraints are used in the refinement to overcome this problem. With constrained refinement a fixed value is used for a certain parameter; e.g. to fix bond lengths and angles, allowing only dihedral angles to vary, thus decreasing the number of parameters to be refined. In comparison, when using restrained refinement, elastic conditions are imposed on parameters; e.g. all bond lengths and bond angles to be within a specific range of values. There are a number of packages available for refining protein structures. In this work CNS least squares refinement (Brunger *et al.*, 1998) and SHELX (Sheldrick, 1998) were used.

3.9.1 **Electron density maps and model building**

During refinement manual model building is required. This involves calculating electron density maps, so that the model can be moved into density where necessary. Two types of electron density maps are normally calculated during model building. Maps that are calculated using *Fo-Fc* as the coefficient provide information about the missing parts of the structure, and emphasize errors in the current model, whilst with a *2Fo-Fc* map an approximation of the electron density of the model and a difference electron density is obtained. Because the phases are initially rough estimates, the first electron density map can be relatively uninformative. To improve the map whatever unit-cell contents that can be discerned in the map is subsequently used to calculate new structure factors during the refinement and the phases of these revised structure factors are used along with the original native amplitudes to calculate a new map.

As the model becomes more accurate, the phases computed from it improve, and the map, computed from the original native structure factors amplitudes and latest phases, becomes even more detailed. The refinement programs adjust the atomic positions to improve the agreement between the amplitudes calculated from the current model and the original measured amplitudes in the native data set. Figure 3.6 shows a flow diagram which illustrates how this refinement ultimately produces a molecular model that agrees with the native data set. The graphics package used to visualize the structure was **QUANTA** (San Diego: Molecular Simulations. 1996); in order to use QUANTA, electron density map files need to be converted into the correct format; this was achieved using the **CCP4** program, **MAPMAN**. With the correct electron density files and the protein coordinate file from the protein refinement the protein model can be visualized.

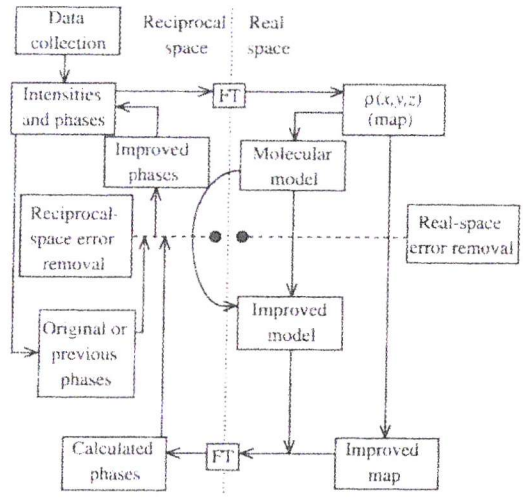

Figure 3.7 A flow diagram of crystallographic structure determination

The Figure is taken from Rhodes 1993

3.9.2 **Convergence and *R*-factor**

The improvement in the quality of the model during refinement can be followed by monitoring the changes in the crystallographic *R*-factor. As refinement converges to the correct structure, the agreement between the observed (F_{obs}) and calculated structure factor amplitudes (F_{calc}) improves. Values for the *R*-factor range from 0-0.60, where 0.60 is achieved when a set of F_{obs} is compared with a random set of amplitudes.

The *R*-factor is related to the residual being minimized and can thus be reduced by refining against an increased number of parameters without actually improving the model. This problem is overcome by monitoring the free *R*-factor (*R*-free) in conjunction with the *R*-factor. The *R*-free gives an idea of the extent of any model-bias and is calculated using 5 % of the total reflections. These reflections are not used in the refinement and thus provide an unbiased assessment whether the refinement is improving the agreement between *Fo* and *Fc*.

Chapter 4

The high resolution structure of cytochrome c_L from *Methylobacterium extorquens*

4.1 Introduction

Cytochrome c_L is a large, soluble *c*-type cytochrome, which is the specific physiological electron acceptor from MDH, and its amino acid sequence bears no relationship to any other type of *c*-type cytochrome (Section 1.15) (O'Keeffe & Anthony, 1980a & b; Beardmore-Gray *et al.*, 1982; Nunn & Anthony, 1988; Anthony, 1992). MDH donates electrons in two single steps to cytochrome c_L; a semi-quinone is formed after the first electron is transferred (Dijkstra *et al.*, 1989). Cytochrome c_L is oxidized by cytochrome c_H (Read *et al.*, 1999). The crystal structure of cytochrome c_L had not been previously solved, although the X-ray crystal structure of the highly related cytochrome c_{551i} from *Paracoccus denitrificans* has been published (Chen *et al.*, 1994). The aim of this work was to grow crystals and solve the structure of cytochrome c_L from *Methylobacterium extorquens.*

Cytochrome c_{551i} is the physiological electron acceptor for methanol dehydrogenase in *P. denitrificans* (Ferguson, 1991). Its crystal structure was solved to 2.4 Å in a three-way crystal complex with amicyanin and methylamine dehydrogenase (Chen *et al.*, 1994). This complex is fortuitous and is not important in the process of methylamine oxidation which involves direct electron transfer between methylamine dehydrogenase and the blue copper protein amicyanin (Davidson & Sun, 2003). As expected, the sequence similarity between cytochrome c_{551i} and cytochrome c_L is high (52 % identity) (Figure 4.1). Cytochrome c_L is larger than cytochrome c_{551i}; the gene sequence revealed it has 172 amino acids (Nunn & Anthony, 1988), whereas cytochrome c_{551i} has 157. The three-dimensional structure for cytochrome c_{551i} revealed a cytochrome *c* tertiary fold, with three central helices surrounding a single haem *c* prosthetic group (Chen *et al.*, 1994). The axial ligands to the haem were provided by a methionine sulphur atom and a histidine nitrogen, as was expected. The high degree of sequence similarity with cytochrome c_L made cytochrome c_{551i} an excellent phasing model for molecular replacement, once suitable crystals and diffraction data for cytochrome c_L had been obtained.

Figure 4.1 The sequence alignment of cytochrome c_L from *M. extorquens* and cytochrome c_{551i} from *P. denitrificans*

The black numbering corresponds to cyt c_L, and the numbering in red corresponds to cyt c_{551i}. Those residues which are blocked in red are acidic, those in blue basic, those in purple hydrophobic and those in green hydrophilic. The three residues in white are Pro, Gly and Ala, and cysteines are represented in yellow blocks.

4.2 **Purification and crystallization of cytochrome c_L**

The purification of cytochrome c_L from *M. extorquens* is described in Section 2.5, and is based on the procedure published by Day and Anthony (1990b). A 15 litre bacterial culture produced a 250 µl protein solution of pure cytochrome c_L, which had a protein concentration of approximately 20 mg/ml. Although this is a poor yield (which is due to the many steps required to produce a pure protein sample), it was enough protein to use with the Molecular Dimensions crystal screen, to search for initial protein crystal hits. Figure 4.2 shows an SDS-PAGE gel of the protein sample which was used for the crystallography experiments.

Crystals of cytochrome c_L were formed using the 'hanging drop' vapor diffusion method (Section 2.7). Hanging drops were obtained by mixing equal volumes (2 µl) of protein solution (20-25 mg/ml cytochrome c_L in 20 mM Tris-HCl buffer, pH 8.0) and a solution from the crystal screen. These drops were suspended above a 1 ml reservoir solution and allowed to equilibrate in a sealed well. Crystals were obtained from three of the one hundred solutions from the screen (Table 4.1). The best crystals were produced from solution 20 of screen I. These conditions produced fewer crystals than the other two sets of conditions but they appeared less needle-like and more spaced out throughout the drop. Table 4.2 shows the subsequent experiments that optimized the conditions for crystal growth. Figure 4.3 shows a crystal which was produced after optimization of the best crystal hit; it was rod-shaped and had dimensions of approximately 900 µm × 100 µm × 100 µm. The crystal was frozen using glycerol as the cryo-protectant, as described in Section 2.10.

4.3 **Data collection and processing**

One hundred and eighty degrees of X-ray diffraction data from a single cytochrome c_L crystal were collected using an ADSC Quantum detector at the ESRF (Grenoble, France beamline ID-19). MOSFLM was used to index the diffraction images and suggested a tetragonal space group of 4 or 422, with unit cell dimensions of a = 66.5 Å, b = 66.5 Å, c = 39.0 Å; as it was a tetragonal point group the angles α, β and γ were 90 °. The data were indexed in the P4 space group to a resolution of 2.0 Å, sorted, scaled and truncated using the programs from the CCP4 suite. After processing the data, the reflection file was viewed using the CCP4 program HKLVIEW, to distinguish between possible space groups (Figure 4.4). No diagonal symmetry was seen in the reflection data, this rules out the point group 422. Systematic absences were also seen along the 00l axes in HKLVIEW (Figure 4.5); this indicated a $P4_3$ or

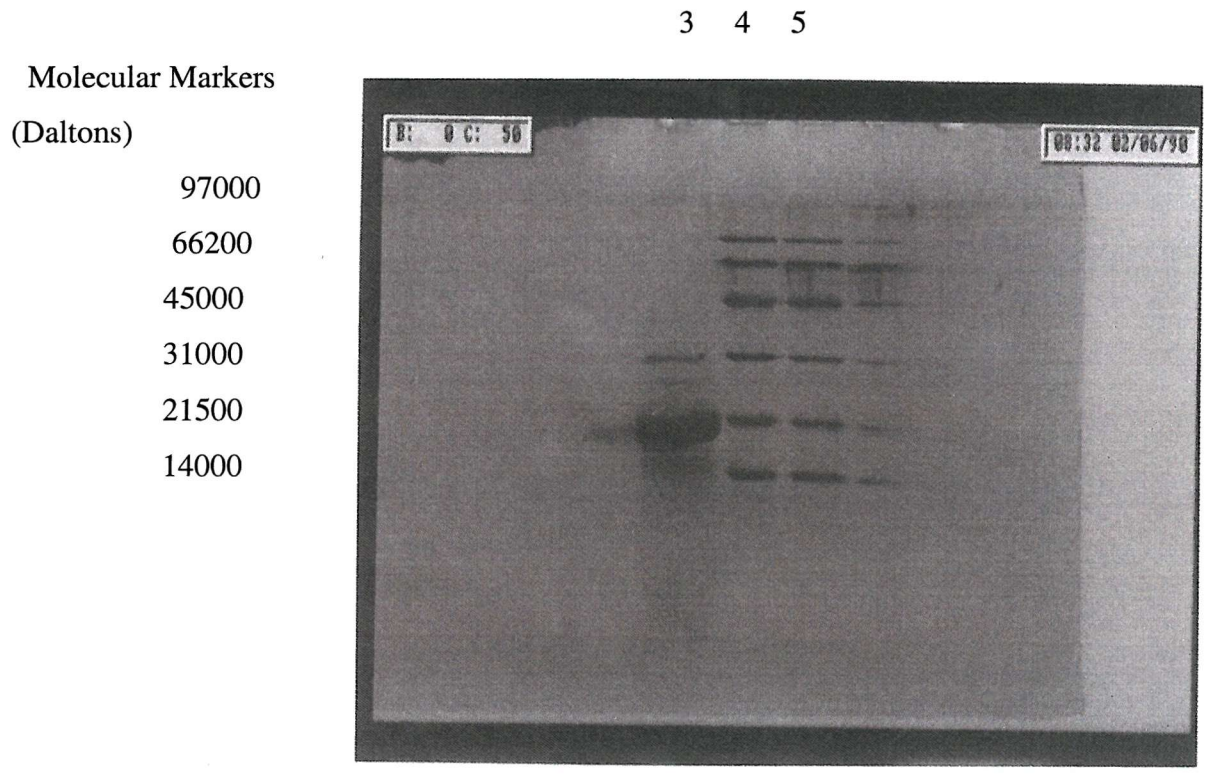

Figure 4.2 SDS-PAGE showing purified cytochrome c_L

Lane 3=Pure cytochrome c_L after the final purification step (anion exchange).

Lane 4= Molecular markers (SDS-PAGE, low range molecular markers, Biorad)

Lane 5= Molecular markers (SDS-PAGE, low range molecular markers, Biorad)

.

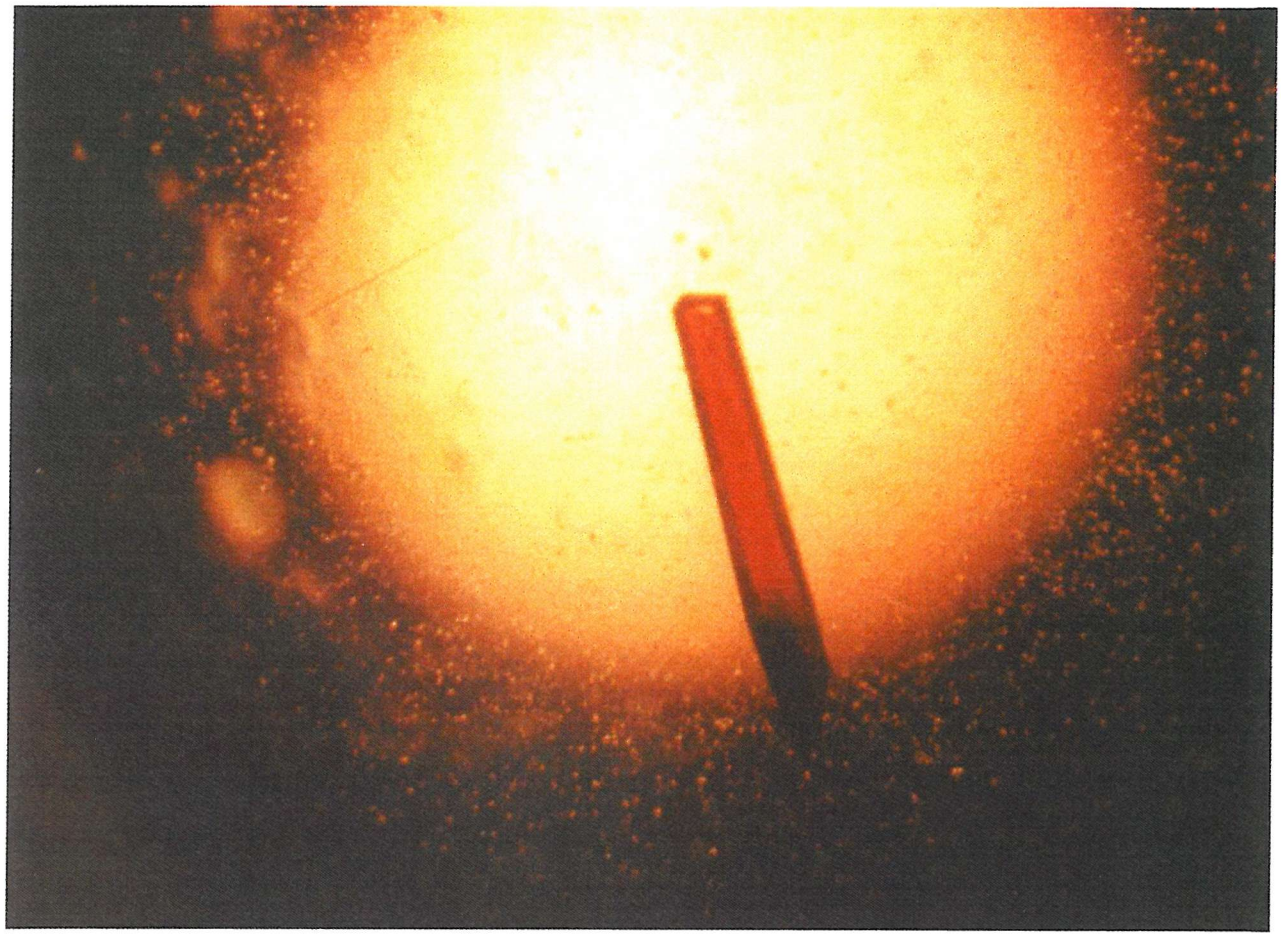

Figure 4.3 A cytochrome c_L crystal

Hanging drops were obtained by mixing equal volumes of protein solution (20 mg/ml cytochrome c_L in 20 mM Tris-HCL buffer, pH 8.0) and a reservoir solution (18 % PEG-8 K, 0.1 M sodium cacodylate and 0.2 M calcium acetate, buffered to pH 6.5). The crystals appeared after a 4 week incubation in the dark, at room temperature. The crystals had the dimensions of approximately 900 μm × 100 μm × 100 μm.

Table 4.1 The three crystal hits obtained from the Molecular Dimensions limited structure screens I and II for X-ray crystallography

Kit Number	Solution Number	Ingredients	Appearance
Screen II	26	30 % PEG-MME 5 k 0.2 M ammonium sulphate 0.1 M MES, pH 6.5	Dark red, thin needles, clustered together
Screen I	14	30 % PEG 8 k 0.1 M sodium cacodylate 0.2 M ammonium sulphate pH 6.5	Dark red, thin needles, clustered together
Screen I	20	18 % PEG 8 k 0.1 M sodium cacodylate 0.2 M calcium acetate, pH 6.5	Dark red, more chunky, rod like crystals

Table 4.2 The optimization of conditions for crystallizing cytochrome c_L

The pH was kept at 6.5 and the concentration of calcium acetate was 0.1 M.

* The best crystals were produced in the drops containing 45 % PEG and a cacodylate concentration of 0.14-0.28 M (shaded)

0 M $(CH_3)_2AsO_2Na$ 0 % PEG 5K MME	0.07 M 0.00 %	0.14 M 0.00 %	0.21 M 0.00 %	0.28 M 0.00 %	0.35 M 0.00 %
0 M 15 %	0.07 M 15 %	0.14 M 15 %	0.21 M 15 %	0.28 M 15 %	0.35 M 15 %
0 M 30 %	0.07 M 30 %	0.14 M 30 %	0.21 M 30 %	0.28 M 30 %	0.35 M 30 %
0 M 45 %	0.07 M 45 %	0.14 M 45 %	0.21 M 45 %	0.28 M 45 %	0.35 M 45 %

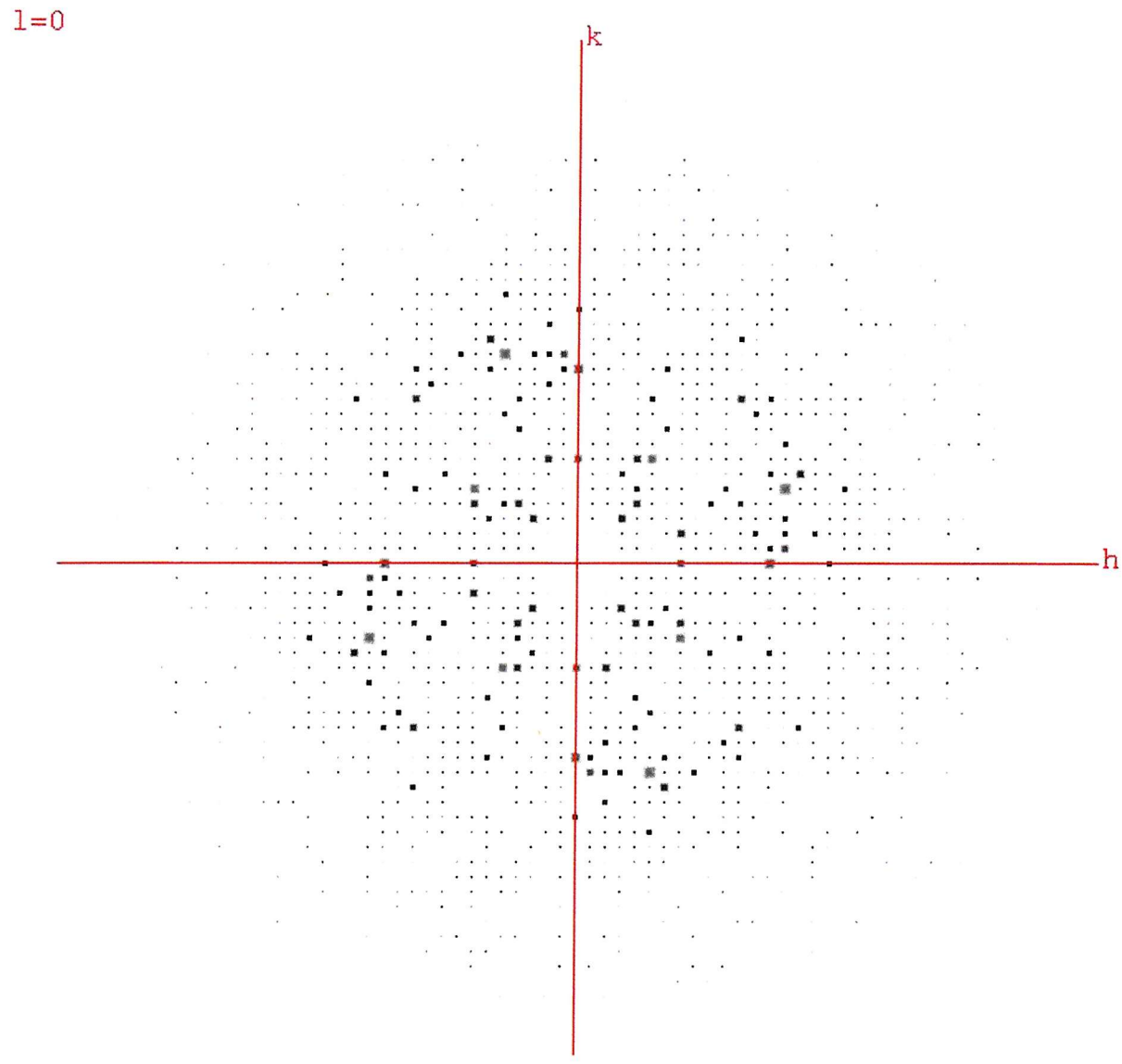

Figure 4.4 The *hk*0 diffraction data from cytochrome c_L viewed along the 00*l* axis

HKLVIEW shows there was no diagonal symmetry in the data, which indicates that the point group is not 422.

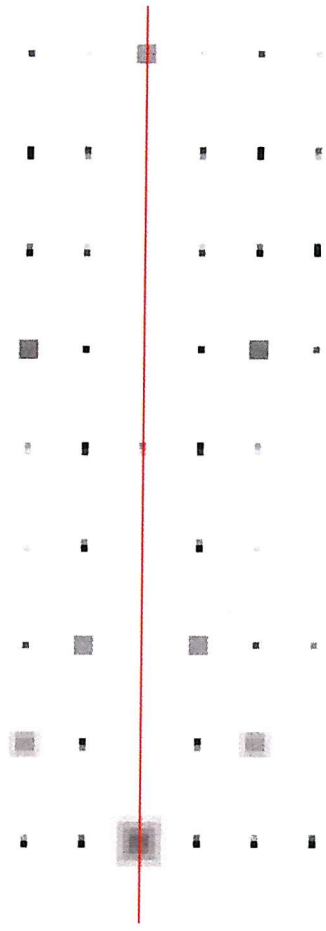

Figure 4.5 Systematic absences along the 00l axes

Systematic absences every four reflections indicates that there is a screw axis in the space group; this suggests a $P4_1$ or a $P4_3$ space group.

$P4_1$ symmetry, and not a P4 space group. Space groups $P4_3$ and $P4_1$ cannot be distinguished on the basis of systematic absences in the diffraction data. To distinguish between these two space groups, the data were processed in both $P4_3$ and $P4_1$ and the reflection files for both space groups were used for molecular replacement, using MOLREP (see below).

4.4 **Molecular replacement studies on cytochrome c_L**

Initial phases for the cytochrome c_L structure were obtained using molecular replacement, using the program MOLREP (Vagin and Teplykov, 1997); the phasing model was cytochrome c_{551i}; the haem and all water molecules were removed from the model. Table 4.3 shows that both sets of reflection data produced identical peaks when running the rotation function; the radius of integration used was 30 Å. MOLREP generated a strong rotation solution ($\alpha = 3.19^{\circ}$ $\beta = 76.29^{\circ}$ $\gamma = 318.21^{\circ}$) of 6.54 σ above the noise (with the next peak being 4.14 σ); this corresponds to the orientation of cytochrome c_L in the asymmetric unit. Table 4.4 shows the translation peaks found when using the orientation from the rotation peak, for both possible space groups. The space group that resulted in the best translation peak was $P4_3$; the translation search gave a strong peak of 7.95 σ above the noise (with the next peak being 3.80 σ). By contrast, when using the data processed in $P4_1$ the translation search produced no discernable peak (Table 4.4). Therefore it was concluded that $P4_3$ was the correct space group. To confirm this, the protein coordinate file from MOLREP was refined using the programs from the CNS program package, and electron density maps were made and visualized using the graphical package QUANTA (San Diego: Molecular Simulations, 1996). The *Fo-Fc* and *2Fo-Fc* electron density maps showed vacant electron density where the haem could be fitted (Figure 4.6). The position of the density for the haem would allow it to be covalently linked to Cys65 and Cys68.

4.5 **Refinement of the cytochrome c_L structure**

The cytochrome c_L structure was refined to a resolution of 2.0 Å using the refinement programs of the CNS suite. All unique reflections (11,712) from the resolution range of 10.0-2.0 Å were used. A test set of reflections (5 %, 587 reflections) were used for the *R*-free calculations. Initially the model was subjected to rigid body refinement, torsion angle simulated annealing and individual B-factor refinement.

Extensive rebuilding and refinement of the model was required. During rebuilding, regions of the model in poor agreement with the electron density were adjusted and the side

Table 4.3 The rotation solutions from MOLREP

The diffraction data were processed in both $P4_1$ and $P4_3$, both reflection files produced the same rotation solution.

a) $P4_1$

Peak Number	α	β	γ	Rf/σ
1	3.19	76.29	318.21	6.54
2	27.27	109.15	150.14	4.14
3	45.28	104.77	168.33	3.62
4	75.47	169.81	207.76	3.56
5	49.82	148.19	47.87	3.55
6	82.55	69.06	109.93	3.53
7	56.60	75.56	125.15	3.51
8	20.95	53.94	274.79	3.47
9	56.39	109.06	290.28	3.44
10	66.69	50.04	267.86	3.41

b) $P4_3$

Peak Number	α	β	γ	Rf/σ
1	3.18	76.29	318.21	6.54
2	27.27	109.15	150.14	4.14
3	45.28	104.77	168.33	3.62
4	75.47	169.81	207.76	3.56
5	49.82	148.19	47.87	3.55
6	82.55	69.06	109.93	3.53
7	56.60	75.56	125.15	3.51
8	20.95	53.94	274.79	3.47
9	56.39	109.06	290.28	3.44
10	66.69	50.04	267.86	3.41

Table 4.4 The translation solutions from MOLREP

The diffraction data which were processed in $P4_3$ produced a discernable translation peak. There was no peak with the $P4_1$ data.

a) $P4_1$

Peak Number	X	Y	Z	Density/σ
1	0.389	0.044	0.00	4.18
2	0.356	0.055	0.00	4.02
3	0.275	0.403	0.00	3.83
4	0.248	0.058	0.00	3.18
5	0.930	0.046	0.00	2.94

b) $P4_3$

Peak Number	X	Y	Z	Density/σ
1	0.250	0.058	0.00	7.95
2	0.013	0.415	0.00	3.80
3	0.427	0.010	0.00	3.22
4	0.358	0.076	0.00	3.06
5	0.319	0.049	0.00	3.00

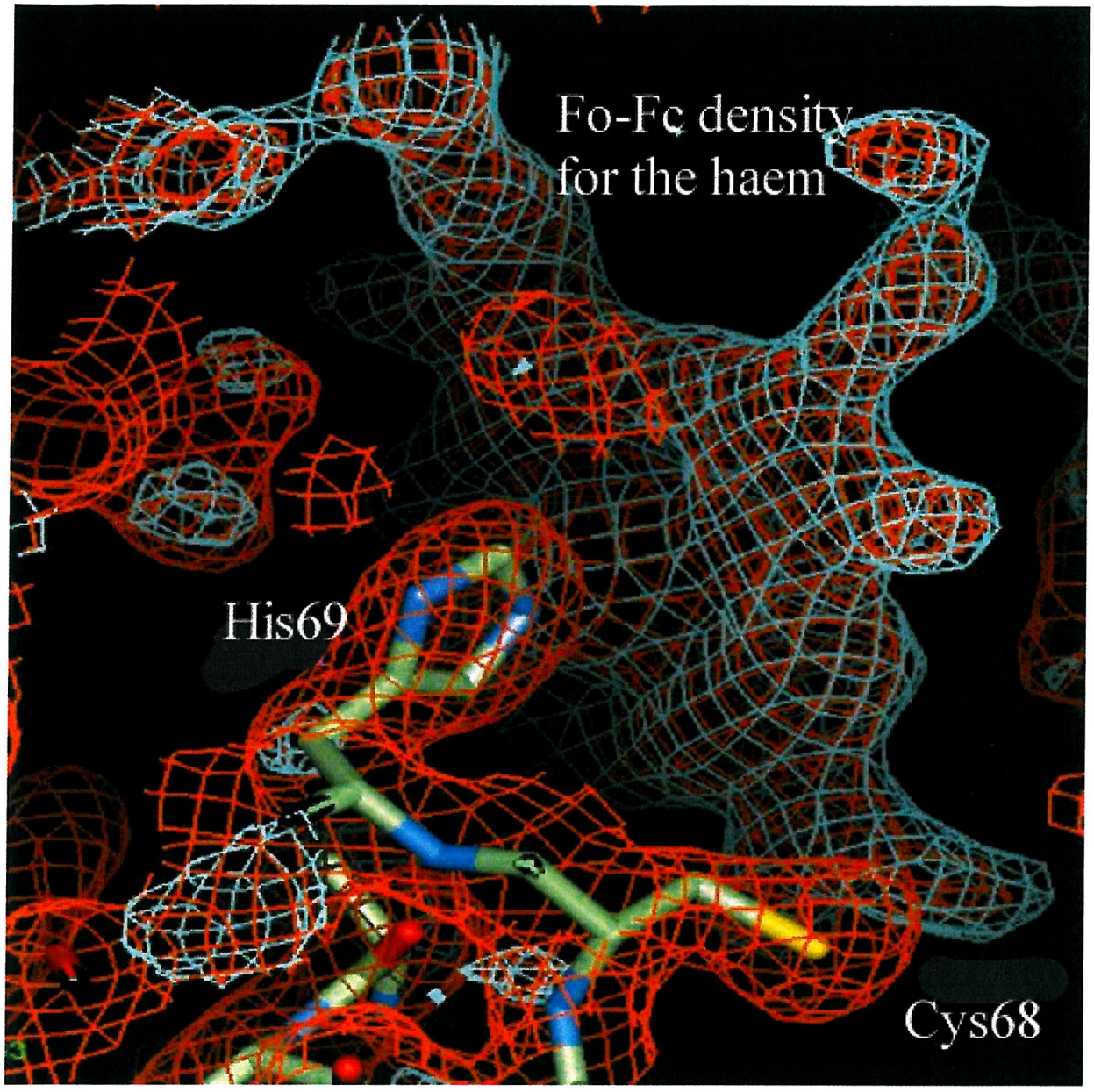

Figure 4.6 The *Fo-Fc* electron density (blue density) which corresponds to the position of the haem in cytochrome c_L

The presence of *Fo-Fc* electron density in this region is further evidence of a correct molecular replacement solution.

chains which lacked electron density were replaced with an alanine residue. After several rounds of refinement the phases for the model improved and *Fo-Fc* electron density returned for these residues which allowed the correct residue to replace the alanine. The amino acid sequence deduced from the X-ray structure matched the sequence deduced from the gene sequence with the exception of two residues at the N-terminus. This region of the protein was difficult to visualize in the electron density maps, consequently both Gln25 and Glu28 were assigned as glycine residues.

After several rounds of rebuilding and refinement, the haem prosthetic group was imported into the electron density maps; Figure 4.7 shows the initial fit of the haem into the electron density. After the haem was imported into the structure, water molecules were incorporated at stereochemically acceptable sites following visual verification of the *2Fo-Fc* maps. The water molecules were kept if, after refinement, they formed hydrogen bonds with chemically-appropiate groups, and had a B-factor of less than 60 $Å^2$. The final model had an *R*-factor of 21.05 %, an *R*-free value of 23.83 %, and consisted of 1124 protein atoms, 1 haem prosthetic group, 1 calcium ion and 78 water molecules.

4.6 **The 1.6 Å resolution structure of oxidized cytochrome c_L from *M. extorquens***

Another data set from a larger crystal (which was grown under the same conditions) was collected. Prior to freezing, individual crystals were soaked for one week in native mother liquor which had been supplemented with 20 mM potassium ferricyanide, this was to fully oxidize the cytochrome. The crystal was frozen, with glycerol as the cryo-protectant.

4.6.1 **Data collection and processing**

X-ray data were collected from the oxidized crystal of cytochrome c_L, using an ADSC Quantum detector at the ESRF (Grenoble, France). The crystal diffracted to approximately 1.6 Å; a single diffraction pattern is shown in Figure 4.8. The unit cell dimensions (a = 65.9 Å, b = 65.9 Å, c = 38.9 Å, α, β, γ angles = 90 °) were determined using MOSFLM. Also MOSFLM determined the space group to be $P4_3$, the same as for the previously solved cytochrome c_L structure. Both a high and a low-resolution data set were collected and processed. Table 4.5 shows the final data processing statistics for the 1.6 Å resolution structure. As the unit cell dimensions are virtually the same as the previously solved cytochrome c_L structure, molecular replacement was not necessary. The structure was solved by using the new reflection file with the slightly altered unit cell dimensions, and the final

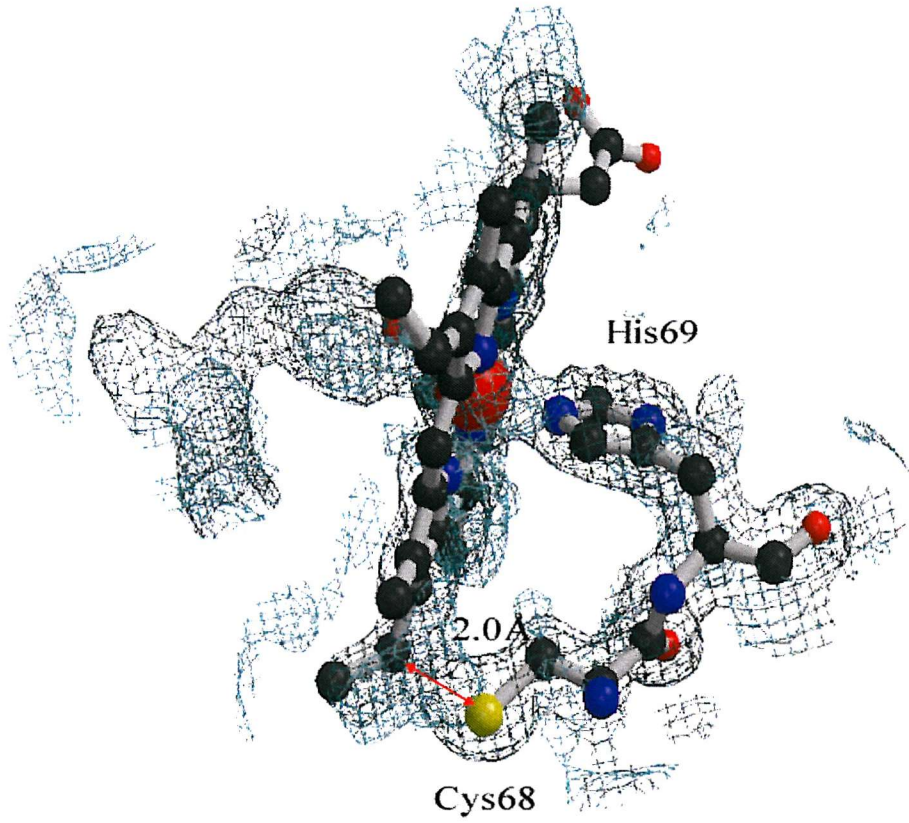

Figure 4.7 The electron density into which the haem prosthetic group was built into.

The haem, once fitted, was in the correct orientation for coordination with His69 and covalent bonding to Cys68. The covalent bond is shown as a red arrow in the Figure.

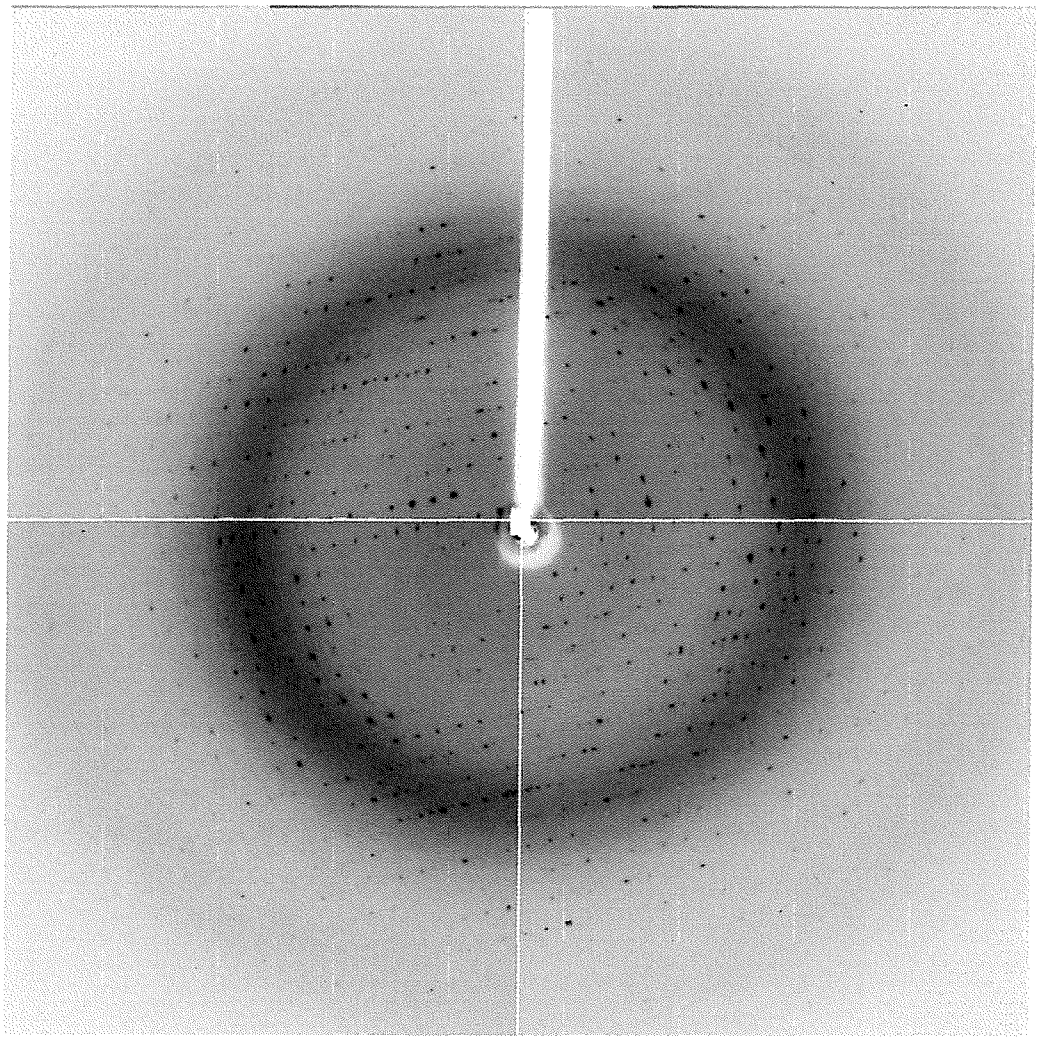

Figure 4.8 A diffraction pattern from an oxidized cytochrome c_L crystal

One hundred and eighty degrees of X-ray diffraction data were collected for a high and low-resolution data set; the crystal diffracted to 1.6 Å.

Table 4.5 The data processing statistics for the 1.6 Å structure of oxidized cytochrome c_L

Total number of reflections	148704
Number of unique reflections	24326
Resolution (Å)	1.6 Å
Completeness (%)	96.1 %
R_{merge} (outer resolution shell)	0.114 (0.221)
Multiplicity	6.4
Average I/σ(I) (outer resolution shell)	5.36 (2.5)

pdb file from the previously solved and refined cytochrome c_L structure.

4.6.2 **Refinement of the 1.6 Å resolution structure of oxidized cytochrome c_L**

After the initial round of refinement, which included a rigid-body refinement, torsion angle simulated annealing and individual isotropic B-factor refinement, the *R*-factor and *R*-free were 28.90 % and 30.67 % respectively. As the resolution of the data was 1.6 Å rather than 2.0 Å, more water molecules could be seen in the electron density maps when they were visualized in QUANTA. Therefore further water molecules were placed at stereochemically acceptable sites following visual verification of the *2Fo-Fc* maps, and were kept if after refinement they had a B-factor of less than 60 $Å^2$. During rebuilding of the model, regions in poor agreement with the electron density were adjusted, and the side chains which lacked electron density were replaced with alanine residues. After several rounds of refinement the phases for the model improved and the *Fo-Fc* density returned for the correct side chains, which were then returned to the model. The final model has an *R*-factor of 20.94 % and an *R*-free of 25.05 %. It consists of 1133 protein atoms, 1 haem group, 1 calcium ion and 173 water molecules. Table 4.6 shows the refinement statistics for the model. The 1.6 Å cytochrome c_L structure was compared with the 2.0 Å structure. There were no obvious differences between the two structures, the distance between the two sulphur atoms in the disulphide bridge was unchanged (2.02 Å and 2.04 Å), the calcium ion ligands were unchanged (as were the Ca^{2+}-oxygen distances) and the residues which were coordinated to the haem iron were His69 and His112 in both structures.

4.7 **The X-ray crystal structure of oxidized cytochrome c_L**

Of the 172 expected amino acid residues in the cytochrome c_L, 25 residues at the N-terminus were absent from the electron density maps. This is the section of the protein which shows least similarity to cytochrome c_{551i} (Figure 4.1). In this N-terminal region of cytochrome c_L and cytochrome c_{551i}, 30 % of the residues are identical and an additional 56.5 % are similar. Of the remaining 134 residues with a direct counterpart, 62 % are exactly the same and an additional 25 % are similar. The Mass spectrometry data (Figure 4.9) showed that the cytochrome c_L which was used for the crystallography was 18-19 kDa. This correlates with the size of cytochrome c_L based on the gene sequence (18,735 Da), which was originally published by Nunn & Anthony (1988). Furthermore the protein was N-terminally blocked, presumably due to the spontaneous formation of pyroglutamate from glutamine at the N-terminal, as found in other bacterial *c*-type cytochromes. This prevented N-terminal

Table 4.6 The refinement statistics for the 1.6 Å structure of oxidized cytochrome c_L

Resolution range	10-1.6 Å
R-factor (%)	20.94
R-free (%)	25.05
Number of reflection in working set	20501
Number of reflections in test set (4.6 %)	1034

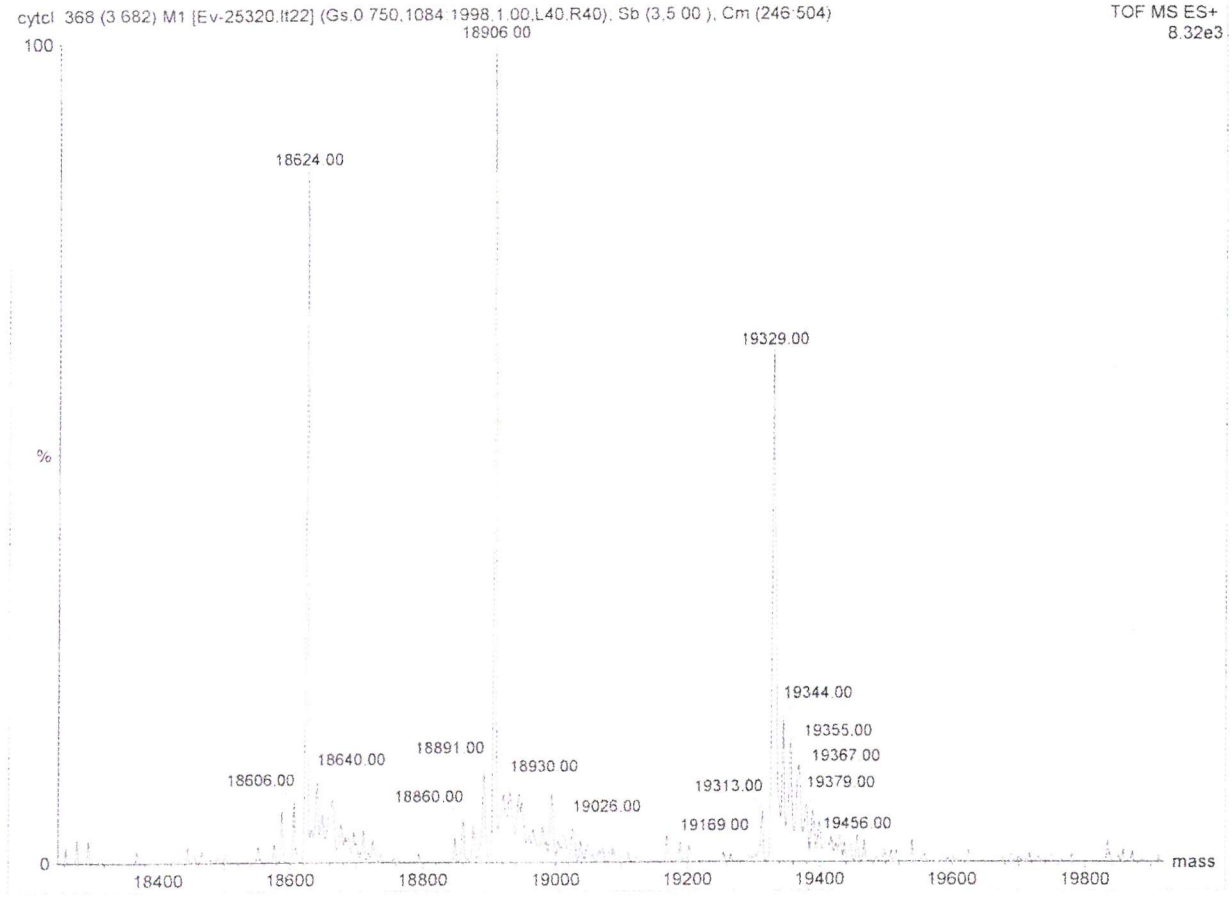

Figure 4.9 Mass spectrometry data from the protein sample which was used to prepare the cytochrome c_L crystals

The data shows that there were three similar sized proteins present in the sample which was used to prepare the cytochrome c_L crystals. All of which are around the mass which was expected from the amino acid sequence (18,735 Da).

sequencing of the cytochrome, as was also the case originally for cytochrome c_L (Nunn & Anthony, 1988). Figure 4.10 indicates where the unseen N-terminal residues would be in the molecule (if they were present), assuming that they were in the same position as the first 25 residues in cytochrome c_{551i}. The Figure shows the complete protein structure of cytochrome c_{551i}, which was used in the molecular replacement search. The non-visible N-terminal region of cytochrome c_L is likely to be a long flexible arm which wraps around the protein exterior. To attempt to trace the electron density for the missing residues several automated refinement programs were used. The programs used were Arp Warp (Morris *et al.*, 2002), Maid (Levitt *et al.*, 2001) and density modification (Cowtan, 1994). Unfortunately none of these programs were able to trace the missing N-terminal fragment. It is therefore possible that this region was removed during the process of crystallization or is disordered in the crystal. If the missing region in cytochrome c_L is similar to the corresponding region in cytochrome c_{551i}, removing this segment creates a more compact protein. This possibly increases the number of crystal contacts and aids crystallization. That cytochrome c_L/cytochrome c_{551i} is difficult to crystallize is highlighted by the fact that cytochrome c_{551i} from *P. denitrificans* could not be crystallized alone and was required to be in a complex with amicyanin (Chen *et al.*, 1994; F. S. Mathews, personal communication).

The remaining 152 amino acids of cytochrome c_L are present in the model, although Glu28 was changed to a glycine residue to compensate for a lack of electron density for the side chain. Figure 4.11 shows the Ramachandran plot of the 152 residues from the protein model; Ala105 and Lys27 were in disallowed regions. The Lysine is at the N-terminal region of the protein where the electron density was poor. It was therefore difficult to build this residue into the available electron density. Ala105 is in a solvent-exposed flexible loop region which connects two helices. Altering the residue to a conformation to suit the Ramachandran plot moved the residue from the areas where it best fit the electron density, and so it was left in the unconventional conformation.

4.7.1 **The oxidation state of the cytochrome c_L crystal**

An absorption spectrum of the cytochrome c_L crystal which was used for the 1.6 Å data collection was performed at the ESRF Cryobench facility (D. Bourgois); this was to determine the oxidation state of the cytochrome (Figure 4.12). Of special interest were the regions around the wavelengths 500-550 nm and 695 nm. Figure 1.24, in Section 1.15.4, shows the absorption spectra of reduced and oxidized cytochrome c_L. Reduced cytochrome c_L has a β-peak at 520 nm and an α-peak at 550 nm; these peaks disappear when the protein is

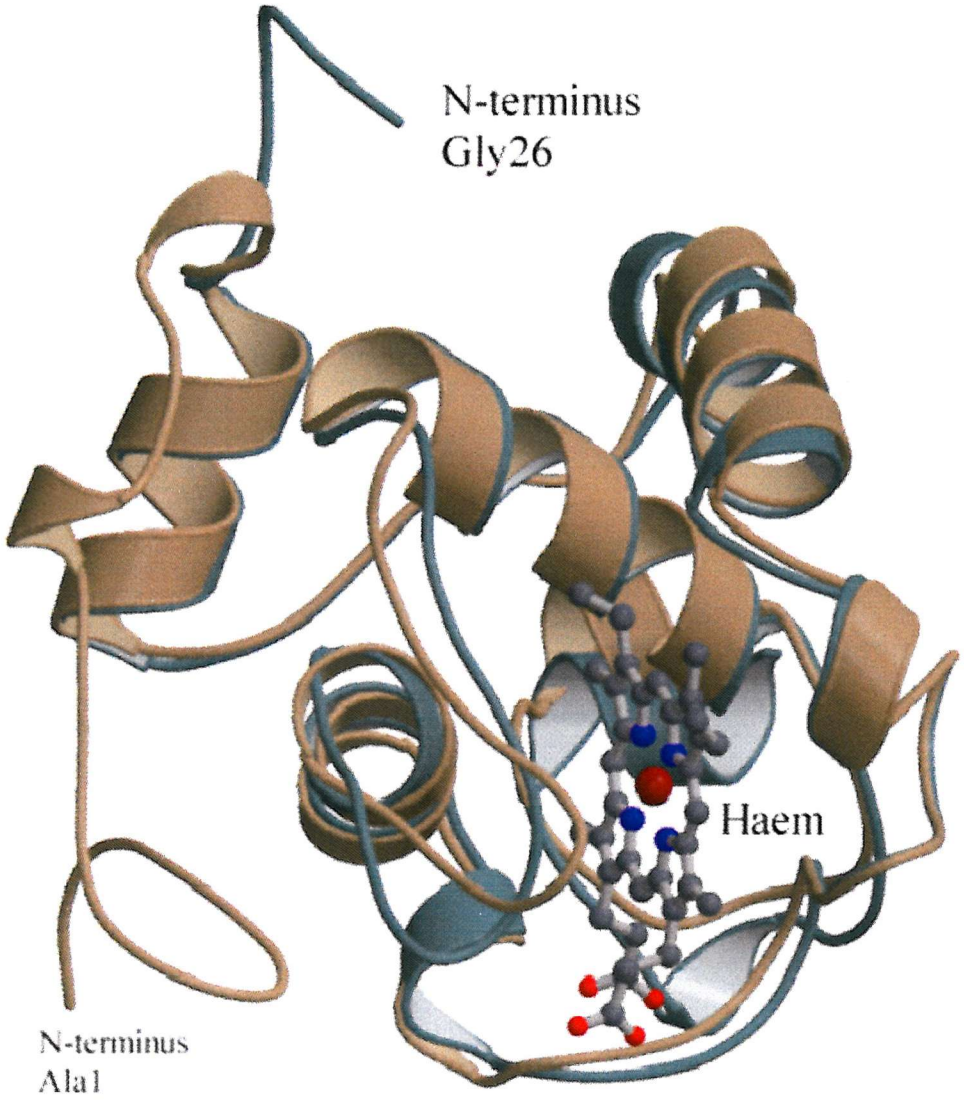

Figure 4.10 The tertiary structure of cytochrome c_L (green) and cytochrome c_{551i} (brown) superimposed together

The 25 N-terminal residues were not seen in cytochrome c_L crystal structure

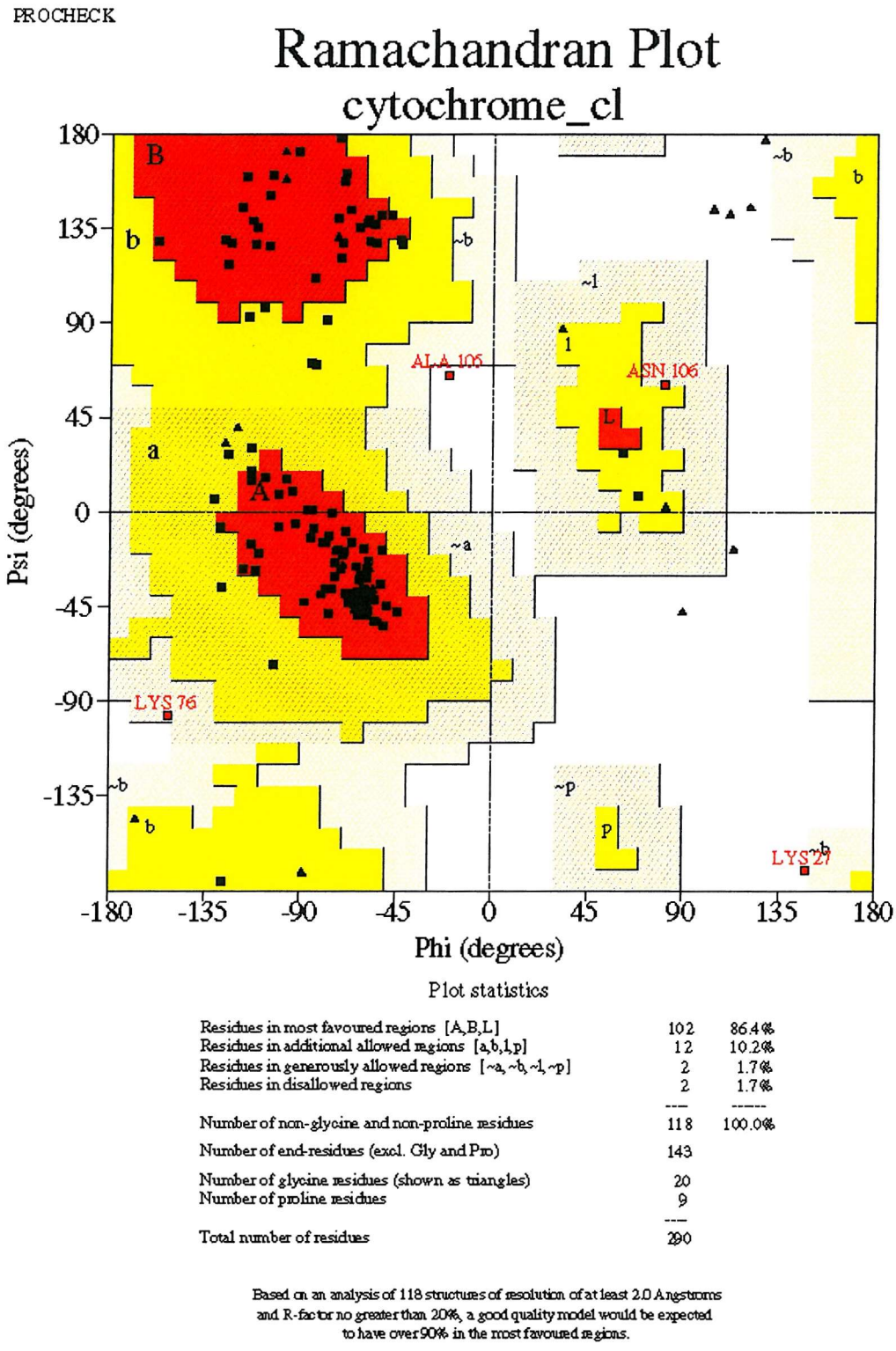

Figure 4.11 A Ramachandran plot of the 1.6 Å structure of oxidized cytochrome c_L

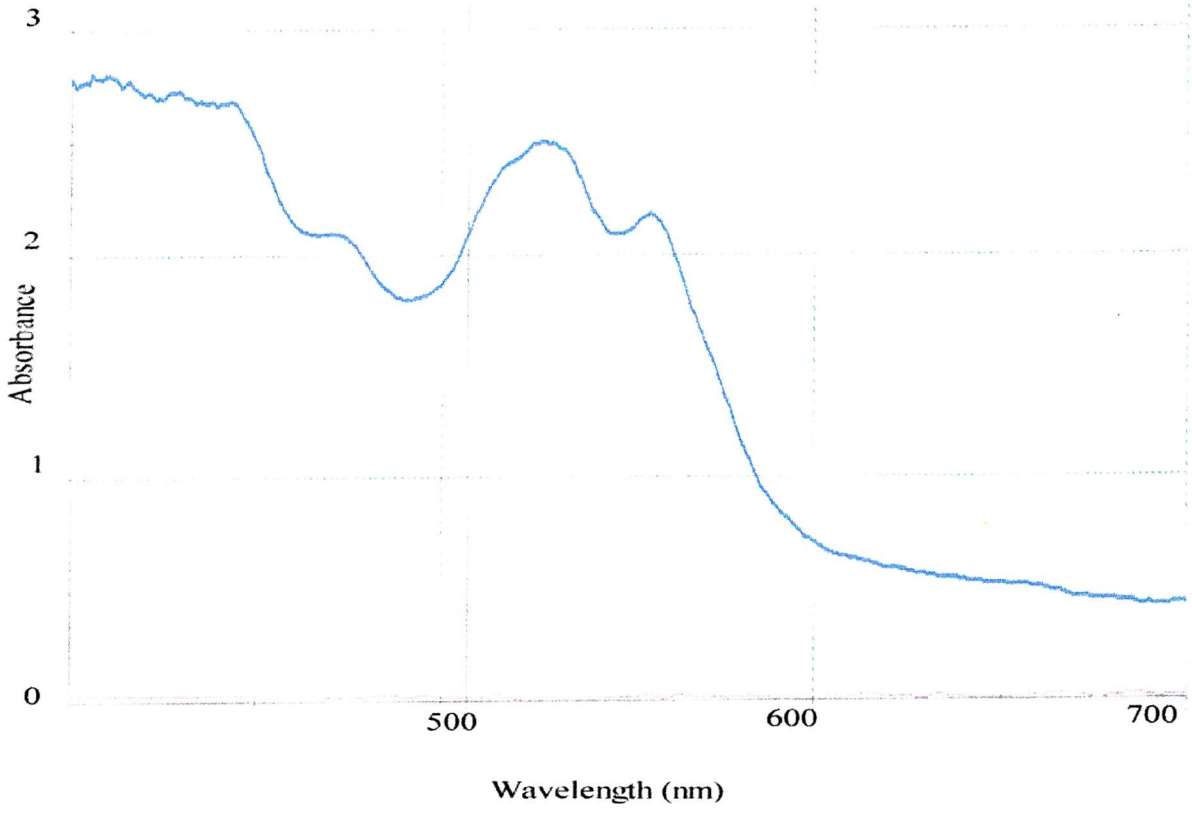

Figure 4.12 An absorption spectrum of the cytochrome c_L crystal which was used for the 1.6 Å data collection

The absorption spectrum shows two broad peaks around 550 nm; this shows the crystal was oxidized. There is no peak at 695 nm; this peak is characteristic of a His-Fe-Me coordination, the absence of such a peak suggests an alternative haem iron coordination in the cytochrome c_L crystal. The region around 400-420 nm could not be measured due to the high optical absorbance of the crystal below 450 nm

oxidized. Oxidation also causes the γ peak at ~415 nm to become smaller and 6 nm blue shifted. The absorption spectrum of the cytochrome c_L crystal which was used for data collection has two broad, very small peaks at 520 nm and 550 nm (Figure 4.12); this shows that the crystal was in the oxidized (ferric) state. Interestingly, there was no 695 nm absorption peak indicating that there was no Met-iron coordination as seen in class I cytochromes *c*, and which has previously been seen in spectra of solutions of the oxidized cytochrome c_L (Beardmore-Gray *et al.*, 1982).

4.7.2 **The tertiary structure of cytochrome c_L**

The text in this section is accompanied by Figures 4.13, 4.14, 4.15 and Table 4.7. The Table summarizes the loops and helical sections of cytochrome c_L, cytochrome c_{551i}, mitochondrial cytochrome *c* (tuna) and cytochrome c_2 from *Rhodospirillum rubrum*. Figure 4.13 shows a stereo picture of cytochrome c_L and Figures 4.14 4.15 show a comparison between the tertiary structures of cytochrome c_L, mitochondrial cytochrome *c* and cytochrome c_2. For convenience these proteins will be abbreviated to cyt c_L, cyt c_{551i}, cyt c_M and cyt c_2.

Cyt c_L is a compact protein which has six α-helical regions (Figure 4.15). The main three helices (helix A, E and C) are highly conserved among class I *c*-type cytochromes and they serve to partially enclose the haem *c* prosthetic group. This is covalently linked to the protein via two thioether bonds to Cys65 and Cys68, and the iron was unexpectedly coordinated to two histidine residues (His112 and His69). Cyt c_L has a single calcium ion bound close to the inner haem propionate (Section 4.13), and a disulphide bridge between Cys53 (helix A), and Cys167, which is at the C-terminal end of the protein (Section 4.12). The remainder of this Section will be a comparison of cyt c_L with cyt c_{551i}, cyt c_M and cyt c_2.

Cyt c_L has an amino acid sequence which is unique amongst *c*-type cytochromes (Figure 4.1). It has many properties typical of class I *c*-type cytochromes, such as a Met-His iron ligation and two covalent bonds from the haem to cysteines residues. But cyt c_L differs from class I *c*-type cytochromes in being larger (18,735 kDa) and having the haem binding sequence begin at Cys65 (the haem binding motif is usually within the first 20 residues for typical class I *c*-type cytochromes). Within the large N-terminal extension of both cyt c_L and cyt c_{551i} there is one large α-helix which I have termed the N-terminal helix (cyt c_L 34-42: cyt c_{551i} 28-36).

Helix A begins at residue 52 and carries on through to the first residue of the haem

Table 4.7 The loops and helices of cyt c_L, cyt c_M (tuna), cyt c_2 and cyt c_{551i}

Structure	Cyt c_L	Cyt c_M	Cyt c_2	Cyt c_{551i}
N-terminal helix	34-42	N/A	N/A	28-36
Loop 1	43-51	N/A	N/A	37-48
Helix A	52-64	2-14	4-14	49-58
Loop 2	65-88	15-49	15-49	59-83
Helix B	89-92	50-55	50-57	84-86
Helix C	94-102	61-69	64-72	88-97
Loop 3	103-118	75-88	83-97	98-112
Helix D	N/A	71-74	74-82	N/A
Helix E	119-130	88-101	98-108	113-124
Loop 4	131-135	102-103	108-112	125-138
Helix F	136-138	N/A	N/A	N/A
Loop 5	139-143	N/A	N/A	N/A
Helix G	144-149	N/A	N/A	139-142
Loop6	150-172	N/A	N/A	143-155

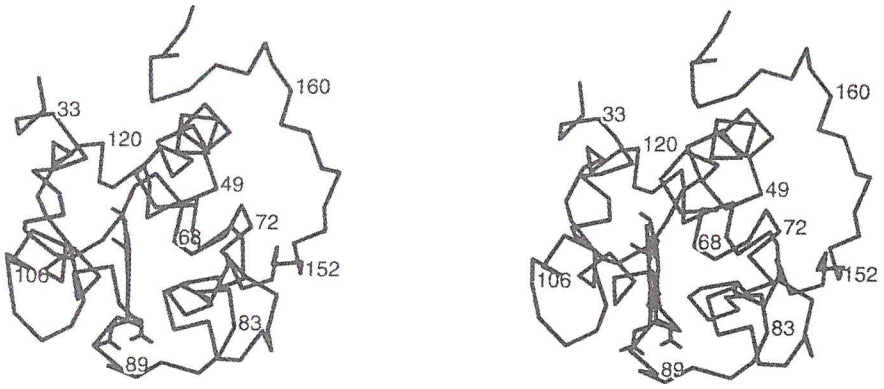

Figure 4.13 A stereo view of the C_α of cytochrome c_L

a) Cytochrome c_2 from *R. rubrum* (cyt c_2)

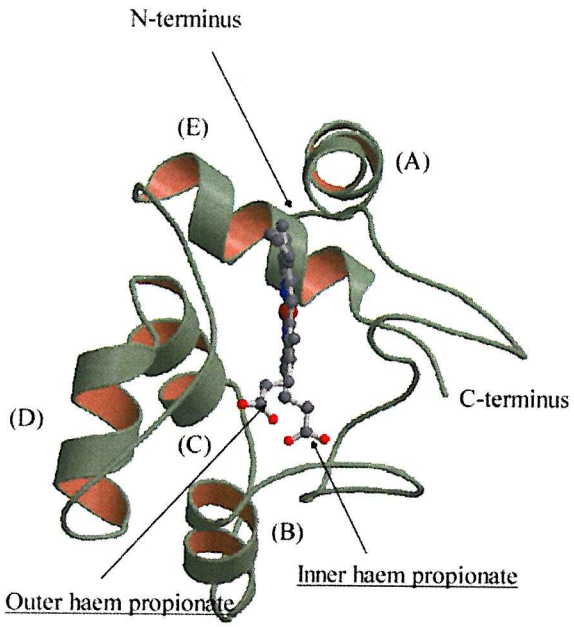

b) Tuna cytochrome *c* (cyt c_M)

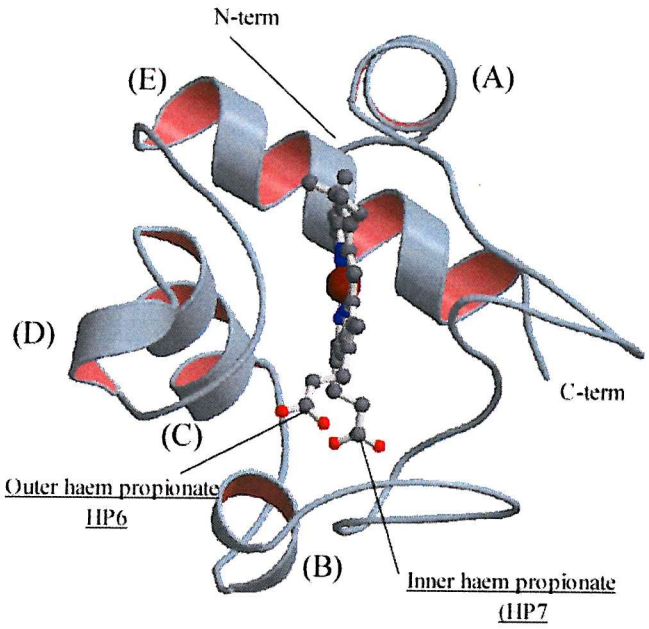

Figure 4.14 **The tertiary structures of (a) cytochrome c_2 and (b) tuna cytochrome *c***

The letters indicate helices (refer to Table 4.7)

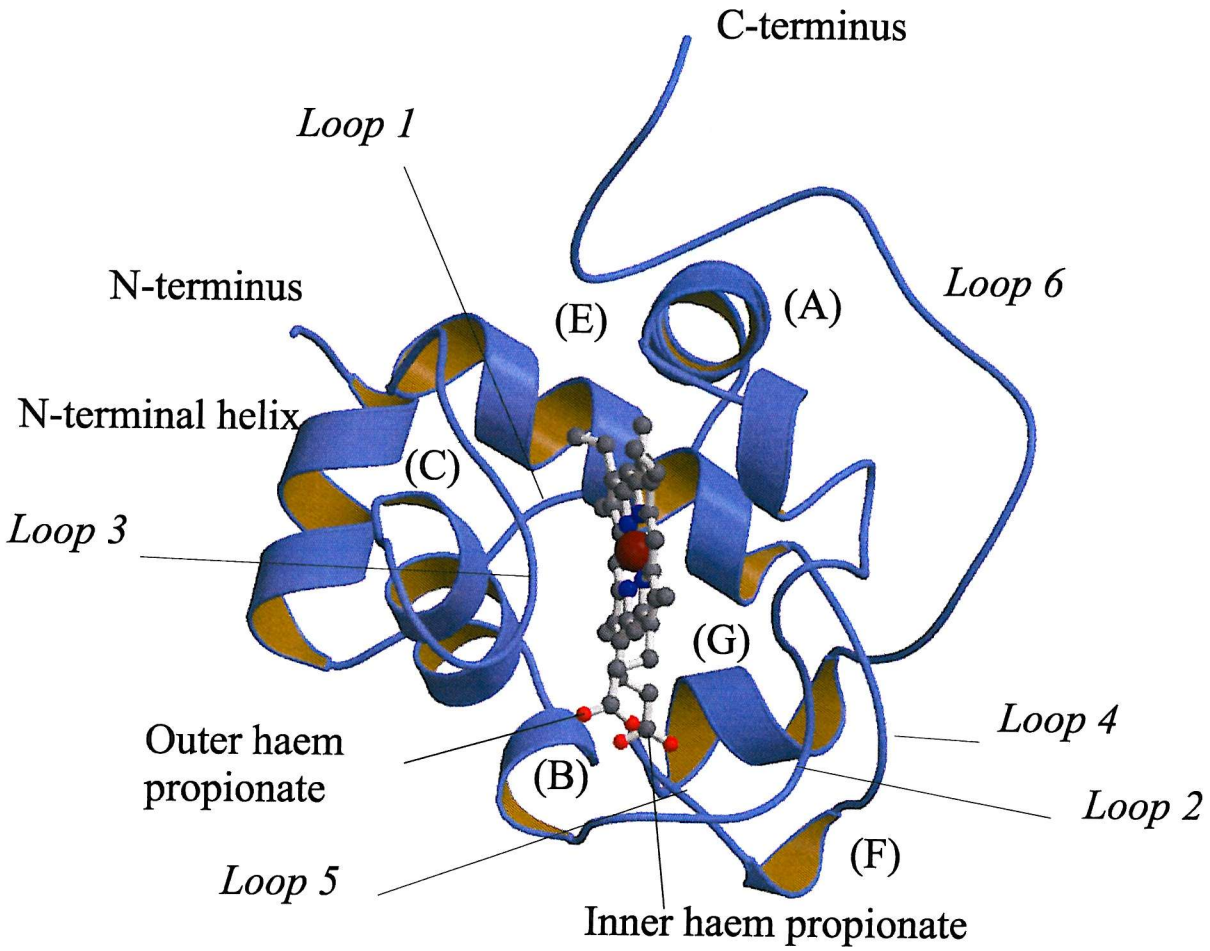

Figure 4.15 The tertiary structure of cytochrome c_L

The letters indicate helices (refer to Table 4.7)

binding motif, Cys65. This helix is conserved throughout the class I cytochrome *c* family and consequently has a counterpart in cyt c_{551i}, cyt c_M and cyt c_2. The first residue prior to the haem binding sequence is Ser64. In both cyt c_M and cyt c_2 this residue is a conserved lysine which hydrogen bonds to a glutamate side chain (cyt c_M; Lys13-Glu90: cyt c_2; Lys13-100) at the beginning of helix E. The serine residue in cyt c_L performs the same role as the lysine, by forming a hydrogen bond with Asn115, which is just before helix E. In cyt c_{551i} the position immediately before the haem binding sequence is Met58, which is not involved in any interactions with another part of the protein.

Loop 2, which travels around the right- hand side and base of cyt c_L (loop 1) connects the haem binding motif with helix B. Within loop 1 there is a conserved proline residue, Pro79 (cyt c_{551i}, Pro73; cyt c_M, Pro30; cyt c_2, Pro30) which forms a hydrogen bond through its carbonyl oxygen to the histidine (His69) coordinated to the iron on the right–hand side of the haem (Section 4.14b and Figure 4.22). Also in loop 1 are the amino acids which are coordinated to the calcium ion (Tyr85, Asp83 and Gly80). Residues in the corresponding loop region in cyt c_M and cyt c_2 (cyt c_M; 15-49: cyt c_2 15-49) interact with the inner haem propionate, Arg38 (cyt c_2; His42), in particular, playing prominent roles. Arg38 interacts with the inner haem propionate via interactions with two water molecules (Wat121 and Wat168); Trp59 is hydrogen bonded to the same propionate (Figure 1.21). The tryptophan is conserved in cyt c_L (cyt c_L: Trp66). In cyt c_L, Arg38 is replaced by Pro81, which does not interact with the propionate and a calcium ion occupies the position that Arg38 occupies in cyt c_M. As a consequence of the steric interference caused by the calcium ion, Trp66 (Trp59 in cyt c_M) is prevented from forming a hydrogen bond with the inner haem propionate. Cyt c_{551i} does not contain a calcium ion or an arginine in the region around the inner haem propionate; the conserved tryptophan (cyt c_{551i}: Trp58) is present but its side chain is not in the correct orientation to form a hydrogen bond with the propionate. In cyt c_{551i} the pocket which has a calcium coordinated in cyt c_L has a bound water molecule.

Helix B is a small helix (Pro89-Thr92) which is followed immediately by helix C (94-102). The first residue of helix C (Asp94) participates in a salt-bridge with Arg129 from helix E which stabilizes the central three-helix core of cyt c_L. Helix C does not contain the highly conserved tyrosine residue (cyt c_M; Tyr67: cyt c_2; Tyr70) that has been postulated to regulate the redox potential, through a hydrogen bond with the sixth ligand to the haem (cyt c_M: Met80) (Berghuis & Brayer, 1992). A phenylalanine (Phe102) replaces this tyrosine in cyt c_L. The residues within helix C of cyt c_L (DVGLFATIF) are mainly hydrophobic. It would appear that no residue within this helix is a suitable replacement for the Tyr67 to hydrogen

bond to the sixth ligand to the haem iron and regulate the redox potential. Figure 4.16 shows Phe102 from cyt c_L and Tyr67 from cyt c_M; Phe102 points away from the haem prosthetic group, whereas Tyr67 points towards the haem and the methionine ligand. In cyt c_L Phe102 also forms a stacking interaction with the other phenylalanine in helix C (Phe98) (Figure 4.17). In cyt c_{551i} the critical tyrosine residue is retained, although as with Phe102 from cyt c_L it is pointing away from the haem, and it also forms the same stacking interaction as is seen in cyt c_L with a neighboring phenylalanine (cyt c_{551i}: Phe92). There is no bond to Met101 in cytochrome c_{551i}

Loop3 (103-117) is the connecting loop between helix C and helix E in cyt c_L; the region does not contain helix D which is seen in cyt c_M and cyt c_2. The larger helices of B and D seem to be the main distinguishing features between the cytochromes c_2 and mitochondrial cytochromes *c*. With the exception of the N and C-terminal extensions it appears that cyt c_L resembles cyt c_M more than cyt c_2. As with cyt c_M helix B is small and cyt c_L does not have helix D, which is quiet prominent in cyt c_2, but not so in cyt c_M

Loop 3 contains the sixth ligand coordinated to the haem iron. This region was particularly difficult to build into the model. Remarkably, it appears that in this crystal structure of cyt c_L a histidine residue (His112) has replaced the expected methionine ligand (Met109), thus creating a bis-histidine coordination to the haem iron (Section 4.9b, Figure 4.34). Such a coordination is well established in transmembrane *b*-type cytochromes. Water soluble cytochromes with bis-histidine haem coordinations are rare. One example of such a coordination is the cytochrome *c´* from *Methylophilus methylotrophus* (Berry *et al.*, 1990). The cytochrome in the oxidized (Fe^{3+}) state has a low-spin, six-coordinated, bis-histidine iron. Both of the histidines are near perpendicular to the haem plane, as is seen in cytochrome c_L. The cytochrome *c´* from *Methylophilus methylotrophus* undergoes radical changes as the protein is reduced; the spin state of the haem iron changes to a high spin configuration, which is accompanied by the removal of one of the histidine ligands to create a 5-coordinate haem iron. The finding that cytochrome c_L has a bis-histidine arrangement is inconsistent with site-directed mutagenesis work on cyt c_L which had demonstrated that Met109 is the sixth ligand to the haem (Afolabi *et al*, 2001). It is also inconsistent with the solution spectrum of oxidized cyt c_L in which the 695 nm band is diagnostic of a Met-iron coordination (Beardmore-Gray *et al.*, 1982). The corresponding loop region in cyt c_{551i} (98-112) has the equivalent methionine (Met103) ligated to the haem iron; the histidine which is ligated to the iron in the crystal form of cyt c_L is not conserved in cyt c_{551i} and is replaced by Met106 (Chen *et al.*, 1994).

Tuna cytochrome *c* (cyt c_M)

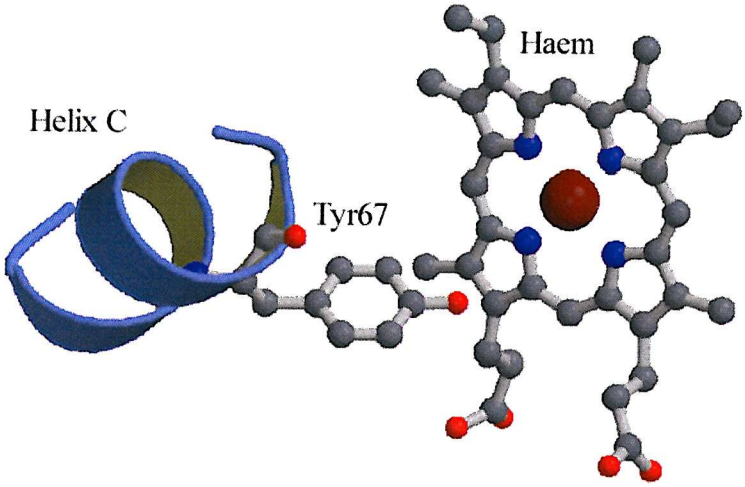

Cytochrome c_L (cyt c_L)

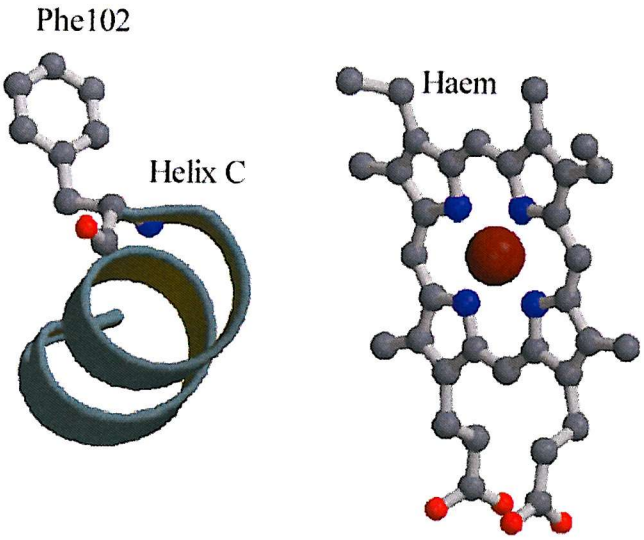

Figure 4.16 The conserved tyrosine in mitochondrial cytochrome *c* (Tyr67) is in effect replaced with a phenylalanine (Phe102) in cytochrome c_L

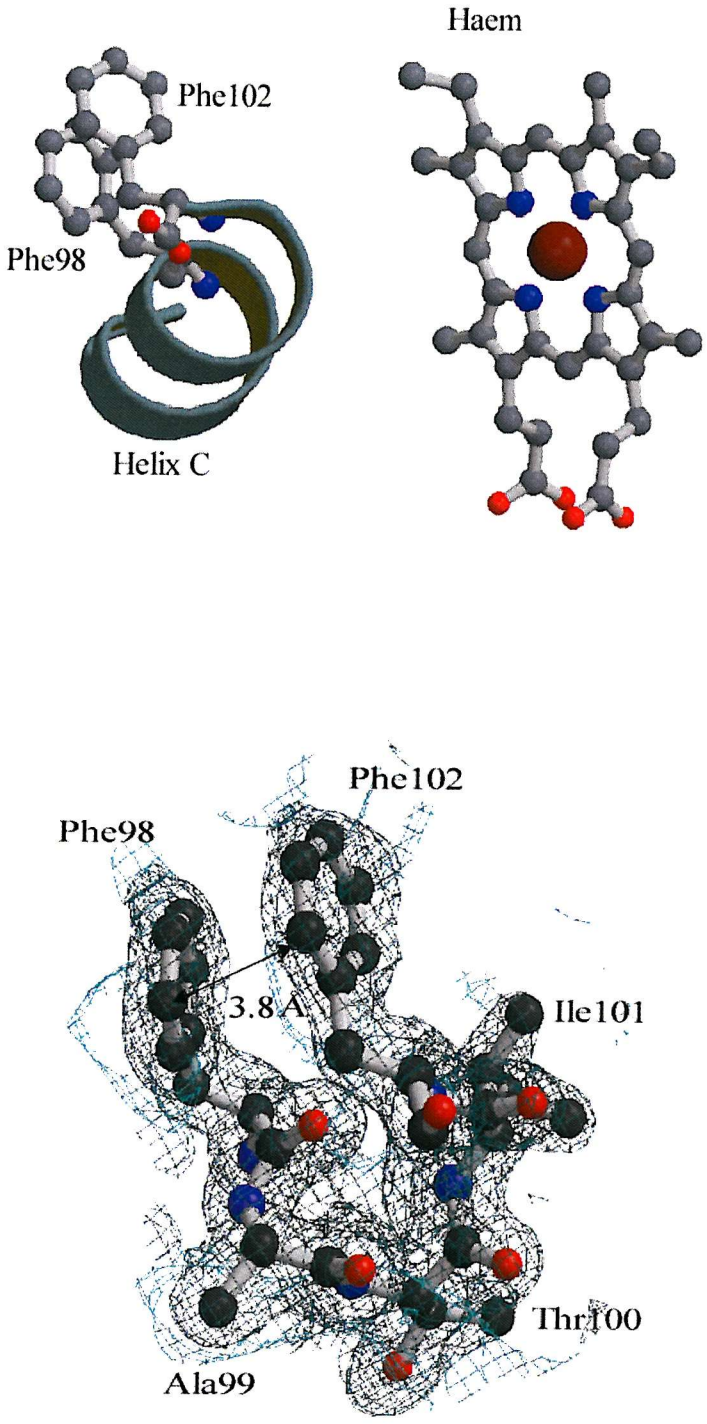

Figure 4.17 The stacking interaction between two nearby phenylalanine residues in helix C of cytochrome c_L

Helix E is a large helix (119-130) and is conserved in all class I *c*-type cytochromes; it forms one of the three helix bundle which partially encloses the haem. In the majority of class I *c*- type cytochromes helix E forms a hydrophobic interaction with helix A; this interaction involves a tyrosine on helix E (cyt c_M; Tyr95: cyt c_2; Tyr107) and a phenylalanine on helix A (cyt c_M; Phe10: cyt c_2; Phe20). A similar interaction between helix A and E is present in cyt c_L (Phe61 and Trp127), the distance between the side chains being the same as in cyt c_M (cyt c_L: 4.2 Å, cyt c_M: 4.1 Å); both interactions are shown in Figure 4.18. What could be more significant in holding these helices together in cyt c_L is a hydrogen bond between Asn56 from helix A and Gln123 from helix E (Figure 4.19). This is a stronger interaction than a hydrophobic interaction and would serve to lock the two helices together tightly. There is also a hydrogen bond at this position in cyt c_{551i} between a glutamate in helix A (cyt c_{551i}: Glu50) and an arginine in helix E (cyt c_{551i}: Arg117).

Cyt c_M and cyt c_2 terminate shortly after helix E (cyt c_M; Ser103: cyt c_2; Lys112). Cyt c_L is uncharacteristically large for a typical class I *c*-type cytochromes. There is an extension of the C-terminus (cyt c_L, 139-172; cyt c_{551i}, 125-157) which loops around the right-side of the protein (Figure 4.15). This C-terminal extension has a high proportion of polar residues; only 6 of the 43 residues are hydrophobic, the remaining 37 residues are all capable of polar/ionic interactions. The C-terminal extension also contains six of the twelve lysine residues that are present in the amino acid sequence. The C-terminal region connects to helix A via several interactions; for example a disulphide bridge is formed between Cys167 and Cys53 (Section 4.12). Also hydrogen bonds are formed between Gln166 in the C-terminal extension and the carbonyl oxygen of Leu46 and the side chain oxygen of Asp50 from helix A (Figure 4.20). Arg55 from helix A also participates in a salt-bridge to the penultimate residue in the structure, Glu172 (Figure 4.21). Another residue which appears to be important in maintaining the structural integrity is Lys136. The side chain of Lys136 forms two hydrogen bonds to the two carbonyl oxygen atoms from Lys147 and Tyr150 (Figure 4.22); this interaction connects helix F and helix G as they fold back on each other.

4.7.3 **Cytochrome c_L contains a disulphide bridge**

Although cytochrome c_L (18.4 kDa) is much larger than cyt c_M (12 kDa), it remains a highly stable protein at extremes of pH. This property is utilized in the protein preparation (Section 2.5), where one of the early steps is to precipitate out contaminating proteins by reducing the pH of the crude extract to pH 4.0. The stability of the protein can partially be explained by the presence of a disulphide bridge between Cys53 and Cys167; this disulphide,

Tuna cytochrome *c* (cyt c_M)

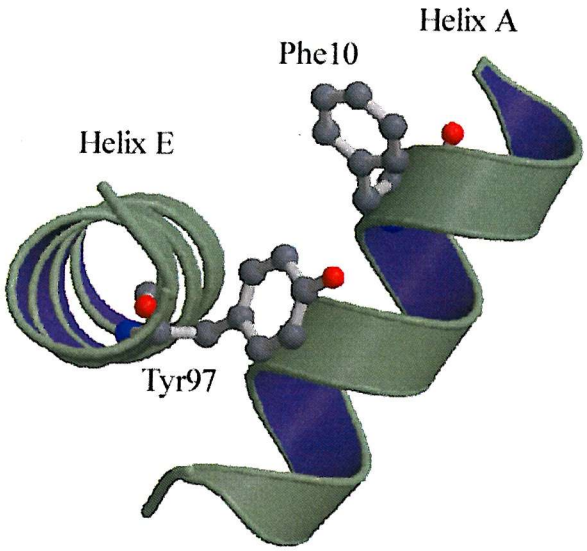

Cytochrome c_L (cyt c_L)

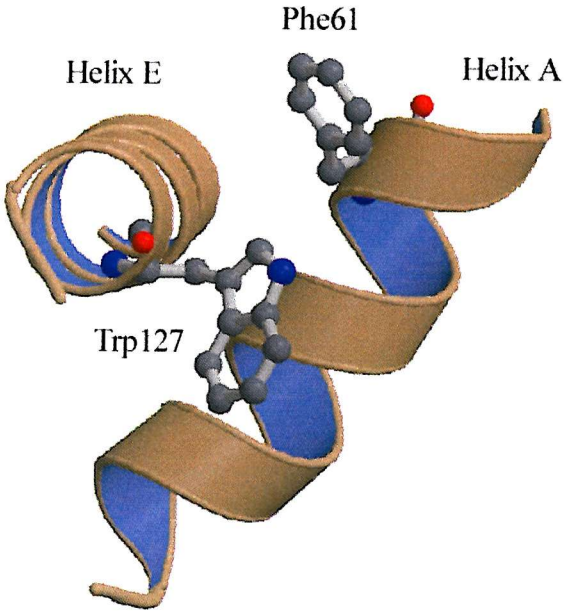

Figure 4.18 The conserved hydrophobic interaction between helix A and helix E in cyt c_M and cyt c_L

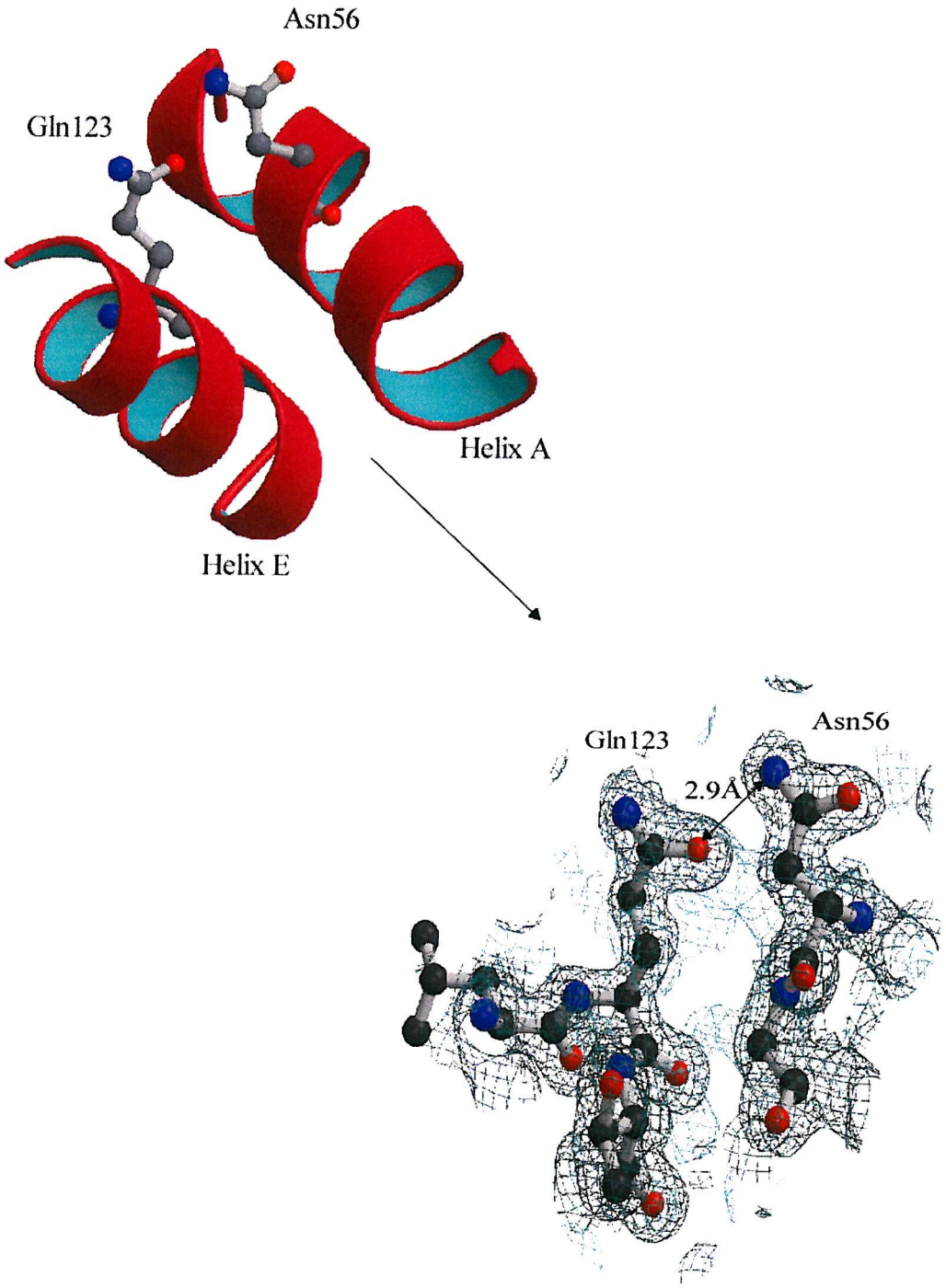

Figure 4.19 The hydrogen bond interaction between Gln123 and Asn56

The interaction helps to lock helix A and helix E together in cyt c_L

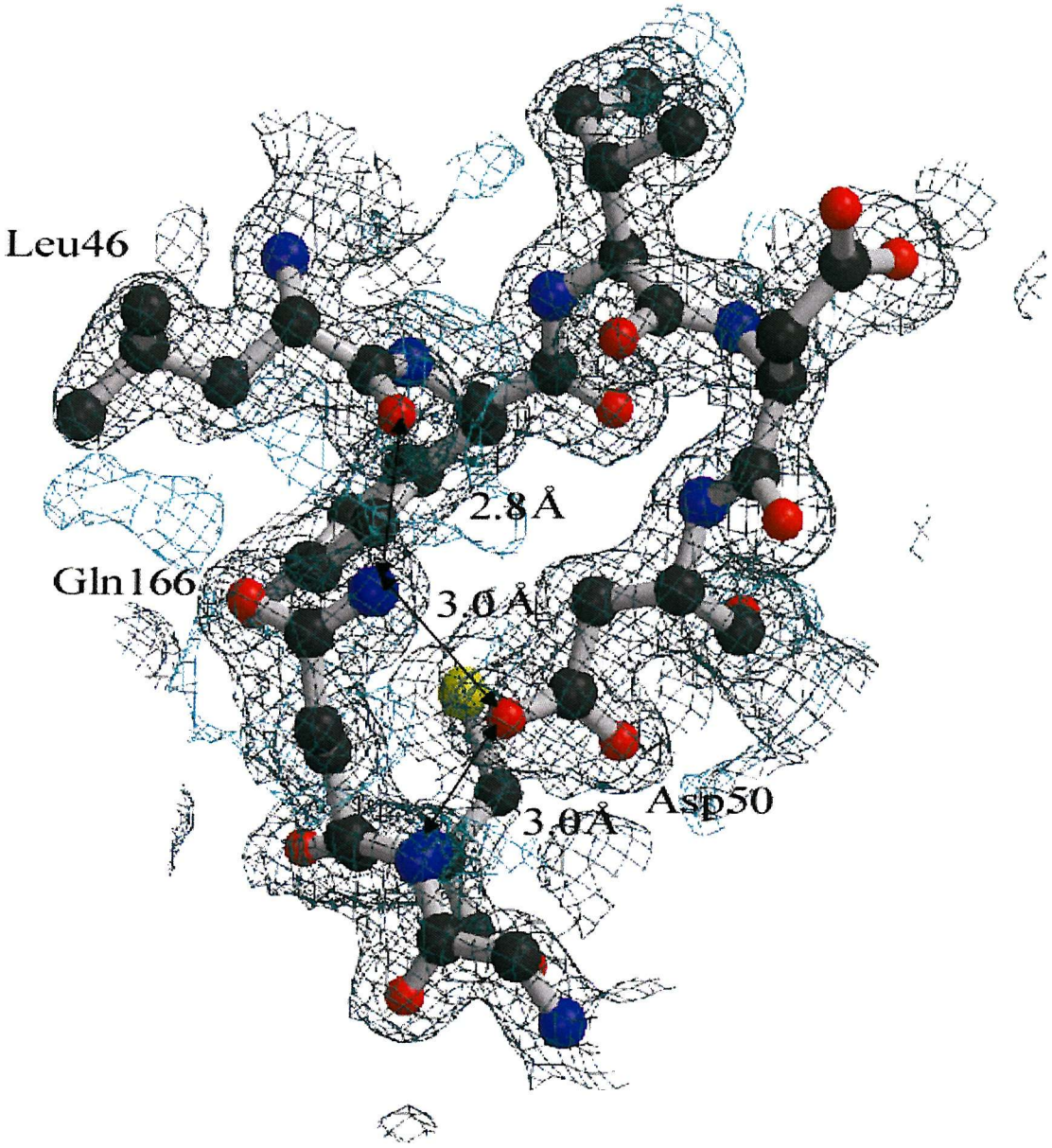

Figure 4.20 The interactions between Gln166 from the C-terminus of the protein and Leu46 and Asp50 from helix A

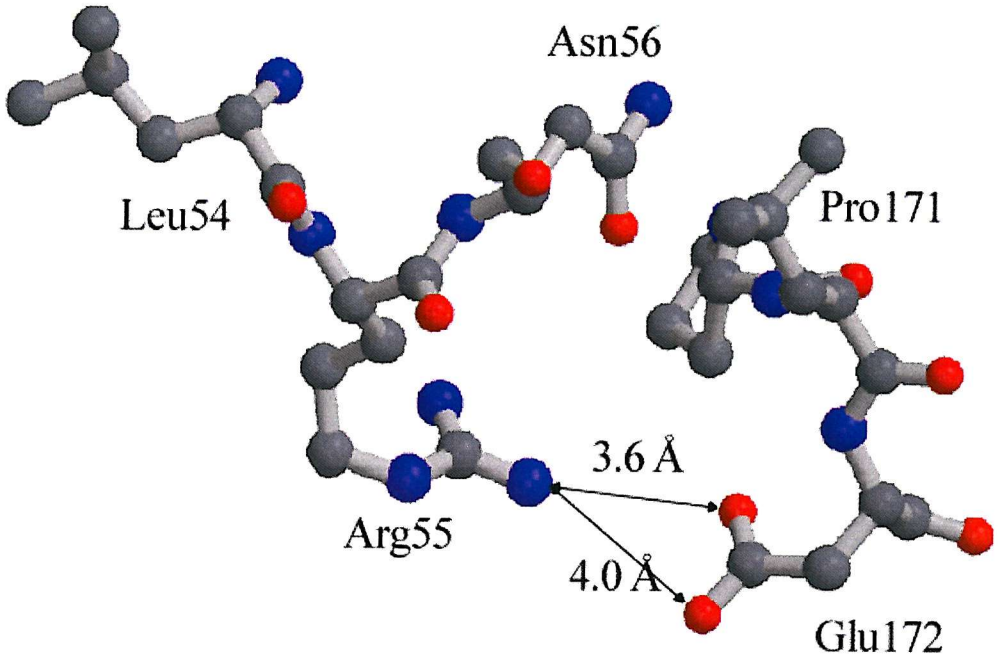

Figure 4.21 The salt-bridge between Glu172 and Arg55

This interaction connects the C-terminus to helix A

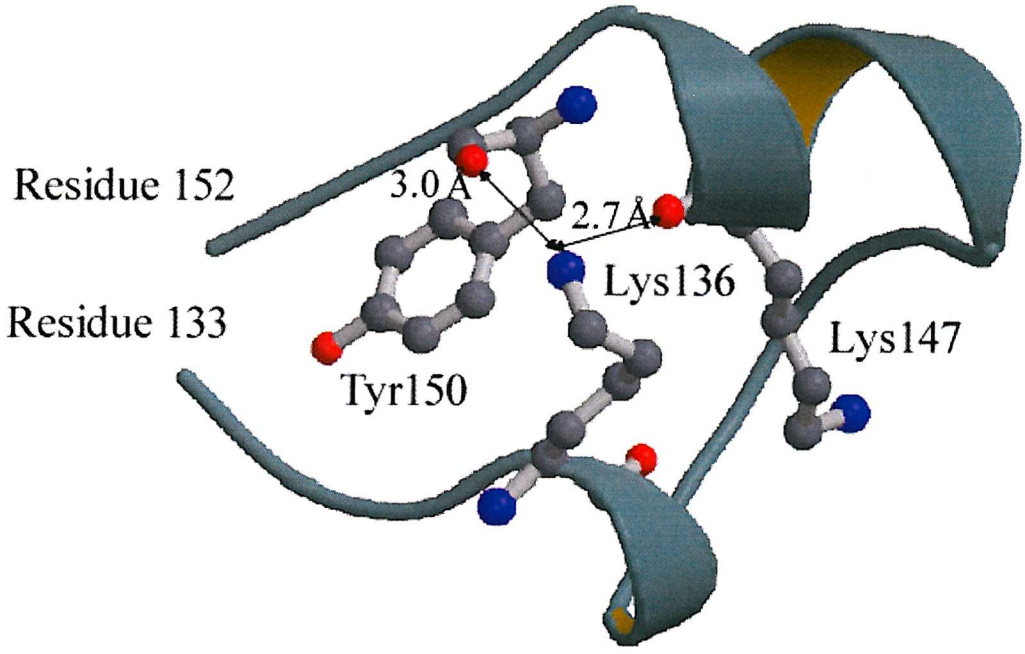

Figure 4.22 The hydrogen bond interactions between Lys136 and the main chain carbonyl oxygen atoms of Lys147 and Tyr150

These interactions connect helix F and helix G.

bridge connects the C-terminus with helix A. In cytochrome c_{551i} Cys53, is replaced by Ile47and Cys167 is replaced by Asp155. Figure 4.23 shows how the C-terminus of cytochrome c_L wraps around the protein to connect to helix A via this disulphide bridge. The electron density is continuous throughout both cysteines in the disulphide bridge and the disulphide bond length is 2.04 Å (Figure 4.24). To see if the disulphide bridge in the crystal could be reduced (to free thiols), the crystal was soaked for one week in mother liquor which had been supplemented with 20 mM sodium dithiothreitol (DTT). This reducing solution had no noticeable effect on the appearance of the crystal, which was subsequently frozen, and data collected at the ESRF in Grenoble. It diffracted well (1.7 Å) and was solved in the same space group and unit cell dimensions as previous structures. The *2Fo-Fc* and *Fo-Fc* electron density maps were calculated, and from this information it could be concluded that the reducing agent had no effect on the disulphide bridge or the overall protein configuration or rigidity. The distance between the sulfur atoms of the disulphide bond was unchanged, indicating that the bond had not been broken by reduction. The reducing agent, it must be noted did not alter the bis-histidine coordination to the haem iron. It should be noted that the redox state of the cytochrome was not confirmed for the reduced cytochrome in the crystal. It is therefore inappropriate to discuss at length the significance of any apparent differences (or similarities) between the 'reduced' and oxidized crystal structures.

Of the published mitochondrial cytochrome *c* sequences (over 100 have been published), the only cytochrome *c* with an internal disulphide bridge is the cytochrome *c* from bullfrog heart (Brems *et al.*, 1982). In this cytochrome the disulphide bridge is formed between Cys20 and Cys102 where it links the N and C-termini. It does not interrupt the central cytochrome *c* fold as was predicted by using the horse heart cytochrome *c* as a model (Betz & Pielak, 1992). This structure has a cysteine at position 102, but there is a valine at position 20. By modeling in a cysteine at position 20 and creating a disulphide link the central cytochrome *c* fold remained unchanged. Several unfolding experiments on bullfrog cytochrome *c* and a V20C yeast cytochrome *c* mutant (using wild-type yeast iso-1-cytochrome *c* as a control) have shown that the stability of the native globular conformation of the mutant is enhanced, relative to control cytochrome *c*, when the protein is exposed to low pH or to high denaturant (guanidine) concentrations, and also that the disulphide bridge encourages the protein to refold more rapidly as the denaturant is diluted out than does the control cytochrome *c* (Betz & Pielak, 1992)

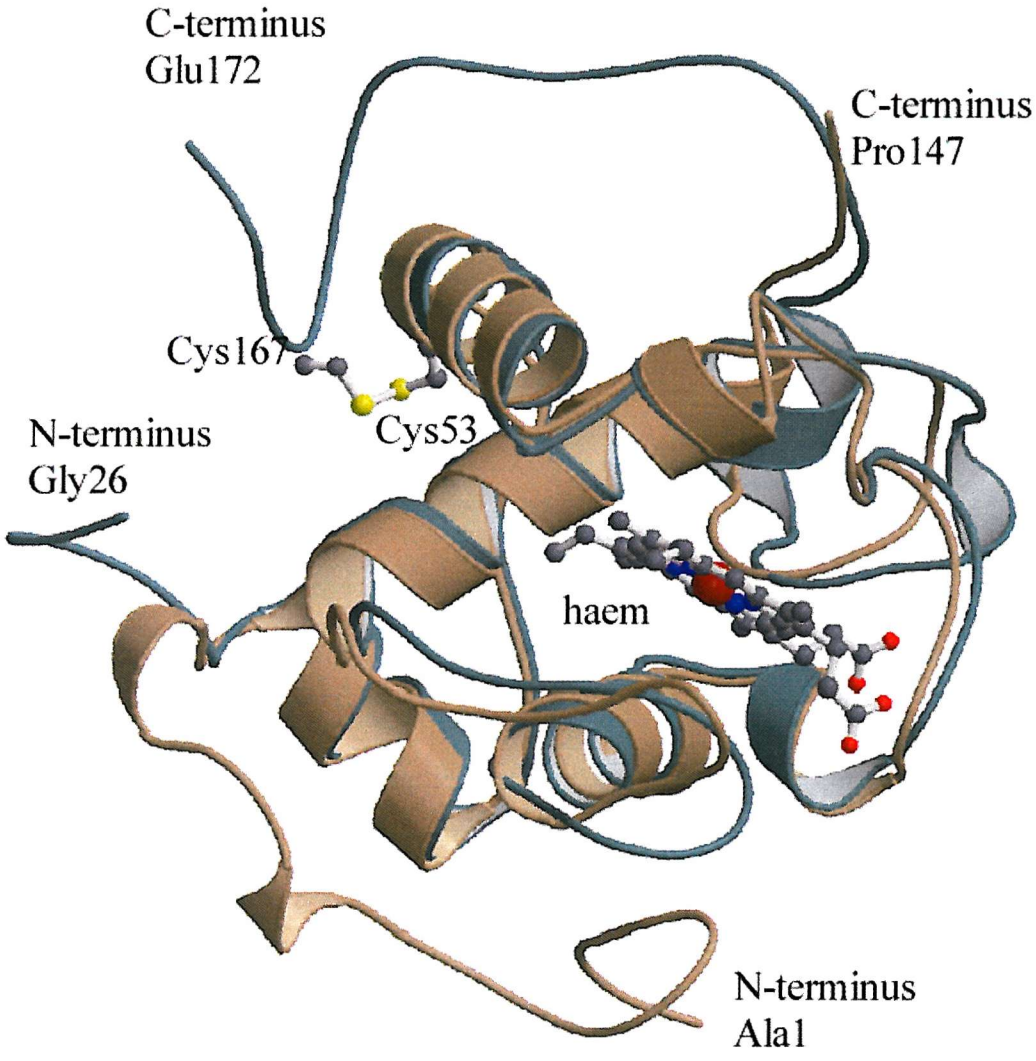

Figure 4.23 The disulphide bond in cytochrome c_L

This feature links the C-terminus with helix A (cytochrome c_L is in green). Cytochrome c_{551i} does not contain a disulphide bridge (cytochrome c_{551i} is shown in brown); the two cysteines are replaced by Ile47 and Asp155.

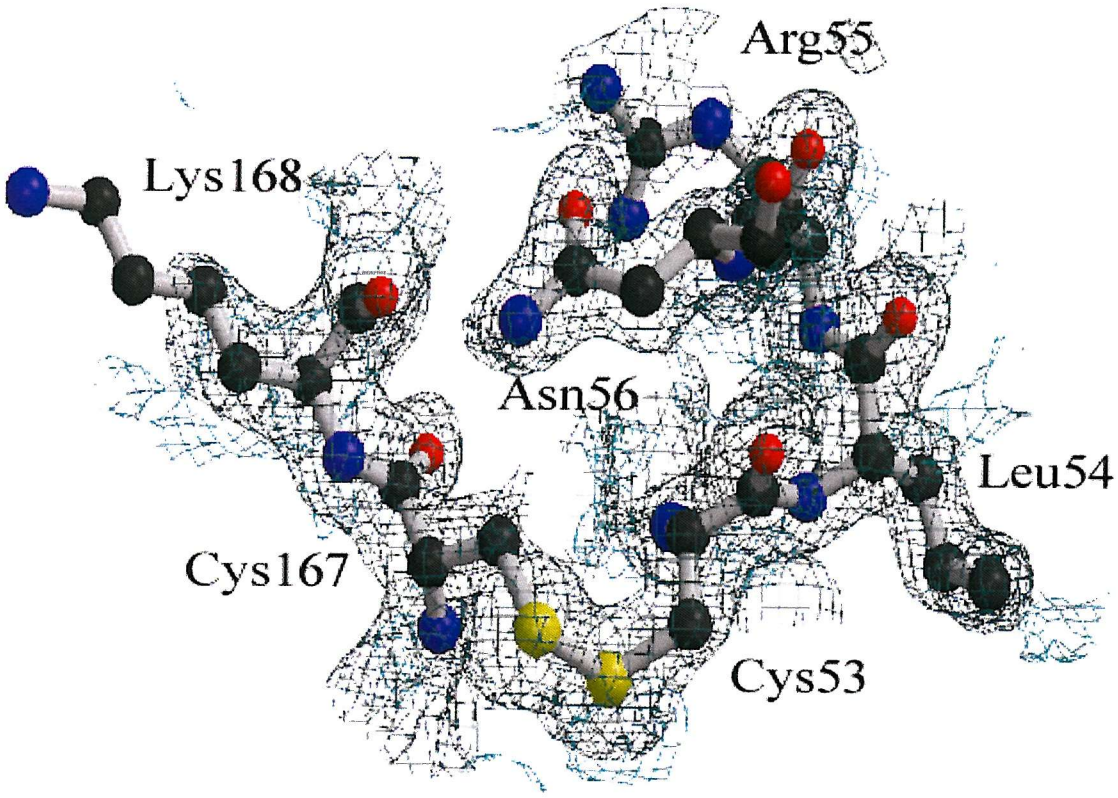

Figure 4.24 The electron density surrounding the disulphide bridge in cytochrome c_L

4.7.4 **Calcium binding to cytochrome c_L**

The X-ray crystal structure of cytochrome c_L has a single calcium ion bound close to the haem prosthetic group (Figure 4.25). The crystal growth conditions contained calcium acetate, which was thought to be the most likely source for the calcium ion. The calcium is coordinated in a classical pentagonal bi-pyramidal arrangement; the ligands to the calcium are provided by four water molecules (Wat6, 7, 8 and 9) and three oxygen atoms, which come from the side chain of Asp83 and the carbonyl oxygen atoms of Gly80 and Tyr85 respectively. All of the calcium-oxygen distances fall within the range of 2.2-2.5 Å, and all the B-factors for the oxygen ligands and the calcium ion itself are below 25 $Å^2$, which suggests that this region of the protein is quite rigid and refined well. The presence of a calcium ion in the cytochrome c_L structure could explain the inhibitory effect of EDTA on methanol oxidation in whole cells of *M. extorquens*. It has previously been suggested that this inhibition is due to EDTA binding to lysine residues on the α-subunit MDH and preventing the 'docked' MDH/cytochrome c_L complex from moving into an optimum position for electron transfer (Dales & Anthony, 1995). Following the discovery of a calcium ion in cytochrome c_L, an alternative explanation could center around EDTA displacing the water ligands to the calcium ion and removing the calcium from the structure. The consequences of such a process could be two-fold. Firstly, the calcium ion could be involved in docking cytochrome c_L with MDH, and by removing the calcium the docking process would be inhibited. Secondly EDTA could inhibit methanol oxidation by denaturing cytochrome c_L by removing the calcium ion from the protein.

Calcium and magnesium ions have previously been shown to bind to mitochondrial cytochrome *c*. Lanthanide ions have been used as probes for calcium binding sites (Moore & Pettigrew, 1990). These are a series of metallic elements in the rare-earth metals in group IIIb which have approximately the same atomic radius and reactivity as calcium, so they can substitute for calcium ions and bind to the same places as a calcium may (Pitcock. & Moore, 2001). Unlike calcium, lanthanide ions exhibit spectroscopic properties, chiefly a pronounced luminescence, which allows a quantitive assessment of binding to the protein. From the studies using lanthanide ions in mitochondrial cytochrome *c* three potential calcium binding sites have been postulated (Moore & Williams). One of these binding sites is at the N-terminus, another is at the C-terminus and the third is near Tyr75 and Met65 (the numbering is from tuna cytochrome *c*). The calcium bound in cytochrome c_L is near none of these sites but is very close to the inner haem propionate (Figure 4.25). Cytochrome c_{551i} is highly

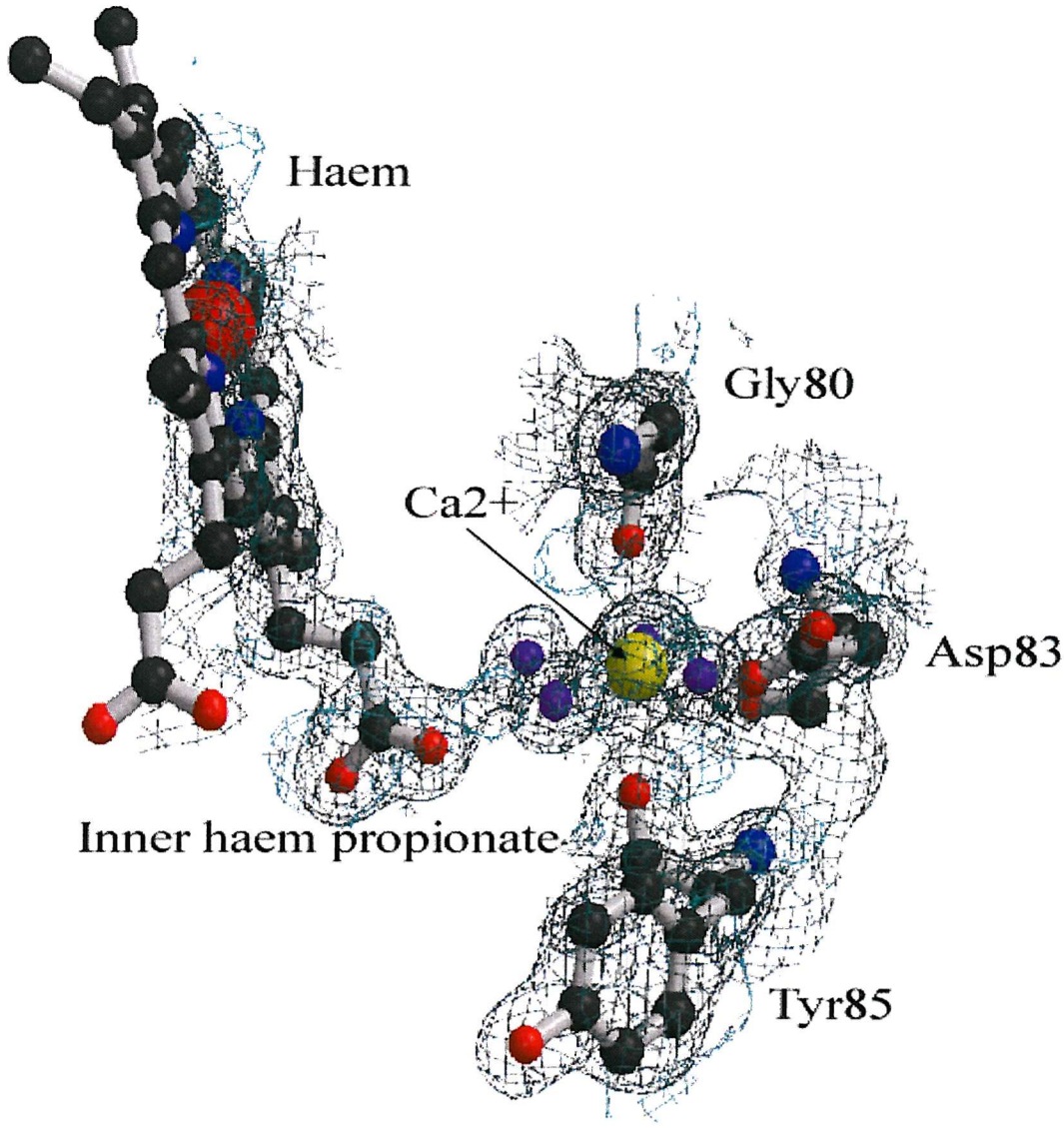

Figure 4.25 The electron density which surrounds the calcium ion in cytochrome c_L

The calcium ion (yellow sphere) is coordinated in a pentagonal bi-pyramidal arrangement to four water molecules (purple spheres) and to Tyr85, Asp83 and Gly80. All of the calcium-oxygen distances fall within the range of 2.2-2.5 Å, and all the B-factors for the oxygen ligands and the calcium ion are below 25 $Å^2$, which suggests that this region of the protein refined well and quite rigid..

homologous to cytochrome c_L in this region. The residues that shape the binding pocket are almost identical, only one of the seven residues is not conserved between the two proteins (Asn84 from cyt c_L is replaced with an alanine in cyt c_{551i}). As a result of the high degree of amino acid conservation in this region the protein backbone for both of the proteins overlap, but no calcium is seen in the cytochrome c_{551i} structure. Cytochrome c_{551i} has a water molecule in this region (Wat1) and there are four oxygen atoms within hydrogen bond distance to this water molecule. Three of these four oxygen atoms are coordinated to the calcium ion in cytochrome c_L; these are the carbonyl oxygen atoms from Tyr77, Gly72 and the side chain oxygen from Asp75. The fourth oxygen within hydrogen bonding distance to Wat1 is a side chain oxygen from Glu31 from amicyanin, the protein with which it forms a complex in the crystal. The ternary structure of methylamine dehydrogenase, amicyanin and cytochrome c_{551i} has since been solved on two other occasions by the same group (pdb coordinates 1MG2 & 1MG3). In both of these structures Wat1 has been replaced with a sodium ion. The B-factor for the sodium ions in both of these structures are similar to those of the other atoms in the structure (9-14 $Å^2$). It therefore seems that there is also a metal ion in cytochrome c_{551i} and, that this metal ion is sodium. Bearing these recent findings from the ternary complex in mind, the calcium ion in 1.6 Å cytochrome c_L model was replaced with a sodium ion and the structure was subjected to another round of refinement, using the programs from the CNS suite. After the refinement the B-factor for the newly incorporated sodium ion was 13.83 $Å^2$ (the B-factor for the calcium ion was 20.05 $Å^2$). Following the refinement, *2Fo-Fc* and *Fo-Fc* electron density maps were calculated and viewed in QUANTA, along with the protein model. The resulting electron density maps revealed a large amount of positive *Fo-Fc* electron density throughout the sodium ion (Figure 4.26); this data would suggest strongly that this position in the molecule should not be occupied by a sodium ion, and that the previous conclusion that a calcium ion occupies this position in cytochrome c_L is correct.

4.8 **The structure of cytochrome c_L determined from crystals grown in the absence of added calcium**

To determine whether the calcium ion in the crystal structure of cytochrome c_L came from the calcium acetate in the mother liquor, or is an inherent feature of cytochrome c_L, crystals of cytochrome c_L were grown using alternative conditions using PEG, ammonium sulphate and MES buffer as the mother liquor. The crystals grown using these conditions were thinner and more needle-like than those grown with cacodylate and calcium acetate, but

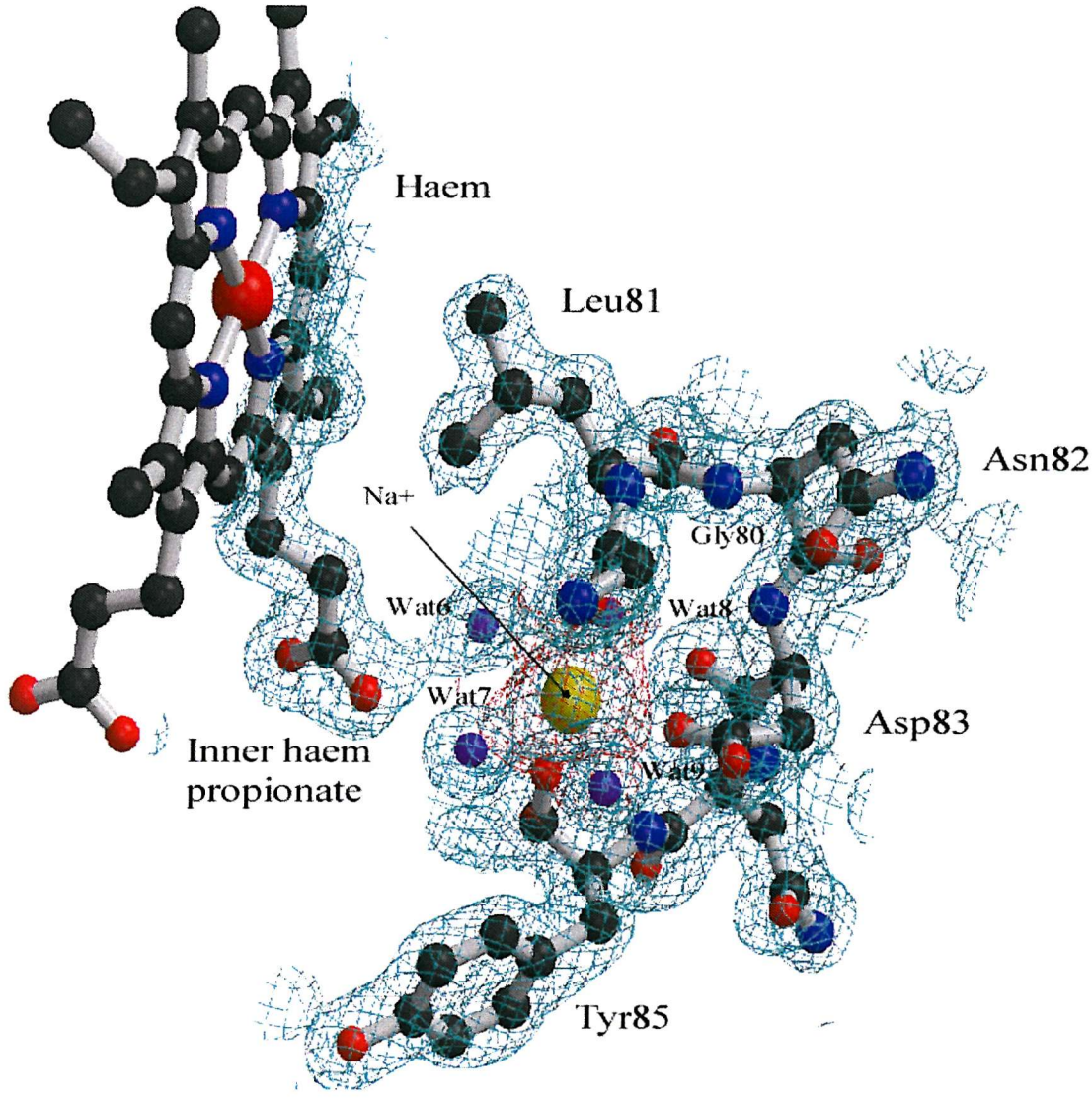

4.26 The electron density which surrounds the sodium ion built into the model of cytochrome c_L

Positive *Fo-Fc* electron density (red) surrounds the sodium ion after it was built into the structure of cytochrome c_L and refined using the programs from the CNS suite. This indicates that the position should not be occupied by a sodium ion and is more-likely occupied by a calcium ion, as previously thought.

they were adequate for data collection at a synchrotron facility (ESRF Grenoble, France). Figure 4.27 shows a single diffraction image from the crystal which diffracted X-rays to approximately 2.8 Å. Autoindexing was done using MOSFLM and the unit cell dimensions and space group which were suggested were similar to those of the cytochrome c_L structure previously solved in this thesis (Figure 4.28), and therefore the data were processed using this unit cell.

The diffraction images were processed in two separate batches (images 20-70, and 70-120); this improved the R_{merge} substantially, reducing it from 17 % to 12 % when the data were scaled. The data processing statistics are shown in Table 4.8. After data processing, the unit cell dimensions had been refined to a = 64.8 Å, b = 64.8 Å, c = 38.7 Å, and as $P4_3$ is a tetragonal space group the angles α, β and γ were 90 °. Although the unit cell dimensions were very similar to those of the previously solved cytochrome c_L structure, molecular replacement was still required to solve the structure. This was almost certainly due to the data being indexed in an alternative manner, which is possible for a $P4_3$ space group. In these situations re-indexing or molecular replacement is required. The phasing model was the 1.6 Å cytochrome c_L structure (Table 4.9). As expected there was a large rotation peak (Rf/sigma value of 8.14), and this rotation solution was used to try to find a positional solution. A large peak was recorded in the translation search, which gave a correlation of the search model to target model of 68 %, with a corresponding *R*-factor of 37.6 %. The protein coordinate file from the molecular replacement and the reflection file from data processing were used for model building and refinement, using QUANTA and the programs from the CNS suite respectively. After one round of refinement, electron density maps were calculated. The electron density maps showed a large region of spherical *Fo-Fc* electron density in the position where there was a calcium ion in the previous structures (Figure 4.29); the sigma levels of the electron density peak reached as high as 7 σ, which would suggest that the peak corresponded to a large atom. A calcium ion was therefore added into the electron density maps and used in subsequent rounds of refinement. The calcium ion refined well, and after a further round of refinement the B-factor for the calcium ion was 23 $Å^2$. Refinement of the protein model was stopped after several rounds of refinement; the final structure had an *R*-factor of 29 % and an *R*-free of 32 % (Table 4.10), which are acceptable values for a structure at 2.8 Å resolution. The 2.8 Å structure was compared with the 1.6 Å cytochrome c_L structure and there appeared to be no major differences. The presence of the calcium ion in this structure suggests that the calcium ion is an integral part of the protein structure and does not

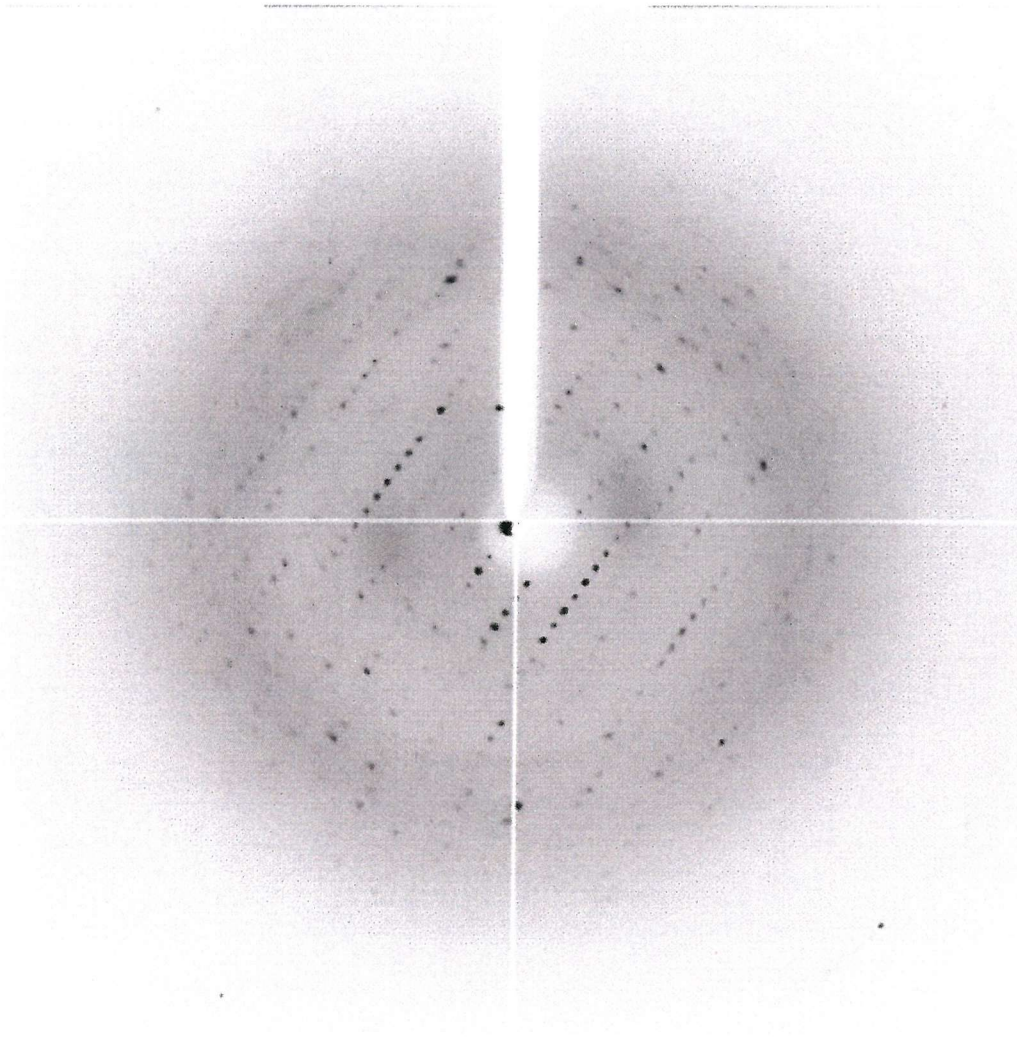

Figure 4.27 A single diffraction pattern from a cytochrome c_L crystal grown in PEG, ammonium sulphate and MES

Using these conditions no calcium was present in the crystallization conditions

```
Only solutions with PENALTY less than 200 are listed, a complete list is given in the terminal window
 No PENALTY  LATT     a        b        c     alpha  beta gamma  Possible spaoegroups
 16 158      mC    37.80   131.94    64.73    89.4  89.8  75.4   C2
 15 153      oC    37.80   131.94    64.73    89.4  90.2 104.6   C222,C2221
 14 149      mC   131.94    37.80    64.73    90.2  90.6  75.4   C2
 13 147      mC    37.80   131.94    64.73    89.4  89.8  75.4   C2
 12 142      oC    37.80   131.94    64.73    89.4  90.2 104.6   C222,C2221
 11 138      mC   131.94    37.80    64.73    90.2  90.6  75.4   C2
 10  26      tP    63.89    64.73    37.80    90.2  92.1  90.5   P4,P41,P42,P43,P422,P4212,P4122,P41212,P4222,P42212 P4322,P43212
  9  23      mC    91.37    90.53    37.80    91.6  91.3  90.8   C2
  8  22      oC    90.53    91.37    37.80    88.7  91.6  89.2   C222,C2221
  7  21      mC    90.53    91.37    37.80    88.7  91.6  89.2   C2
  6  14      oP    37.80    63.89    64.73    90.5  90.2  92.1   P222,P2221,P21212,P212121
  5  14      mP    37.80    63.89    64.73    90.5  90.2  92.1   P2,P21
  4  10      mP    63.89    37.80    64.73    90.2  90.5  92.1   P2,P21
  3   5      mP    37.80    64.73    63.89    90.5  92.1  90.2   P2,P21
  2   1      aP    37.80    63.89    64.73    89.5  90.2  87.9   P1
  1   0      aP    37.80    63.89    64.73    90.5  90.2  92.1   P1

Select a solution AND a spacegroup from list above (eg 3 p42) or 0 to abandon or T to change min I/sig(I):␣
```

Figure 4.28 The autoindexing by MOSFLM of the diffraction patterns from a cytochrome c_L crystal which was grown in the absence of calcium

MOSFLM suggested a unit cell which was previously used to solve the 1.6 Å cytochrome c_L structure (solution number 10)

Table 4.8 The data processing statistics for the 2.8 Å resolution structure of cytochrome c_L crystallised in the absence of calcium

Total number of reflections	7902
Number of unique reflections	2612
Resolution (Å)	2.8 Å
Completeness (%)	91.1 %
R_{merge} (outer resolution shell)	0.115 (0.290)
Multiplicity	2.4
Average I/σ(I) (outer resolution shell)	5.7 (2.0)

Tables 4.9 The molecular replacement result for the 2.8 Å resolution structure of cytochrome c_L crystallized in the absence of calcium

The search model was the 1.6 Å resolution structure of cytochrome c_L.

a) The rotation search

Peak Number	α	β	γ	Theta	Phi	chi	Rf/σ
1	49.17	1.34	219.85	179.06	-175.34	90.99	8.14
2	35.67	166.18	244.79	94.43	165.44	169.39	4.34
3	49.83	168.35	259.67	92.49	165.08	169.46	4.01

b) The translation search

Peak Number	X	Y	Z	Density/σ	R-fac	Corr
1	0.580	0.156	0.00	29.54	0.376	0.684
2	0.690	0.125	0.00	9.07	0.541	0.340
3	0.640	0.148	0.00	6.25	0.536	0.343
4	0.531	0.181	0.00	5.68	0.534	0.345
5	0.219	0.322	0.00	4.87	0.544	0.304

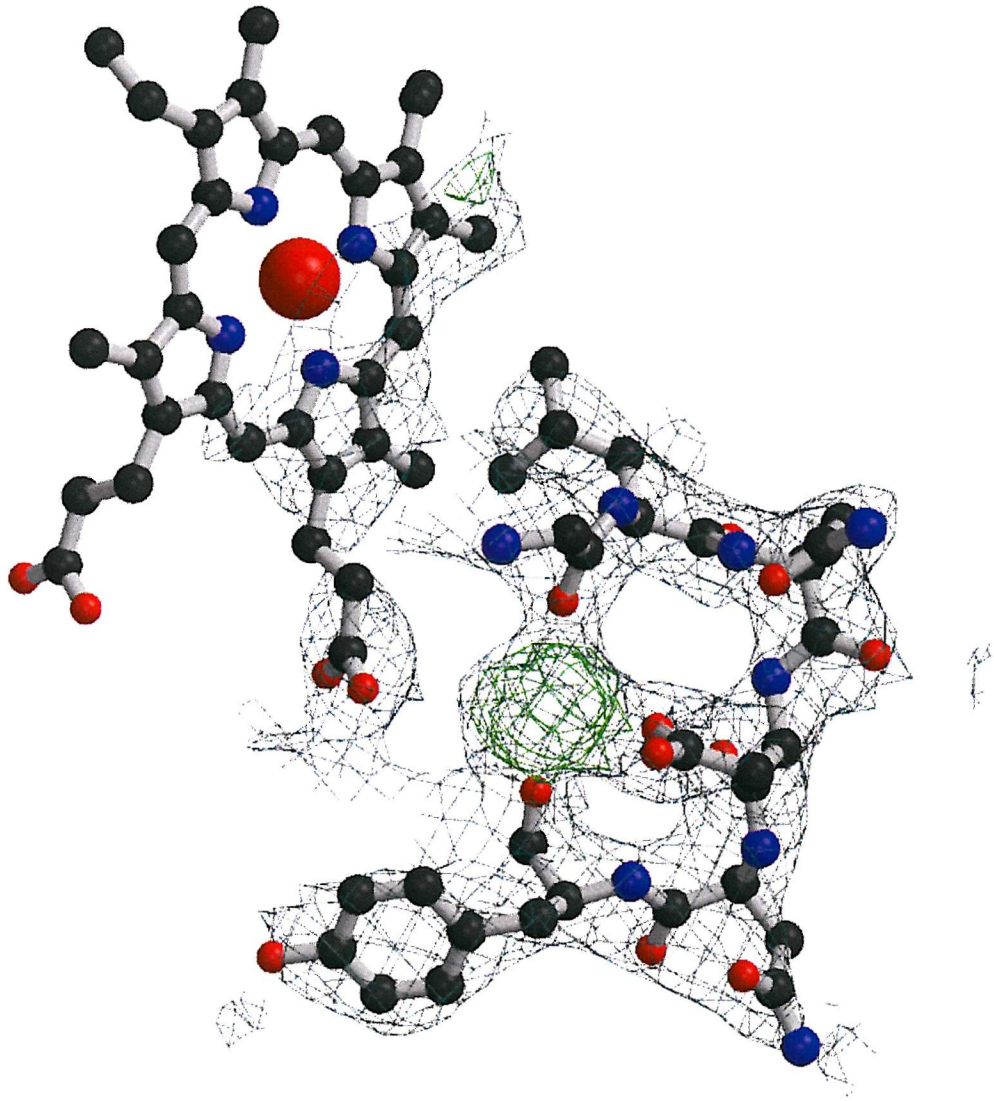

4.29 A region of *Fo-Fc* electron density in the position where there was a calcium ion in the 1.6 Å structure of cytochrome c_L

The *Fo-Fc* electron density map is contoured at the 5 σ level (shown in green) and the *2Fo-Fc* map at the 1 σ level (shown in dark blue). The crystal was prepared in the absence of calcium. The prescence of a calcium ion in this structure suggests that the calcium is an inherent feature of the protein

Table 4.10 The final refinement statistics for the 2.8 Å resolution structure of cytochrome c_L which was prepared in the absence of calcium

Resolution range	10-2.8 Å
R-factor (%)	28.7 %
R-free (%)	32.0 %
Number of reflection in working set	4083
Number of reflections in test set (4.6 %)	196

come from the mother liquor. Whether its role is mainly structural or functional is difficult to determine purely from structural information. The region surrounding the inner propionate is highly conserved throughout the cytochrome *c* family (Section 4.11). The usually conserved arginine (cyt c_M : Arg38), has been proposed to contribute to a high redox potential by way of the positive charge on the guanidine group which effectively neutralizes the negatively charged inner haem propionate, thus diminishing its potential electrostatic effect on the haem iron (Moore & Pettigrew, 1990). In cyt c_L this arginine is absent. It is quite possible that the calcium ion in cytochrome c_L performs a similar role by providing a positive charge close to the inner haem propionate. As with Arg38 in cyt c_M there is a water molecule between the positive charge (calcium) and the propionate oxygen (Figure 4.24). Mutation of Arg38 to alanine in mitochondrial cytochrome *c* alters several properties of the protein. In the wild-type cytochrome *c* the arginine provides two hydrogen bonding groups which interact with the conserved water molecules, Wat121 and Wat168. The stability of the R38A cytochrome remains unaltered, this is probably because the position which was occupied by the arginine side chain now contained two additional water molecules, thus allowing the original hydrogen bonding framework to remain (Lo *et al.*, 1995).

Arg38 contributes to the high redox potential through two mechanisms, either via direct electrostatic stabilization of the reduced state of the haem group by the positively charged guanidinum side chain, or through an electron-withdrawing effect on the haem though the hydrogen-bonding network involving the conserved water molecules, Wat121 and Wat168 and the inner haem propionate of the haem. Mutation of the conserved arginine always reduces the redox potential (Moore & Pettigrew, 1990). Arg38 could also have an additional role to protect the haem from solvent by providing enough binding energy to stabilize the loop region of 36-59 (tuna). The inner haem propionate is usually protected from bulk solvent through hydrogen bonds with a conserved tyrosine (Tyr46), a conserved water molecule (Wat26) and the conserved arginine (Arg38) (Berghuis & Brayer, 1991). Cytochrome c_L has a different arrangement around the inner haem propionate and is more exposed to solvent, and it is likely that this arrangement around the inner haem propionate contributes to the unusual pH dependence of redox potential which has been previously reported in this protein (O'Keeffe & Anthony, 1980b). Figure 4.30 shows how both of the haem propionate groups in cyt c_L are exposed to the external solvent. By contrast, in mitochondrial cytochrome *c* the haem propionate groups are completely protected from bulk solvent via conserved residues on the protein (Figure 4.31). Like cytochrome c_L, cytochrome c_H has an exposed region about the inner propionate, although the outer propionate is not as

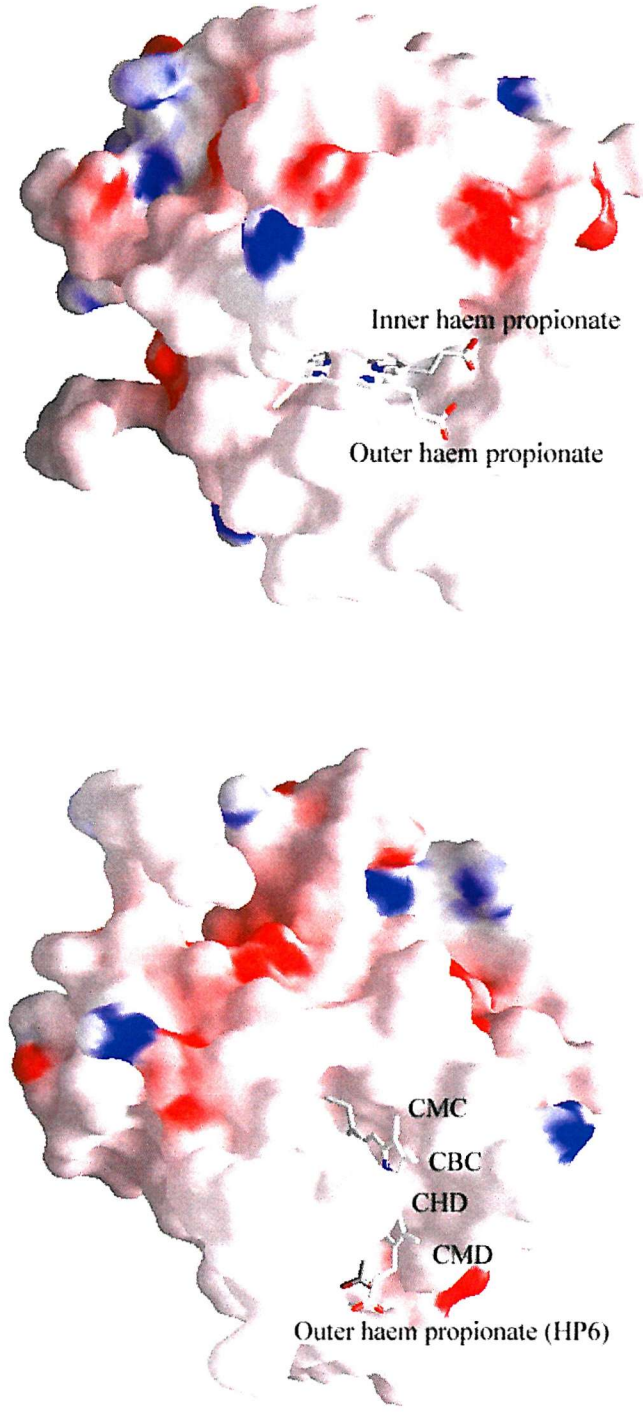

Figure 4.30 The exposed haem propionates in cytochrome c_L

Both of the propionates in the haem of cyt c_L are exposed to bulk solvent (top diagram) along with the CMC, CBC, CHD and CMD atoms (bottom diagram).

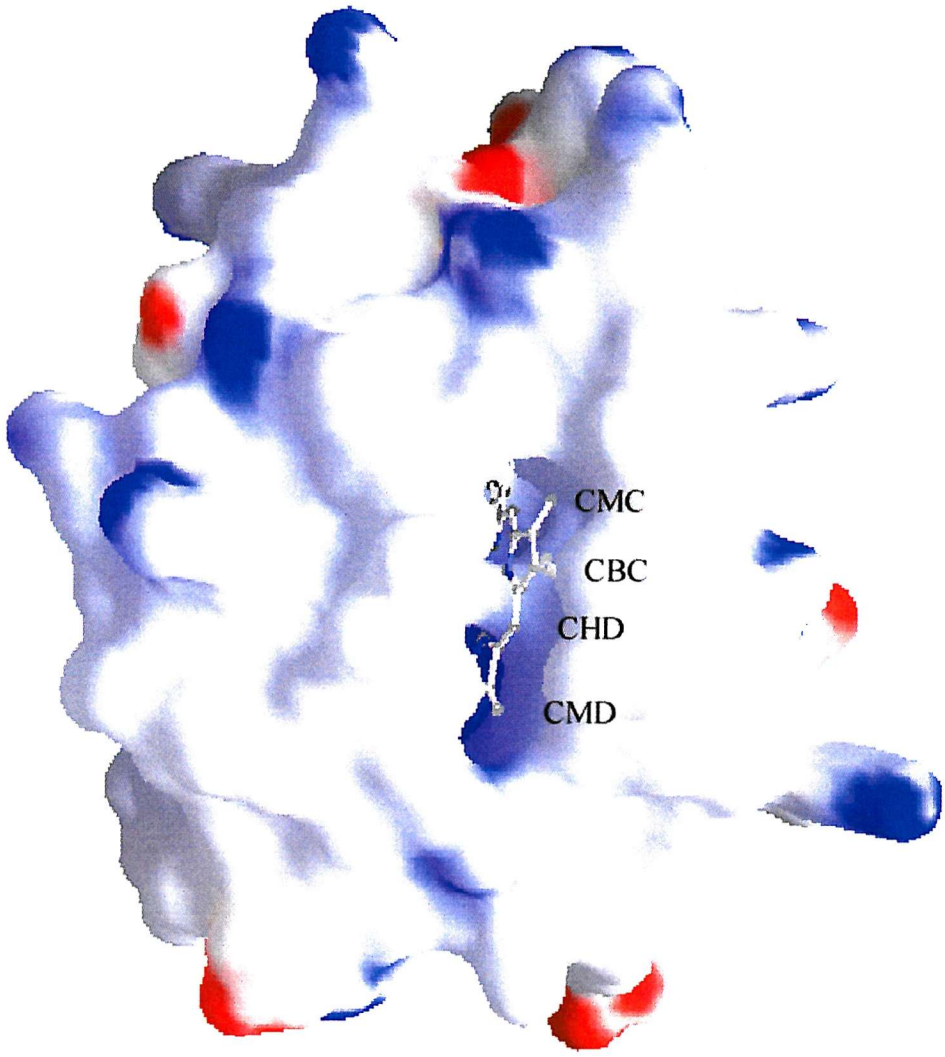

Figure 4.31 The extent of haem exposure in tuna cytochrome *c*.

Both of the propionates in the haem of cyt c_M are completely protected from bulk solvent, although the atoms at the haem edge are exposed for electron transfer (CMD, CHD, CBC and CMC).

exposed as it is in cytochrome c_L.

4.9 **The region surrounding the haem prosthetic group**

a) Haem conformation

In all highly refined X-ray crystal structures of cytochromes *c*, the haem prosthetic group is distorted from a planar configuration, and can be described as ruffled or saddle-shaped. The cause of this distortion is most likely due to the thioether linkages from the protein to the haem. This conclusion is based on the observation that in mitochondrial cytochrome *c* the pyrrole rings bearing the thioether bonds are tilted more than the others. In cytochrome c_L the conformation of the haem group is like that of all other highly refined cytochrome *c* structures in being slightly non-planar and dome-shaped (Figure 4.32).

b) The protein ligands to the haem

The haem in cytochrome c_L forms a thioether linkage with cysteines 65 and 68 and the iron is coordinated to a histidine NE2 atom (His69); these two features define the protein as a *c*-type cytochrome. The definition of a class I cytochrome *c* also includes methionine as the 6^{th} ligand to the haem iron. The distance between the His69 NE2 atom and the Fe^{3+} is 2.04 Å (Figure 4.33), which is in accordance with other cytochrome structures. The NE1 atom of His69 is hydrogen bonded to the carbonyl group of a nearby proline residue (Pro79). Although such a hydrogen bond is not an absolute requirement for histidine to coordinate to haem iron, it is thought that it serves to orientate the imidazole ring perpendicular to the plane of the haem, and in the process bisecting the angle between the iron-pyrrole bonds (Figure 4.34b). There are a number of reasons for this orientation. Firstly in a model where the histidine lies along the iron-pyrrole bond there will be substantial steric interaction between the histidine C-2 and C-4 hydrogen atoms and the pyrrole nitrogen atoms (Figure 4.34a). Secondly, the 3d orbitals from the iron which extend out of the porphoryrin ring, and could interact with the N_{pz} orbitals of the histidine ligand, are prevented from doing so by the rotation around the Fe-His bond, and it has been suggested that the interaction between the electrons in these orbitals would be unfavorable due to electron-electron repulsion. The amino acid residues which surround His69 are mainly hydrophobic (Leu81, Phe61 and Ile128 and Gly78), which is typical of *c*-type cytochromes. This hydrophobic environment contributes to the high redox potential (Moore & Pettigrew, 1990).

The sixth ligand to the haem iron in cytochrome c_L was surprisingly provided by another histidine residue (His112), creating a bis-histidine coordination. Both of the histidine

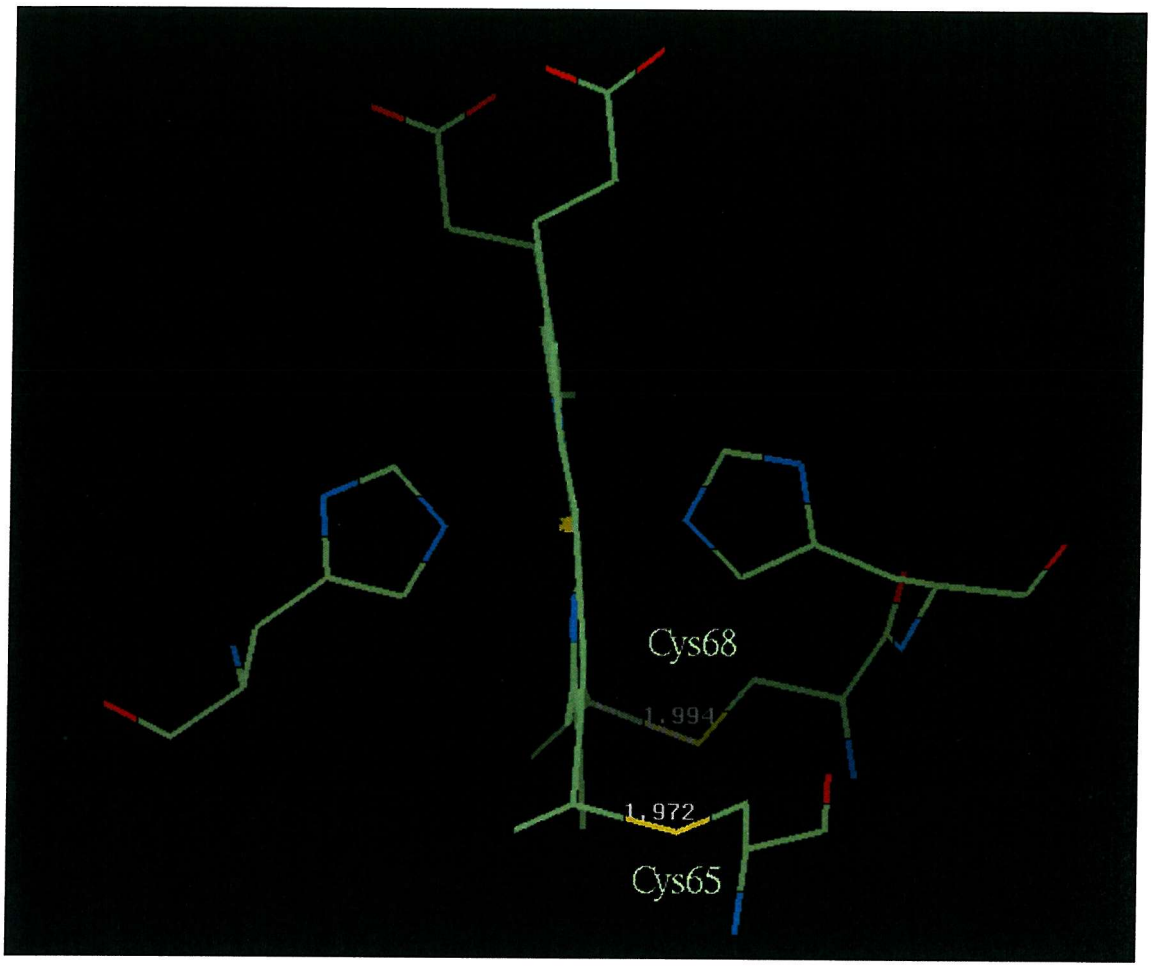

Figure 4.32 The two thioether linkages from Cys65 and Cys68 to the haem.

The Figure shows how the haem is slightly dome-shaped

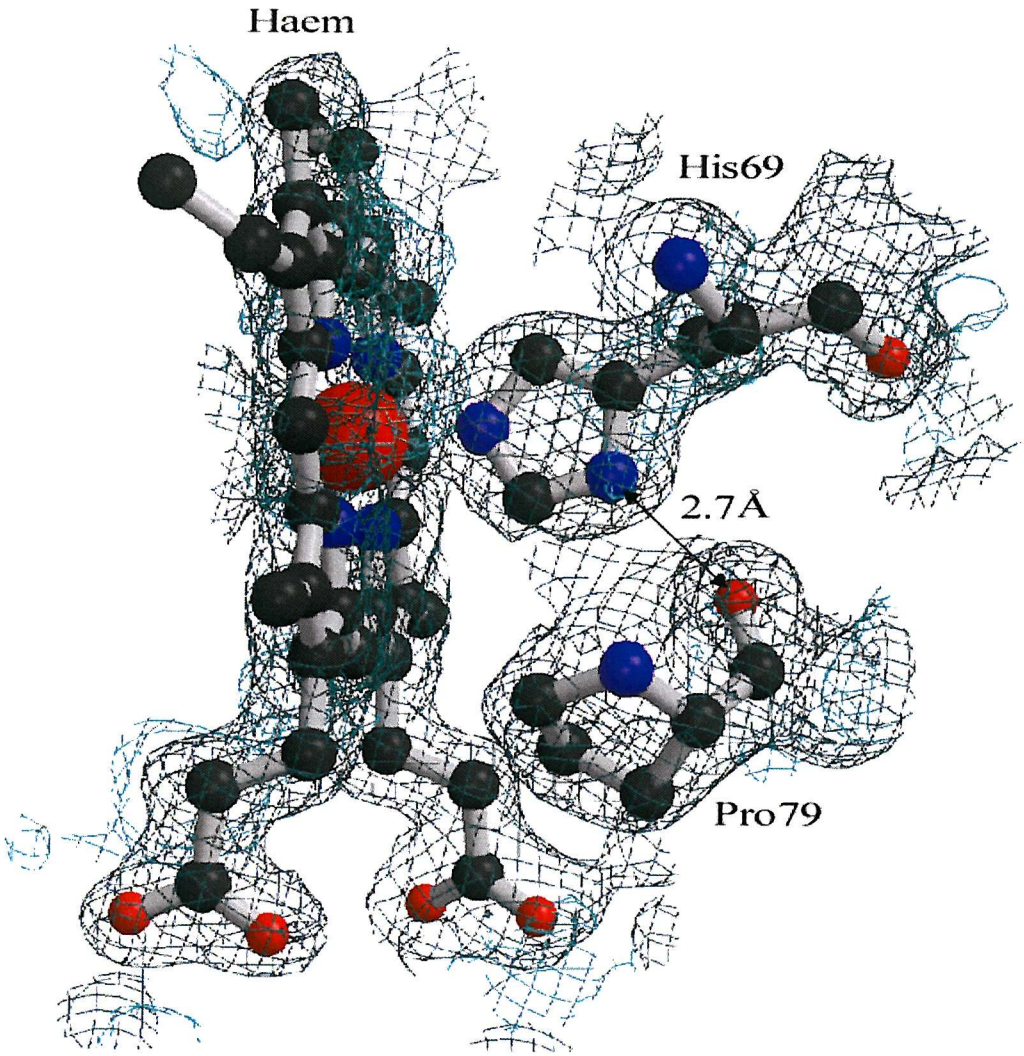

Figure 4.33 The hydrogen bonding of the His69 ligand which is coordinated to the haem Fe^{3+}

The NE2 atom from His69 is hydrogen bonded to the proline carbonyl atom.

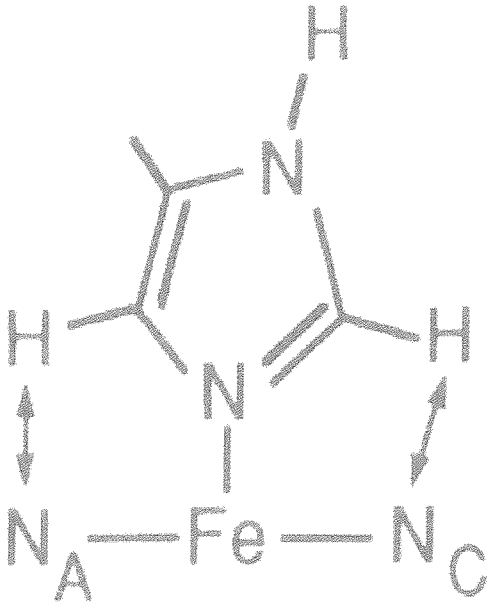

Figure 4.34a The steric interference between the hydrogens on the ligand with the nitrogen of the haem.

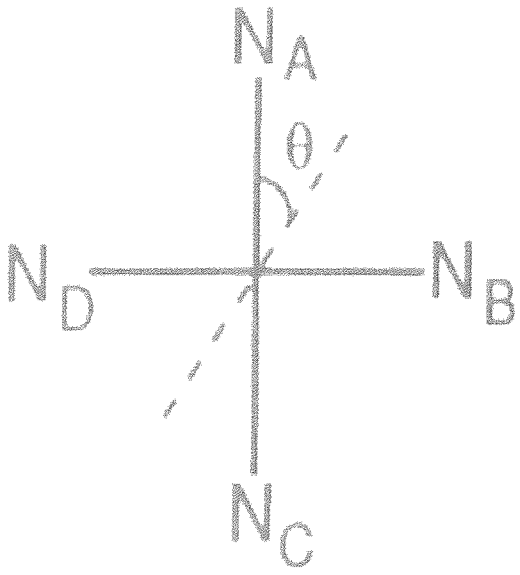

Figure 4.34b The orientation of the histidine side chain, relative to the haem. The histidine imidazole ring bisects the Fe-pyrrole bonds.

residues are roughly perpendicular to the plane of the haem (Figure 4.35). Both His69 and His112 refined well during the course of structural determination; the average B-factors for the atoms in His69 were 19.36 $Å^2$ and His112 were 26.69 $Å^2$. There was no *Fo-Fc* electron density surrounding either histidine after several rounds of refinement. The hydrogen bonding pattern surrounding His112 is slightly different from the pattern surrounding His69.The His112 NE1 atom is hydrogen bonded to the carbonyl of Met109 and not to the carbonyl of the nearby Pro113 (Figure 4.36) which is 3.7 Å from the NE1 atom (Figure 4.36). The NE1 atom also forms a hydrogen bond with a nearby water molecule (Wat84); the B-factor for this water is quite high (31 $Å^2$), indicating that it is relatively mobile. The finding that His112 forms a hydrogen bond through its NE1 atom to a nearby carbonyl is important. Previously it was thought that the histidine had to be hydrogen bonded specifically to a proline residue to maintain a perpendicular orientation with respect to the haem. Clearly this is not the case in cytochrome c_L in which the carbonyl group belongs to a methionine (Met101). A bis-histidine coordination is quite rare in *c* type cytochromes; the 6th ligand to the haem iron is usually provided by a methionine, which is the case with the related cytochrome c_{551i}. The distance between the histidine and the iron is between 2.0-2.1 Å for both histidines, which is in accordance with other cytochrome *c* structures. Sulphur is a good electron acceptor and therefore favours the electron-rich reduced state, and it is this which largely accounts for the Met-Fe-His cytochromes *c* having a more positive redox potential compared with the His-Fe-His cytochromes.

Conclusions drawn from previous spectroscopic and site-directed mutagenesis studies on cytochrome c_L are inconsistent with the X-ray crystal structure described here. The three methionines (Met109, Met108 and Met121) in cytochrome c_L were mutated separately by site-directed mutagenesis to alanines and the cytochromes were assayed for activity and the absorbance spectra recorded (a 695 nm absorbance band signifies a Met-Fe-His iron coordination). The M109A protein was the only mutant to lose activity and to lack the 695 nm absorbance band in the oxidized state. It was therefore concluded that Met109 is the sixth ligand to the haem in wild type cytchrome c_L. This methionine is conserved in cyt c_{551i} in which it is the sixth ligand to the haem.

There are several factors which may have contributed to the different haem iron coordination in the crystal. It may be that the protein preparation caused a change to the coordination of the iron. During the protein preparation the pH of crude extract is reduced to pH 4 to remove contaminating proteins; the pH is subsequently raised back to pH 8.0 immediately after this cut. This pH cut is unlikely to have brought about the change in

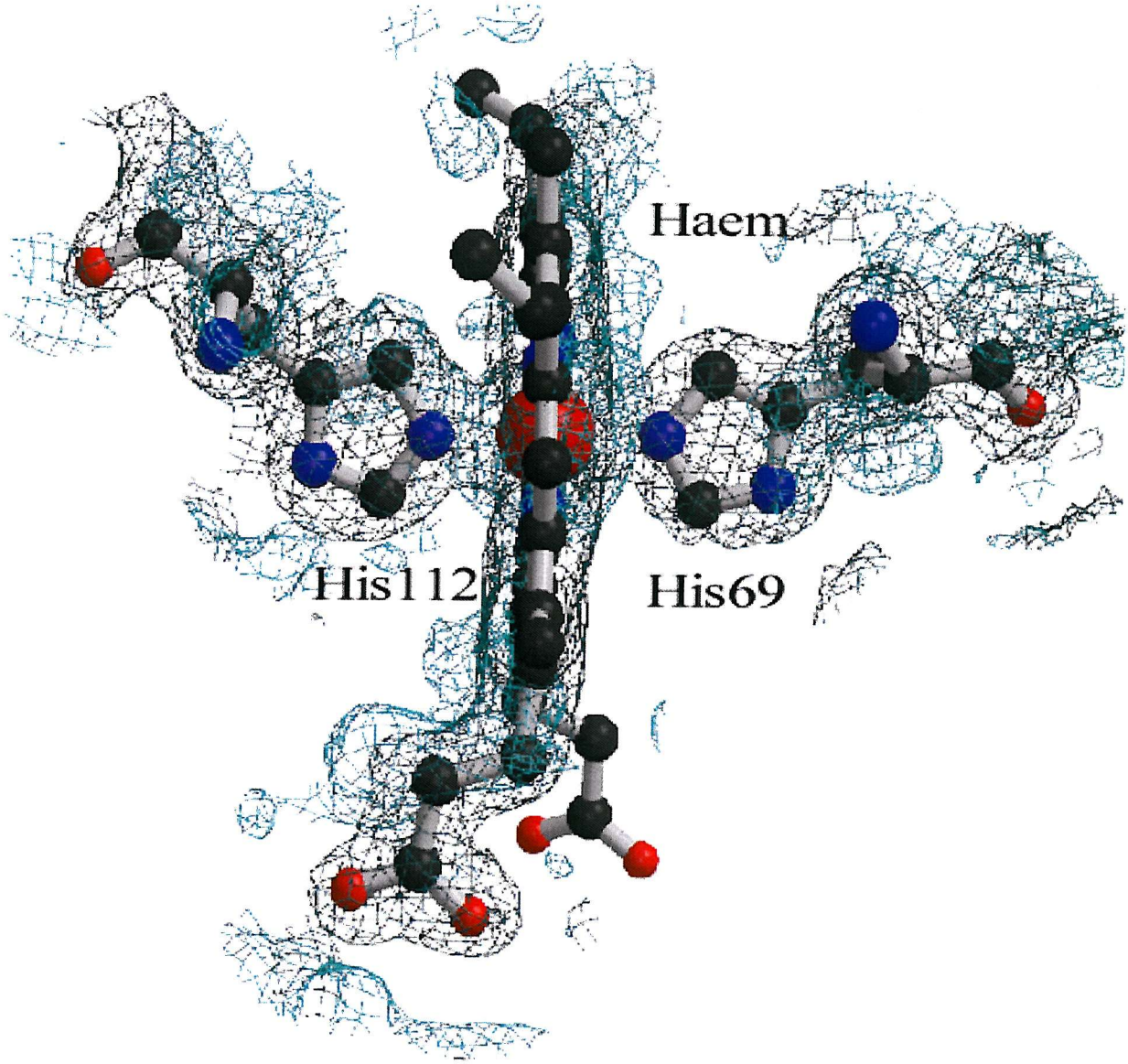

Figure 4.35 The geometry of the bis-histidine coordination to the haem iron in the 1.6 Å X-ray crystal structure of cytochrome c_L

Both of the histidine side chain rings are perpendicular to the plane of the haem

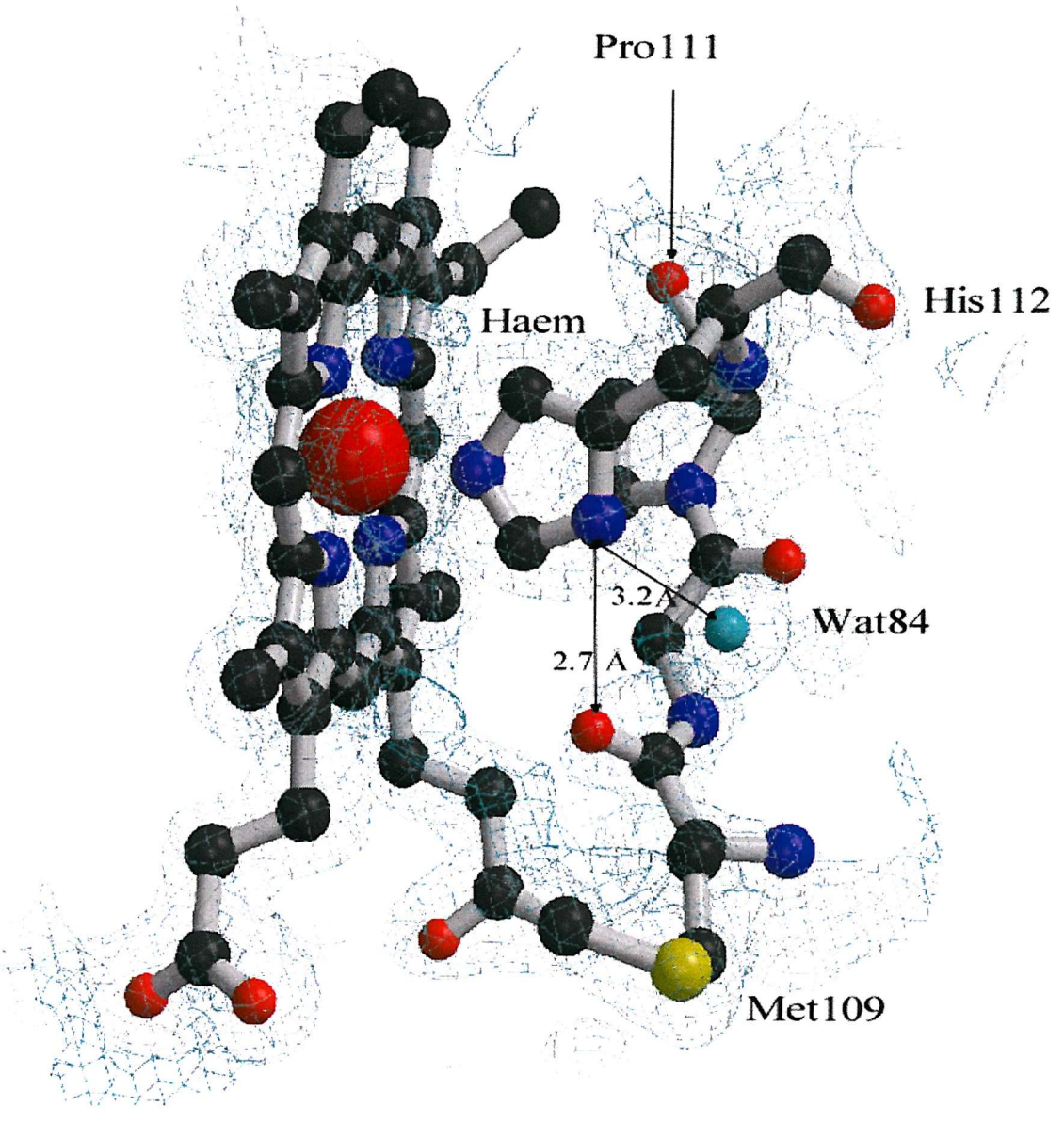

Figure 4.36 The hydrogen bonding of the His112 side chain

The distance of the NE2 atom from His112 to the carbonyl of Pro111 is too long (3.7 Å) to form a hydrogen bond (as found in other class I *c*-type cytochromes).

coordination as cytochromes are extremely compact and stable at extremes of pH, in addition, cytochrome c_L has been prepared this way for years with no problems.

The N-terminal proteolysis which may have taken place during crystallization could have made the protein less stable and prone to unfolding. Although the N-terminal arm is most likely to be a flexible region of protein, this region (1-25), which is absent from the electron density maps and presumed to be absent from the protein in the crystal, may have interacted with the loop region (Loop3: Table 4.7) containing Met109 when coordinated to the haem. Both His112 and Met109 are residues in loop 3 (Section 4.11). If these residues in the loop became exposed to bulk solvent after the removal of the N-terminal arm, this could have caused the Met109 to dissociate from the haem iron and be replaced by His112.

The methionine ligation to the haem iron is always strengthened by a hydrogen bond to the methionine sulfur, which is almost always provided by a tyrosine from helix C (Cyt c_M: 67). Cytochrome c_L is unique in that it appears to have no residue in helix C which is capable of hydrogen bonding to the methionine ligand. The region is almost exclusively hydrophobic. The lack of a hydrogen bond to the methionine is likely to weaken the interaction between the methionine and the haem iron and cause it to be easily dissociated and be replaced by an alternative ligand. The reaction of cytochrome c_L with CO reflects the readily-dissociable nature of the iron-methionine bond; 72 % of a cytochrome c_L solution reacts with CO in a CO-saturated solution at 25 °C, whereas only 36 % of cytochrome c_H reacts with CO under identical conditions (O'Keeffe & Anthony, 1980b).

Others factors which have been shown to disturb the haem iron coordination have been studied in mitochondrial cytochrome *c*. The Fe-Met bond is sensitive to changes in the hydrogen bonding patterns around the haem propionates. Chemical modifications which have stopped the hydrogen bonding capacity of Arg38 have been shown to cause a change in the coordination of the iron, as indicated by the loss of the 695 nm absorption band (Wallace & Rose, 1983). The calcium ion in this region of cytochrome c_L is likely to influence the interactions of the propionate with its protein surroundings. The presence of calcium in the 2.8 Å cytochrome c_L structure suggests that it is an important feature of cytochrome c_L, and that it is present in the native protein when in solution. However, if the calcium had just been incorporated during the crystallization then it could have influenced the coordination of the iron as the protein was removed from solution. Chemical modification of the conserved tryptophan which forms a hydrogen bond to the inner haem propionate in mitochondrial cytochrome *c* (cyt c_M; Trp59) was also shown to alter the coordination to the haem iron. The

tryptophan side chain was chemically modified to remove its capacity to hydrogen bond to the inner haem propionate. This caused a change in the haem iron coordination, demonstrated by the loss of the 695 nm absorption band (Aviram & Schejter, 1971). However, mutating the tryptophan to a phenylalanine, which would also be unable to hydrogen bond to the inner haem propionate, did not alter the coordination. The alternative conclusion is that a bulky residue is required in this position, which need not, however be a tryptophan, and a hydrogen bond to the propionate may not be essential.

Cytochrome c_L undergoes an autoreduction process in the absence of MDH if the pH is raised to pH 10 (Beardmore-Gray *et al.*, 1982). During this process the methionine is replaced by an alternative strong field ligand (Beardmore-Gray *et al.*, 1982), which, from the structure reported in this thesis, is most likely to be His112. This process could be reversed by decreasing the pH to 7.0; the 695 nm band did not re-appear on oxidation with ferricyanide at pH 10. When reduced with dithiothreitol at pH 7.0 cytochrome c_L loses the 695 nm absorption band (Beardmore-Gray *et al.*, 1982). The dissociation of the iron methionine bond that occurs on raising the pH to 10 or reducing it with DTT does not occur in cytochrome c_L when the protein undergoes reduction by MDH. It is unlikely that at pH 8.0 (the pH of the TRIS buffer during protein preparation) the methionine would be displaced by the histidine due to the autoreduction process as the pK for this process is pH 10. The conditions for crystallography are carried at pH 6.5, so again this pH should have no effect on the iron-methionine bond.

c) The hydrogen bonding pattern surrounding the haem propionates.

Just as the haem macrocycle interacts with hydrophobic residues, the haem propionates interact with polar residues. A common hydrogen-bonding pattern involving the propionates is difficult to define and may not exist, although there are several common features. It is notable that the inner haem propionate is close to a species which can carry a positive charge. In most cases this is a conserved arginine (cyt c_M: Arg38), but in the case of cytochrome c_L the charge is provided by a calcium ion.

A tryptophan (cyt c_M: 59) is conserved in all mitochondrial cytochromes *c* and has a counterpart in most bacterial cytochromes *c*. Although widespread, a tryptophan in this structural position is not essential for a class I cytochromes. This was shown by the W59F mutants of mitochondrial cytochrome *c*, which retained all wild type properties, raising the question, why does this substitution not occur in any naturally-occurring cytochromes *c*? This may be due to protein stability, as it is worth mentioning that Trp59 and Arg38 do form a

main chain hydrogen bond in mitochondrial cytochrome *c*; the backbone nitrogen from Trp59 forms a strong hydrogen bond (2.6 Å) to the backbone oxygen atom from Arg38. By replacing Arg38 with a Ca^{2+} ion, as in cytochrome c_L, the possibility for this hydrogen bond is taken away, which allows the tryptophan to adopt the alternative conformation that is seen in cytochrome c_L. In this alternative conformation the main chain nitrogen and the side chain of Trp86 hydrogen bond to a water molecule (Wat13), and not to the inner haem propionate (Figure 4.37)

In the case of most mitochondrial cytochromes *c* and bacterial cytochromes c_2 the outer haem propionate (HP6) has no direct interaction with solvent; this is prevented from by forming hydrogen bonds with the side chains of a buried threonine or serine and the main chain of a lysine residue. By contrast, the outer haem propionate in cytochrome c_L is highly exposed to solvent (Figures 4.38 and 4.39). It forms only one hydrogen bond to an amino acid side chain (Tyr88), which is also coordinated to the calcium ion through its carbonyl group; there are also no conserved threonine or asparagine residues in the region. A conserved asparagine (tuna: Asn52) and threonine (tuna: Thr78) have both been implicated in redox-related conformation changes in mitochondrial cytochromes *c* (Section 1.13.1). Figures 4.38 and 4.39 also show that the inner haem propionate in mitochondrial cytochrome *c* is prevented from forming hydrogen bonds with bulk solvent by its hydrogen bonding to a conserved tyrosine (tuna: Tyr 48), and also the long side chain of Arg38 shields the propionate from the bulk solvent. Because of the rearrangement around the propionate, due to the bound calcium ion, in cytochrome c_L, this propionate is hydrogen bonded to two water molecules, Wat7 and Wat8, both of which are coordinated to the calcium ion. The exposed nature of this inner haem propionate could contribute to the unusual pH-dependence of redox potential as proposed by O'Keeffe & Anthony (1980b).

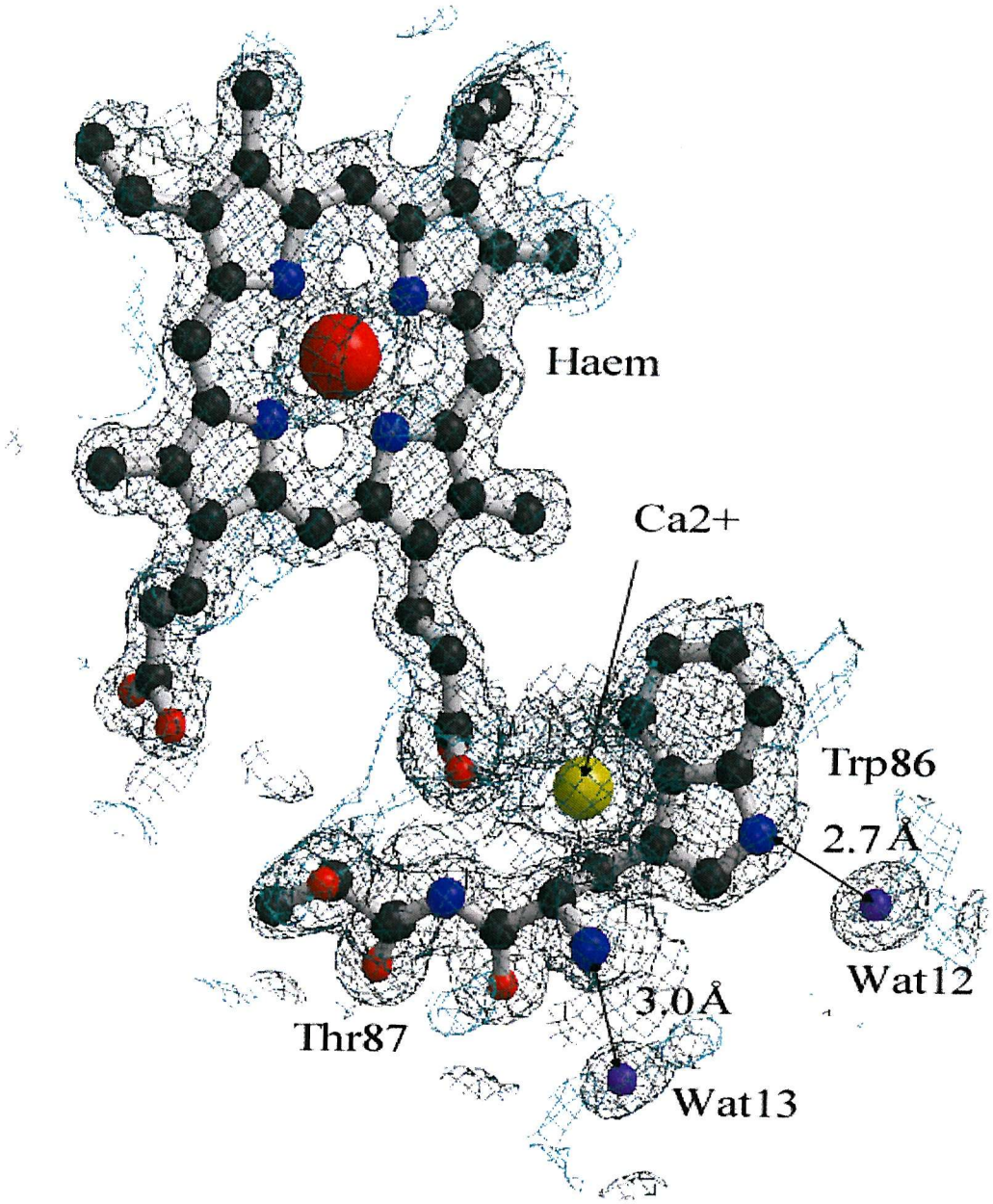

Figure 4.37 The hydrogen bonding interactions of Trp88 from cytochrome c_L

Trp88 is hydrogen bonded to Wat13 and Wat12 via the carbonyl nitrogen and the indole nitrogen respectively; it does not interact with the inner haem propionate or the calcium ion.

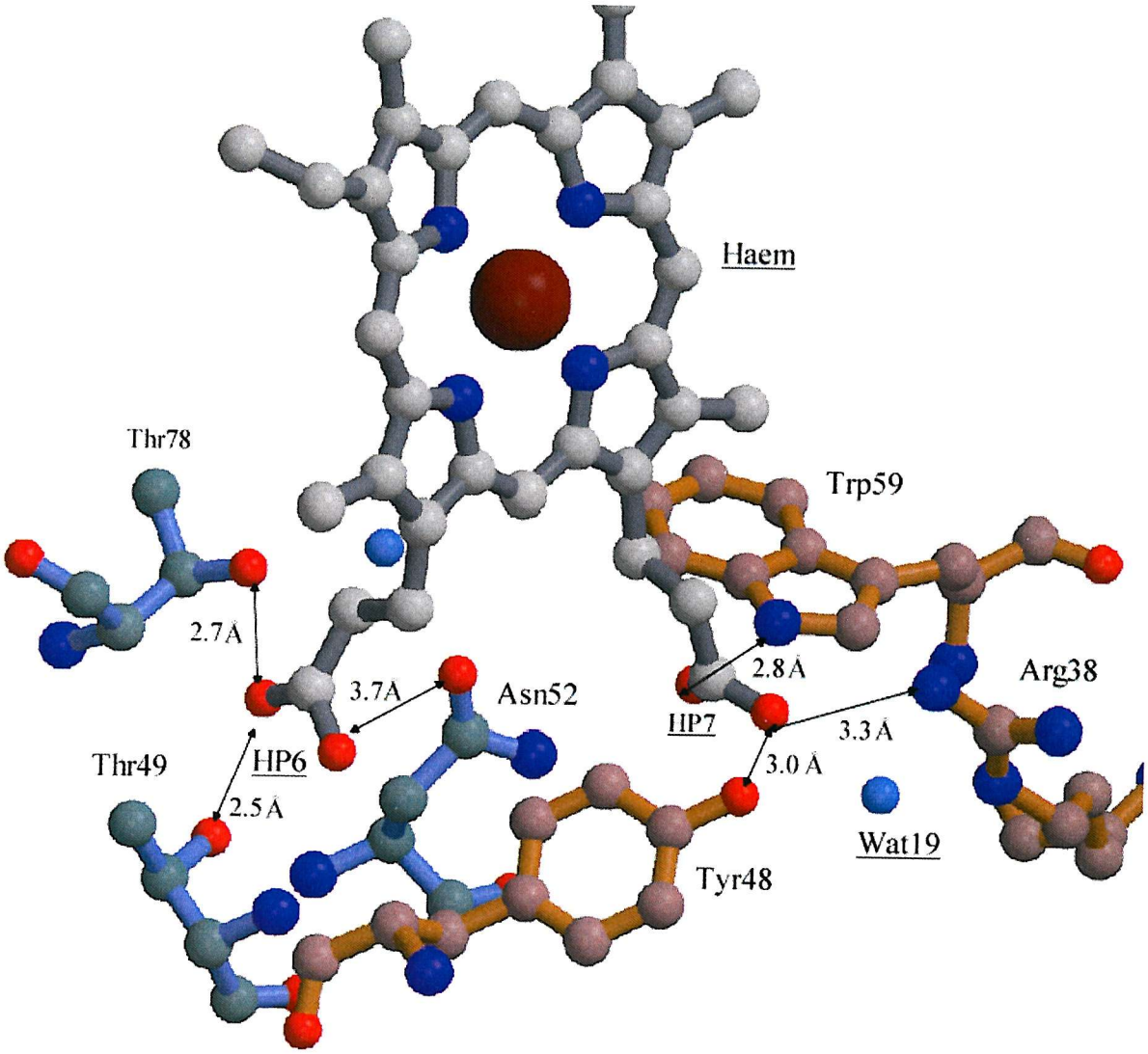

Figure 4.38 The hydrogen bonding pattern around the haem propionates in oxidized tuna cytochrome *c*

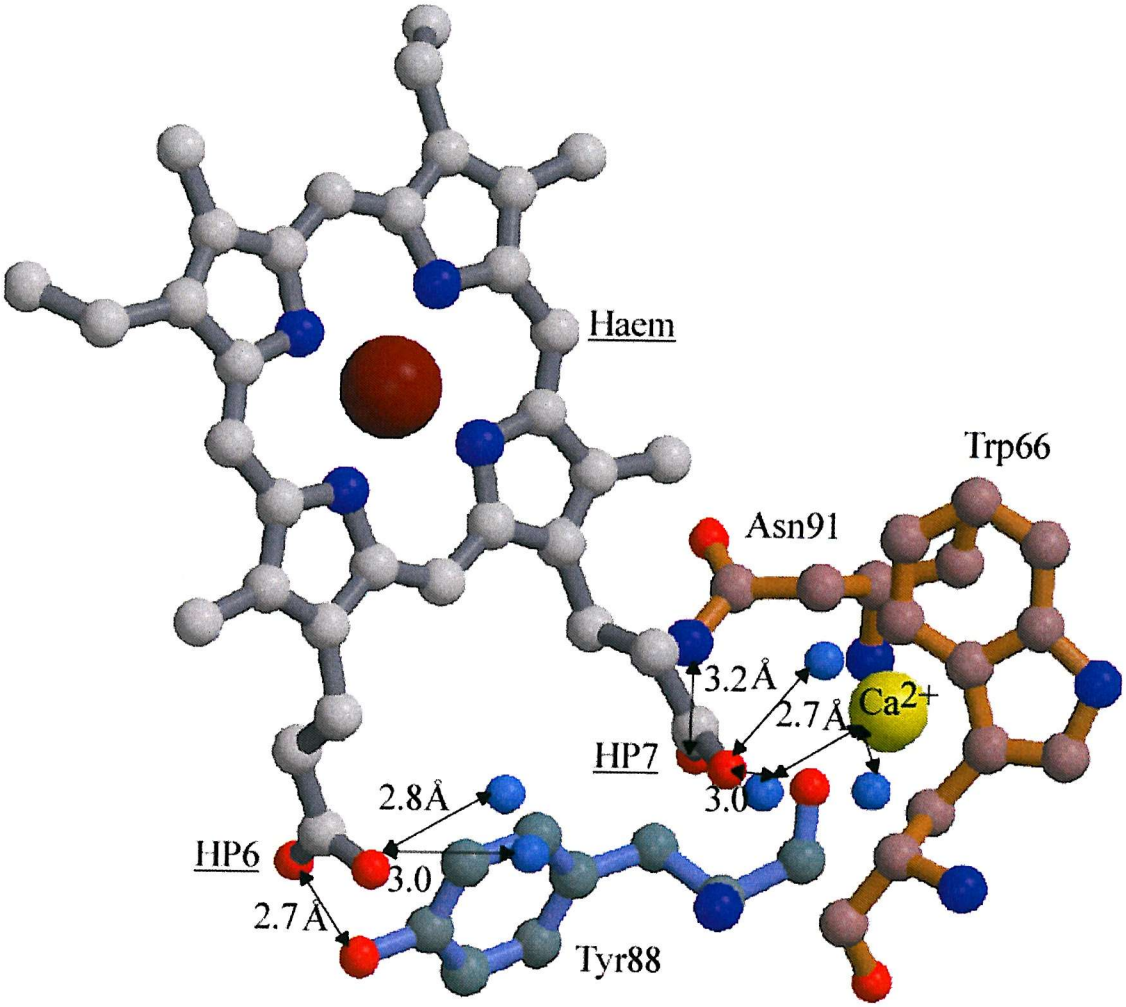

Figure 4.39 The hydrogen bonding pattern surrounding the haem propionates in oxidized cytochrome c_L

Chapter 5

Characterisation and the X-ray crystal structure of methanol dehydrogenase from the *Methylobacterium extorquens* mutant *mxaC31*

5.1 Introduction

In *Methylobacterium extorquens* there are at least 30 genes which are involved in the oxidation of methanol; these also include those genes which are involved in the synthesis of PQQ (Section 1.17). The genes which code for the α and β-subunits of MDH (*mxaF* and *mxaI*) are present in the gene cluster, *mxaFJGIR(S)ACKLD* (Amaratunga *et al.*, 1997). A mutation in any of the three genes *mxaA, K* or *L* creates an organism which produces inactive MDH (mxaAKL-MDH) and is unable to grow on methanol. The activity of MDH from the mutant organisms can be reestablished by reconstituting purified MDH with high concentrations of calcium ions at a high pH (Richardson & Anthony, 1992). Further experiments on MDH from *mxaA* (mxaA-MDH) led to the characterization of the enzyme with barium and strontium in the active site (Goodwin & Anthony, 1996: Goodwin *et al.*, 1996). This leaves two genes from the *mxaACKLD* group which code for proteins whose function is unknown; these genes are *mxaC* and *mxaD*. An insertion mutation has been introduced into the *mxaC* gene of *M. extorquens* to create methanol oxidation mutant, *mxaC31*, which is unable to grow on methanol (Toyama *et al.*, 1998). In this Chapter the characterization and X-ray crystal structure of MDH purified from *mxaC31* (mxaC31-MDH) has been carried out; this was to determine if *mxaC* codes for a protein that is involved in inserting calcium into the active site of MDH.

5.2 Growth of *mxaC31* and purification of MDH

The growth medium which was used to grow *mxaC31* contained methylamine hydrochloride as the carbon source and the antibiotic used was kanamycin (300 μg/ml). The expression of MDH in the mutant bacteria was approximately the same as in wild type bacteria; a 15 litre bacterial culture yielded approximately 180 mg of MDH. The molecular weight of the α-subunit of MDH was estimated from SDS-PAGE (Figure 5.1). This shows that the α-subunit of wild type-MDH and mxaC31-MDH migrated to the same position on SDS-PAGE. The mxaC31-MDH was inactive when it was assayed in the standard dye-linked assay system (Section 2.3), although the enzyme activity could be recovered by incubating

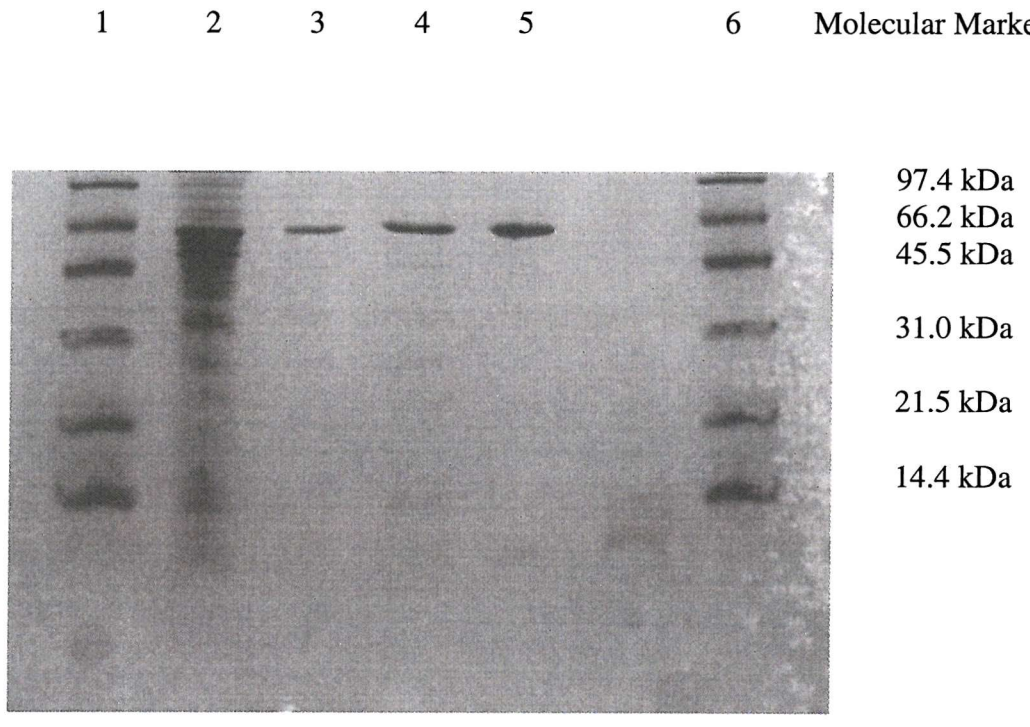

Figure 5.1 SDS-PAGE showing wild type-MDH (lane 4) and mxaC31-MDH (lane 5). Molecular markers are in lanes 1 and 6

The Figure shows that the α-subunit of mxaC-MDH and wild-type-MDH migrate to approximately the same position on SDS-PAGE.

the MDH with high concentrations of calcium, strontium or barium ions (see below).

5.3 **Reconstitution of mxaC31-MDH with calcium, strontium or barium ions.**

For MDH to recover enzyme activity it was incubated at a high pH (9.0) with the divalent ions Ca^{2+}, Sr^{2+}or Ba^{2+} at 25 °C; the enzyme remained inactive when it was incubated with Mg^{2+} ions. Figures 5.2 and 5.3 show the recovery of active enzyme was dependent on the concentration of the divalent ion, and on the time of incubation. It was fully reconstituted after 90 minutes incubation with 40 mM Ca^{2+}; neither the substrate nor the activator (ammonia) was necessary for the reconstitution.

The maximum enzyme specific activity was different when MDH was reconstituted with Ca^{2+}, Sr^{2+}or Ba^{2+} (measured using the standard dye-linked assay). Ca-MDH had the highest activity of 669.5 nmoles/mg/min, compared with 361 nmoles/mg/min for Sr-MDH and 209 nmoles/mg/min for Ba-MDH. The concentration of divalent ions that was required to give half the maximum activity also varied when MDH was reconstituted with the three different ions; it required 29.0 mM for Ba-MDH, 27.13 mM for Sr-MDH and 12.53 mM for Ca-MDH. These results reflect the relative sizes of the three ions; barium is the largest, followed by strontium and finally calcium.

5.4 **The absorbance spectrum of mxaC31-MDH**

Absorption spectrum changes occurred as mxaAKL-MDH was reconstituted with Ca^{2+} (Richardson & Anthony., 1992: Goodwin *et al.*, 1996). The absorption spectrum of unreconstituted mxaAKL-MDH was considerably different from wild type-MDH (Figure 5.4). The characteristic absorption peak at 345 nm is absent in mxaAKL-MDH and an absorption peak at 520 nm is seen, suggesting that PQQ is bound differently in the active site. The absorption spectrum of unreconstituted mxaC31-MDH (Figure 5.5a) was similar to mxaAKL-MDH, where the characteristic peak at 345 nm is absent. Following the reconstitution of mxaC31-MDH with calcium, strontium or barium, the absorption spectrum changed to resemble the absorption spectrum of wild type-MDH (Figure 5.5b).

5.5 **The effect of pH on reconstitution**

The pH optimum for the reconstitution of holo-MDH from *mxaC31* was approximately 10.0 (Figure 5.6), as was the case with mxaA-MDH. The observed pK of 8.5-9.0 would suggest that a single arginine, lysine or tyrosine residue plays some part in the

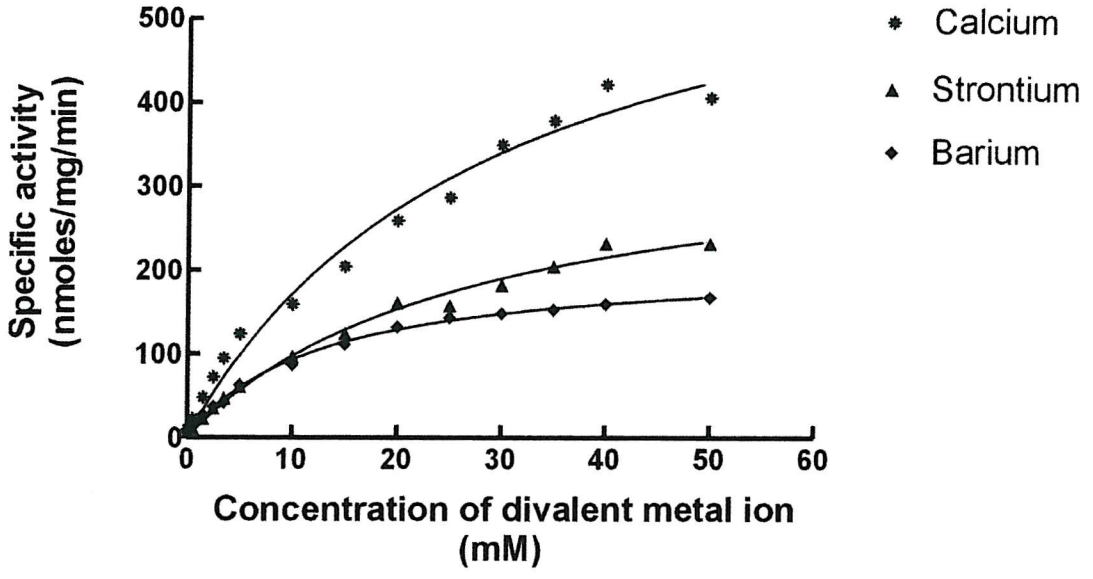

Figure 5.2 The specific activity of mxaC31-MDH after reconstitution for 1 hr at 25 °C, pH 9.0 with various concentrations of divalent cations (the activity was measured using the standard dye-linked assay)

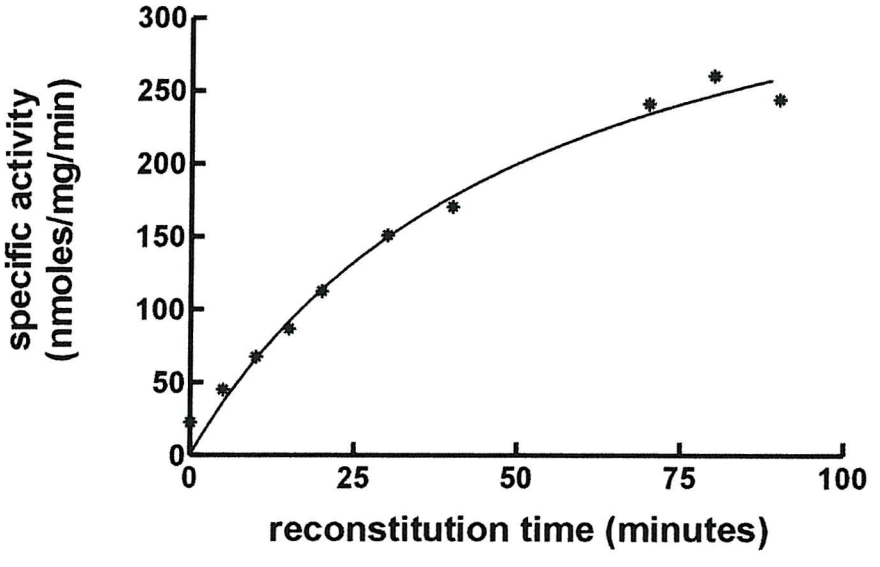

Figure 5.3 The specific activity of mxaC31-MDH after reconstitution with 40 mM Ca^{2+} at 25 °C, pH 9.0, for various time spans (assayed using the standard dye-linked assay)

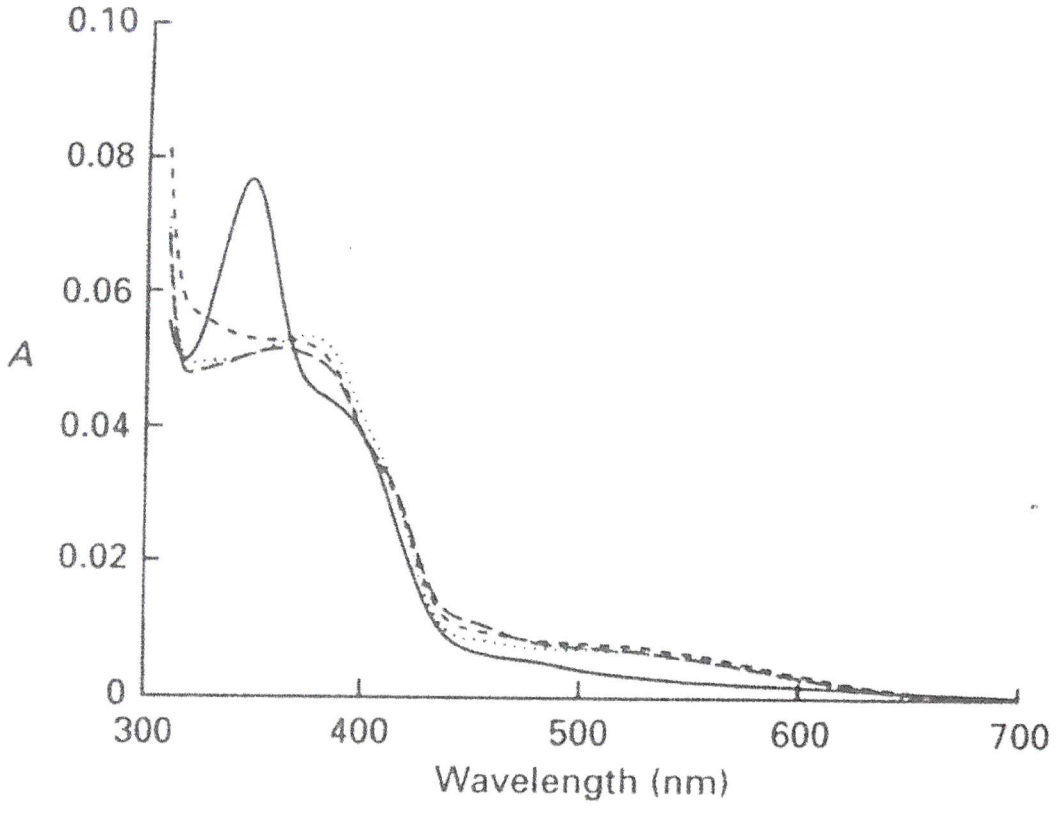

Figure 5.4 The absorption spectrum of MDH from wild type *M. extorquens* and from the *mxaA, mxaK* and *mxaL* mutants

Spectra of MDH (1 mg/ml) were recorded in 100 mM potassium phosphate buffer, pH 7.0, at 20 °C, — wild type MDH; – – – MxaA; ------ MxaK; ····· MxaL.

a)

Unreconstituted mxaC31-MDH

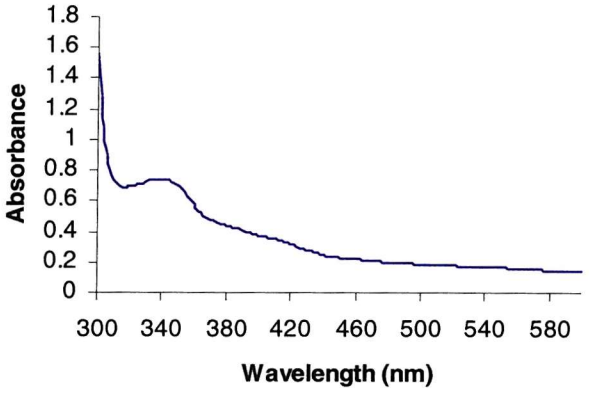

b)

Reconstituted mxaC31-MDH (reconstituted with 40 mM $CaCl_2$)

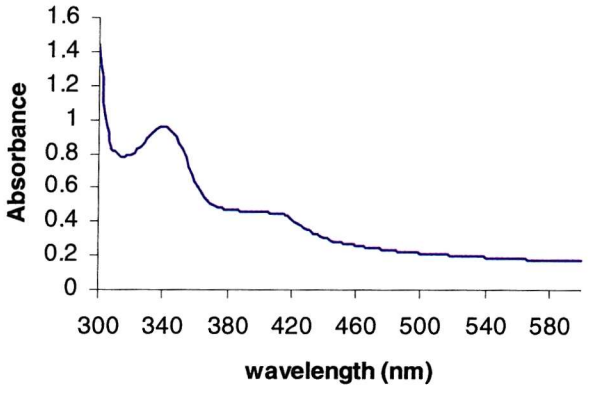

Figure 5.5 The absorption spectrum of mxaC31-MDH before reconstitution, and after reconstitution with 40 mM $CaCl_2$

The absorption spectrum of MDH (2 mg/ml) was recorded in 20 mM Tris/HCL buffer, pH 8.0, at 20 °C.

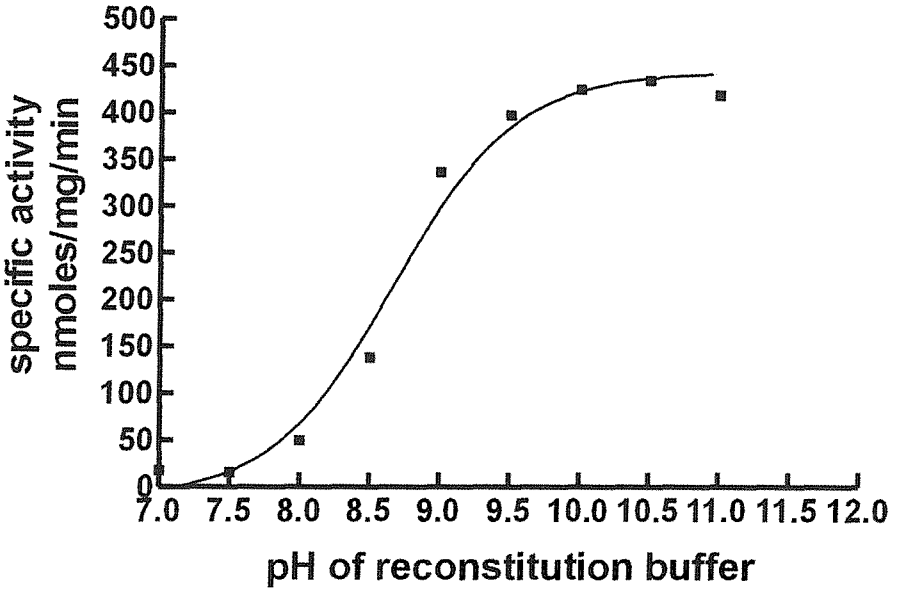

Figure 5.6 The effect of pH on the reconstitution process

The enzyme was reconstituted with 40 mM Ca^{2+} for 1 hr, 25 °C at different pH values, and assayed for activity using the standard dye-linked assay.

incorporation process (Goodwin *et al.*, 1996). Although between pH 8.0-10.0 cysteine residues in disulphide bridges can undergo a process known as thiol exchange. This would require a reducing environment to initially break the disulphide bridge and also a nearby thiol group to reform the disulphide bridge. The active site of mxaC31-MDH was expected to be somewhat different to the active site of wild type-MDH. To pinpoint these differences the X-ray crystal structures of unreconstituted mxaC31-MDH was undertaken (Section 5.7-5.15).

5.6 **Properties of reconstituted holo-MDH**

The mxaC31-MDH had a different tolerance to high temperatures after it was reconstituted with Ca^{2+}, Sr^{2+} or Ba^{2+} (Figure 5.7). Wild type-MDH was relatively stable to thermal inactivation and retained most of its activity after a 10 minute incubation at 64.0 °C (Figure 5.8). The mxaC31-MDH appeared to be most stable to heat treatment when it was reconstituted with strontium (Sr>Ca>Ba); the enzyme reconstituted with strontium remained active after a 10-minute incubation at temperatures above 70 °C. Furthermore, Sr-MDH had the lowest rate of inactivation (Figure 5.8). After the enzyme had been reconstituted with either of the three divalent ions and subsequently incubated at 64 °C, Sr-MDH retained enzyme activity for a longer time period than the other two enzymes.

These data are similar to data from MDH from *Paracoccus denitrificans* which had strontium in the active site instead of calcium. Strontium was incorporated into MDH by growing *P. denitrificans* in a strontium-rich growth medium (Harris & Davidson, 1994a, b). At temperatures in the transition region for stability, the rate constants for inactivation of Sr-MDH were two-fold lower than those for Ca-MDH. However, Arrhenius plots yielded a lower activation energy for Sr-MDH than for Ca-MDH (640 KJ/mol and 699 KJ/mol respectively). Further analysis suggested that the difference in the rate of inactivation at high temperatures of the Sr-MDH and Ca-MDH was a consequence of a favorable gain in entropy (Harris & Davidson, 1994b). The difference in thermal stability of Ca-MDH and Sr-MDH in both *P. denitrificans* and *M. extorquens* can be explained by the calcium coordination in the active site. Calcium is coordinated to six ligands in the active site; three atoms are from PQQ and three from the protein residues (Section 1.9: Figure 1.3). This arrangement allows a calcium ion (0.99 Å) to fit tightly into the cavity created from the C-5 carbonyl, the C-7 carboxylate oxygen and the quinoline N6 of PQQ. The larger ionic radius of Sr^{2+} (1.13 Å) would cause a steric perturbation in the positioning of the PQQ or the glutamate or asparagine side chains which are coordinated to the calcium. The replacement of the calcium

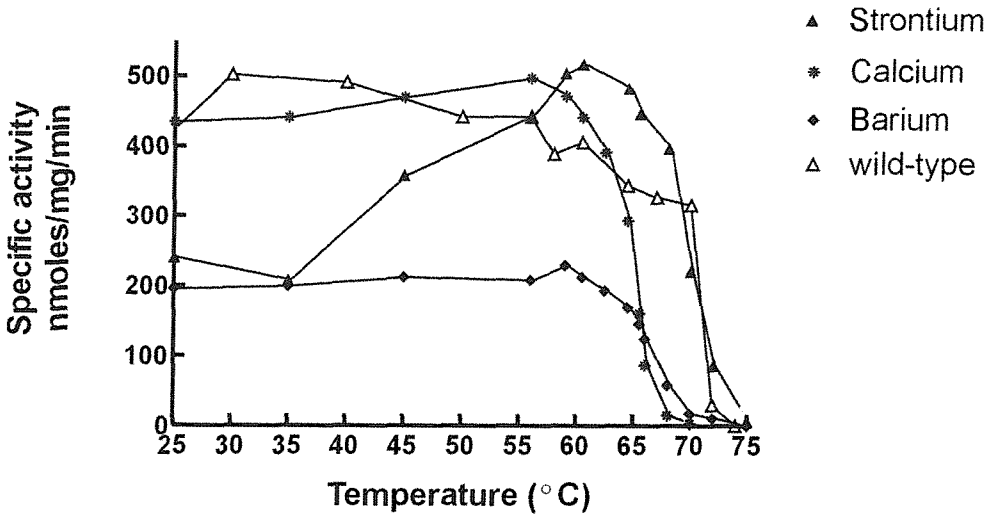

Figure 5.7 The stability of mxaC31-MDH

The activity of mxaC31-MDH measured using the dye-linked assay at various temperatures after it was reconstituted with calcium, strontium and barium for 1 hr, pH 9.0.

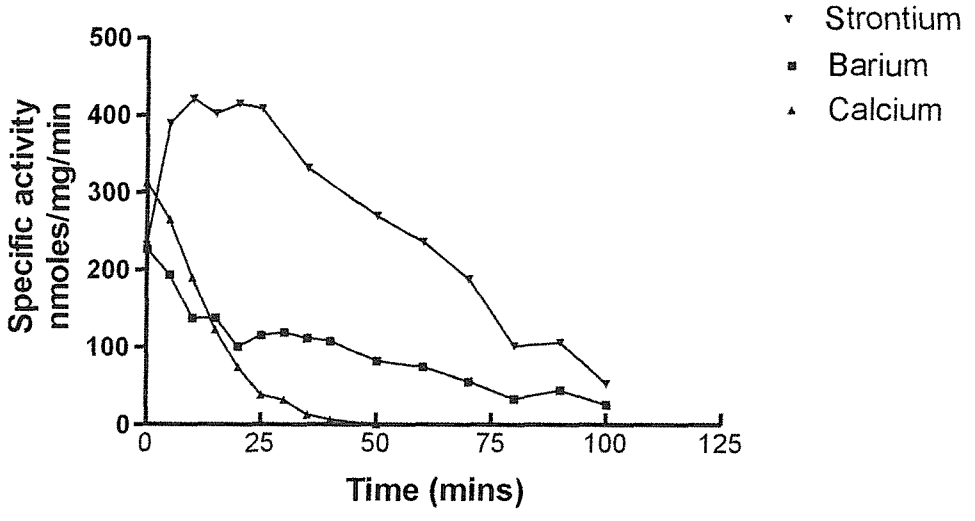

Figure 5.8 The effect of heat (64 °C) on the inactivation of mxaC31-MDH

The mxaC31-MDH was reconstituted with 40 mM divalent ions for 1hr, pH 9.0 at 25 °C and then incubated at 64 °C for various amounts of time before the activity was measured.

with strontium could therefore result in changes in the numbers or strength of the hydrogen bonds to the PQQ, which could change the solvation environment of PQQ and cause differences in the thermal stability of MDH. Previous studies on mxaAKL-MDH showed the effect of NH_4Cl concentration on activity was different when the protein was reconstituted with Ca^{2+}, Sr^{2+} or Ba^{2+} (Goodwin & Anthony, 1996). This was also the case for mxaC31-MDH (Figure 5.9). Ba-MDH has a lower affinity for methanol than Ca-MDH and this facilitated the study of the effect of ammonia on substrate binding to the enzyme. From work on Ba-MDH it appears the affinity of the enzyme for methanol decreases with increasing concentration of the activator; this observation is consistent with the conclusion that although methanol and ammonia are essential for activity, each binds more strongly to the enzyme in the absence of the other. This suggests that the binding site for ammonia is likely to be independent of, but very close to the methanol binding site (Goodwin & Anthony, 1996).

5.7 **X-ray crystallography of mxaC31-MDH**

The aim of the work described here was to use X-ray crystallography to determine the structure of un-reconstituted and barium-reconstituted mxaC31-MDH.

5.7.1 **Crystallization of MDH from *mxaC31***

The same conditions were used to crystallize mxaC31-MDH as were used to crystallize wild type MDH (Afolabi *et al.*, 2001); the mother liquor contained 15 % PEG 6 K and 100 mM Tris/HCl at pH 9.0. The MDH was buffered with 100 mM Tris, pH 8.0 and had a final concentration of 20 mg/ml. The crystals were obtained using the hanging drop method; one example of the crystals that were produced is shown in Figure 5.10.

5.7.2 **Data processing of unreconstituted mxaC31-MDH**

X-ray diffraction data from a single crystal were collected using an ADSC Quantum detector at the ESRF (Grenoble, France). A single diffraction pattern of unreconstituted mxaC31-MDH is shown in Figure 5.11; the crystal diffracted X-rays to 1.2 Å. The unit cell dimensions and space group for MDH were estimated using MOSFLM (a = 62.9 Å, b = 73.62 Å c = 88.08 Å, α = 86.09 β = 104.11 and γ = 109.68, space group P1). MDH has previously been solved in a triclinic cell (Ghosh *et al.*, 1995). A high and a low-resolution data set were collected and processed using the programs of the CCP4 suit. HKLV1EW was used to confirm the space group. Reflection data from a P1 space group would show no extra mirror

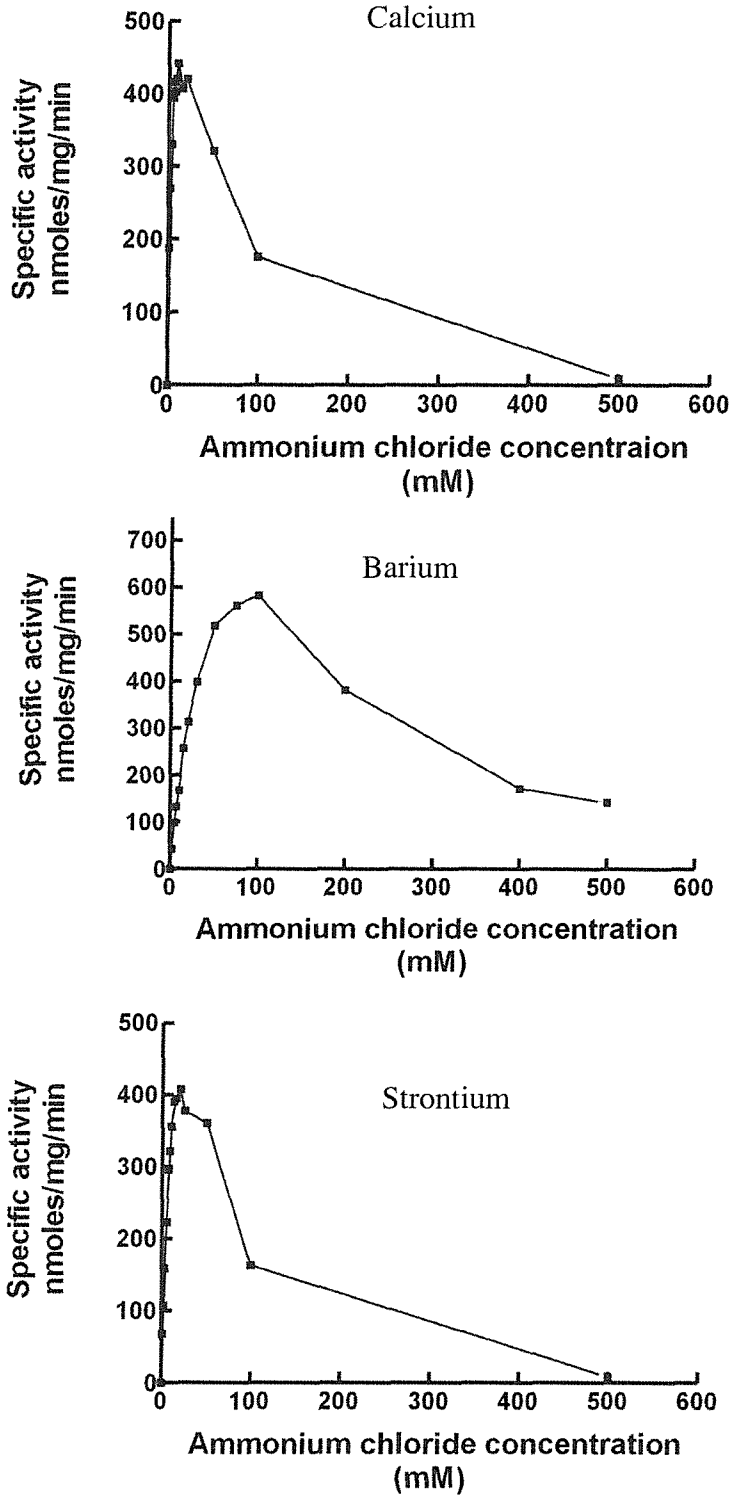

Figure 5.9 The effect of ammonium concentration on the activity of the mxaC31-MDH

The enzyme was reconstituted with 40 mM divalent ions for 1 hr 25 °C, pH 9.0 and then assayed using the dye-linked assay with various amounts of ammonia in the reaction buffer and 10 mM methanol.

Figure 5.10 Crystals of unreconstituted mxaC31-MDH

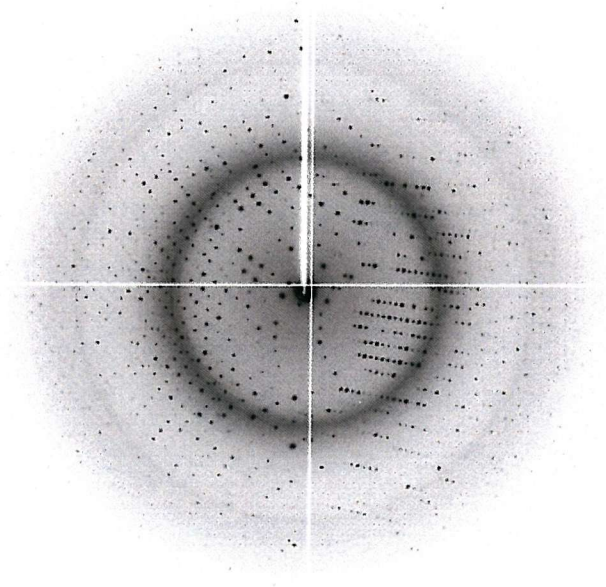

Figure 5.11 A high-resolution diffraction pattern for mxaC31-MDH

The crystal diffracted the X-rays from a synchrotron source to 1.2 Å.

planes in the diffraction data and, as Figure 5.12 shows, there was no additional symmetry in the diffraction data. A solvent content of 52 % was calculated using the Mathews coefficient. Table 5.1 shows the final data processing statistics.

5.7.3 **Molecular replacement studies on mxaC31-MDH**

Molecular replacement, using the program MOLREP was used to obtain initial phases (Vagin & Teplykov, 1997). The phasing model consisted of a single $\alpha_2\beta_2$ tetramer, with the PQQ and metal ions removed (this thesis). Table 5.2 shows the five peaks that were found when running the cross-rotation function; two significant peaks were found, which corresponded to the two possible orientations of the search molecule due to its internal symmetry. In P1 a translation function is not necessary as the position of the molecule in the cell is arbitrary. The protein coordinate file from MOLREP was subsequently used for refinement and model building.

5.7.4 **Refinement of the 1.2 Å mxaC31-MDH structure**

The refinement and model building were undertaken using the programs from the CNS suite and QUANTA respectively. Initially, isotropic refinement was performed within the resolution range of 33.3-1.2 Å. After the first round of refinement the *R*-factor and the *R*-free were 28.35 % and 28.74 % respectively. The *Fo-Fc* electron density at this stage was sufficient to build in the two PQQ molecules (Figure 5.13) and 366 water molecules; the water molecules were added using the QUANTA program X-SOLVATE. After three further rounds of model building and refinement the *R*-factor was 21 % and the *R*-free was 22 %, it was at this stage that the data were refined anisotropically.

5.7.5 **Anisotropic refinement**

The crystal which was used for the data collection diffracted to 1.2 Å; this allowed the model to be refined anisotropically. Crystallographic refinement programs adjust the x, y, z coordinates of the atoms, the occupancy and the B-factor for each atom in the structure. The B-factor can either be refined by a single number, indicating that the thermal motion is the same in all directions, or by six numbers (six directions), in which the thermal motion in each direction can differ, giving a more realistic model of thermal motion for each atom. For anisotropic refinement to be feasible, at least 2.25 times more observations are needed than is required to do isotropic B-factor refinement; the number of observations per atom rises from

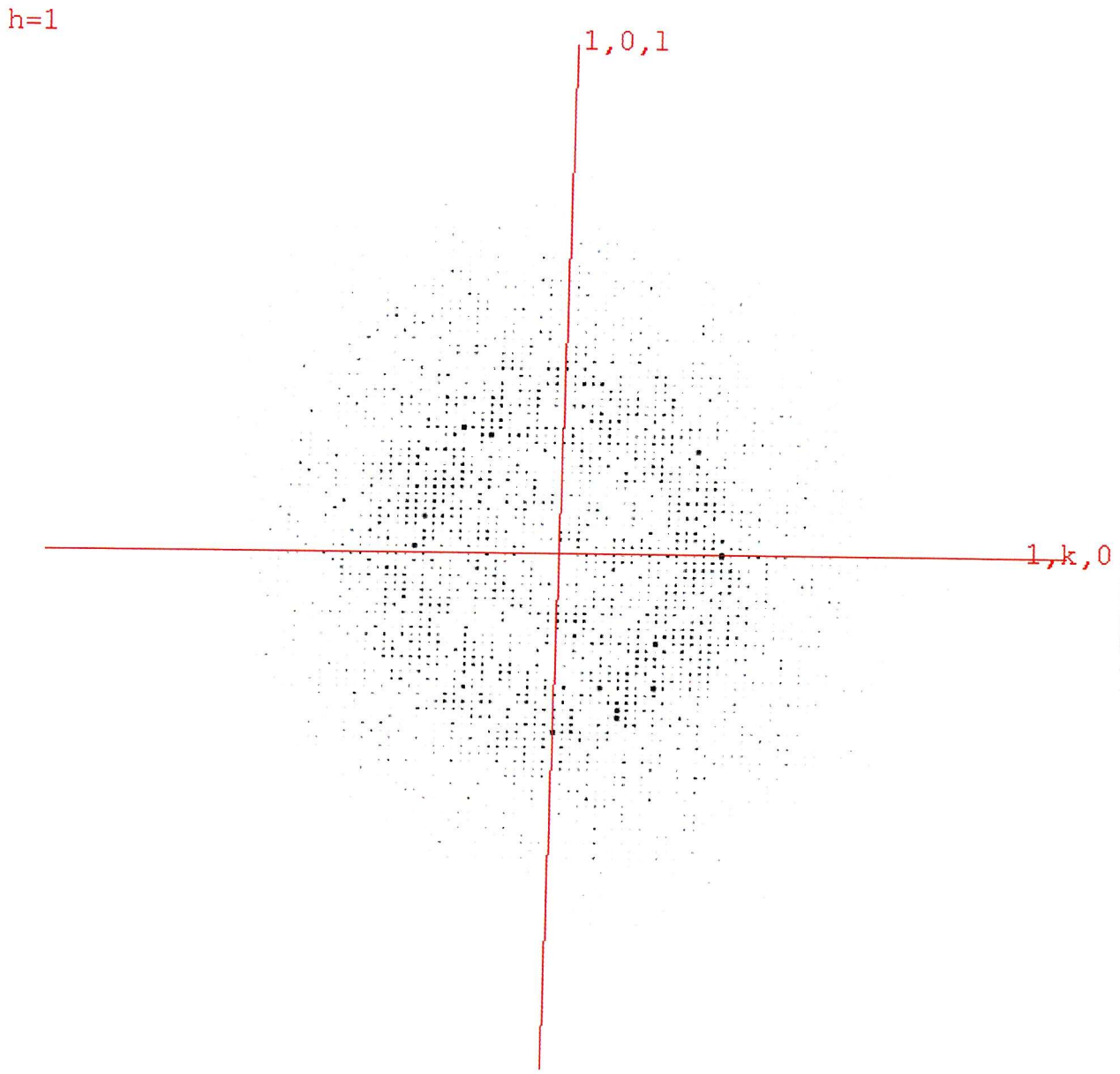

Figure 5.12 HKLVIEW of the diffraction data

There is no extra symmetry in the upper layers of the diffraction data; this is further evidence of a P1 space group.

Table 5.1 The final data processing statistics for mxaC31-MDH

Total number of reflections	724568
Number of unique reflections	373341
Resolution (Å)	1.20
Completeness (%)	90.3
R_{merge} (outer resolution shell)	10.3 (44)
Multiplicity	2.0
Average I/σ (outer resolution shell)	2.3 (1.3)

Table 5.2 The 5 cross-rotation functions performed with MOLREP

Peak number	α	β	γ	Rf/σ
1	300.5	54.43	120.0	47.45
2	83.43	118.41	274.43	47.21
3	276.20	122.87	299.51	5.68
4	28.14	159.67	349.06	5.67
5	52.31	57.08	220.01	5.61

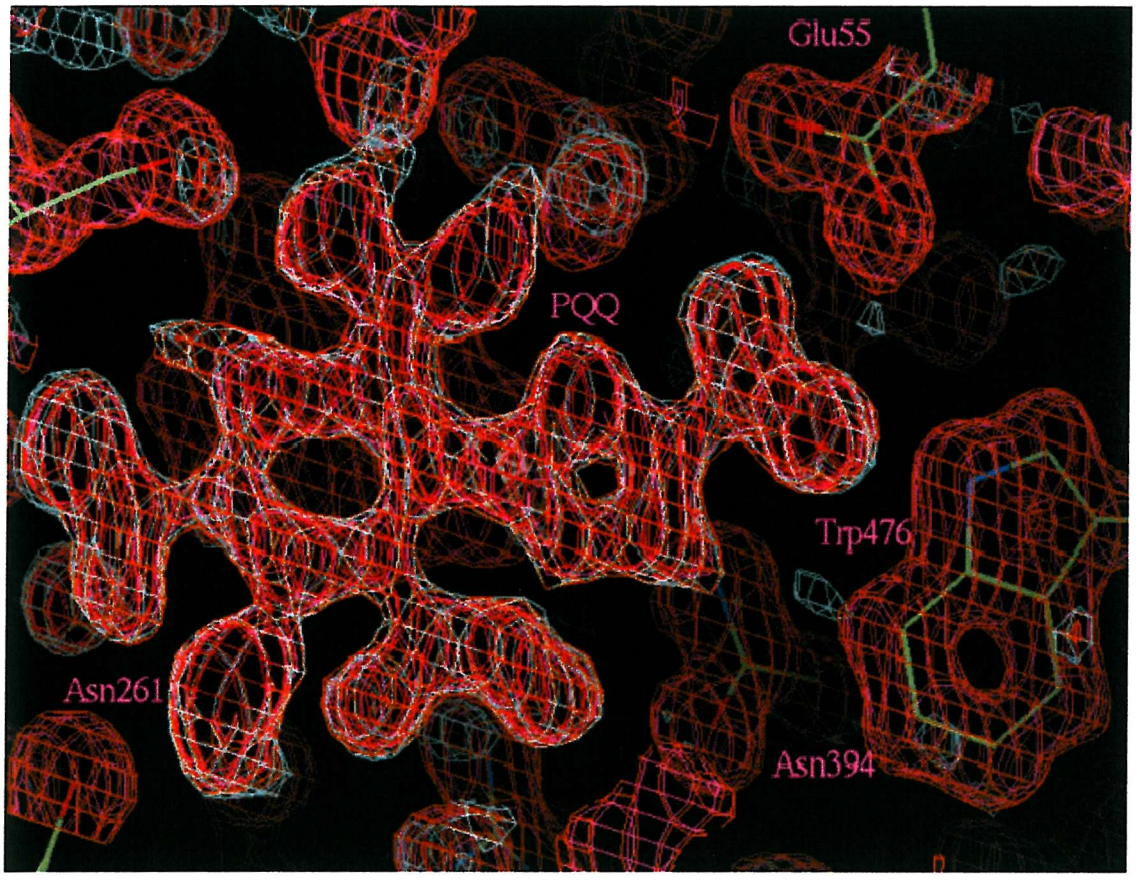

Figure 5.13 The active site electron density of mxaC31-MDH

The Figure shows the *Fo-Fc* electron density into which a PQQ molecule was built. The *Fo-Fc* electron density map is contoured at the 2 σ level and the *2Fo-Fc* map at the 1 σ level.

four (isotropic refinement) to nine (anisotropic refinement). Thus anisotropic refinement is only feasible with high resolution structures, which inherently have more reflections and therefore more observations.

Anisotropic refinement was performed using SHELX (Sheldrick., 1998). Cross-validation of the refinement was carried out at all stages, where 5 % of the available reflections were chosen at random for inclusion into the *R*-free set. The initial round of anisotropic refinement reduced the *R*-factor from 21 % to 14 % and the *R*-free from 22 % to 16 %. After three more rounds of anisotropic refinement the protein model had a final *R*-factor of 12.20 % and *R*-free of 14.50 %. Table 5.4 shows the final refinement statistics for the model. It is unusual for a protein as large as MDH (one $\alpha_2\beta_2$ tetramer is approximately 149 kDa) to diffract to atomic resolution, it is usually only small peptides and small molecules that diffract to these resolutions.

5.7.6 **The absorption spectrum of the mxaC31-MDH crystal**

The absorption spectrum of the unreconstituted mxaC31-MDH crystal is shown in Figure 5.14. The spectrum confirms that the MDH used for the X-ray crystallography had not reconstituted (an absorbance spectrum of a wild type-MDH crystal is shown in Fig 5.15). Although the crystal absorbance spectrum of mxaC31-MDH is poor and difficult to interpret (because of the high optical density of the crystal), it is clearly different from the crystal spectrum of wild type-MDH (Figure 5.15).

5.7.7 **The 1.2 Å structure of mxaC31-MDH**

The tertiary structure of mxaC31-MDH is the same as wild type-MDH from *M. extorquens* (Figure 5.16). The protein exhibits the same propeller fold which makes up a superbarrel structure of eight radially arranged β-sheets (the 'propeller blades'). A Ramachandran plot revealed that four out of the 1336 residues in the $\alpha_2\beta_2$ tetramer were in disallowed regions (Figure 5.17), these were Lys19 and Asp105 from both of the α-subunits. These residues are in disallowed regions in all of the MDH structures which have been solved in this thesis, and are therefore not a result of the mutation in the *mxaC* gene. The Ramachandran chart plots the acceptable combinations of ϕ (phi) angle and φ (psi) angles. These two angles denote the rotation about the single bonds either side of the side chain of the amino acid in question. The ϕ bond is between the α-carbon of the amino acid and the adjacent N-H bond, and the φ bond is between the α-carbon of the amino acid and the

Table 5.3 The final refinement statistics for the 1.2 Å mxaC31-MDH structure

Resolution range (Å)	10-1.2
R-factor (%)	12.2
R-free (%)	14.5
Number of reflection in working set	354472
Number of reflections in test set	18636

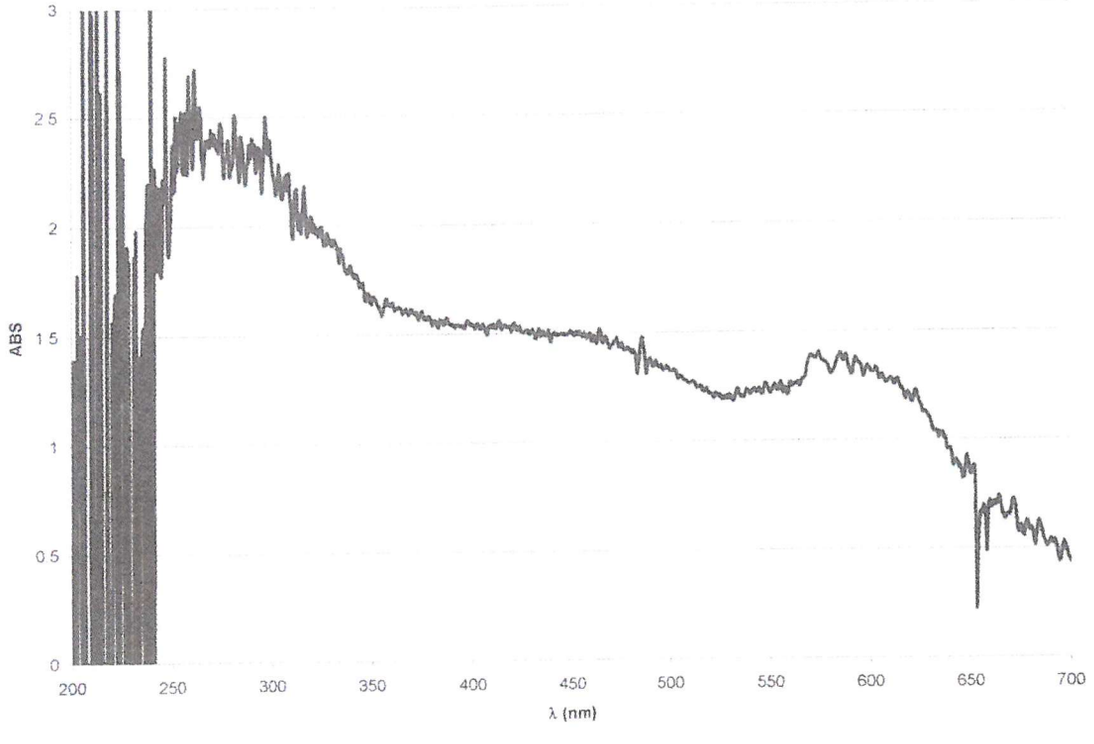

Figure 5.14 The absorption spectrum of an unreconstituted mxaC31-MDH crystal

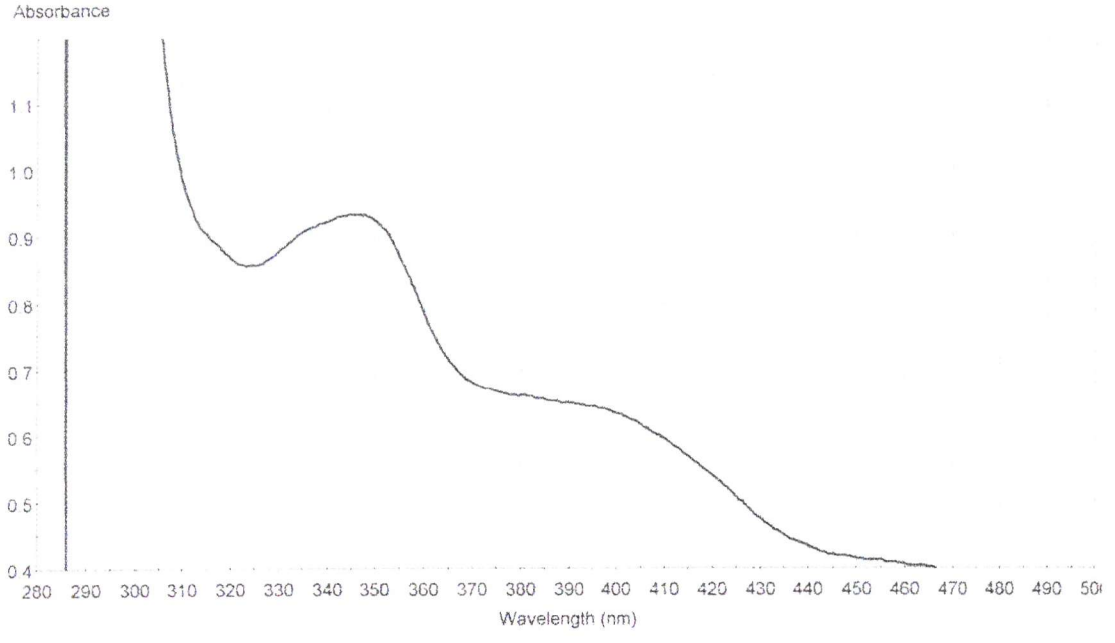

Figure 5.15 The absorption spectrum of a wild type-MDH crystal

The wild type crystal clearly exhibits a peak at 340-345 nm. The peak is apportioned to absorption by PQQ.

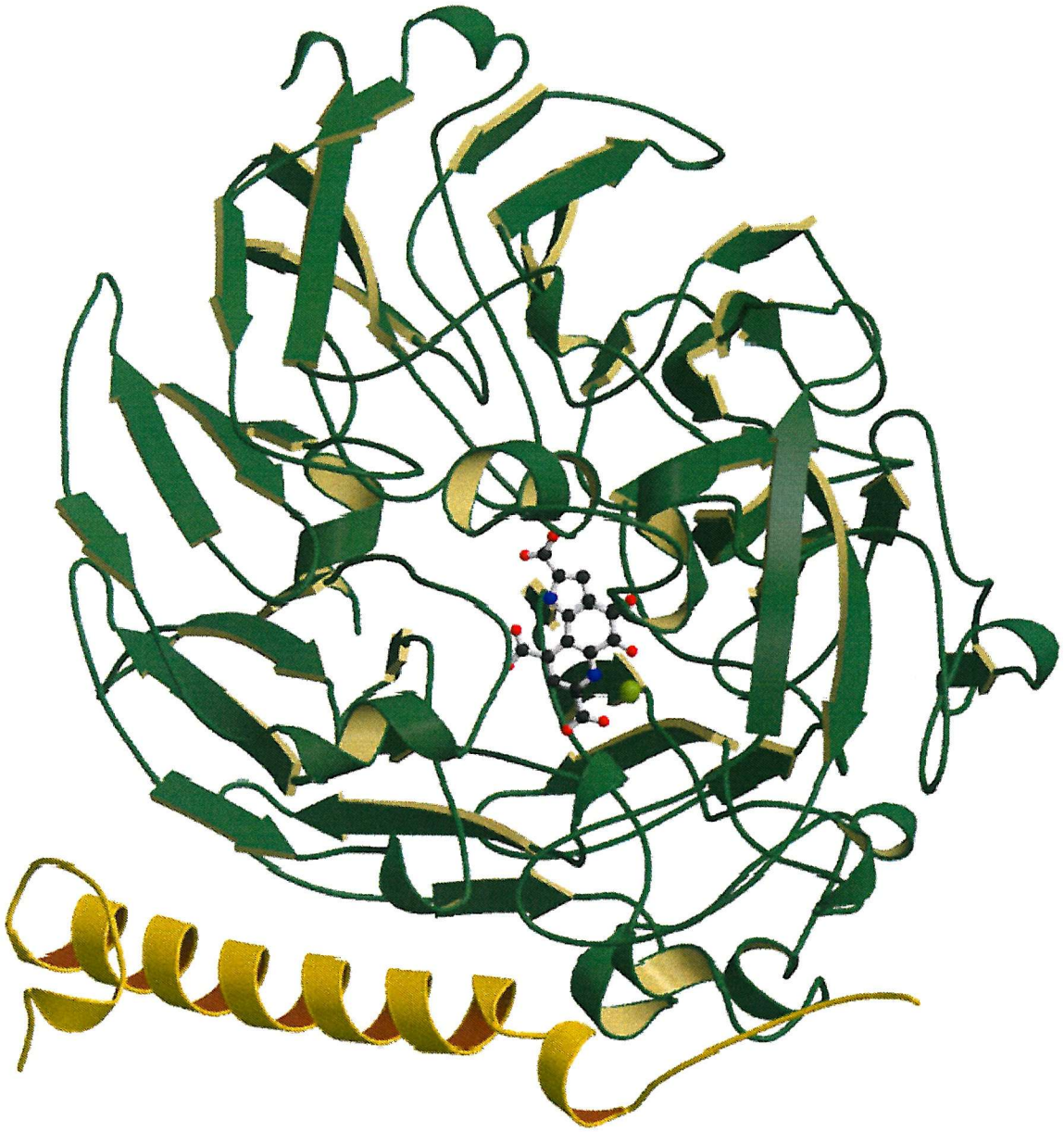

Figure 5.16 The tertiary structure of mxaC31-MDH

The Figure shows that the mutant bacteria, as expected, produced MDH with an identical tertiary structure to wild type-MDH (Figure 1.5).

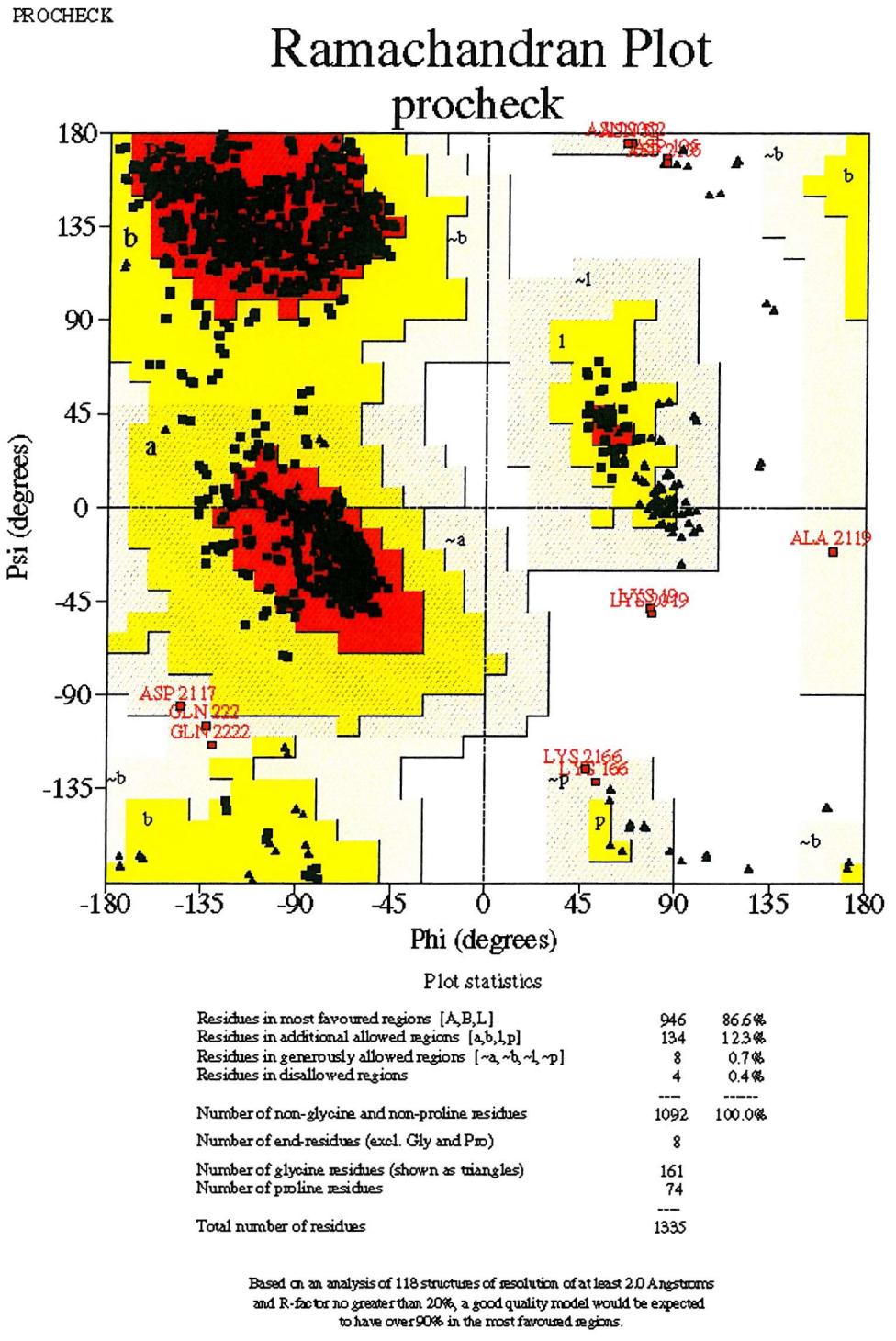

Figure 5.17 A Ramachandran plot of the 1.2 Å mxaC31-MDH structure

Four residues were in disallowed regions, these are Lys19 and Asp105 from both of the α-subunits. Lys19 is involved in a tight turn and is in the same conformation in both α-subunits and Asp105 follows immediately after the disulphide bridge between Cys103 and Cys104.

adjacent carbonyl carbon; these angles are labeled in Figures 5.18 and 5.19. Both Lys19 and Asp105 occupy the electron density extremely well (Figure 5.18 and 5.19) and were therefore kept in the disallowed conformation.

Asp105 follows the disulphide bridge formed between Cys103 and Cys104. There are two factors which may contribute to Asp105 being in a disallowed regions of the Ramachandran plot. Firstly the eight-member disulphide ring structure which is formed from the adjacent cysteines residues may force the Asp105 side chain to adopt a position which would minimize steric interference between itself and the ring, causing the Asp105 side chain to adopt a position which gave an unusual combination of phi and psi angles. Secondly, the side chain of Asp105 forms a hydrogen bond to the side chain of Asn52 (Figure 5.16). This interaction may be important in the transfer of electrons from the reduced PQQ to cytochrome c_L (Section 6.3 & Figure 6.5), thus Asp105 may have to adopt this conformation in order to maintain this interaction.

Lys19 is at the beginning of the α-subunit. The two residues prior to Lys19 are the typical residues which can orchestrate tight turns in protein structures (Pro17 and Gly18). The backbone nitrogen from Lys19, hydrogen bonds to the carbonyl oxygen from Pro17, this interaction helping to stabilize the turn. The side chain nitrogen atom from Lys19 makes two hydrogen bonds to nearby water molecules.

5.7.8. **The calcium coordination in the active site**

The calcium ion in the active site of MDH is thought to serve two functions. Firstly, it acts as a Lewis acid and polarizes the PQQ C-5 carbonyl bond, which in turn makes the PQQ C-5 atom susceptible to attack by a hydride from the substrate (see Section 1.10). Secondly, the calcium is coordinated to three PQQ atoms (the oxygen from the C-7 carboxylate, the N-6 atom from the quinoline ring and the oxygen atom from the C-5 carbonyl group); these interactions would be expected to fix the PQQ in the correct conformation for catalysis. There are variations on the standard calcium coordination in MDH. The D303E MDH active site mutant has a hepta-coordinated calcium ion (Afolabi *et al.*, 2001); the extra carbon in the glutamate side chain brought the carboxylate close enough to coordinate to the calcium ion. The decrease in the apparent affinity for methanol in the D303E-MDH (K_m increases form 3 μM to 250 mM), and the decrease in the stability of the transition state complex are consistent with the observed changes in the active site region. These include the extra ligand

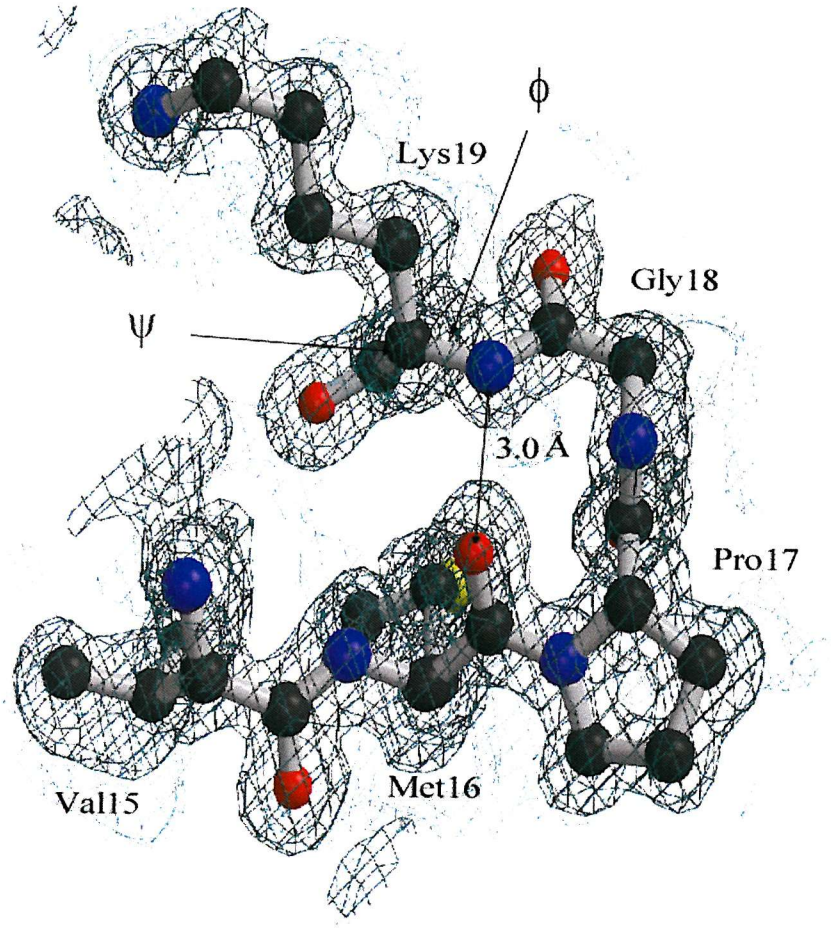

Figure 5.18 The electron density which surrounded Lys19 from the α-subunit of mxaC31-MDH

Lys19 was in a disallowed region of the Ramachandran plot (Figure 5.15) but, as the Figure shows, the lysine residue fits the electron density very well and was therefore left unaltered.

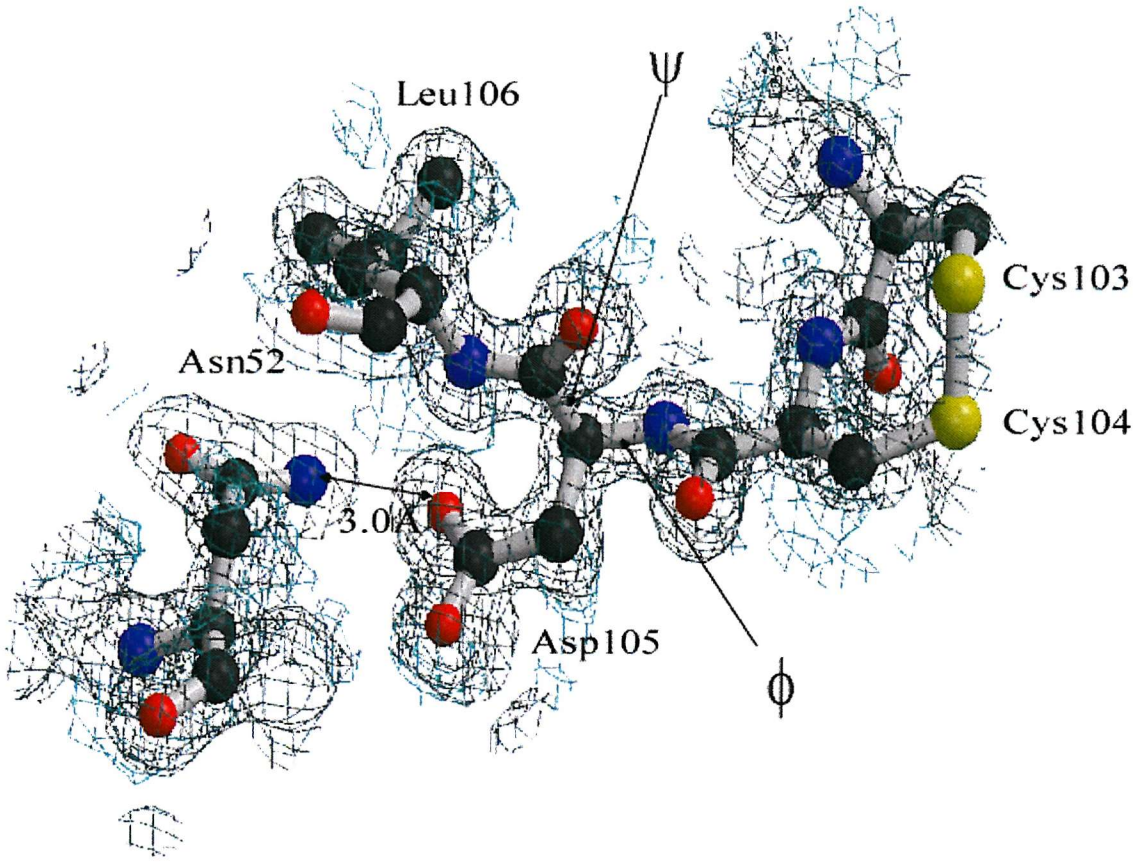

Figure 5.19 The electron density which surrounded Asp105 in the α-subunit of mxaC31-MDH

The Figure shows orientation of Asp105 and the hydrogen bond with Asn52. Asp105 is in a disallowed region of the Ramachandran plot, although the residue fits the electron density very well and was therefore left unaltered.

to the Ca^{2+} and the replacement of the Asp303 hydrogen bond with Arg331 with a Glu303 hydrogen bond to the O5 of PQQ.

Laboratory experiments have characterized mxaC31-MDH as inactive until it was reconstituted with Ca^{2+}, Sr^{2+} or Ba^{2+} ions, which would suggest that the X-ray studies would reveal an altered active site structure which lacks the calcium ion or perhaps contains a water molecule. Figure 5.20 shows the active site of mxaC31-MDH. A region of oval shaped positive *Fo-Fc* electron density was seen. The σ level for this peak was above 6 σ, suggesting that it should be occupied by an atom with a high electron distribution, such as a metal ion. To rule out a water molecule occupying the electron density, a water molecule was built into the electron density map and refined anisotropically. The subsequent electron density maps showed a great deal of positive *Fo-Fc* electron density surrounded the water molecule (Figure 5.21), strongly suggesting that the density should not be occupied by a water molecule.

Recent work on wild type mGDH showed that it is active when it is reconstituted with PQQ and magnesium (James & Anthony, 2003), but it is inactive when reconstituted with PQQ and calcium. In light of these findings it was conceivable that the protein produced from the *mxaC* gene could help remove a magnesium ion from the active site of MDH and aid the insertion of a calcium ion in its place. To test this theory a magnesium ion was built into the active site of the model in place of the water molecule. The model was again refined anisotropically to a resolution of 1.2 Å, using the refinement programs from SHELX. The resulting protein coordinate file which was output after the refinement programs gave good temperature factors for both of the magnesium ions in the model (18 $Å^2$ and 19 $Å^2$ respectively); this is a useful guide to how well the metal ion refined, but the electron density maps give a truer reflection of the refinement. The *Fo-Fc* and *2Fo-Fc* electron density maps were therefore calculated. Figure 5.22 shows that the magnesium ion did not refine particularly well in the structure. The Figure shows an area of negative *Fo-Fc* electron density (red) at the center of the density peak and two regions of positive *Fo-Fc* electron density (green) peaks either side of the negative electron density. Subsequently the occupancy of the magnesium ion was refined anisotropically but, unfortunately this refinement was unsuccessful, the SHELX program aborting during the refinement. From the electron density maps it can be concluded with a fair degree of certainty that a magnesium ion does not occupy this region of electron density.

Finally a calcium ion was built into this region of electron density and refined anisotropically to 1.2 Å, using the programs of SHELX. Initially the occupancy of the

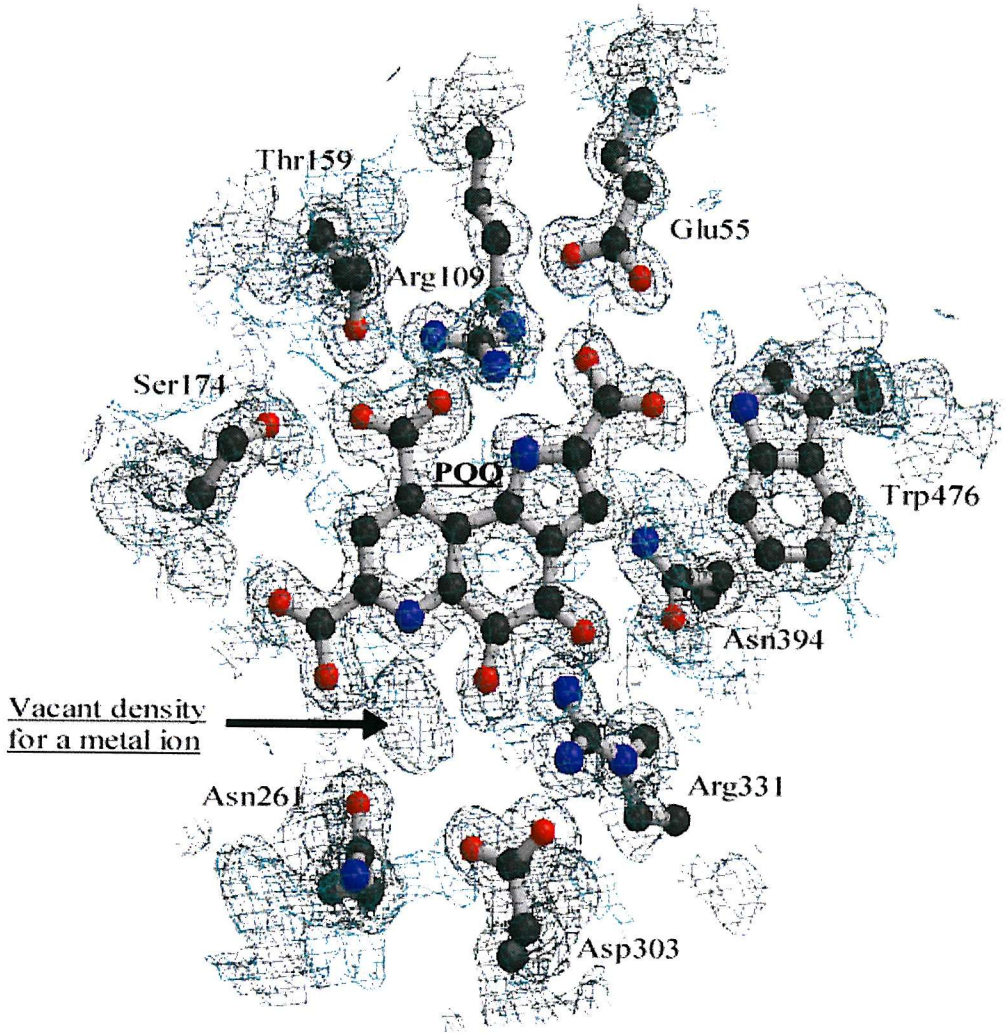

Figure 5.20 The oval shaped *Fo-Fc* electron density in the mxaC31-MDH structure

In this Figure Glu177 was removed in order to clearly see the electron density more clearly.

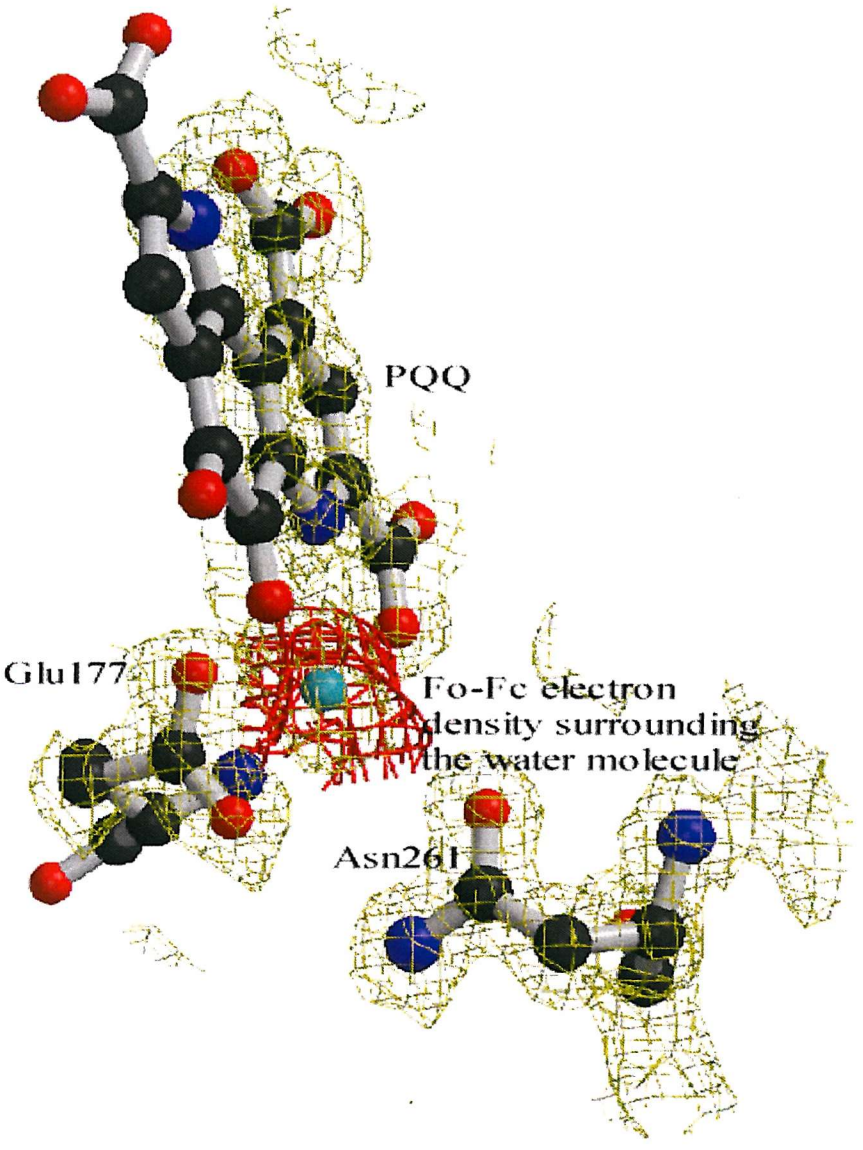

Figure 5.21 The positive *Fo-Fc* electron density which surrounded the active site water molecule after one round of anisotropic refinement

The positive *Fo-Fc* electron density surrounding the water molecule (green sphere) which was modeled into the active site suggested that the position should not be occupied by a water molecule.

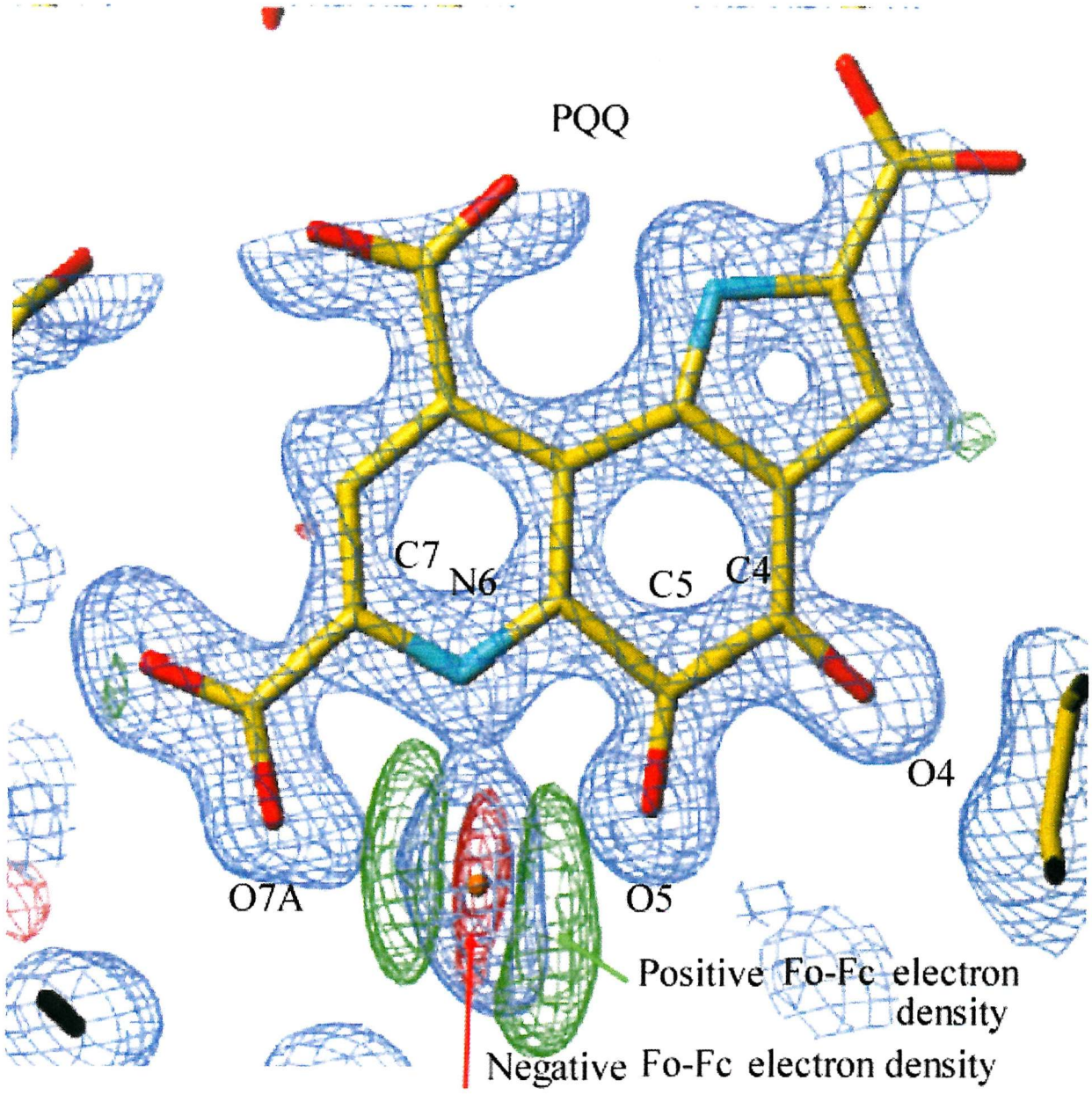

Figure 5.22 The positive and negative *Fo-Fc* electron density which surrounded the active site magnesium ion after one round of anisotropic refinement

The electron density maps strongly suggest that a magnesium ion should not occupy the active site cavity, although the B-factors for the magnesium ion were acceptable.

calcium ion was set to fully occupied. After the model was refined the B-factors for both of the calcium ions in the structure were over 30 Å^2 (31.32 Å^2 & 30.03 Å^2); this was significantly higher than the B-factors for calcium ions in previous MDH structures. It was thought that the B-factor for the calcium ions may be high due to them not fully occupying the active site, with this in mind the refinement programs were repeated, but with the occupancy of the calcium ions set to 60 % (0.6) occupied. Over the course of the refinement if the calcium ions were underrepresented, in terms of occupancy, then this number would increase towards 1.0 (100 % occupied). After the anisotropic refinement the calcium ion occupancy remained around 0.6 (60 % occupied, 0.647 & 0.592 for the two sites), although the B-factors were reduced down towards 20 Å^2 (23.03 Å^2 & 22.59 Å^2). The *Fo-Fc* and *2Fo-Fc* electron density maps were calculated. The region surrounding the PQQ and active site metal ion is shown in Figure 5.23. Although there is positive *Fo-Fc* density towards the base of the oval shaped density, there is no negative *Fo-Fc* electron density surrounding the calcium ion. From the data derived from the X-ray crystal structure of mxaC31-MDH it can be assumed that there is a calcium ion in the active site, but that it only partially occupies this position.

Having established that there is a calcium ion present in the binding site, although not at full occupancy, what, if any other differences are there between mxaC31-MDH and wild type-MDH? The active site structures of wild type-MDH and mxaC31-MDH were compared, to look for subtle conformational changes in the active site (Figure 5.24 & Figure 5.25). The distances between the calcium ion and its coordinated atoms were different in mxaC31-MDH, although the orientation of all of the ligands relative to the calcium remained the same. The atom which showed the most significant change in distance to the calcium ion was Asn261. The distance from the side chain of Asn261 to the calcium ion increased from 2.61 Å (wild-type) to 3.13 Å (*mxaC31*). A distance of 3.13 Å is too long for the atom to be coordinated to the calcium ion; the distance of an oxygen ligand to a calcium ion is ideally between 2.2 and 2.5 Å. The Asn261 is in the same orientation as it is in wild type-MDH and it is similarly hydrogen bonded in the active site (Figure 5.26); it is these interactions which orientate the asparagine rather than its coordination to the calcium ion. It was thought possible that the electron density may reflect the presence of a methanol molecule in the active site, but this idea can be ruled out due to the unacceptable close proximity of the methyl group to the PQQ molecule.

From these high resolution data it can be concluded that the active site metal ion binding site is not fully occupied in the mxaC31-MDH enzyme, and that the protein, which is

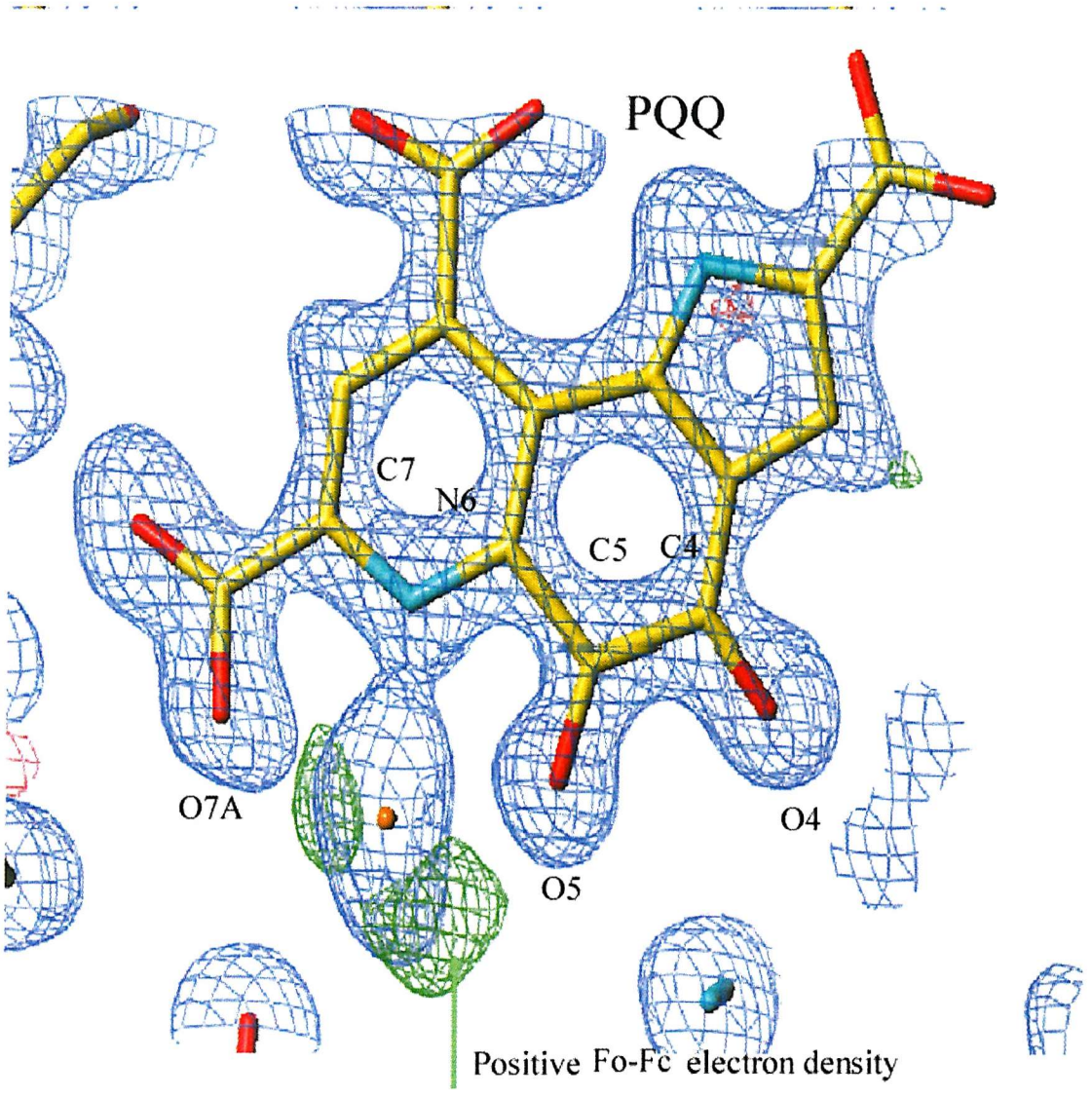

Figure 5.23 The electron density which surrounded the active site calcium ion after one round of anisotropic refinement

The calcium ion which was modeled into the active site cavity and refined anisotropically fitted the electron density quite well; the electron density maps showed little positive *Fo-Fc* (green) no negative *Fo-Fc* electron density.

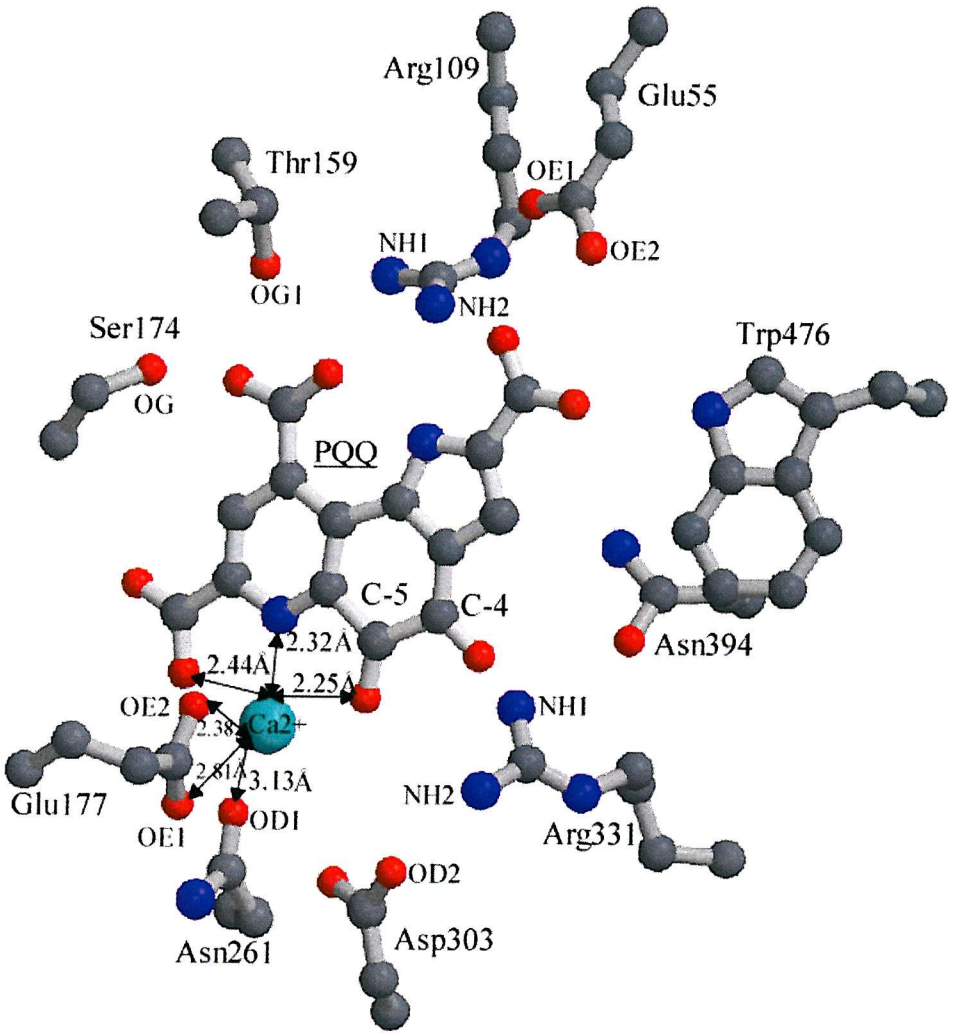

Figure 5.24 The active site structure of mxaC31-MDH

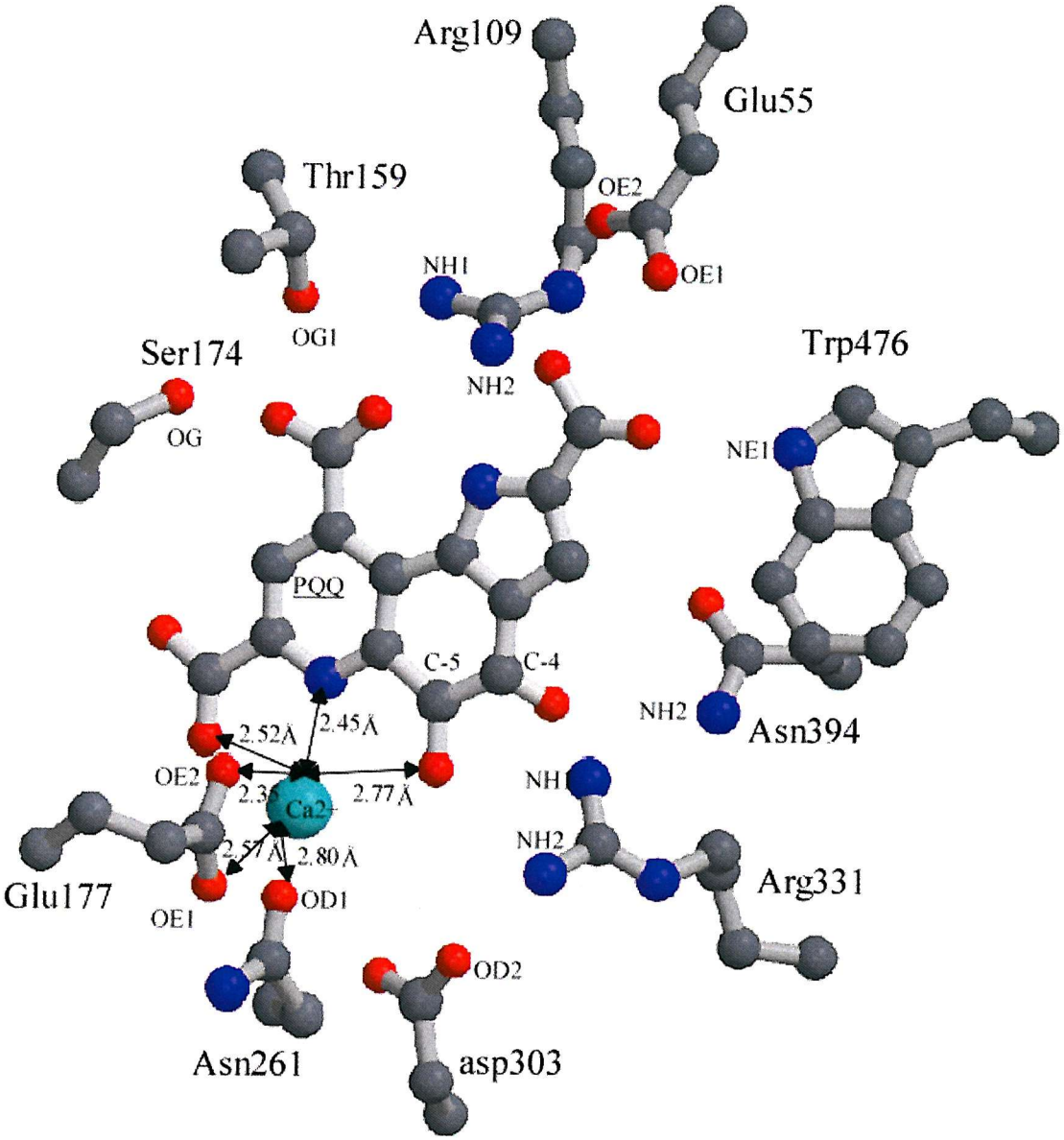

Figure 5.25 The active site structure of wild type-MDH

The Figure is taken from a 1.94 Å X-ray structure of MDH (Ghosh *et al.*, 1995).

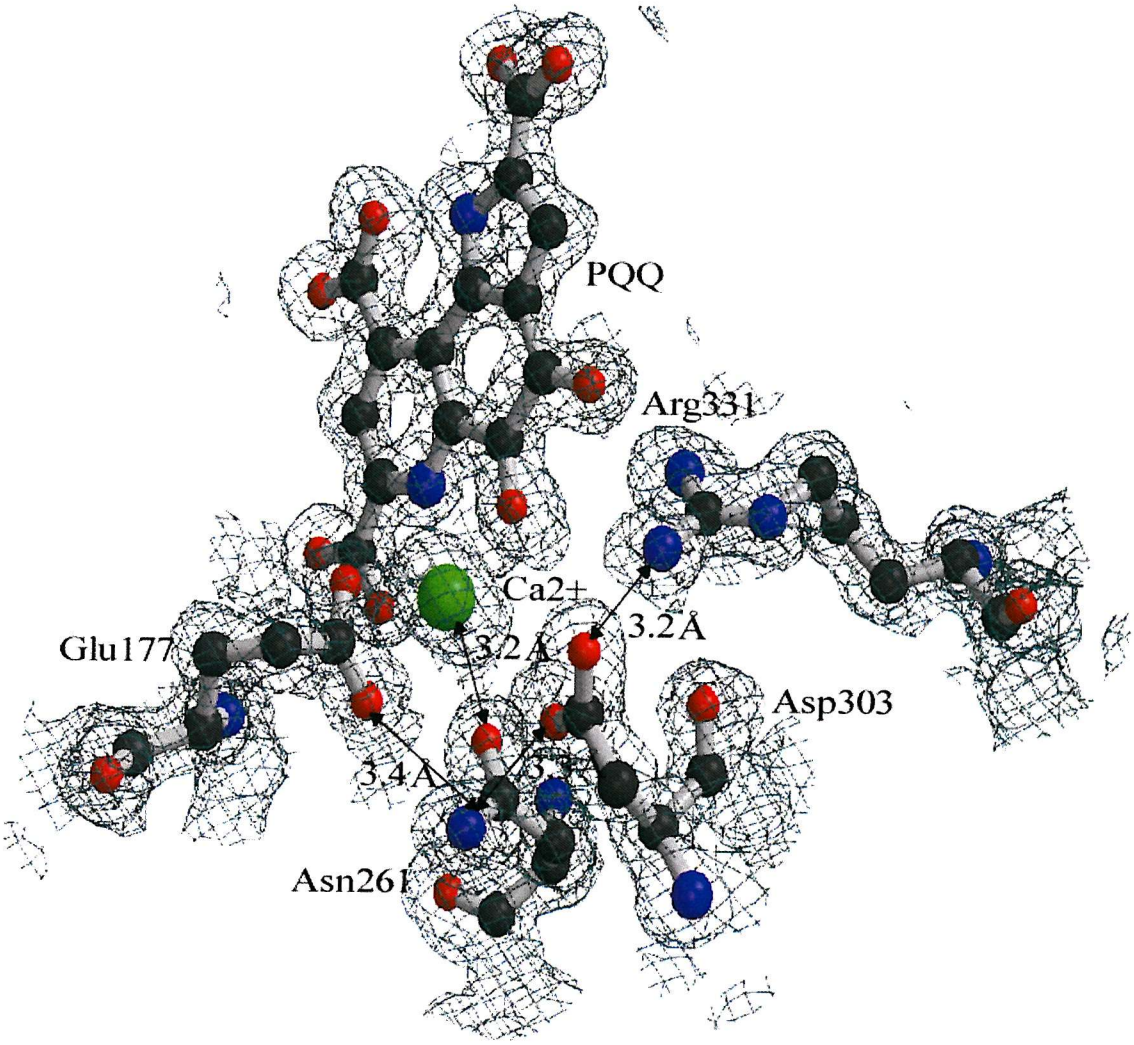

Figure 5.26 The hydrogen bond interactions of Asn261 with Asp303 and Glu177 in mxaC31-MDH

These interactions orientate the side chain of Asn261.

encoded by the *mxaC* gene, is essential in incorporating calcium into the active site to establish enzyme activity. It is therefore likely that the *mxaA,C,K,L* genes each produce proteins which contribute to the insertion of calcium into the active-site, although a mutation in the *mxaC* gene does not lead to an enzyme which is totally free of calcium ions.

5.8 **Molecular replacement studies of the MDH from *mxaC31* reconstituted with barium ions.**

An attempt was made to crystallize mxaC31-MDH in the presence of barium, in order to form a crystal of the active MDH with barium in the active site (at this stage it was assumed that the metal ion binding site was vacant). The crystal conditions were the same as were used before (PEG, Tris pH 9.0), although the mother liquor was supplemented with 20 mM $BaCl_2$. The crystals were grown at 4 °C and appeared after approximately 4 weeks.

One hundred and eighty degrees of X-ray diffraction data were recorded from one crystal at the ESRF facility in Grenoble, France. As with all other MDH crystals, the X-ray reflections were sharp and diffracted to a high resolution (approximately 2.0 Å) (Figure 5.27). The data were processed using MOSLFM, which suggested a unique unit cell with a monoclinic space group (a = 55.39, b = 93.96, c = 107.12, α = 90.0, β = 99.87, γ = 90.0, space group $P2_1$). After the data were indexed, sorted, scaled and truncated, the resulting reflection file was used in molecular replacement. The final data processing statistics are shown in Table 5.5. The overall R_{merge} for the data was 12.7. This indicates firstly, that the space group in which the data was processed was correct, and secondly, that the quality of the data was good.

5.8.1 **Molecular replacement studies on the mxaC31-MDH crystallized in the presence of barium**

Molecular replacement, using the program MOLREP was used to obtain initial phases (Vagin & Teplykov, 1997). The phasing model consisted of a single $\alpha_2\beta_2$ tetramer, with the co-factor and metal ions removed (this thesis). Table 5.6 shows the five peaks that were found when running the cross-rotation function; no significant peaks were found (Table 5.6). As the search model is identical to the target model, this was somewhat unexpected. To try and find a molecular replacement solution the parameters in the molecular replacement search were altered. The radius of integration, which was used in the rotation search, was varied from 20 Å up to 60 Å, and still no rotation solution was found. The resolution cut-off

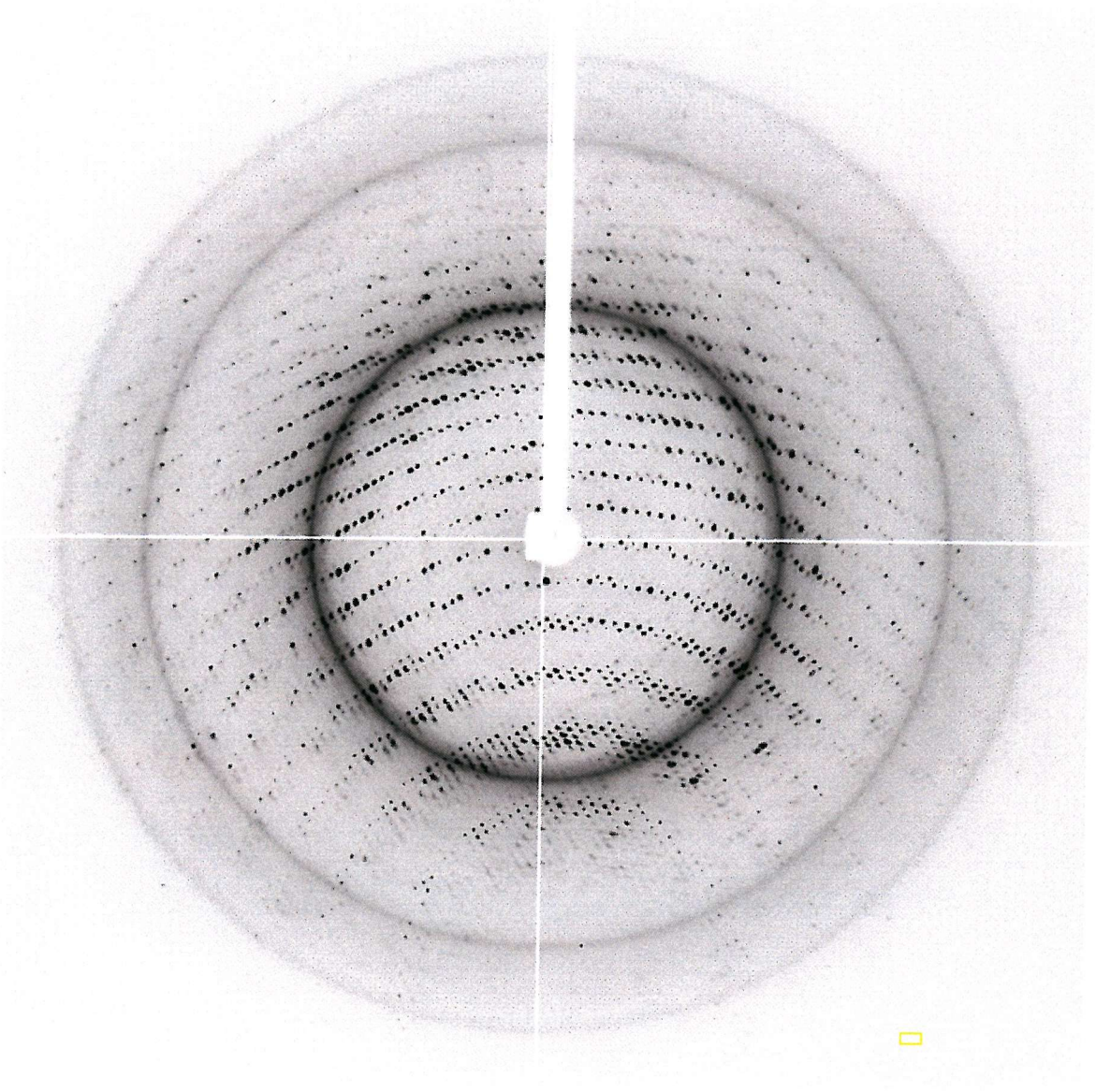

Figure 5.27 A diffraction image of mxaC31-MDH which was reconstituted with 20 mM $BaCl_2$

Table 5.5 The final data processing statistics for mxaC31-MDH after it was reconstituted with barium.

Total number of reflections	201074
Number of unique reflections	66685
Resolution (Å)	2.0
Completeness (%)	98.8 (98.8)
R_{merge} (outer resolution shell)	12.7 (27.4)
Multiplicity	2.9 (2.9)
Average I/σ(I) (outer resolution shell)	3.7 (2.2)

was also altered, with 0.5 Å increments, from 3.0-5.0 Å, and each time no rotation peak was found. There are two possible explanations for the lack of a molecular replacement solution. If MOSFLM has estimated the unit cell and space group correctly, the barium may have substantially altered the three-dimensional structure of MDH, and consequently it was not possible to get a molecular replacement solution using MDH as the model. Several other models were used in the molecular replacement search, such as ethanol dehydrogenase, and still no solution was found. The second possible reason for the failure to obtain a molecular replacement solution is that the crystal may be twinned. In this situation your crystal really consists of two or more crystals, orientated such that their diffraction patterns exactly overlap. When there is twinning, each twin makes an independent contribution to the structure factors and therefore to the peaks in the Patterson map, making it extremely difficult to obtain an overlap of Patterson vector maps with those from the search model After several months of molecular replacement studies this aspect of the work was halted.

Table 5.6 The five cross-rotation functions performed with MOLREP

Peak number	α	β	γ	Rf/σ
1	14.56	77.37	107.78	4.62
2	357.50	79.98	89.32	4.42
3	19.0	74.18	116.85	4.33
4	317.95	59.50	52.87	4.33
5	2.98	87.97	90.26	4.28

Chapter 6

The X-ray crystal structure of MDH from the *Methylobacterium extorquens* methanol oxidation mutant *mxaD11*

6.1 Introduction

The methanol oxidation mutant *mxaD11* was produced by the Toyama group (Toyama *et al.*, 1998). The *mxaD* gene is in the *mxaACKLD* gene cluster, the rest of the genes in this group being important in calcium insertion into the active site of MDH. The protein coded for by *mxaD* is a 17 kDa, periplasmic protein (Toyama *et al.*, 2003). Unlike bacteria which have a mutation in any of the other genes in the *mxaACKLD* cluster, *mxaD11* is able to grow on methanol, although only at a reduced rate (30 % of the growth measured with wild type *M. extorquens*). MDH from *mxaD11* (mxaD11-MDH) is over-expressed and has a higher specific activity than wild type-MDH when measured in the dye-linked assay system (three times higher than the wild type value). The rate of interaction between MDH and cytochrome c_L was higher with the proteins in the soluble crude extract from wild type *M. extorquens*, which contained some mxaD protein, than with the proteins from the *mxaD11* mutant, which contained no mxaD protein. The rates of methanol oxidation by whole cells were only 20 % of the wild type rates, which sufficiently explains the lower growth rate of the mutant. These findings, along with the previous observation that the electron transfer rates from MDH to cytochrome c_L are too low to account for whole cell respiration has led to the proposal that the protein encoded for by *mxaD* modifies MDH somehow to improve the electron transfer to cytochrome c_L. X-ray crystallography was again used as a tool to look at the structure of MDH from the methanol oxidation mutant *mxaD11* to investigate whether the protein encoded for by *mxaD* modified MDH in comparison to wild-type MDH.

6.2 Crystallization of MDH from *mxaD11*

The mxaD11-MDH which was used for the X-ray crystallography was provided by the Toyama group; its purity is shown in Figure 6.1. MDH crystals were formed using the hanging drop method; the crystallization conditions were the same as those described in Section 5.8 (15 % PEG 8 K, 100 mM Tris-HCl, pH 9.0). The crystals which appeared after a few days were fragile and they deteriorated rapidly. To produce more robust, stable crystals, they were grown at 4 °C instead of at room temperature. The crystals which appeared after a

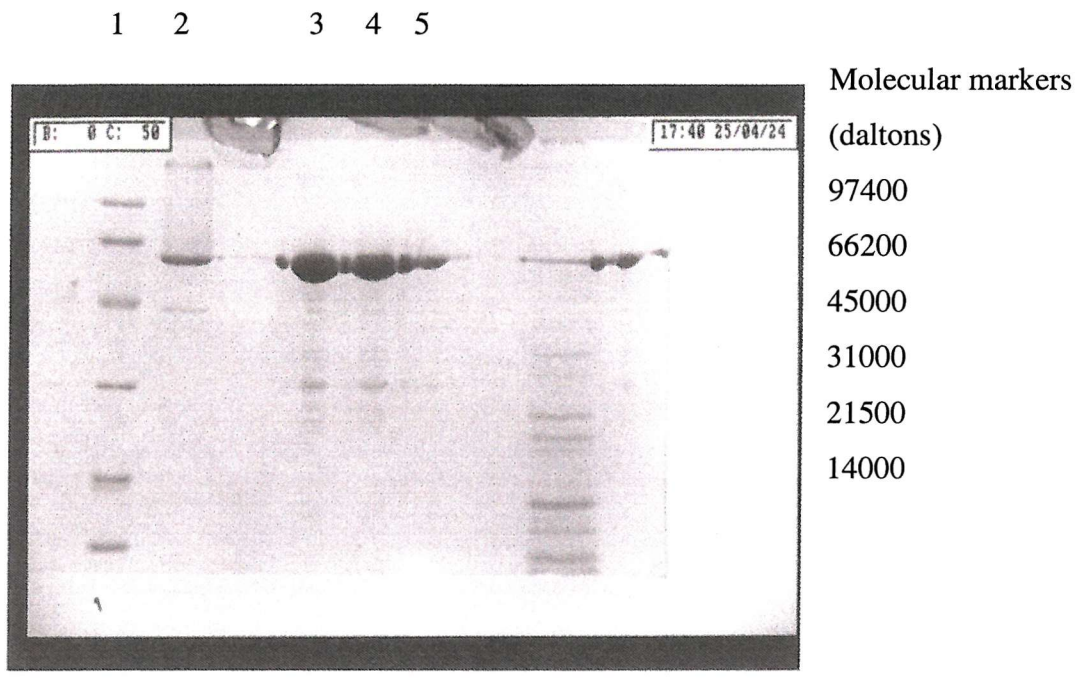

Figure 6.1 SDS-PAGE showing an MDH preparation from *mxaD11* (lanes 3 and 4)

Molecular markers are in lane 1.

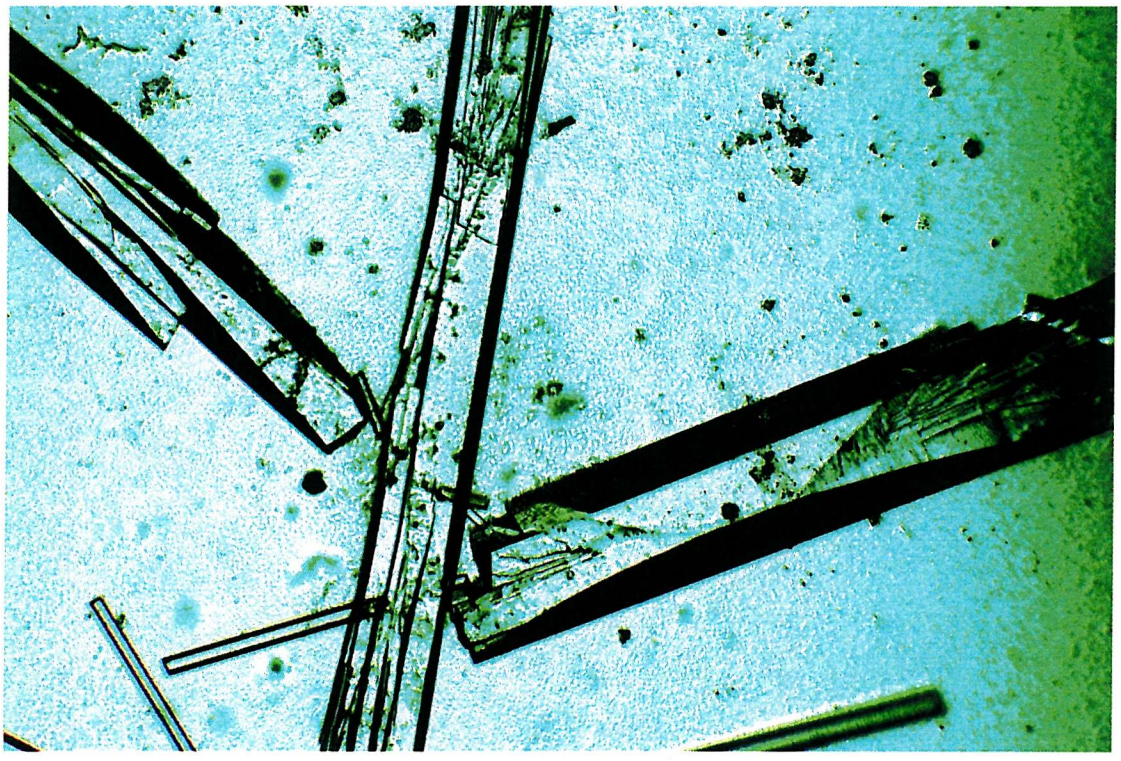

Figure 6.2 Crystals of mxaD11-MDH

The crystals were grown at 4 °C and took two weeks to appear. The crystal conditions were the same as those previously used to grow MDH crystals (15 % PEG 8K, 100 mM Tris, pH 9.0). The crystals were large and rod-shaped with the dimensions of 1 mm x 0.15 mm x 0.15 mm. The crystals had similar dimensions and shape to those of wild-type MDH which were grown at an earlier stage of the project.

few weeks were large and had sharp edges (Figure 6.2). One hundred and eighty degrees of X-ray diffraction data were collected from a single crystal at the ESRF facility in Grenoble, France; the crystal diffracted to approximately 1.5 Å.

6.2.1 **Data processing of MDH from *mxa*D11**

A high and a low-resolution data set were collected from a single crystal using an ADSC Quantum detector. The unit cell dimensions and space group were determined using MOSFLM (a = 66.3 Å, b = 107.6 Å c = 187.4 Å, space group $P2_12_12_1$). The data were processed in the $P2_12_12_1$ space group, sorted, scaled and truncated using the programs of the CCP4 suite. These unit cell dimensions and space group are the same as a previous MDH crystal from wild type *M. extorquens* (Section 6.4, table 6.5). HKLVIEW was used to confirm the space group; there were systematic absences every two spots along the h, k, and l axis, which suggested there was a screw axis along each axis. Table 6.1 shows the final data processing statistics.

6.2.2 **Molecular replacement studies on MDH from *mxa*D11**

As the unit cell was the same as that of native MDH, molecular replacement is not strictly necessary. Nevertheless, we decided to use MOLREP to compensate for any slight differences in the orientation of the molecule in the mutant crystal. The search model consisted of a single $\alpha_2\beta_2$ tetramer, with the co-factor and metal ions removed (this thesis). The rotation search found two significant peaks (Table 6.2), which corresponded to the two possible orientations of the search molecule due to its internal symmetry. The first rotation peak was used to find the position of the molecule in the unit cell. The translation search found one peak (Table 6.3), which had a correlation between the data and the model of 64 % and a corresponding *R*-factor of 37 %. The protein model from molecular replacement and the reflection file from truncate were used in the CNS refinement package.

6.2.3 **Refinement of the 1.5 Å MDH structure from *mxa*D11**

The model was refined using the programs from the CNS suite, and the electron density was visualized using QUANTA. Three rounds of isotropic refinement was performed within the resolution range of 33.3-1.5 Å; the two PQQ molecules and two calcium ions were fitted into vacant *Fo-Fc* electron density after the first round of refinement, and water molecules were added using the QUANTA program X-SOLVATE. Table 6.4 shows the final

Table 6.1 The final data processing statistics for the 1.5 Å mxaD11-MDH structure

Total number of reflections	171773
Number of unique reflections	10327
Resolution (Å)	1.50
Completeness (%)	85 (85)
R_{merge} (outer resolution shell)	10.5 (33.5)
Multiplicity	8.3 (5.4)
Average I/σ (outer resolution shell)	5.0 (2.4)

Table 6.2 The 5 cross-rotation functions performed with MOLREP

Peak number	α	β	γ	Rf/σ
1	176.75	0.00	2.95	16.37
2	28.13	33.26	27.31	15.38
3	54.57	60.56	55.17	3.00
4	175.08	9.93	170.21	3.00
5	100.01	72.06	102.28	2.88

Table 6.3 The 5 translation functions performed with MOLREP

Peak number	X	Y	Z	R-factor	Corr
1	0.00	0.00	179.0	0.373	0.644
2	0.00	0.00	179.0	0.489	0.361
3	0.00	0.00	179.0	0.500	0.354
4	0.00	0.00	179.0	0.499	0.355
5	0.00	0.00	179.0	0.499	0.355

Table 6.4 The final refinement statistics for the 1.5 Å mxaD11-MDH structure

Resolution range (Å)	30-1.5 Å
R-factor (%)	18.32
R-free (%)	20.03
Number of reflection in working set	172242
Number of reflections in test set	9110

refinement statistics for the protein model. The final protein model consisted of 1335 amino acids, 2 molecules of PQQ, 2 calcium ions, 985 water molecules and 6 molecules of glycerol.

6.2.4 **The active site structure of mxaD11-MDH**

The tertiary structure of mxaD11-MDH was the same as wild type-MDH. A comparison of the active sites showed that there was no significant difference between the two proteins (Figure 6.3); the only difference which is visible in the electron density maps concerns Asp303. This residue initiates the reaction mechanism by abstracting a proton from the substrate. It forms several interactions in the active site, where it is hydrogen bonded to a water molecule, Asn261 and Arg331 (Figure 6.4). The Asp303 is somewhat closer to the calcium ion (3.1 Å) than in previous MDH structures (wild type: 3.5 Å); furthermore, the *Fo-Fc* density electron density map reveals areas of positive difference density around Asp303 (Figure 6.4). It is possible that this electron density could represent an alternative configuration for the Asp303 side chain, which would bring one of the side chain oxygen atoms to within 3 Å of the calcium ion, changing the calcium co-ordination from six to seven atoms; this would create a similar active site structure to the one seen in the D303E mutant (Afolabi *et al.*, 2001). Although bearing in mind that there were no similar regions of electron density surrounding Asp303 in the other α-subunit of the dimer, it is difficult to confidently assign an alternative conformation for the active site aspartate.

In conclusion the 1.5 Å X-ray crystal structure of mxaD11-MDH does not reveal anything about how the 17 kDa protein produced by the *mxaD* gene contributes to the oxidation of methanol. The structure shows no great deviation from wild type-MDH; the same residues are in disallowed regions of the Ramachandran plot for mxaD11-MDH as wild type-MDH (Lys19 and Asp105 from both α-subunits) and the active site is almost identical. These results suggest that the mxaD protein does not modify the gross structure, or the active site of MDH to allow an enhanced rate of interaction with cytochrome c_L, as had previously been suggested (Toyama *et al.*, 2003).

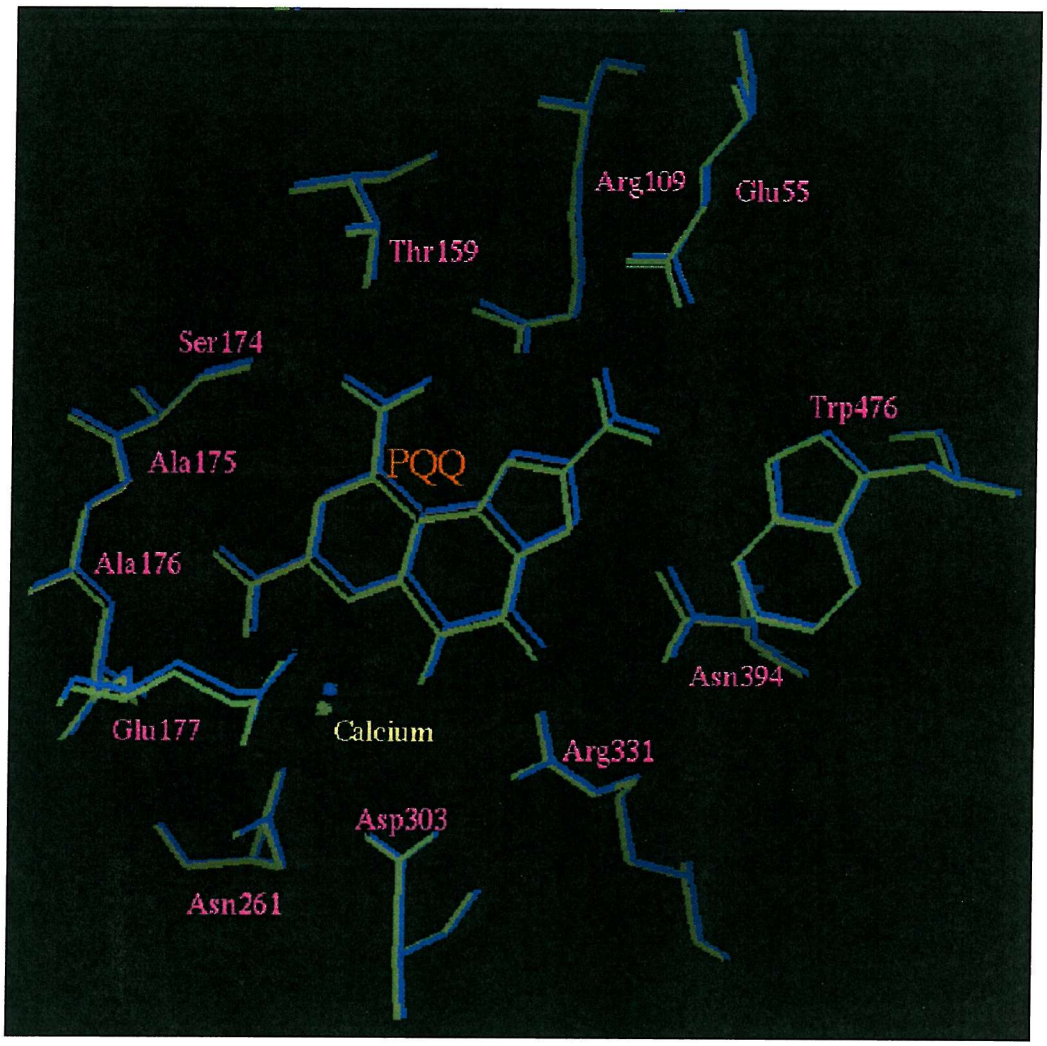

Figure 6.3 The active site of wild type-MDH (blue) and mxaD11-MDH (green)

There was no significant difference between the two active site structures.

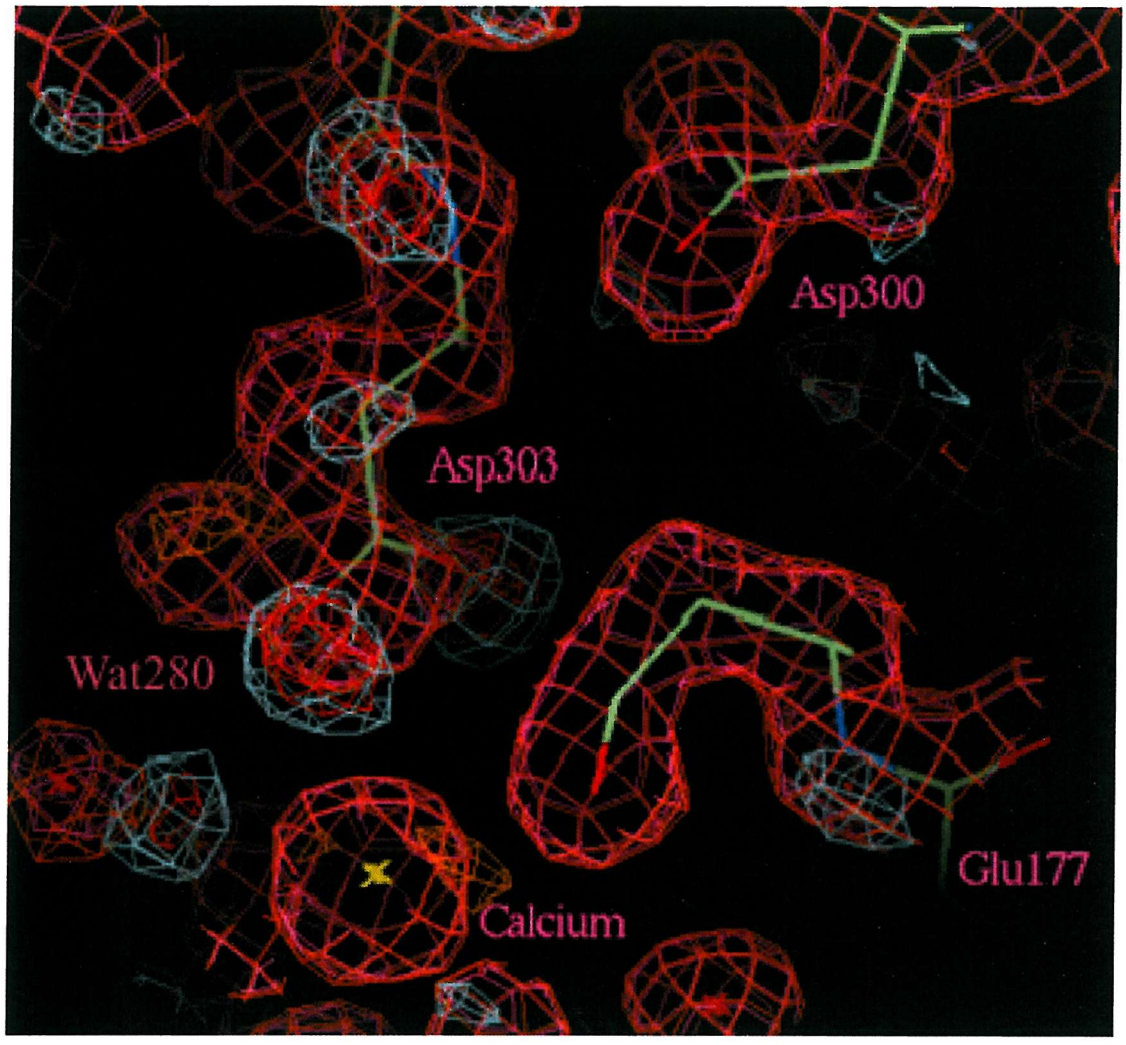

Figure 6.4 The electron density which surrounds the Asp303 side chain oxygen atoms of mxaD11-MDH

The Figure shows the Asp303 side chain occupying the positive difference density (blue); this represents an alternative conformation to Asp303 in wild type-MDH. The conformation brings the side chain to within 3 Å of the active site calcium ion.

Chapter 7

General summary

7.1 Introduction

The aim of the thesis work was to understand the structural basis of electron transfer during methanol oxidation in the methylotrophic bacteria, *Methylobacterium extorquens*. The crystal structures of the cytochrome c_H and methanol dehydrogenase had previously been determined at 2.0 Å and 1.94 Å resolution respectively (Read *et al.*, 1999, Ghosh *et al.*, 1995). This line of research has been furthered by the determination of the crystal structure of cytochrome c_L, the second protein in the electron transfer pathway, at 1.6 Å. Furthermore, the structure of MDH has now been determined at 1.2 Å, making it one of the largest proteins determined at atomic resolution to date. Although attempts to co-crystallize complexes of MDH with cytochrome c_L were unsuccessful, the determination of the structure of cytochrome c_L enabled modeling of the complex based upon the recently determined structure of the *Pseudomonas putida* HK6 quinohaemoprotein alcohol dehydrogenase (Chen *et al.*, 2002).

7.2 Cytochrome c_L

Rod shaped crystals (~ 1 x 0.1 x 0.1 mm) of cytochrome c_L were grown in the dark and in the presence of calcium over a period of a month. X-ray data were collected at the ESRF (Grenoble) to 1.6 Å resolution and the space group determined as $P4_3$. The structure was determined by molecular replacement with the homologous cytochrome c_{551i} from *Paracoccus denitrificans* at 2.4 Å as the search model (Chen et al., 1994). After several rounds of refinement the final model, containing 1 haem group and 1 calcium ion had an *R*-factor of 20.9 % (*R*-free 25.1 %).

As expected, the tertiary structure of cytochrome c_L is similar to that of cytochrome c_{551i} (Figure 4.10). In both of the cytochromes, the 'cytochrome *c*' fold, composed of three central α-helices partially enclosing the haem group is conserved (Figure 4.14b). Both hydrophobic and

hydrogen bond interactions serve to maintain this central core of the protein Although both cytochromes are unique in possessing C-terminal extended regions, in cytochrome c_L the extension is tethered to the body of the molecule by an additional disulphide bridge, making it one of only a few *c*-type cytochromes which contain two cysteines in addition to those which form a covalent bond to the haem. In the case of cytochrome c_L the two extra cysteines are Cys53 and Cys167; Cys53 is located in helix A whereas Cys167 is at located in strand at the C-terminus end of the protein (Figure 4.22).

Another unexpected finding was the presence of a tightly-bound calcium ion in close proximity to the inner haem propionate, interacting with it through a water ligand (Figure 4.24). The calcium ion is bound in a classical pentagonal-bipyramidal arrangement, with four of the ligands provided by water molecules and three by protein oxygen atoms. In the vast majority of class I *c*-type cytochromes this position is occupied by an arginine residue which also interacts with the propionate through a conserved water molecule and modulates the redox potential (Moore & Pettigrew, 1990). The presence of a positive charge so close to the propionate carboxylate in cytochrome c_L may contribute to the high redox potential (256 mV) exhibited by cytochrome c_L

To ascertain the source of the calcium ion, crystals were grown in the absence of calcium. Although smaller, the crystals diffracted X-rays to 2.8 Å and the initial electron density maps retained a large spherical peak of *2Fo-Fc* and positive *Fo-Fc* electron density at the calcium binding site. A calcium ion was built into the electron density maps and refined; subsequent electron density maps showed no negative or positive *Fo-Fc* electron density surrounding the calcium ion. Furthermore, the B-factors for the calcium ion were in accordance with the other atoms in the structure. From these findings it was concluded that the calcium ion is an inherent feature of the protein and not merely a crystallization artifact.

The protein ligands to the haem iron in the homologous cytochrome c_{551i} are His64 and Met101 (Chen *et al.*, 1994). Site-directed mutagenesis and spectroscopic studies have implicated Met109 as the corresponding sixth ligand to the haem iron in cytochrome c_L (Afolabi *et al.*, 2001). Unexpectedly, the X-ray structure of cytochrome c_L demonstrates that the haem ligands are actually two histidines (69 and 112) (Figure 4.33). This bis-histidine haem coordination may have arisen from the N-terminal proteolysis which is apparent in the structure. The N-terminal region is likely to have interacted with the flexible loop which contains Met109, and as a

consequence of its removal the loop region is more flexibile and exposed to solvent, facilitating a change in the haem iron coordination from Met109 to the stronger His112. Dissociation of Met109 from the iron is consistent with the exceptional reactivity of cytochrome c_L with carbon monoxide; this reaction relies on CO displacing one of the haem iron protein ligands. In the case of cytochrome c_L approximately 72 % of the molecules bind CO in a CO-saturated solution, suggesting the existence of a labile Met-Fe bond (O'Keeffe & Anthony, 1980). Furthermore, NMR studies on cytochrome c_L suggest that the methionine coordinated to the haem has an unusual configuration when compared with other cytochromes *c*, or other small bacterial cytochromes; the pattern of the methionine ligand proton resonances were unusual insofar as none of the methylene protons resonate at a lower frequency than the ε-CH_3 group (Teixeira *et al.*, 1993). An unusual methionine orientation may be permitted due to the absence of a 'conserved' hydrogen bond to a nearby tyrosine (Tyr67 in tuna mitochondrial cytochrome *c*), which is observed in the majority of Met-His ligated haems. Another crystal structure in which the methionine bond to the haem iron had been broken was the cytochrome c_2 from *Rhodopseudomonas palustris*. In this case the methionine was replaced by an exogenous ammonia molecule. A couple of factors were thought to contribute to the displacement of the methionine to the haem iron. Firstly, the protein was crystallized at a basic pH (pH 8.5); previous studies under typical denaturing conditions, including high-pH values and the prescence of exogenous ligands, have shown that the detachment of the methionine axial ligand is a basic step in the folding/unfolding pathway of *c*-type cytochromes. Secondly, the hydrogen bond from the conserved tyrosine to the haem ligated methionine is weaker than in most class I *c*-type cytochromes, allowing the methionine to dissociate from the haem iron easily (Geremia *et al.*, 2002).

7.3 **Methanol dehydrogenase**

Small rod shaped crystals (~ 0.3 x 0.1 x 0.1 mm) of *mxaC31*-MDH and larger rod shaped crystals (~ 1 x 0.1 x 0.1 mm) of *mxaD11*-MDH, both from methanol oxidation mutants of *M. extorquens* mutants, were grown in the dark over the period of a month. Both mutations have been proposed to alter the structure of MDH; the *mxaC31* gene codes for a protein involved in calcium insertion into MDH (Chapter 5) and the *mxaD11* gene product was thought to somehow

modify MDH to improve the electron transfer to cytochrome c_L (Toyama *et al.*, 2003). Both crystal forms grew under the previously published conditions, but in the absence of calcium. X-ray data were collected at the ESRF (Grenoble) to 1.2 Å (*mxaC31*-MDH) and 1.5 Å (*mxaD11*-MDH) resolution and the space groups determined as P1 and $P2_12_12_1$ respectively. Both structures were determined by molecular replacement with the MDH structure at 1.94 Å as the search model (Ghosh *et al.*, 1995). After several rounds of refinement the final models of *mxaC31*-MDH and *mxaD11*-MDH each contained 2 PQQ groups and 2 calcium ions per dimer and had *R*-factors of 12.20 % (*R*-free 15.58 %) and 18.32 % (*R*-free 20.03 %) respectively. Although no gross structural changes were observed in the MDH structures from both methanol oxidation mutants, the calcium occupancy in *mxaC31*-MDH was only 60%, consistent with the proposed role of the *mxaC31* gene product in calcium insertion. The conformation of the PQQ in the active site of mxaC31-MDH is identical to that in WT-MDH although calcium is not coordinated to all of the PQQ molecules in the crystal. It can therefore be surmised that the PQQ conformation is not significantly dependent on calcium coordination. The structural similarity of *mxaD11*-MDH to wild-type-MDH does not account for its greater activity in the dye-linked assay and implies that the lower rate of methanol oxidation in whole cells of this mutant should not be specifically attributed to a change in structure, but that the protein coded for by the *mxaD* gene is somehow involved (Toyama *et al.*, 2003).

7.4 **The conformation of the PQQ prosthetic group**

The conformation of PQQ in MDH has created a certain amount of debate. For the remainder of this section refer to Figures 1.2 for clarification of the atom names of PQQ and Figure 1.3 for the interactions of PQQ with its immediate protein environment. X-ray crystal structures of the sodium and potassium salts of PQQ show the tricyclic ring to be planar in conformation (Ishida *et al.*, 1989; van Koningsveld., 1985), and that the three carboxylate groups can be either co-planar or twisted out of the plane. It was not certain whether the conformation of the PQQ from these crystals was an inherent property of the PQQ or a result of the crystal packing, as the PQQ forms extended hydrogen bonding and metal ion coordination networks. Due to this confusion the conformations of PQQ in different oxidation states were studied using *ab initio* molecular orbital theory (Zheng & Bruice, 1997). These studies produced models which

suggested that free-PQQ is not totally planar, both the C-4 and C-5 carbonyl oxygen atoms were twisted slightly out of the tricyclic plane to resist repulsive interactions. In addition, only two out of the three carboxyl groups (C-2 and C-7) were coplanar with the tricyclic ring; the carboxyl group of C-9 was twisted out of the plane.

The first crystal structure of MDH from *M. extorquens* was solved to 1.94 Å resolution. The C-4 carbonyl was shifted from the plane of the PQQ ring by 40 ° (Ghosh *et al.*, 1995), whereas the C-5 carbonyl stayed within the plane of the PQQ ring (Figure 7.1). This conformation was postulated to be the structure of the semi-quinone form of PQQ (Ghosh & Anthony, 1998). This would be consistent with the proposal that these carbonyl groups are twisted out of the PQQ plane to resist repulsive interactions (see above), although a movement of 40 ° from planarity would seem unnecessary; the chemical groups on C-4 and C-5 in the semi-quinone structure would not require more protection from each other than when in the quinone or quinol forms.

The second high-resolution structure which showed PQQ in an unusual conformation was the 1.90 Å crystal structure of MDH from *M. methylotrophus* (Figure 7.2). In contrast to the MDH structure from *M. extorquens* it was the groups attached to the C-5 PQQ atom which was twisted out of the plane of the PQQ ring and not the C-4 carbonyl. The explanation for the conformation was that the C-5 was in a tetrahedral arrangement; this conformation is only encountered when considering the hydride transfer mechanism and as such, was used as further evidence for the hydride transfer mechanism for the oxidation of methanol by MDH (Zheng *et al.*, 2001). All of the MDH structures solved in this work have been solved to a higher resolution than 1.90 Å (Table 7.1), and in each of these structures the conformation of the PQQ was planar. An absorbance spectrum was taken from a wild type MDH crystal which was used to obtain a 1.7 Å data set (Figure 5.15). The characteristic peak at 345 nm confirmed that the PQQ was either in a reduced or a semi-quinone oxidation state; the final protein model showed PQQ in a planar conformation. The hydroxyl groups on the PQQ C-5 and C-4 atoms were expected to be planar when the prosthetic group is reduced, as a result this 1.7 Å structure conformation was postulated to represent the reduced form of PQQ. There are differences in the active site of the 1.7 Å MDH structure, compared to the postulated 1.94 Å semi-quinone PQQ structure (where the C-4 is twisted out of the PQQ ring). In the semi-quinone conformation the C-4 and C-5 carbonyl oxygen atoms are hydrogen bonded to the NH1 and NH2 atoms of Arg331, in addition,

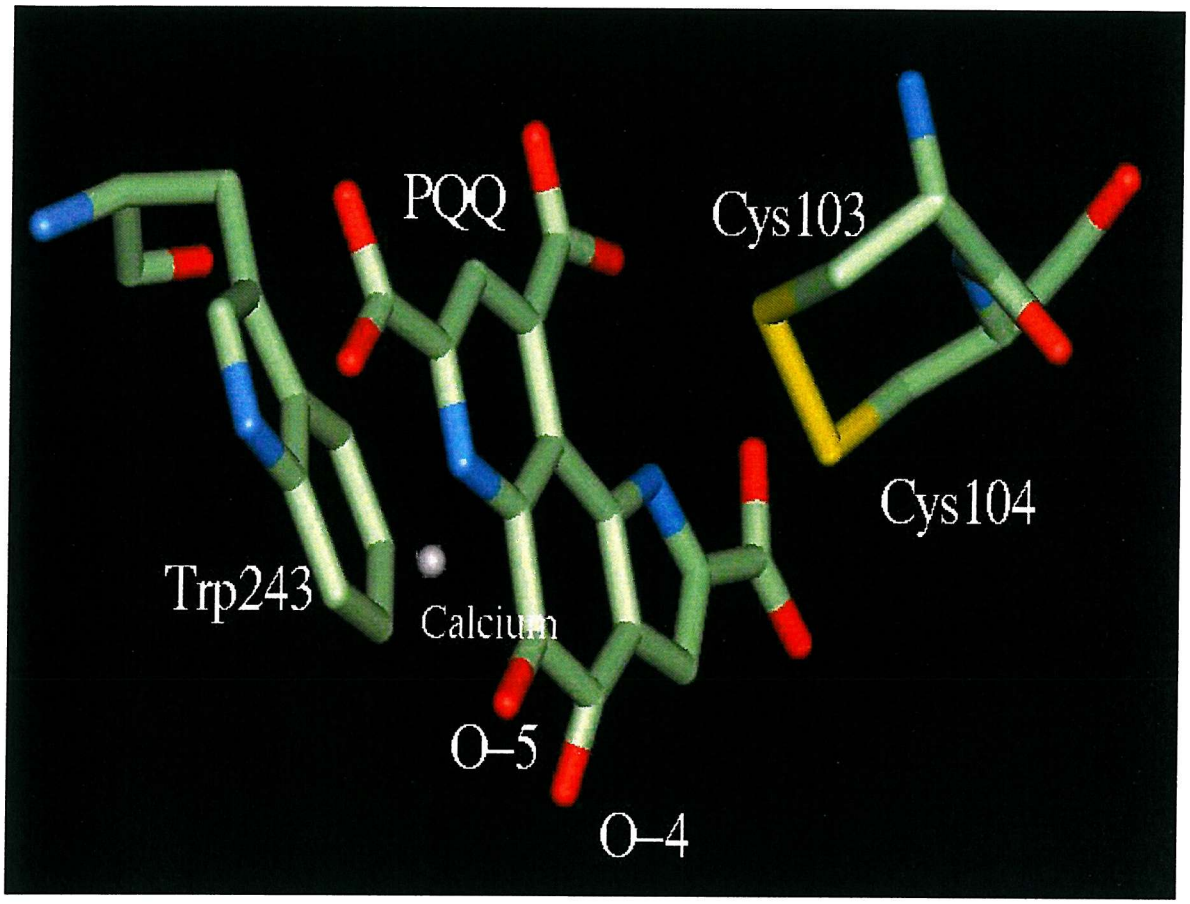

Figure 7.1 The conformation of the PQQ prosthetic group from the 1.94 Å resolution crystal structure of MDH from *M. extorquens*

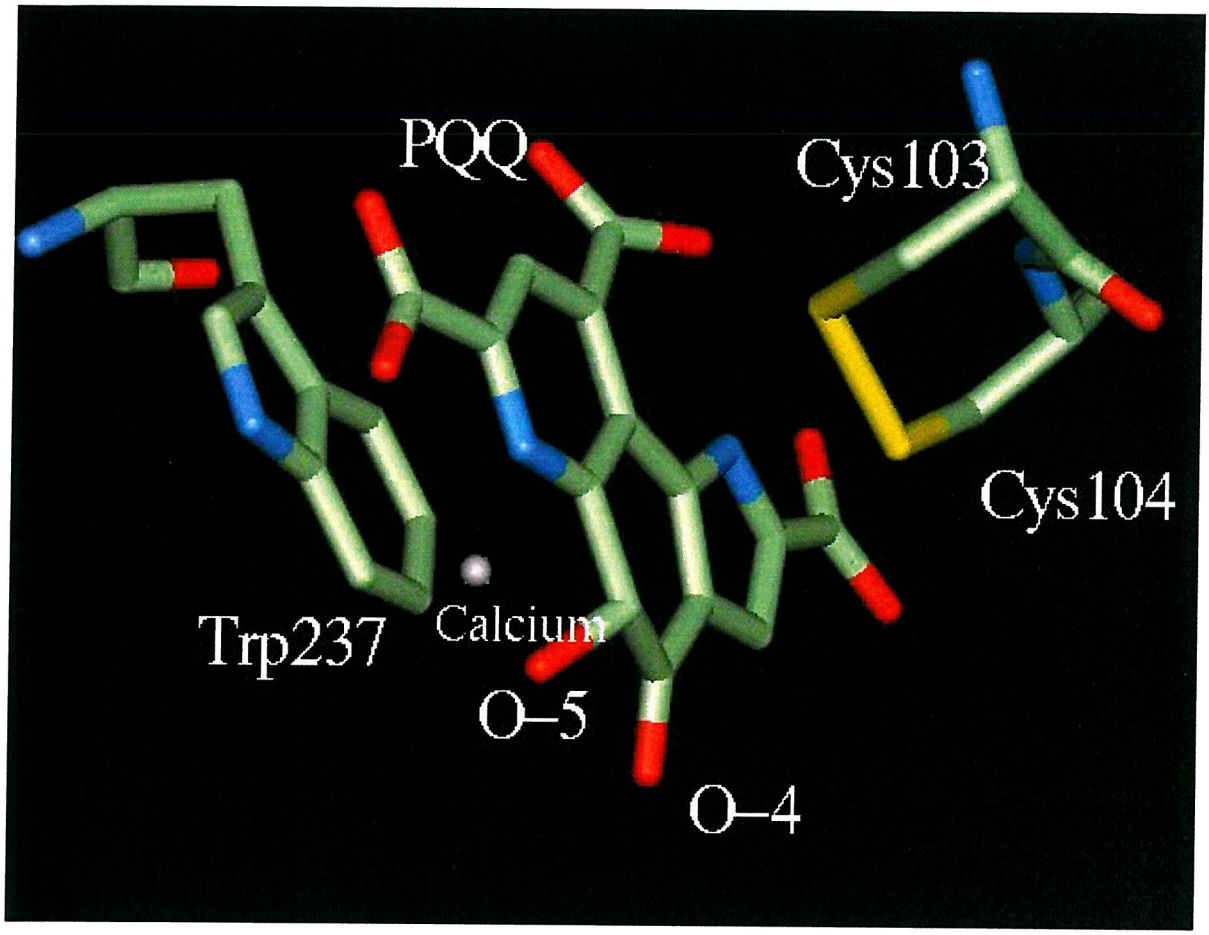

Figure 7.2 The conformation of the PQQ from the 1.90 Å resolution structure of MDH from *M. methylotrophus* (Zheng *et al.*, 2001)

Table 7.1 A Summary of the MDH structures solved during the course of this work.

Protein	Space group	Resolution	*R*-factor	*R*-free
MDH from wild-type *M.extorquens*	$P2_12_12_1$	1.7 Å	18.23 %	20.08 %
MDH from *mxaD11 M.extorquens*	$P2_12_12_1$	1.8 Å	19.57 %	22.26 %
MDH from *mxaD11 M.extorquens*	$P2_12_12_1$	1.5 Å	18.32 %	20.03 %
MDH from *mxaC31 M.extorquens*	P1	1.2 Å	12.20 %	15.58 %

the C-4 oxygen atom makes a hydrogen bond interaction with the amide NH2 of Asn394. By creating a planar PQQ conformation (the 1.7 Å MDH structure) these interactions remain, although the hydrogen bond distance of the C-4 carbonyl oxygen-ArgNH1 increases from 2.70 Å to 3.16 Å. The length of the hydrogen bond from C-4 to Asn394 shows no significant difference between the planar and non-planar structures of MDH. All other high resolution PQQ-containing structures (soluble glucose dehydrogenase and the quinohaemoprotein alcohol dehydrogenases) show a planar PQQ conformation. It is difficult to explain the PQQ C-4 conformation in the 1.94 Å MDH structure. If it does indeed represent the semi-quinone structure of PQQ, compared to the postulated structure of reduced PQQ (see above), only slight modifications of the existing hydrogen bond network are seen, the most substantial of these involves the side chain of Arg331. The short 2.7 Å hydrogen bond between the PQQ O-5 atom and the Arg331 NH_1 atom could serve to stabilize the semi-quinone free-radical. Once the semi-quinone has been fully reduced the need for this protection is removed, which allows the PQQ to 'relax' into a planar conformation.

7.5 **Electron transfer from PQQ to cytochrome c_L**

Upon re-oxidation of the quinol form of PQQ to the quinone form, two electrons are sequentially passed to two molecules of cytochrome c_L (Frank *et al.*, 1988). During the dissociation of the first molecule of cytochrome c_L from MDH, and the binding of the second cytochrome c_L, the PQQ in MDH remains in the semi-quinone form. Although the structure of the MDH / cytochrome c_L complex has yet to be determined, it is reasonable to assume that electrons pass from the reduced PQQ to the haem of cytochrome c_L via the shortest distance. Based on the recently determined structure of the quinohaemoprotein alcohol dehydrogenase from *Pseudomonas putida* HK6 (Chen *et al.*, 2002), it has been possible to superimpose MDH onto the PQQ domain and cytochrome c_L onto the cytochrome domain, in order to model their relative orientations within the MDH / cytochrome c_L complex (Figure 7.3). The model suggests how the two proteins would interact in the bacterial periplasm, provided that the orientation of the redox partners is related to the quinohaemoprotein, as is suggested by the conservation of amino acids and water molecules within the PQQ domain of the quinohaemoprotein and

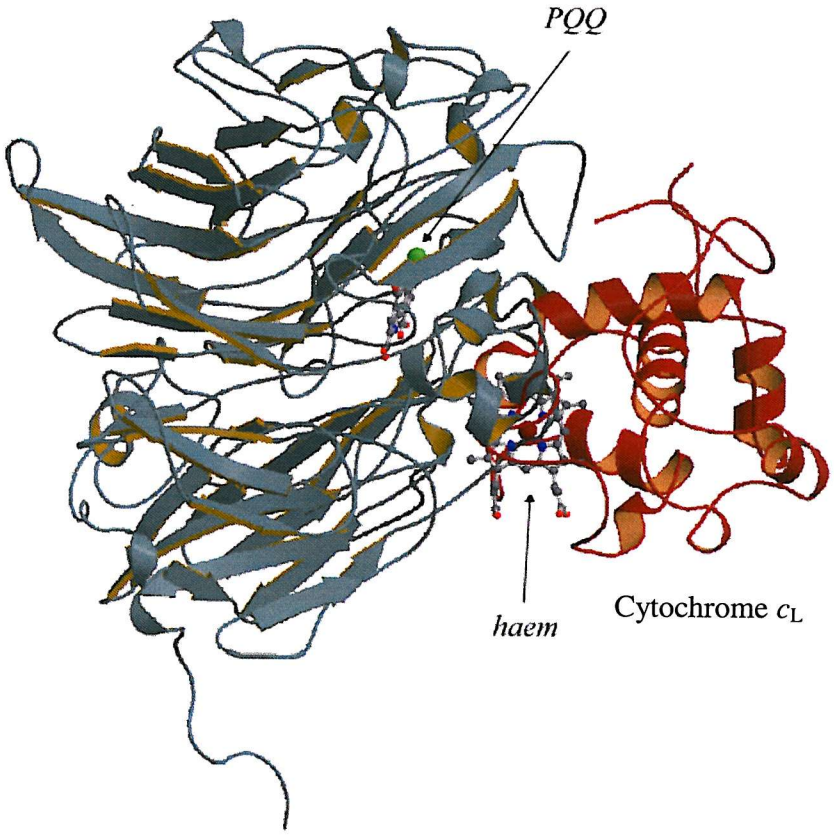

Figure 7.3 A model of the interaction between MDH and cytochrome c_L.

This postulated complex is based on the protein structure of the quinohaemoprotein alcohol dehydrogenase from *Pseudomonas putida* HK6 (Chen *et al.*, 2002).

methanol dehydrogenase (see below). It should be emphasized that Figure 7.3 only provides an approximation of the interaction of the redox partners.

The structures of the quinohaemoprotein alcohol dehydrogenases have provided insights into how electrons are passed from the PQQ-containing to the haem *c* containing domains (Section 1.13). Studies of the enzyme from *Comamonas testeroni* have suggested several pathways for electron transfer, all of which involve active site amino acids, specifically Asp118, Arg67, Glu185, Cys116, Cys117 and internally-bound water molecules (Figure 1.14). The similarity between the active site of MDH and the PQQ domain of the quinohaemoprotein suggests that the electron transfer from MDH to cytochrome c_L may follow a similar pathway involving the PQQ, Asp105, Asn52, Glu177, Cys103, Cys104, and internally bound water molecules. The high-resolution structures presented in this thesis demonstrate that all of the components of the postulated electron transfer pathway are conserved in MDH. The shortest electron transfer route modelled on the QH-ADH structure is depicted in Figure 7.4. Upon the re-oxidation of the quinol form of PQQ in MDH, protons must be released into the periplasm. Based on the calculations from the QH-ADH complex, this is likely to be by way of a similar hydrogen bonded network of proton donor and acceptor groups involving the side chains of Asp303, Arg331, Glu177 and a channel of water molecules leading out from the active site into the periplasm (Figure 7.4) (the red line).

The proposed complex between cytochrome c_L and MDH, along with the suggested routes for electron transfer and proton translocation, suggests several areas for future research. Amino acids which are potentially crucial to electron transfer and proton translocation could be mutated to alternative residues to examine their role in methanol oxidation in *M. extorquens*; obvious examples would be Asp105 and Asn52. Attempts to mutate either Cys103 or Cys104 have been attempted previously, although this mutation compromises the protein structure to such an extent that very little of the MDH is expressed by the bacteria.

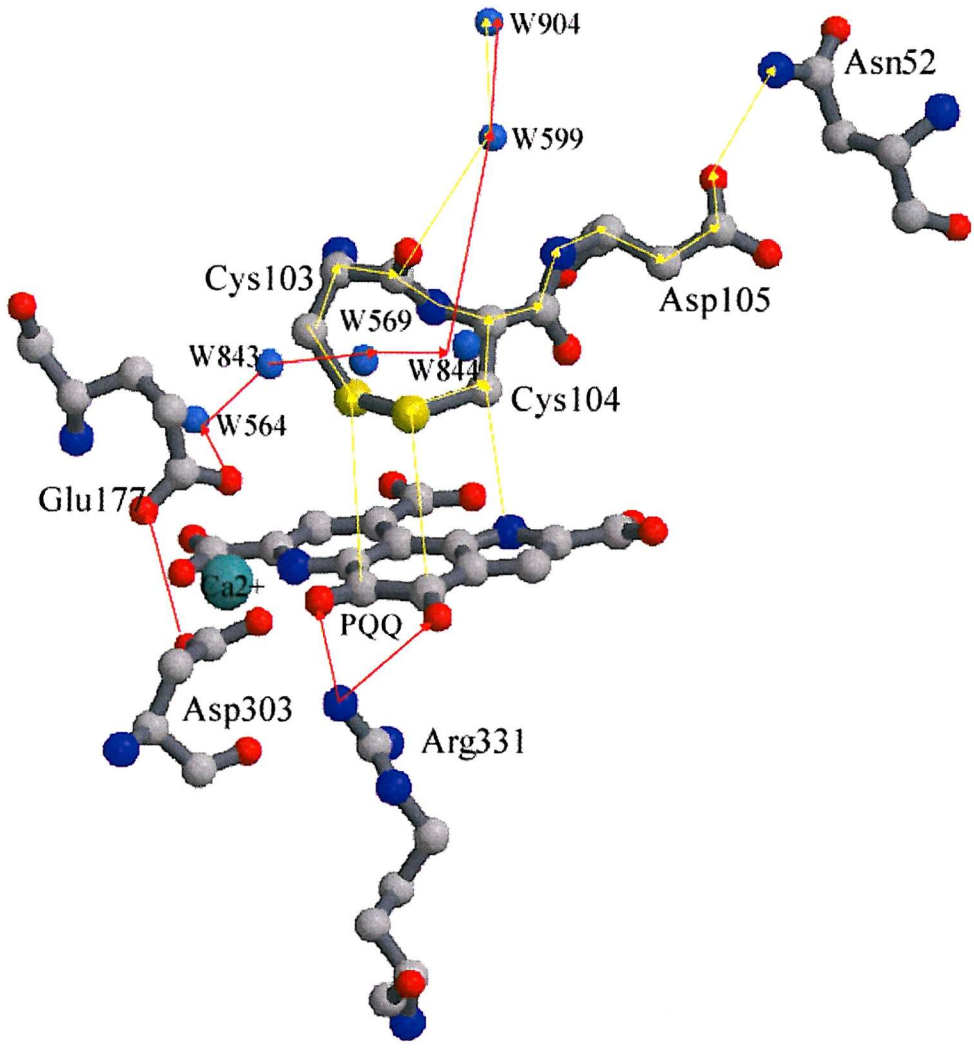

Figure 7.4 A postulated electron transfer pathway from the reduced PQQ towards cytochrome c_L (shown in yellow), and a proposed pathway for protons to be released into the periplasm (shown in red).

These postulated pathways are based on the pathways proposed from the protein structure of the quinohaemoprotein from *Pseudomonas putida* HK6 (Chen *et al.*, 2002).

References

Afolabi, P. R., Mohammed, F., Amaratunga, K., Majekodunmi, O., Dales, S. L., Gill, R., Thompson, D., Cooper, J. B., Wood, S. P., Goodwin, P. M. and Anthony, C. (2001). Site-directed mutagenesis and X-ray crystallography of the PQQ-containing quinoprotein methanol dehydrogenase and its electron acceptor, cytochrome c_L. *Biochemistry.* **40 (33).** 9799-9809.

Amaratunga, K., Goodwin, P. M., O'Connor, C. D. and Anthony, C. (1997). The methanol oxidation genes mxaFJGIR(S)ACKLD in Methylobacterium extorquens (vol 146, pg 31, 1997). *FEMS microbiology letters.* **150 (1).** 175-177.

Ambler, R. P., Daniel, M., Hermoso, J., Meyer, T. E., Bartsch, R. G., Kamen, M. D. (1979). Cytochrome c_2 sequence variation among recognized species of purple non-sulfur photosynthetic bacteria. *Nature.* **278.** 659-660.

Anderson, D. J. and Lidstrom, M. E. (1988). The MoxFG region encodes 4 polypeptides in the methanol-oxidising bacterium *Methylobacterium sp*AM1. *J. Bacteriology.* **170 (5).** 2254-2262.

Anderson, D. J., Morris, C. J., Nunn, D. N., Anthony, C. and Lidstrom, M. E. (1990). Nucleotide sequence of the Methylobacterium extorquens AM1 MoxF and MoxJ genes involved in methanol oxidation. *Gene.* **90 (1).** 173-176.

Anthony, C. (1992). The *c*-type cytochromes of methylotrophic bacteria. *Biochim. Biophys. Acta* **1099**, 1-15.

Anthony, C. (1986). The bacterial oxidation of methane and methanol. *Adv. Microbiol. Physiol.* **27**, 113-210.

Anthony, C. (1982). *The biochemistry of Methylotrophs.* Academic press, London.

Anthony, C. (1996). Quinoprotein-catalysed reactions. *Biochemical. J.* **320**, 697-711

Anthony, C. (1988). Quinoproteins and energy transduction. In: Anthony C (ed) Bacterial Energy Transduction. pp.293-316. Academic press, London.

Anthony, C and Zatman, L. J. (1967). The microbial oxidation of methanol: The prosthetic group of alcohol dehydrogenase of *Pseudomonas* sp. M27; A new oxidoreductase prosthetic group. *Biochemical. J.* **104**, 960-969.

Anthony, C. Ghosh, M. and Blake, C. C. F. (1994). The structure and function of methanol dehydrogenase and related quinoproteins containing pyrrol0quinoline quinone. *J. Biochemical.* **304**. 665-674.

Anthony, C. and Ghosh, M. (1998). The structure and function of the PQQ-containing quinoprotein dehydrogenases. *Prog. Biophy* and *Mol Biol.* **69 (1)**. 1-21.

Avezoux, A., Goodwin, M. G. and Anthony, C. (1995). The role of the novel disulphide ring in the active site of the quinoprotein methanol dehydrogenase from *Methylobacterium extorquens. Biochemical. J.* **307**. 735-741.

Anthony, C. and Williams, P. A. (2003). The structure and mechanism of methanol dehydrogenase. *Biochim. Biophys. Acta.* **164**. 18-23.

Aviram, I and Schejter, A. (1971). Modification of the tryptophanyl residue of horse heart cytochrome *c*. *Biochim. Biophys. Acta.* **244**. 3773-3778.

Axelrod, H. L., Feher, G., Allen, J. P., Chirino, A. J., Day, M. W., Hsu, B. T. and Rees, D. C. (1994). Crystallisation and X-ray structure determination of cytochrome c_2 from *Rhodobacter Sphaeroides* in three crystal forms. *Acta. Cryst. Sec D. Biolgical Crystallography.* **50**. 596-602.

Balabin, I. A. and Onuchic, J. N. (2000). Dynamically controlled protein tunneling paths in photosynthetic reaction centers. *Science.* **290 (5489)**. 114-117.

Beardmore-Gray, M., O'Keeffe, D. T. and Anthony C. (1982). The autoreducible cytochromes *c* of the methylotrophs, *Methylophilus methylotrophus* and *Pseudomonas* AM1. *Biochemical. J.* **207**. 161-165.

Benning, M. M., Meyer, T. E., Holden, H. M. (1994). X-ray structure of the cytochrome c_2 isolated from *Paracoccus denitrificans* refined to 1.7 Å resolution.
Benning, M. M., Wesenger, G., Caffrey, M. S., Bartsch, R. G., Meyer, T. E., Cusanovich, M. A.,

Betz, S. F. and Pielak, G. J. (1992). Introduction of a disulphide bond into cytochrome *c* stabalizes a compact denatured state. *Biochemistry*. **31 (49)**. 12337-12344.

Berghuis, A. M., Guillemette, J. G., Smith, M. and Brayer, G. D. (1994). Mutation of tyrosine-67 to phenylalanine in cytochrome *c* significantly alters the local haem environment. *J. Mol. Biol.* **235 (4)**. 1326-1341.

Berguist, A. M. and Brayer, G. D. (1992). Oxidation state-dependant conformational changes in cytochrome *c*. *J. Mol. Biol.* **223 (4)**. 959-976.

Berry, M. J., George, S. J., Thompson, A. J., Santos, H. and Turner, D. L. (1990). Cytochrome *c*" from methylophillus methylotrophus- an example of a bis-histidine coordinated Fe^{3+} haem with near perpendicular orientation of the ligands. *Biochemical. J.* **270 (2)**. 413-417.

Bourgeois, D., Vernede, X., Adam, V., Fioravanti, E. and Ursby, T. (2002). A microspectrophotometer for UV-visible absorption and fluorescence studies of protein crystals. *J. Applied. Cryst.* **35**. 319-326.

Bushnell, G., Louie, G. V. and Brayer, G. D. (1990). High-resolution three-dimensional structure of horse heart cytochrome *c*. *J. Mol. Biol.* **214**. 585-595.

Brems, D. N., Cass, R. and Stellwagen, E. (1982). Conformational transitions of frog heart ferricytochrome *c*. *Biochemistry*. **21**. 1488-1493.

Bruger, *et al.* (1998). *Acta crystallographica.* **D54**. 905-921.

Chan, H. T. C. and Anthony, C. (1991). The interaction of methanol dehydrogenase and cytochrome c_L in the acidophilic methylotrophs *Acetobacter methanolicus*. *Biochemical. J.* **280**.139-146.

Chan, H. T. C. and Anthony, C. (1992). The mechanism of inhibition by EDTA and EGTA of methanol oxidation by methylotrophic bacteria. *FEMS Microbiology letters*. **96**. 231-234.

Chen, Z. W., Matsushita, K., Yamashita, T., Fujii, T., Toyama, H., Adachi, O., Bellamy, H. and Mathews, S. F. (2002). Structure at 1.9 Å resolution of a quinohaemoprotein alcohol dehydrogenase from *Pseudomonas putida* HK5. *Structure*. **10**. 1-20.

Chen, L. Y., Durley, R. C. E., Mathews, F. S. and Davidson V. L. (1994). Structure of an electron transfer complex- Methylamine dehydrogenase, amicyanin and cytochrome c_{551i}. *Science*. **264 (5155)**. 86-90

Colby, J. and Zatman, L. J. (1972). Hexose phosphate synthase and tri-carboxylic-acid cycle enzymes in *Bacterium* 4B6, an obligate methylotrophs. *Biochemical. J.* **128**, 1373-1376.

Collaborative Computational Project Number 4. (1994). "The CCP4 suite: programs for protein crystallography". *Acta Cryst.* **D50**. 760-763.

Cowtan, K. (1994). An automated procedure for phase improvement by density modification. *Joint CCP4 and ESF-EACBM Newsletter on Protein Crystallography*. **31**. p34-38.

Cox, J. M., Day, D. J. and Anthony, C. (1992). The interaction of methanol dehydrogenase and its electron acceptor, cytochrome c_L in methylotrophic bacteria. *Biochimica et Biophysica Acta.* **1119 (1)**. 97-106.

Cozier, G. E., Lan, I.. and Anthony, C. (1995). The structure of the quinoprotein alcohol dehydrogenase of *Acetobacter aceti* modeled on that of methanol dehydrogenase from *Methylobacterium extorquens*. *Biochemical. J.* **308**. 375-379.

Cozier, G. E., Salleh, R. A, and Anthony, C. (1990). Characterization of the membrane quinoprotein glucose dehydrogenase from Escherichia coli and characterization of a site-directed mutant in which histidine-262 has been changed to tyrosine. *Biochemical. J.* **340**. 639-647.

Crennell, S. J., Garman, E. F., Laver, W. G., Vimr, E. R. and Taylor, G. L. (1993). Crystal structure of a bacterial sialidase (from *Salmonella typhimurium* LT2) shows the same fold as an influenza virus neuraminidase. *Proc. Natl. Acad. Sci. USA*. **90**. 9852-9856.

Dai, S. D., Schwendtmayer, C., Schurmann, P., Ramaswamy, S.and Eklund, H. (2000). Redox signaling in chloroplasts: Cleavage of disulfides by an iron-sulfur cluster. *Science*. **287 (5453)**. 655-658.

Dales, S. L. and Anthony, C. (1995). The interaction of methanol dehydrogenase and its cytochrome electron acceptor. *Biochemical. J.* **312**. 261-265 Part 1.

Davidson, V. L. (1993) Methylamine dehydrogenase. In: Principles and applications of quinoproteins.

Davidson, V. L. and Zhu, Z. Y. (2000). Reaction products and intermediates of tryptophan tryptophylquinone enzymes. *J. Mol. Catalysis. B-enzymatic*. **8 (1-3)**. 69-83.

Davidson, V. L. and Sun, D. P. (2003). Evidence for substrate activation of electron transfer from methylamine dehydrogenase to amicyanin. *J. Am. Chem. Soc*. **125 (11)**, 3224-3225.

Dijkstra, M., Frank, J and Duine, J. A. (1989). Studies on electron transfer from methanol dehydrogenase to cytochrome c_L, both purified from Hyphomicrobium X. *Biochemical. J.* **257**, 87-94.

Day, D. J and Anthony, C. (1990a). Methanol dehydrogenase from *Methylobacterium extorquens* AM1. *Methods Enzymology*. **188**. 210-216.

Day, D. J and Anthony, C. (1990b). Cytochrome c_L from *Methylobacterium extorquens* AM1. *Methods Enzymology*. **188**. 298-303.

Drenth, J. (1994). *Principles of protein X-ray crystallography*. Springer-Verlag, New York, Inc
Duine, J. A., Frank, J. and Longejan, J. A. (1987). Enzymology of quinoproteins. In: *Avdances in Enzymology*, New York: John Wiley and Sons, p 169-212.

Duine, J. A. (1991). Quinoproteins-Enzymes containing the quinonoid co-factor pyrroloquinoline quinone, topoquinone or tryptophan-tryptophan quinone. *Euro. J. Biochem.* **200 (2)**, 271-284.

Elliot, E. J. and Anthony, C. (1988). The interaction between methanol dehydrogenase and cytochrome *c* in the acidic methylotroph. *Acetobacter methanolicus. J. Gen. Microbiol.* **134**. 369-377.

Faber, H. R., Groom, C. R., Baker, H. M., Morgan, W. T., Smith, A., Baker, E. N. (1995). 1.8 Å crystal-structure of the C-terminal domain of rabbit serum hemopexin. *Structure*. **3 (6)**. 551-559.

Ferguson, S. J. (1991). The functions and synthesis of bacterial *c*-type cytochromes with particular reference to *Paracoccus denitrificans* and *Rhodobacter capsulatus*. *Biochimica et. Biophysica. Acta*. **1058 (1)**. 17-20.

Frank, J., Vankrimpen, S. H and Verviel, P. E. J. (1989). On the mechanism of inhibition of methanol dehydrogenase by cyclopropane-derived inhibitors. *Euro. J. Biochem.* **184 (1)**. 187-195.

Frank,J., Dijkstra, M., Duine, A. J. and Balny, C. (1988). Kinetic and spectral studies on the redox forms of methanol dehydrogenase from *Hyphomicrobium*. *Euro. J. Biochem.* **174**. 331-338.

Frauenhoff, M. M. and Scott, R. A. (1992). The role of tyrosine-67 in the cytochrome *c* haem crevice structure studies by semisynthesis. **14 (2)**. 202-212.

Fulop, V., Moir, J. W. B., Ferguson, S. J. and Hajdu, J. (1995). The anatomy of a bifunctional enzyme: structural basis for the reduction oxygen to water and synthesis of nitric oxide by cytochrome cd_1. *Cell.* **81**. 369-377.

Geremia, S., Garau, G., Vaccari, L., Sgarra, R., Viezzoli, M. S., Calligaris, M. and Randaccio, L. (2002). Cleavage of the iron-methionine bond in c-type cytochromes: Crystal structure of oxidized and reduced cytochrome c_2 from *Rhodopseudomonas palustris* and its ammonia complex. *Pro. Sci.* **11 (1)**. 6-17.

Ghosh, R. and Quayle, J. R. (1981). Purification and properties of the methanol dehydrogenase from *Methylophilus methylotrophus*. *J. Biochemical.* **199 (1)**. 245-250.

Ghosh, M., Anthony, C., Harlos, K., Goodwin, M. J. and Blake, C. C. F. (1995). The refined structure of the quinoprotein methanol dehydrogenase from *Methylobacterium extorquens* at 1.94 Å. *Structure*. **3**. 177-187.

Giacovazzo, C., Monaco, H. L., Viterbo, D., Scordari, F., Gilli, G., Zanotii, G and Catti, M. (1992). *Fundamentals of crystallography*. Oxford University P, New York

Goodwin, M. G. and Anthony, C. (1986). Characterisation of a novel methanol dehydrogenase containing barium instead of calcium. *Biochemical. J.* **318**. 673-679.

Goodwin, M. G., Avezous, A., Dales, S. L. and Anthony, C. (1986). Reconstitution of the quinoprotein methanol dehydrogenase from active Ca^{2+}-free enzyme with Ca^{2+}, Sr^{2+} or Ba^{2+}. *Biochemical. J.* **319**. 839-842.

Grabarek, Z. and Gergely, J. (1990). Zero-length crosslinking procedure with the use of active esters. *Analytical Biochem.* **185 (1)**. 131-135.

Goodwin, P. M. and Anthony, C. (1998). The biochemistry, physiology and genetics of PQQ and PQQ-containing enzymes. *Advances in Microbiol Physiology*. **40**, 1-80.

Harris, T. K. and Davidson, V. L. (1994a). Replacement of enzyme bound calcium with strontium alters the kinetic properties of methanol dehydrogenase. *Biochemical. J.* **300**. 175-182

Harris, T. K. and Davidson, V. L. (1994b). Thermal stability of methanol dehydrogenase is altered by the replacement of enzyme bound Ca^{2+} with Sr^{2+}. *Biochemical. J.* **303**. 141-145.

Hauge, J. G. (1964). Glucose dehydrogenase of *Bacterium anitratum*: an enzyme with a novel prosthetic group. *J. Biol. Chem.* **239**, 3630-3639.

Harrenga, A., Reincke, B., Ruterjans, H., Ludwig, B.and Michel, H. (2000). Structure of the soluble domain of cytochrome c_{552} from Paracoccus denitrificans in the oxidized and reduced states. **295 (3)**. 667-678.

Hirohide Toyama, Hideko Inagaki, Kazunobu Matsushita, Christopher Anthony and Osao Adachi, The role of the MxaD protein in the respiratory chain of *Methylobacterium extorquens* during growth on methanol. *Biochim. Biophys. Acta.* **164.** 372-375

Ishida, T., Doi, M., Tomita, K., Hayashi, H., Inoue, M. and Urakami, T. (1989). Molecular and crystal structure of PQQ (methoxatin), a novel coenzyme of quinoproteins: Extensive stacking character and metal ion interaction. *J. Am. Chem. Soc.* **111**. 6822-6828.

Itoh, S. Kawakami, H. and Fukuzumi, S. (1997). Modelling of the chemistry of the quinoprotein methanol dehydrogenase. Oxidation of methanol by a calcium complex of co-enzyme PQQ via the addition-elimination mechanism. *J. Am. Chem. Soc.* **119 (2)**. 439-440.

Iwata, S., Ostermeier, C., Ludwig, B. and Michel, H. (1995). Structure at 2.8 Å resolution of cytochrome-*c*-oxidase from *Parracoccus denitrificans*. *Nature*. **376**. 660-669.

James, P. J. and Anthony, C. (2003). The metal ion in the active site of membrane glucose dehydrogenase of *Escherichia coli*. *Biochim. Biophys. Acta*. **164**. 200-205.

Karplus, P. A. and Schultz, G. E. (1989). Substrate binding and catalysis by glutathione-reductase as derived from the refined enzyme-substrate crystal structures at 2.0 Å resolution. *J. Mol. Biol.* **210 (1)**. 163-180.

Kurnikov, I. V. (2000). University of Pittsburgh, Pittsburgh.

Laemmli, U. K. (1970). Cleavage of structural proteins during the assembly of the head of the bacteriophage T4. *Nature*. **227**, 680-685.

Lambright, D. G., Sondek, J., Bohm, A., Skiba, N. P., Hamm, H. E., Sigler, P. B. (1996). The 2.0 Å crystal structure of a heterotrimeric G protein. *Nature*. **379**. 311-319.

Leslie, A. G. W. (1992). Joint-CCP4 and ESF-EACMB. *Newsletter on protein crystallography* **No26**, Daresbury laboratory, Warrington, U.K.

Leslie, A. G. W. (1994). Mosflm user guide.

Levitt, D. G. (2001). A new software routine that automates the fitting of protein X-ray crystallographic electron-density maps. *Acta. Cryst. Section D-Biol Chem.* **57**. 1013-1019 Part 7.

Li, J., Brick, P., O'Hare, M. C., Skarzynski, T., Lloyd, L. F., Curry, V. A., Clark, I. M., Bigg, H. F., Hazleman, B. L., Cawston, T. E. and Blow, D. M. (1995). Structure of a full-length porcine synovial collagenase reveals a C-terminal domain containing a calcium-linked four bladed propeller. *Structure*. **3**. 541-549.

Lidstrom, M. E., Anthony, C., Biville, F., Gasser, F., Goodwin, P., Hanson, R. S. and Harms, N. (1994). New unified nomenclature for genes involved in the oxidation of methanol in gram-negative bacteria. *Fems Microbiology letters*. **117 (1)**. 103-106.

Lo, T. P., Komarpanicucci, S., Sherman, F., McLendon, G. Brayer, G. D. (1995). Structural and functional effects of multiple mutations at distil sites in cytochrome *c*. *Biochemistry*. **34 (15)**. 5259-5268.

Louie, G. V. and Brayer, G. D. (1990). High-resolution refinement of yeast iso-1-cytochrome *c* and comparisons with other eukaryotic cytochromes *c*. *J. Mol. Biol.* **214**. 527-555.

Luntz, T. L., Schejter, A., Garber, E. A. E. and Margoliash, E. (1989). Structural significance of an internal water molecule studied by site-directed mutagenesisof tyrosine-67 in rat cytochrome *c*. *Proc. Nat. Acad. Sci., USA*. **86**. 3524-3528.

Matsushita, K., Toyama, H., Ameyama, M., Adachi, O., Dewanti, A. and Duine, J. A. (1995). Soluble and membrane bound quinoprotein D-glucose dehydrogenase of the *Acinetobacter caloaceticus*- the binding process of PQQ to the apoenzymes. *Bioscience Biotecnology and Biochemistry*. **59 (8)**. 1548-1555.

Mattevi, A., Vanoni, M. A., Todone, F., Rizzi, M., Teplyakov, A., Coda, A., Bolognesi, M. and Curti, B. (1996). Crystal structure of D-amino acid oxidase: A case of active site mirror-image convergent evolution with flavocytochrome b(2). *Proc. Nat. Aca. Sci. USA*. **93 (15)**. 7496-7501.

Mattevi, A., Fraaije, M. W., Mozzarelli, A., Olivi, L., Coda, A. and vanBerkel, W. J. H. (1997). Crystal structures and inhibitor binding in the octameric flavoenzyme vanillyl-alcohol oxidase: The shape of the active-site cavity controls substrate specificity. *Structure*. **5 (7)**. 907-920.

Mitchell, E., Khun, P and Garman, E. (1999). Demystifying the synchrotron: A first time user's guide. *Structure* 7, **No 5** R111-R121.

Moore, G. R. and Pettigrew, G. W. (1990). Cytochromes *c*: Evolutionary, structural and Physicochemical aspects. Springer-verlag, London.

Morris, R. J., Perrakis, A. and Lamzin, V. S. (2002). ARP/wARP's model-building algorithms. I. The main chain. *Acta. Cryst. Section D-Biol Chem*. **58**. 968-975 Part 6.

Moser, C. C., Page, C. C, Farid, R. and Dutton, P. L. (1992). Biological electron transfer. *J. Bioenergetics and Biomembranes*. **27 (3)**. 263-274.

Mutzel, A. and Gorisch, H. (1991). Quinoprotein ethanol dehydrogenase-Preparation of the apo-form and the reconstitution with pyrrolequinoline quinone and Ca^{2+} or Sr^{2+} ions. *Agr. Biol. Chem*. Tokyo. **55 (7)**. 1721-1726.

Nunn, D. N., Day, D. J. and Anthony, C. (1989). The second subunit of methanol dehydrogenase of *Methylobacterium extorquens*. *Biochemical. J*. **260**. 857-862.

Nunn, D. N. and Anthony, C. (1988). The nucleotide sequence and deduced amino acid sequence of the *Methylobacterium extorquens* AM1, a novel class of *c*-type cytochrome. *Biochemical. J*. **256 (2)**. 673-676.

Ochi, H., Hata, T., Tanaka, N., Kakudo, M., Sakurai, T., Aihara, S. and Morita, Y. (1983). Structure of rice ferricytochrome *c* at 2.0 Å resolution. *J. Mol. Biol*. **166**. 407-418.

Oubrie, A., Rozeboom, H. J., Kalk, K. H., Huizinga, E. G. and Dijkstra, B. W. (2002). Crystal structure of quinohaemoprotein alcohol dehydrogenase from *Comamonas testeroni*; structural basis for substrate oxidation and electron transfer. *J. Biol. Chem.* **277**. 3727-3732.

Oubrie, A., Rozeboom, H. J., Kalk, K. H., Olsthoorn, A. J. J., Duine, J. A.and Dijkstra, B. W. (1999). Structure and mechanism of soluble quinoprotein glucose dehydrogenase. *EMBO Journal*. **18 (19)**. 5187-5194.

O'Keeffe, D. T. and Anthony, C. (1978). The microbial metabolism of C1 compounds. The stoicheiometry of respiration-driven proton translocation in *Pseudomonas* AM1 and in a mutant lacking cytochrome *c*. *Biochemical. J.* **170**. 561-567.

O'Keeffe, D. T. and Anthony, C. (1980a). The two cytochromes *c* in the facultative methylotroph *Pseudomonas* AM1. *Biochemical. J.* **192**. 411-419.

O'Keeffe, D. T. and Anthony, C. (1980b). The interaction between methanol dehydrogenase and the autoreducible cytochromes *c* of the facultative methylotroph *Pseudomonas* AM1. *Biochemical. J.* **190**. 481-484.

Page, C. C., Moser, C. C., Chen, X. X.and Dutton, P. L. (1999). Natural engineering principles of electron tunnelling in biological oxidation-reduction. *Nature*. **402 (6757)**. 47-52.

Pettigrew, G. W. and Moore, G. R. (1987). Cytochromes *c*: Biological aspects. Springer-verlag, London.

QUANTA96. (1996). X-ray structure analysis user's reference, June1996. San Diego: Molecular Simulations.

Pidcock. and Moore, G. R. (2001). Structural characteristics of protein binding sites for calcium and lanthandine ions. http://link.springerny.com/link/service/jpurnal/00775/01/00214/s007750100214ch002html

Rayment, I. and Holden, H. M. (1991). Molecular structure of cytochrome c_2 isolated from *Rhodobacter capsulatus* determined at 2.5 Å resolution. *J. Mol. Biol.* **220 (3)**. 673-685.

Read, J., Gill, R., Dales, S. L., Cooper, J. B., Wood, S. P. and Anthony C. (2000). The molecular structure of an unusual cytochrome c(2) determined at 2.0 angstrom; the cytochrome c_H from *Methylobacterium extorquens*. *Protein Science*. **8 (6)**. 1232-1240.

Redinbaugh, M. G and Turley, R. B. (1986). Adaption of the bicinchoninic acid proteins assay for the use with microtiter plates and sucrose gradient fractions. *Anal. Biochem.* **153**. 267-271.

Rhodes, G. (1993). *Crystallography made crystal clear: A guide for users of macromolecular molecules*. Academic press.

Richardson, I. W. and Anthony, C. (1992). Characterisation of mutant forms of of the quinoprotein methanol dehydrogenase lacking an essential calcium ion. *Biochemical. J.* **287**. 709-715.

Rossman, M and Blow, D. (1962). The detection of sub-units within the crystal asymmetric unit. *Acta Crystallographica*. **15**. 45-52

Salisbury, S. A., Forrest, H. S., Cruise, W. B. T. and Kennard, O. (1979). A novel coenzyme from bacterial from bacterial primary alcohol dehydrogenase. *Nature*. **280**, 843-844.

Santos, H. and Turner, D. L. (1988). Characterisation and NMR studies of a novel cytochrome *c* isolated from *Methylophilus methylotrophus* which shows a redox-linked change of spin-state. *Biochimica et. Biophysica. Acta*. **954 (3)**. 277-286.

Satoh, A., Kim, J. K. Miyahara, I., Devreese, B., Vandenberghe, I., Hacisalihoglu, A., Okajima, T., Kuroda, S., Adachi, O., Duine, J. A., Van Beeumen, J., Tanizawa, K. and Hirotsu, K. (2002). Crystal structure of quinohemoprotein amine dehydrogenase from Pseudomonas putida-

Identification of a novel quinone cofactor encaged by multiple thioether cross-bridges. *J. Biol. Chem.* **277 (4)** 2830-2834.

Senn, H., Keller, R. M., Wuthrich, K. (1980). Different chirality of the axial methionine in homologous cytochromes *c* determined by NMR and CD spectroscopy. *Biochem. Biophys. Res. Commun.* **92.** 1362-1369.

Senn, H. and Wuthrich, K. (1985). Amino acid sequence, haem iron coordination geometry and functional properties of mitochondrial and bacterial *c*-type cytochromes. *Quat review Biophys.* **18.** 111-134.

Sheldrick, G. M. (1998). In direct methods for solving macromolecular structures. 131-141 and 401-411. Oxford university press, Oxford.

Sogabe, S. and Miki, K. (1995). Refined crystal structure of ferrocytochrome c_2 from *Rhodopseudomonas viridis* at 1.6 Å resolution. *J. Mol. Biol.* **252 (2).** 235-247.

Sondek, J., Bohm, A., Lambright, D. G., Hamm, H. E. and Sigler, P. B. (1996). Crystal structure of a G_A protein dimer at 2.1 Å resolution. *Nature.* **379.** 369-374.

Stowell, M. H., McPhillips, T. M., Rees, D. C., Soltis, S. M., Abresch, E. and Feher, G. (1997). Light-induced structural changes in photosynthetic reaction center: Implications for mechanism of electron-proton transfer. *Science.* **276.** 812-816.

Smith, P. K., Krohn, R.I., Hermanson, G. T., Mallia, A. K., Garther, F.H., Provenzano, M.D., Fujimoto, D. C., Goeke, N. M., Olsen, B. J. and Klesk, D.C. (1985). Measurement of protein using bicinchonoic acid. *Anal. Biochem.* **150.** 76-85.

Takano, T. and Dickerson, R. E. (1981a). Conformational changes of cytochrome *c*-Ferrocytochrome-*c* structure refined at 1.5 Å. *J. Mol. Biol.* **153 (1).** 79-94.

Takano, T. and Dickerson, R. E. (1981a). Conformational changes of cytochrome *c*-Ferricytochrome-*c* structure refined at 1.8 Å. *J. Mol. Biol.* **153 (1)**. 95-115.

Teixeira, M., Campos, A. P., Aguiar, A. P., Costa, H. S., Santos, H., Turner, D. L and Xavier, A. V. (1993). Pitfalls in assigning heme axial ligands by EPR; *c*-type cytochromes with atypical Met-His ligation. *FEBS.* **317 (3)**. 233-236.

Toyama, H., Fujii, A., Matsushita, K., Shinagawa, E., Ameyama, M. and Adachi, O. (1995). 3 distinct quinoprotein alcohol dehydrogenases are expressed when *Pseudomonas putida* is grown in different alcohols. *J. Bacteriology.* **17 (9)**. 2442-2450.

Toyama, H., Anthony. C. and Lidstrom, M. (1998). Construction of insertion and deletion *mxa* mutants of *Methylobacterium extorquens* AM1 by electroporation. *FEMS Microbiology Letters.***166**. 1-7.

Vagin, A. and Teplyakov, A. (1997). MOLREP: an automated program for molecular replacement. *J. App. Cryst.* **30**. 1022-1025 Part 6.

Van Koningsveld, H., Jansen, J. C., Jongejan, J. A., Jzn, J. F. and Duine, J. A. (1985). Structure of the 2, 4- dintrophenylhydrazine adduct of pyrroloquinoline quinone (PQQ) dimethy ethyl triester C24H18N6011. *Acta. Cryst. Sec C. Chem Comm.* **41**. 89-92.

Van Spanning, R. J. M., Wansell, C. W., Deboer, T., Hazelhaar, M. J., Anazawa, H., Harms, N., Oltmann, L. F. and Stouthamer, A. H. (1991). Isolation and characterization of the MoxJ, MoxG, MoxI and MoxR and the resultant effect on methylotrophic growth. *J. Bacteriology.* **173 (21)**. 6948-6961.

Varghese, J. N., Laver, W. G. and Colman, P. M. (1983). Structure of the influenza virus glycogen antigen neuraminase at 2.9 Å resolution. *Nature.* **303**. 35-40.

Wallace, C. J. A. and Rose, K. (1983). The semisynthesis of analogues of cytochrome *c*. Modifications of arginine residues 38 and 91. *Biochemical. J.* **215**. 651-658.

Weber, K.T and Osbourne, M. (1975). Proteins and sodium dodecyl sulphate: molecular weight determination on polyacrilamide gels and related procedures. *The proteins.* 3^{rd} edition. 179-223.

Westbrook, E. M and Naday, I. (1997). Charge coupled device based area detectors. *Methods in Enzymology*. **276**. 244-268.

White, S., Boyd, G., Mathews, F. S., Xia, Z. X., Dia, W. W., Zhang, Y. F., Davidson, V .L. (1993). *Biochemistry*. **32 (48)**: 12955-12958

Wilkström, M., Krabb, K., Saraste, M. (1981). Cytochrome oxidase: a synthesis. Acedemic press, New York, London.

Woolfson, M. M (1997). *An introduction to X-ray crystallography*. Cambridge University Press, Inc.

Xia, Z. X., Dai, W. W., Zhang, Y. F., White, S. A., Boyd, G. D. and Mathews, F. S. (1996). Determination of the gene sequence and the three-dimensional structure at 2.4 angstrom resolution of methanol dehydrogenase from *Methylophilus* W3A1. *J. Mol. Biol.* **259 (3)**. 480-501.

Xia, Z. X., He, Y. N., Dai, W. W., White, S. A., Boyd, G. D. and Mathews, F. S. (1999). Detailed active site configuration of a new crystal form of methanol dehydrogenase from *Methylophilus* W3A1 at 1.9 angstrom resolution. *Biochemistry*. **38 (4)**. 1214-1220.

Xia, Z. X., Dai, W. W., Xiong, J. P., Hao, Z. P., Davidson, V. L, White, S. A, Mathews, F. S. (1992). The 3-dimensional structures of methanol dehydrogenase from 2 methylotrophic bacteria at 2.6- Angstrom resolution. *J. Biol. Chem.* **267 (31)**. 22289-22297

Yamada, M., Sumi, K., Matsushita, K., Adachi, O. and Yamada, Y. (1993). Topological analysis of quinoprotein glucose dehydrogenase in *Escherichia coli* and its ubiquinone-binding site. *J. Biol. Chem.* **268 (17)**. 12812-12817.

Zarnt, G., Schrader, T. and Andreesen, J. R. (2001). Catalytic and molecular properties of the quinohemoprotein tetrahydrofurfuryl alcohol dehydrogenase from Ralstonia eutropha strain Bo. *J. Bacteriology*. **183 (6)**. 1954-1960.

Zarnt, G., Schrader, T. and Andreesen, J. R. (1997). Degradation of tetrahydrofurfuryl alcohol by Ralstonia eutropha is initiated by an inducible pyrroloquinoline quinone-dependent alcohol dehydrogenase. *Applied and Environmental microbiology*. **63 (12)**. 4891-4898.

Zheng, Y. J., Xia, Z. X., Chen, Z.W. and Mathews, F. S. (2001). Catalytic mechanism of quinoprotein methanol dehydrogenase: a theoretical and X-ray crystallographic investigation. *Proc. Nat. Aca. Sci. USA*. **98**. 432-434.

Zheng, Y. J. and Bruice, T. C. (1997). Conformation of coenzyme pyrroloquinoline quinone and role of Ca2+ in the catalytic mechanism of quinoprotein methanol dehydrogenase. *Proc. Nat. Aca. Sci. USA*. **94 (22)**. 11881-11886.

Zheng, Y. J., Xia, Z. X., Chen, Z. W., Mathews, F. S. and Bruice, T. C. (2001). Catalytic mechanism of quinoprotein methanol dehydrogenase: A theoretical and x-ray crystallographic investigation. *Proc. Nat. Aca. Sci. USA*. **98 (2)**. 432-434.